Vibration of floor structures subjected to crowd-rhythmic activities

Youssef El Asri

THESE DE DOCTORAT DE

L'INSTITUT NATIONAL DES SCIENCES APPLIQUEES RENNES
En cotutelle avec
L'UNIVERSITE DE LIEGE

ECOLE DOCTORALE N° 647
Sciences pour l'Ingénieur – SPI.bzh
Spécialité : Génie civil

Par
Youssef EL ASRI

Vibration of floor structures subjected to crowd-rhythmic activities

Thèse présentée et soutenue à l'INSA de Rennes, le 24/02/2023
Unité de recherche : CTICM / LGCGM
Thèse N° : 23ISAR 06 / D23 - 06

Rapporteurs avant soutenance :

Anas BATOU	Professeur, University of Liverpool (Royaume-Uni)
Jean-Marc BATTINI	Professeur, KTH Royal Institute of Technology (Suède)

Composition du Jury :

Président :	Anas BATOU	Professeur, University of Liverpool (Royaume-Uni)
Examinateurs :	Jean-Marc BATTINI	Professeur, KTH Royal Institute of Technology (Suède)
	Luis COSTA-NEVES	Professeur assistant, Universidade de Coimbra (Portugal)
	Cédric SCHWARTZ	Professeur associé, Université de Liège (Belgique)
	Federica TUBINO	Professeur associé, Università di Genova (Italie)
Co-encadrant :	Maël COUCHAUX	Maître de conférences, INSA de Rennes
Directeur de thèse :	Mohammed HJIAJ	Professeur, INSA de Rennes
Co-directeur de thèse :	Vincent DENOËL	Professeur, Université de Liège (Belgique)

Invité(s)

Mladen LUKIĆ	Directeur de projets, Centre Technique Industriel de la Construction Métallique (France)

Intitulé de la thèse :

Vibration of floor structures subjected to crowd-rhythmic activities

Youssef EL ASRI

En partenariat avec :

Université de Liège

الحمد لله على الإنعام بنعمة الإيمان والإسلام
قد خلق بفضله الإنسانا فضله بالنطق واللسانا
يفيض نوره على عقولنا حتى بدا الخفي من معقولنا
وجاعل التفكير في آياته سبيل وصل الحق في اعتقاده
من أجل ذا نص الكتاب المحكم الله لا يخشاه إلا عالم
فأحمد الله على ما سهلا حمدا ينيل من مزاياه العلى
حمدا يدوم بدوام الأبد ثم صلاته على محمد
أفضل من بعث للأنام وخير من قد قام بالمقام
فهو الشريف يا فداه أمي ووالدي وإخوتي وعمي
والحمد لله على التمام ومنه أرجو أحسن الختام
وأسأل الله تعالى العصمة في القول والفعل فتلك النعمة
وأن يزكي عملي ويعرضا عن سوئه وأن ينيلنا الرضا

يوسف العسري
(منتقى من عدة أرجوزات)

Abstract

Nowadays, building floors are prone to excessive vibrations induced by human actions, especially when a group of people performs rhythmic activities in a coordinated manner. Resulting effects on the floor occupants vary from perception, discomfort or even panic. A reliable model for rhythmic activities, taking into account the experimentally observed group effect, is thus essential for the serviceability assessment of such structures. However, design guidelines dealing with the subject are mainly based on time domain load models for a single person exciting a floor structure, and little information is given about the response calculation of floors when subjected to crowd-rhythmic activities.

This thesis addresses the development of a spectral load modelling approach characterizing rhythmic activities induced by a single person or a group of individuals. The proposed model comprises a Power Spectral Density (PSD) function for a single person, combined with coordination factors for multiple individuals. For that purpose, a floor specimen was designed on which a test campaign involving two particular types of rhythmic activity (jumping, skipping) was conducted. In this experiment, up to 16 individuals were asked to perform rhythmic activities in a coordinated manner while exposed to audible and visual stimulus. Parameters of the PSD function for a single person are identified by means of a least-squares procedure. It is found that specific load parameters characterize the human motion associated to each investigated activity. Recommendations for the choice of such parameters for design purposes are then proposed depending on the comfort level defined by the stakeholders. Moreover, coordination factors for multiple individuals are obtained from best-fit functions describing the variation of crowd forces against group size. Resulting coordination factors are described by hyperbolic functions for jumping activities against decreasing exponential functions for skipping activities. The developed crowd load models are then verified by means of response measurements on a full-scale structure and their scope extended to a maximum number of 32 individuals. It is concluded that the coordination stimulus has an influence on the developed load model between the two previous experiments, but it is deemed plausible that this model could be used for similar situations encountered in real life. Comparison of the proposed load models and existing models in the literature are performed afterwards, and remarkable differences are highlighted in terms of individual and crowd forces as well as numerical responses computed for three different floor structures.

In addition, methods for predicting the response of floors subjected to crowd-rhythmic activities are proposed. These methods are based on the developed spectral load model and the random vibration theory. The assessment of floors against human discomfort could then be carried out using these methods, in accordance with the vibration acceptability criterion agreed by the stakeholders. This includes various facilities such as sports venues, fitness centres, gymnasiums, grandstands, etc. The findings of this work might also represent a first step of a procedure to be implemented in future Eurocodes editions for practical application.

Acknowledgements

The work presented in this thesis was conducted at the Centre Technique Industriel de la Construction Métallique (CTICM) in France, with the academic supervision of INSA Rennes and University of Liège. I would like to first thank the members of the defence committee for taking their time to assess my research work.

I would like to express my gratitude to all my supervisors during this thesis, Professor Mohammed HJIAJ and Sen. Lec. Maël COUCHAUX from INSA Rennes, Professor Vincent DENOËL from University of Liège, and Dr. Mladen LUKIĆ from CTICM, for their continuous support as well as their fruitful advices and discussions along the research period. Thanks also go to all colleagues of CTICM and INSA Rennes for their assistance and everyday company during my presence at these institutions.

The FCBA technical centre is gratefully acknowledged for providing the necessary area to perform experiments on the floor specimen, together with Briand CM Company which furnished the parking floor for vibration tests. The participation of all individuals in the two test campaigns presented in this thesis is also highly appreciated.

Finally, I owe my thanks to every person who participated directly or indirectly in the completion of this research work.

Résumé étendu

De nos jours, la construction des planchers de bâtiments a connu des développements remarquables. En effet, l'usage de matériaux plus résistants et plus légers a permis la construction de structures plus légères, plus minces et plus flexibles, tout en satisfaisant les critères de vérification à l'Etat Limite Ultime. Il en résulte une diminution des fréquences propres et des amortissements, remettant ainsi en cause le comportement vibratoire de ces planchers à l'Etat Limite de Service. En particulier, les occupants perçoivent de plus en plus couramment les vibrations des planchers, ce qui peut engendrer des problèmes d'inconfort voire même de panique.

La prise en compte des effets vibratoires sur les planchers doit alors être menée dès la phase de dimensionnement. Toutefois, la prise en considération de l'effet de ces vibrations est assez limitée dans les Eurocodes. En guise d'illustration, l'Annexe Nationale Française à l'Eurocode 3 [6] propose des fréquences propres minimales au-delà desquelles le confort vibratoire des planchers est supposé acceptable. Cependant, l'expérience a montré que des planchers souffrent de véritables problèmes vibratoires même lorsque ces critères fréquentiels sont satisfaits. En réalité, le comportement vibratoire des planchers est régi par de nombreux paramètres modaux autres que la fréquence propre (masse généralisée, coefficient d'amortissement, déformée modale). Concernant les vibrations d'origine humaine, le cas de chargement le plus défavorable correspond à des activités rythmiques pratiquées par un groupe de personnes ayant un certain degré de coordination (voir Figure 1).

Figure 1: Groupe de personnes sur un plancher (modifié de [75])

Face à cette situation, deux éléments principaux doivent être établis pour un dimensionnement adéquat de tels planchers :

- Un modèle de charge communément accepté pour les activités rythmiques de foule ;
- Une méthode de calcul de la réponse vibratoire des planchers soumis à ces activités.

L'objectif de cette thèse est de contribuer à mieux répondre aux problématiques engendrées par les points précédents, actuellement indisponibles pour la pratique courante. En premier lieu, une nouvelle approche de modélisation des activités rythmiques de groupe dans le domaine fréquentiel, dont les paramètres du modèle sont déterminés sur base d'essais expérimentaux, est établie. En second lieu, des procédures pour l'évaluation de la réponse des planchers induite par ces activités sont proposées.

Une revue de la littérature a été d'abord effectuée dans le Chapitre 2, en se basant sur la subdivision courante du problème en trois parties : la source vibratoire (modèle de charge), le chemin de transmission (réponse du plancher) et le récepteur (limites d'acceptabilité des vibrations). L'étude est limitée aux activités rythmiques avec perte de contact avec le sol qui causent le maximum de vibrations aux planchers.

Dans un premier temps, les principaux documents dont dispose l'ingénieur pour évaluer le confort vibratoire des planchers soumis aux activités rythmiques sont présentés. Il s'agit de deux guides pratiques, à savoir le guide SCI P354 [81] et le guide AISC DG11 [63]. L'évaluation du confort des planchers à l'aide de ces guides se base sur deux éléments essentiels :

- Des modèles analytiques exprimés principalement dans le domaine temporel. Pour le cas d'une seule personne sollicitant un plancher, les modèles existants sont de deux types : décomposition en série de Fourier suivant un nombre d'harmoniques (voir Figure 2(a)) ou impulsions successives basées sur un modèle d'impulsion défini (voir Figure 2(b)). Les paramètres de ces modèles ont été initialement déterminés par des méthodes théoriques.
- Des limites d'acceptabilité des vibrations vis-à-vis des occupants, sur la base des directives fournies par les normes de confort vibratoire en vigueur (ISO 2631-1 [46], ISO 2631-2 [48], ISO 10137 [45] et DIN 4150-2 [25]).

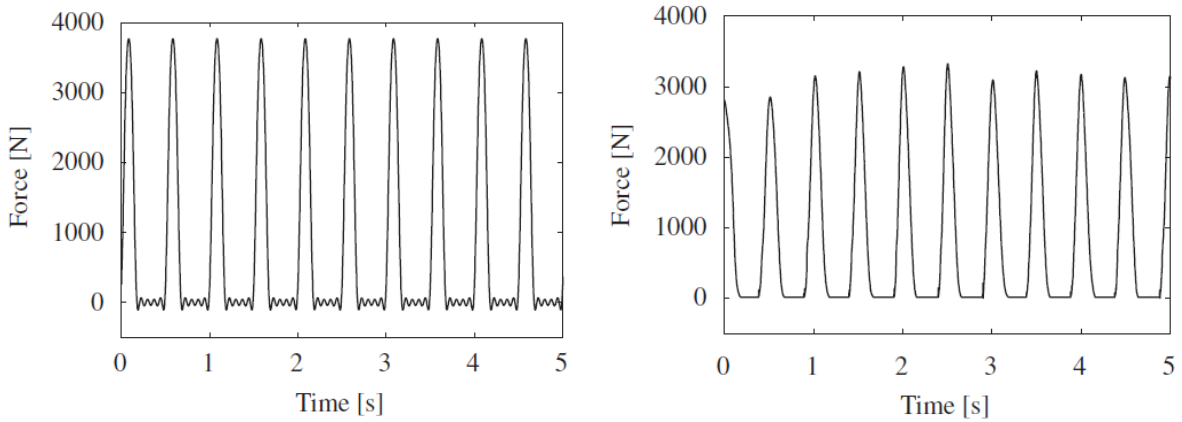

(a) Série de Fourier (b) Impulsions successives

Figure 2: Modèles de charge temporels [50]

Dans un second temps, les principales recherches visant le développement des modèles de charge rythmiques sont détaillées. Dans le domaine temporel, une amélioration des modèles analytiques décrits précédemment est effectuée en déterminant leurs paramètres sur la base de mesures expérimentales pour s'approcher d'activités réelles. Toutefois, l'inconvénient majeur d'une telle modélisation réside dans le fait que la personne est supposée répéter la même action durant le mouvement. En réalité, ceci n'est pas possible au vu des variations de fréquences et

amplitudes d'un impact à l'autre (« effets d'intra-variabilités »). L'activité humaine est plutôt considérée comme un processus stochastique quasi-périodique à bande étroite. Des modèles ont donc été développés dans le domaine fréquentiel, notamment en terme de densité spectrale de puissance.

Pour le cas d'un groupe de personnes sollicitant un plancher (voir Figure 1), le chargement total n'est pas égal à la somme des chargements individuels, puisque chaque personne possède un rythme de mouvement différent de l'autre (« effets d'inter-variabilités »). Une réduction du chargement total est donc considérée dans les modèles temporels en y introduisant des coefficients de coordination dépendant du degré de synchronisation entre individus. Pour les modèles fréquentiels, le chargement de foule est caractérisé par la densité spectrale d'une seule personne ainsi qu'une fonction de corrélation pour prendre en compte la coordination entre personnes.

La réponse vibratoire des planchers soumis aux modèles de charge précédemment présentés est calculée pour les modèles de charge temporels en résolvant l'équation de mouvement découplée (après décomposition modale) par des méthodes numériques (Newmark-β par exemple). En revanche, une approche de vibrations aléatoires est utilisée pour obtenir la réponse sous chargement fréquentiel de la foule. Cette réponse pourra être comparée aux limites d'acceptabilité fournies par les normes décrites ci-dessus pour évaluer le confort vibratoire des planchers soumis aux activités rythmiques de foule.

La majorité des recherches évoquées dans le Chapitre 2 sont dédiées au développement de modèles de charge temporels pour les activités rythmiques. Ce type de modèle est caractérisé par des pics étroits pour chaque harmonique du chargement, négligeant ainsi les « effets d'intra-variabilités » évoqués précédemment. Ceci conduit à des amplitudes plus grandes au niveau de chaque harmonique et plus faibles au niveau de leur voisinage. Une surestimation de la réponse vibratoire en cas de résonance est donc envisageable. L'effet inverse pourra se produire hors résonance. De plus, ces modèles ne permettent d'exciter qu'un seul mode propre dominant à la fois, ce qui n'est pas approprié pour une large gamme de planchers caractérisés par des modes propres proches en fréquence (planchers à travées ou à panneaux multiples par exemple).

Il s'avère donc nécessaire de disposer d'un modèle de charge fréquentiel, sur la base d'une caractérisation expérimentale des activités rythmiques de foule. Le Chapitre 3 présente le développement de cette dernière, à partir d'un plancher de dimensions réduites. Une campagne d'essais a ainsi été conduite sur un plancher de laboratoire de type mixte acier-béton ayant 8 m de longueur et 7 m de largeur (voir Figure 3). Les caractéristiques du plancher sont celles couramment rencontrées dans la pratique. Le comportement dynamique du plancher a été analysé en modélisant la structure par la méthode des éléments finis (éléments coques pour la dalle en béton et éléments poutres pour les poutres, les poteaux, le bac acier et les connecteurs). Une étude paramétrique menée à l'aide de ce modèle a permis de choisir une configuration de plancher dont un seul mode propre a une fréquence inférieure à 10 Hz (correspondant à la fréquence maximale d'excitation humaine), de manière à éliminer la contribution des modes supérieurs dans cette gamme de fréquences.

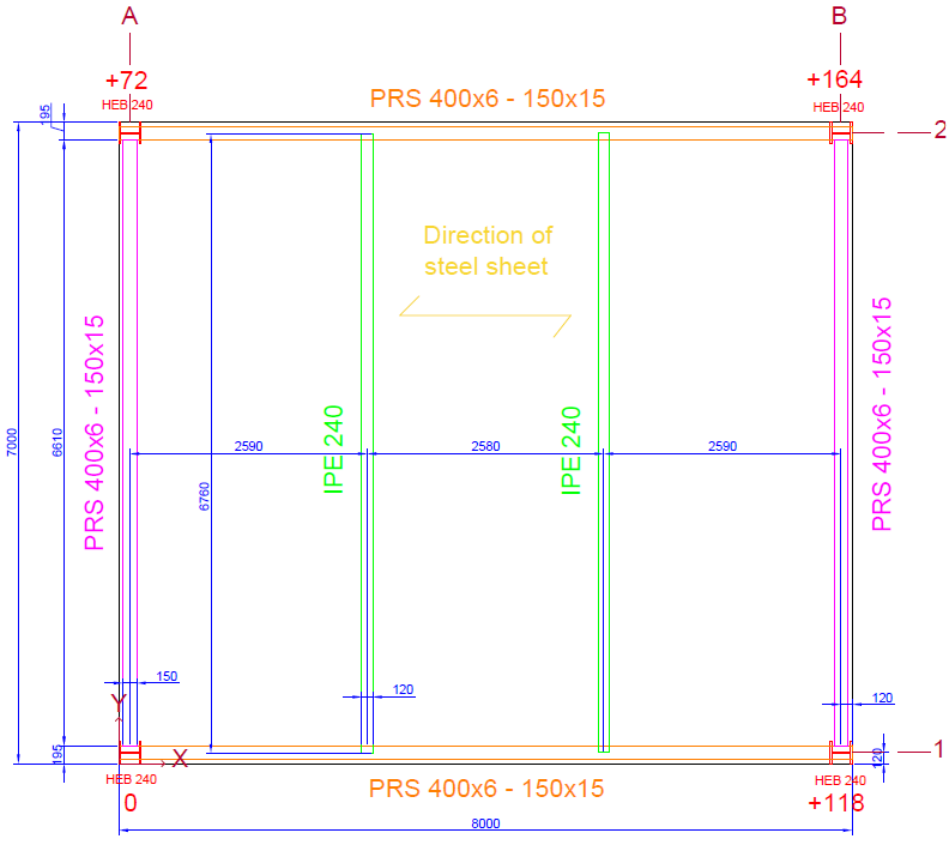

Figure 3: Vue en plan du plancher de laboratoire (dimensions en mm)

Des essais statiques ont d'abord été réalisés afin d'estimer la raideur du plancher en des points spécifiques et en les comparant avec les résultats numériques. Ensuite, les propriétés modales du plancher (fréquences propres, coefficients d'amortissement, déformées modales) ont été déterminées à l'aide d'une analyse modale expérimentale en utilisant un marteau instrumenté (voir Figure 4). Un seul mode, ayant une fréquence propre de 7,65 Hz, a bien été obtenu dans la gamme de fréquences d'intérêt. La comparaison des résultats expérimentaux et numériques a révélé des fréquences propres inférieures pour le cas numérique (différence de 5 % pour le mode fondamental). Le plancher modélisé est en fait plus souple que la réalité car certains assemblages entre les poutres ont été considérés comme articulés alors qu'ils sont semi-rigides.

Figure 4: Marteau instrumenté utilisé pour l'analyse modale

Des mesures de vibration du plancher faisant intervenir des groupes de personnes ont été ensuite menées. Des cellules de force ont été placées sous les quatre poteaux afin de mesurer les réactions dynamiques correspondantes au cours du mouvement, et un capteur LVDT a été utilisé pour mesurer le déplacement dynamique du plancher. La majorité des recherches dans la littérature se focalisent sur l'analyse du « saut normal » étant donné qu'il produit les efforts maximaux. Néanmoins, d'autres activités sont plus récurrentes (comme dans les salles de sport ou de fitness, les gymnases, les stades, etc.) et peuvent même donner des amplitudes plus grandes que le saut normal. Par conséquent, quatre activités rythmiques ont été sélectionnées pour les essais de vibration, à savoir deux activités de saut (le « jumping jack » et le « quick jumping ») ainsi que deux activités de course sur place (« skipping » sur les pointes de pied et « skipping » sur la plante de pied). Les tailles de groupe envisagées étaient de 1, 2, 4, 8 et 16 individus avec une densité d'environ 0,3 personne/m², ce qui a nécessité la participation de 33 personnes. Il a été demandé aux participants de pratiquer les quatre activités en suivant les mouvements d'un coach expérimenté et une bande sonore (voir Figure 5).

Figure 5: Illustration d'essais rythmiques avec 16 personnes sur le plancher de laboratoire

Dans le but de surmonter les limitations des modèles temporels (exposées dans le Chapitre 2) et d'apporter une modélisation plus simplifiée par rapport aux modèles existants par champs aléatoires, un modèle de charge fréquentiel est établi dans le Chapitre 4 pour représenter les activités rythmiques de foule. L'approche proposée est basée sur un modèle spectral pour une seule personne combiné avec des coefficients de coordination pour le cas d'une foule.

Le modèle de charge proposé pour une seule personne émane d'une simplification du modèle de densité spectrale de puissance établi par Xiong et Chen [89]. Les paramètres définissant le modèle développé sont la fréquence d'excitation f_p, le coefficient d'amplitude α (lié au pic d'harmonique) et le coefficient d'énergie δ tenant compte de la distribution d'énergie autour des harmoniques d'excitation (comme illustré à la Figure 6).

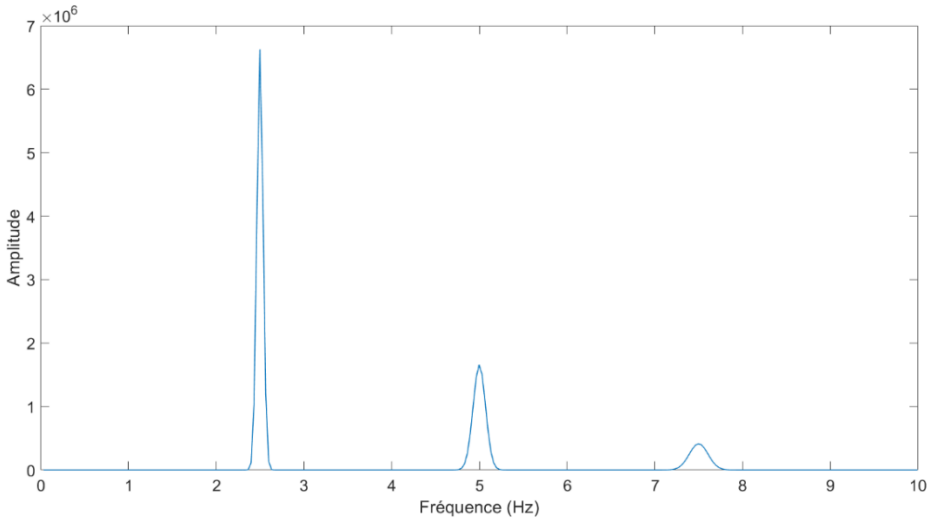

Figure 6: Illustration du modèle de charge spectral proposé (avec une fréquence d'excitation de 2 Hz)

L'identification de ces trois paramètres est réalisée sur la base de mesures expérimentales de forces vibratoires pour l'activité rythmique étudiée. Pour ce faire, une méthode basée sur la technique des moindres carrés est établie, en utilisant l'algorithme de Levenberg-Marquardt adapté à un problème non-linéaire. Cette approche permet de prendre en compte l'intégralité du signal pour l'optimisation, contrairement aux méthodes d'identification existantes basées soit sur le pic d'harmonique, soit sur le calcul d'énergie par harmonique. Les variabilités observées durant le mouvement peuvent donc être prises en compte. Une étude synthétique est conduite afin de déterminer la gamme des conditions initiales permettant d'obtenir la solution optimale du problème d'identification, et de tester la robustesse du modèle proposé face aux bruits de mesure. De plus, une procédure pour calculer des coefficients d'amplification dynamique équivalents est présentée pour pouvoir comparer ultérieurement le modèle proposé avec les principaux modèles temporels existants.

L'inclusion de l'effet de groupe dans le modèle est ensuite effectuée sur la base des mesures des forces de foule pour un nombre donné de personnes. La variation de la valeur RMS (ou valeur efficace) de ces forces, en fonction de la taille de groupe, est caractérisée par une fonction optimisée à partir de la méthode des moindres carrés. Le choix de cette grandeur vient du fait qu'elle est couramment adoptée par les guides d'évaluation du confort vibratoire des occupants d'un plancher. Le coefficient de coordination est alors calculé en divisant la valeur RMS de la force équivalente d'une personne au sein du groupe (force de foule divisée par la taille de groupe) par celle de la force d'une seule personne présente sur le plancher.

La combinaison du modèle spectral pour une seule personne et des coefficients de coordination mène à un modèle final dédié aux activités rythmiques de foule. La méthode de validation d'un tel modèle est détaillée en calculant les valeurs RMS des réponses numériques et expérimentales.

Les enregistrements temporels des forces et déplacements (six séquences par activité et par taille de groupe, donnant lieu à 120 enregistrements au total) relatifs aux essais présentés dans le Chapitre 3 ont été post-traités. Il en résulte des signaux de base utilisés pour déterminer les paramètres du modèle proposé en appliquant les méthodes d'identification décrites ci-dessus. En premier lieu, les paramètres du modèle de charge spectral pour une seule personne ont été

déterminés pour les quatre activités étudiées. Les modèles ainsi paramétrés sont généralement proches des forces mesurées (comme illustré à la Figure 7). Les paramètres obtenus dépendent effectivement du type de stimulation adopté lors des essais, mais ils sont donnés dans une gamme de variation (moyenne ± écart-type) rendant les modèles applicables à d'autres situations. Une différence notable des paramètres des modèles pour les différentes activités a été également observée en termes de valeurs moyennes et écart-types, montrant que chaque activité possède un rythme de mouvement distinct de l'autre. L'énergie du chargement est assez concentrée au niveau de chaque harmonique sauf pour le « quick jumping », tandis que l'amplitude associée présente la plus grande fluctuation étant donnée la variation d'impact sur le sol d'une séquence à l'autre. Des recommandations pour le choix des paramètres des modèles ainsi obtenus sont alors fournies pour le dimensionnement des planchers soumis aux activités rythmiques, en fonction du degré de confort défini par les parties prenantes (moyen ou conservatif).

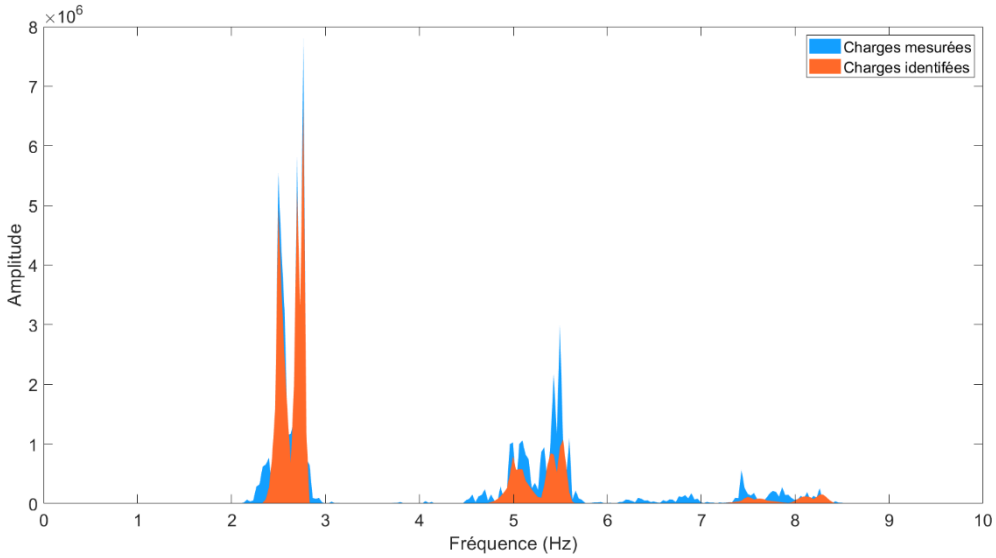

Figure 7: Comparaison des forces mesurées et des modèles de charge identifiés (cas du « skipping » sur la plante de pied)

Par la suite, les coefficients de coordination ont été extraits sur la base des valeurs RMS des forces de foule. Il en résulte que les individus arrivent à coordonner leurs mouvements plus facilement en pratiquant les activités de saut comparativement aux activités de course sur place. De plus, chaque type d'activité possède sa propre loi de décroissance du coefficient de coordination en fonction de la taille de groupe : hyperbolique pour les activités de saut (voir Figure 8(a)) et puissance pour les activités de course sur place (voir Figure 8(b)). Le type de contact avec le sol a également une influence sur la synchronisation des individus. Les coefficients de coordination pour le « skipping » sont plus importants pour le cas du contact sur la plante de pied par rapport à celui du contact sur les pointes de pied. Les modèles de foule ainsi établis ont été utilisés pour calculer la valeur RMS des déplacements en les comparant aux valeurs mesurées au même point. L'écart obtenu était acceptable, avec une différence relative moyenne allant de 7,2 % à 21,8 %.

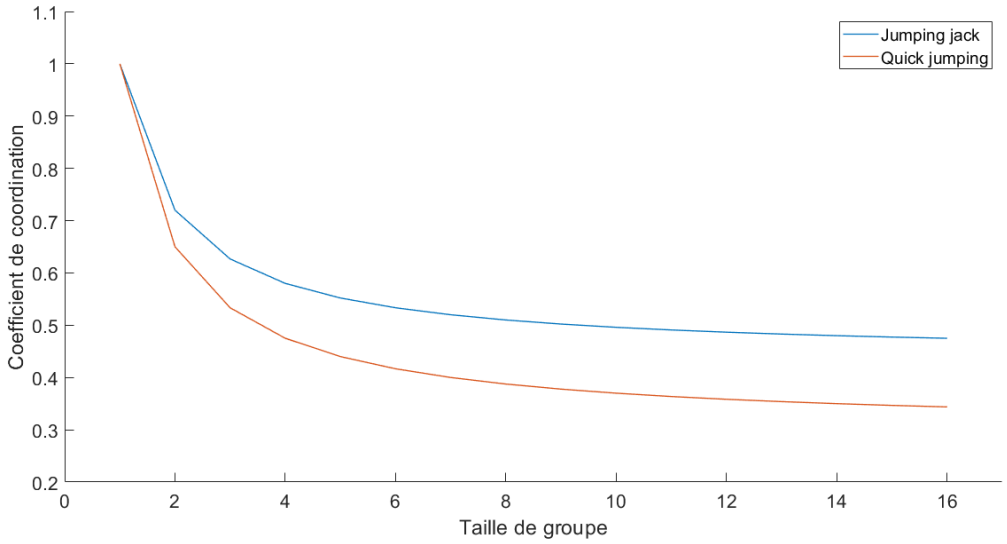

(a) Activités de saut

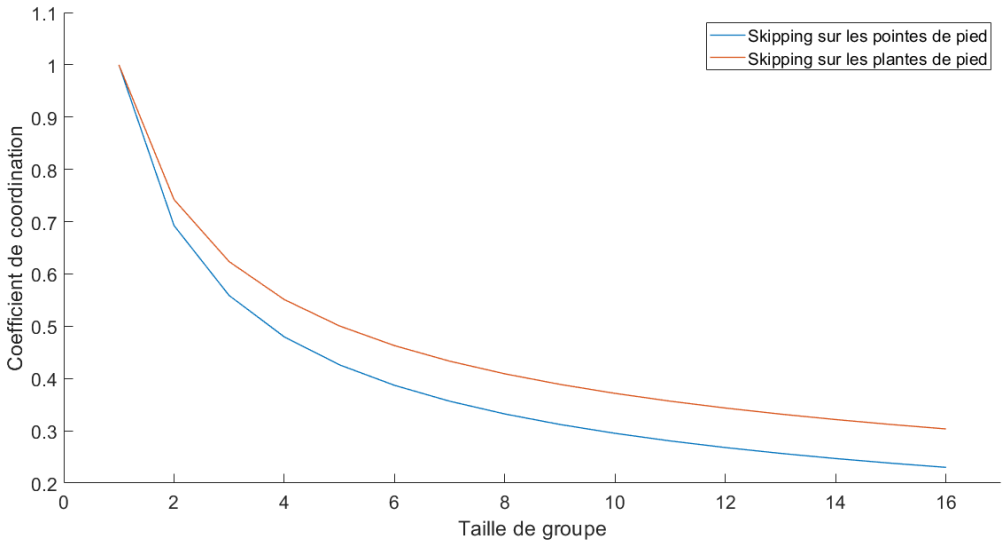

(b) Activités de course sur place

Figure 8: Variation du coefficient de coordination en fonction de la taille de groupe

Afin de tenir compte des caractéristiques des structures rencontrées dans la pratique et d'étendre l'étude à des tailles de groupes plus larges, une investigation à grande échelle des activités rythmiques devrait être effectuée. Dans cette optique, des essais in-situ réalisés sur un bâtiment de parking aérien à trois étages sont présentés dans le Chapitre 5. Le plancher est de type mixte acier-béton, situé au 1er étage du bâtiment. La zone étudiée du plancher a une longueur de 22,5 m et une largeur de 15,785 m (voir Figure 9(a)). Dans un premier temps, les propriétés modales du plancher ont été déterminées moyennant une analyse modale expérimentale par le biais d'un excitateur dynamique (« shaker », voir Figure 9(b)). 20 modes propres ont été identifiés dans la gamme de fréquences d'intérêt (inférieures à 10 Hz). La fréquence propre du mode fondamental valant 3,56 Hz montre que le plancher est à faible fréquence (au sens du guide SCI P354 [81]) et donc sensible aux vibrations humaines.

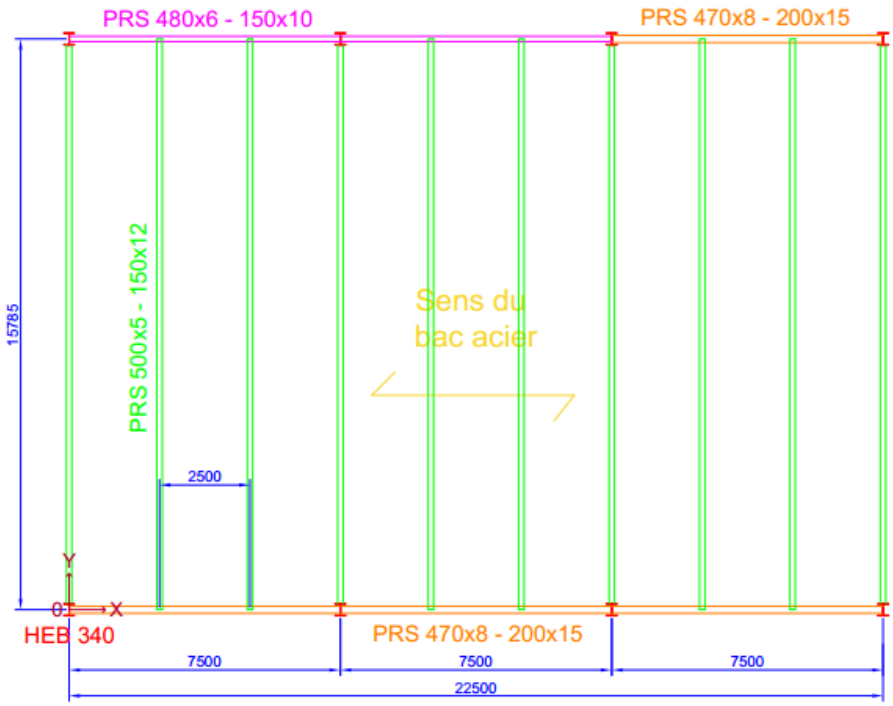

(a) Vue en plan du plancher (dimensions en mm)

(b) Shaker excitant le plancher

Figure 9: Configuration du plancher de parking

Dans un second temps, des essais de vibration sous excitations humaines ont été réalisés pour deux activités rythmiques (« jumping jack » et « skipping » sur la plante de pied), avec des groupes de 2, 4, 8, 16 et 32 personnes (voir Figure 10). Des conditions identiques à celles des essais rythmiques en laboratoire ont été adoptées ici, et les réponses ont été mesurées à l'aide d'accéléromètres câblés.

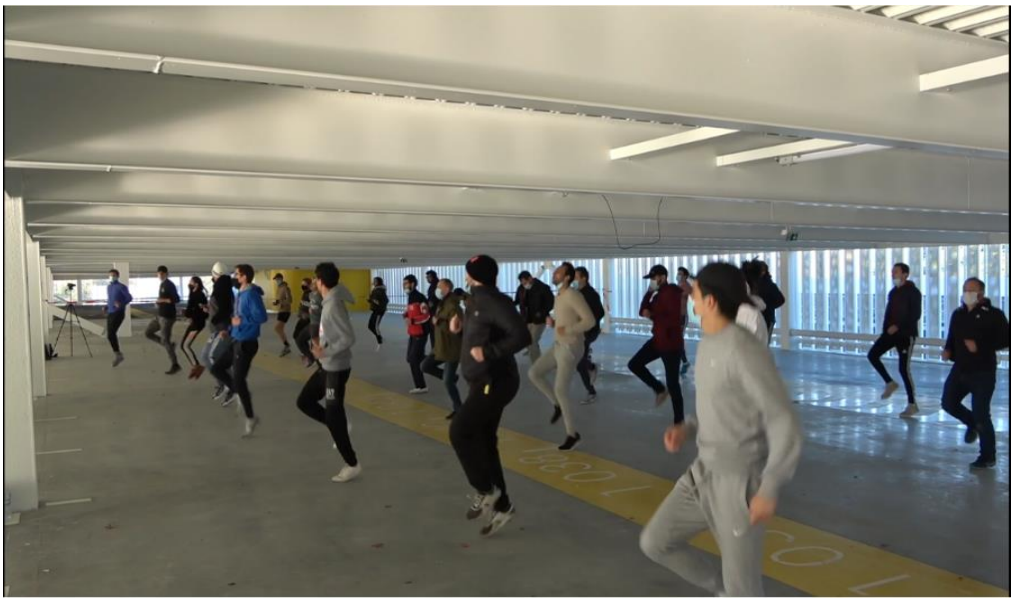

Figure 10: Illustration d'essais rythmiques avec 32 personnes sur le plancher de parking

Après post-traitement des réponses vibratoires, la valeur RMS des accélérations mesurées a été évaluée et comparée aux valeurs numériques calculées en utilisant les modèles de charge de foule établis dans le Chapitre 4 et la base modale dominante du plancher (comme illustré à la Figure 11). La différence relative moyenne entre les résultats numériques et expérimentaux était de 9,8 % et 17,5 % pour l'activité « jumping jack » et l'activité « skipping » sur la plante de pied, respectivement. Cet écart est probablement dû à la différence de stimulation (coach et bande sonore) entre les deux essais réalisés.

Cette étude a permis également d'étendre le domaine d'application des coefficients de coordination de 16 à 32 personnes. En effet, l'utilisation de la courbe hyperbolique obtenue précédemment pour les activités de saut (voir Figure 8(a)) a été jugée valide jusqu'à 32 personnes. En revanche, l'usage de la loi de puissance pour les activités de course sur place (voir Figure 8(b)) entraîne une sous-estimation de la réponse vibratoire, ce qui a conduit à proposer un plateau constant entre 16 et 32 personnes pour ces activités.

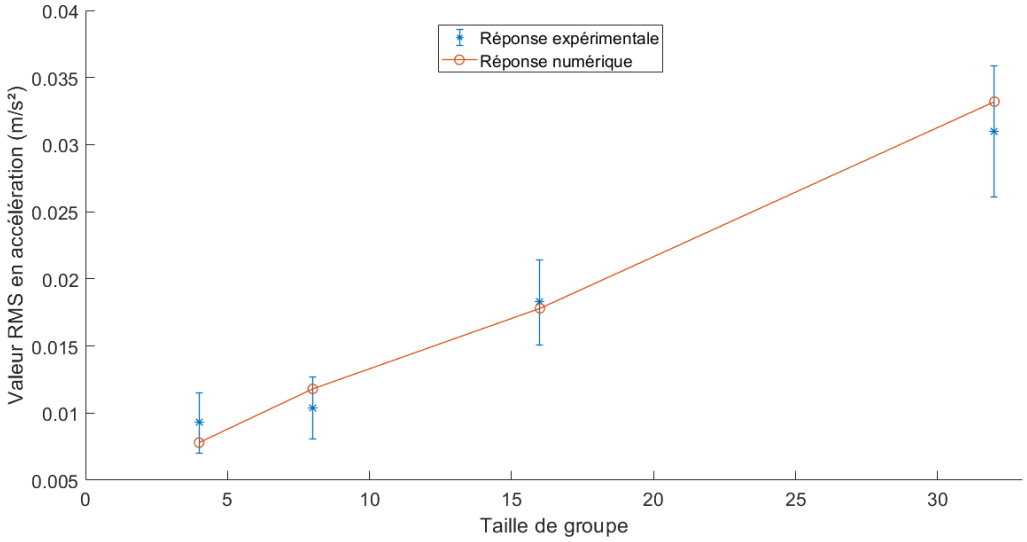

Figure 11: Comparaison des accélérations expérimentales et numériques (cas du « jumping jack »)

Une comparaison des modèles spectraux proposés avec les modèles de la littérature présentés dans le Chapitre 2 a été ensuite entreprise. Pour les forces d'une seule personne, les coefficients d'amplification dynamique équivalents montrent que l'amplitude du 1er harmonique est similaire dans les différents modèles. En revanche, les amplitudes des harmoniques supérieurs sont plus grandes pour le modèle proposé car celui-ci prend en compte l'augmentation de la propagation d'énergie en fonction de l'ordre d'harmonique. Pour les effets de groupe, les coefficients de coordination des activités de saut figurant dans la littérature se subdivisent en trois catégories : lois linéaires avec palier constant, lois de décroissance en puissance et lois de décroissance graduelle. Les coefficients proposés se situent dans la troisième catégorie avec des valeurs moins conservatives. Les mêmes tendances en puissance entre les modèles ont été observées pour les activités de course sur place avec des coefficients du modèle établi plus élevés pour des grandes tailles de groupe. Les modèles proposés ont été également confrontés aux trois principaux modèles temporels de foule existants dans la littérature en terme de réponse vibratoire. Ces modèles ont été appliqués pour évaluer à la fois la réponse du plancher de laboratoire (à un seul mode) et du plancher de parking (multimodal). Il s'est avéré que les modèles proposés sont moins sensibles à la fréquence d'excitation que les modèles temporels et permettent d'exciter simultanément plusieurs modes ayant des fréquences propres proches. Une comparaison avec le modèle de Xiong et Chen [89] a été également effectuée en se basant sur les résultats expérimentaux d'un plancher existant obtenus par Xiong et al. [91]. Bien qu'il fournisse des résultats conservatifs pour des petites tailles de groupe, le modèle proposé prend bien en compte la diminution du degré de coordination observée expérimentalement surtout pour un grand nombre d'individus.

L'analyse de la variation du déplacement du plancher de laboratoire en fonction de la taille de groupe entreprise dans le Chapitre 4 (comme illustré à la Figure 12) a montré que la réponse décroît plus rapidement que la force induite par la foule. La raison réside dans le fait que l'amplitude moyenne du mode fondamental est inversement proportionnelle au nombre de personnes, en raison de leurs plus grandes distances par rapport au centre du plancher où l'amplitude modale est maximale. Cette observation a conduit à considérer que les charges appliquées en différentes positions d'excitation (utilisées dans la méthode exacte de calcul de

réponse) peuvent être réduites à une seule charge équivalente appliqué à l'endroit ayant l'amplitude moyenne du mode fondamental. Ceci mène à développer un modèle de charge rythmique équivalent appliqué à cette position.

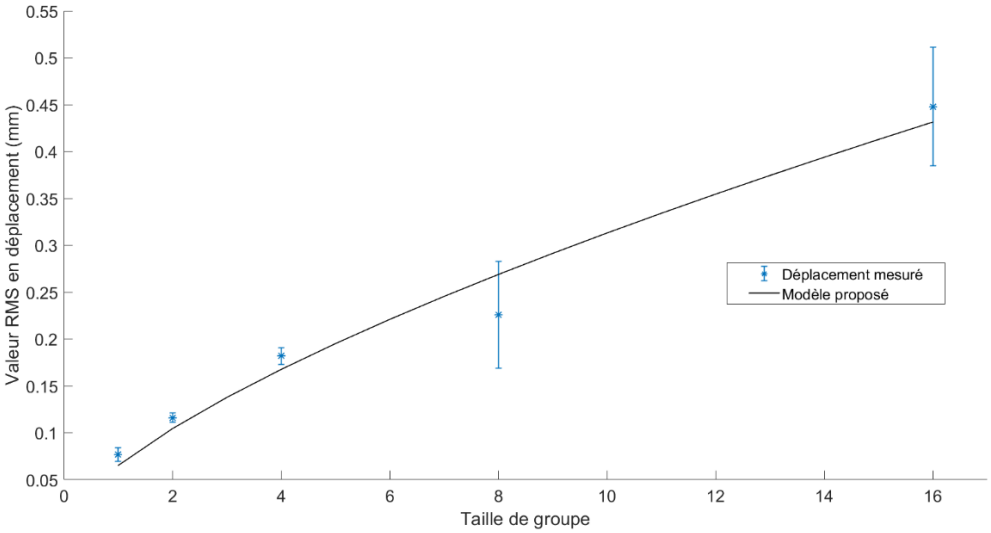

Figure 12: Variation du déplacement du plancher de laboratoire en fonction de la taille de groupe (cas du « jumping-jack »)

L'établissement d'une procédure complète de détermination de la réponse vibratoire constitue l'objet du Chapitre 6. Pour rappel, les guides d'évaluation du confort vibratoire évoqués dans le Chapitre 2, s'appliquent principalement aux planchers soumis aux activités rythmiques pratiquées par une seule personne. Aucune indication explicite n'est fournie pour le calcul de la réponse des planchers pour le cas d'une foule. Certains détails concernant la prise en compte du chargement rythmique de foule existent dans les normes en vigueur, mais demeurent insuffisants.

Le modèle équivalent décrit plus haut a été utilisé pour proposer une méthode générale de calcul de la réponse vibratoire des planchers soumis à des activités rythmiques. Une étude de sensibilité a été ainsi effectuée dans le but d'étudier l'influence des paramètres de chargement et des propriétés modales du plancher sur la réponse vibratoire. Une dépendance étroite entre cette dernière et la fréquence d'excitation ainsi que la fréquence propre du plancher a été mise en évidence. De plus, les accélérations calculées par la méthode exacte (utilisant le modèle spectral de foule) et la méthode générale (utilisant le modèle équivalent) étaient sensiblement proches.

Afin d'établir une méthode pratique applicable par les ingénieurs, une procédure simplifiée d'évaluation de la réponse vibratoire a été proposée pour les planchers satisfaisant certaines conditions (mode fondamental dominant, déformée modale proche d'une sinusoïde classique). Cette méthode est basée sur une approximation de la fonction exponentielle caractérisant le modèle de charge proposé, tout en en recommandant des paramètres de calcul (déformée modale, distribution des individus). L'application de cette méthode est illustrée sur un plancher existant destiné à un usage de bureaux.

Les conclusions majeures du présent travail sont résumées dans le Chapitre 7. L'objectif a été de développer une approche simplifiée de modélisation des activités rythmiques de foule sur les planchers. Deux campagnes d'essais ont été menées pour la caractérisation et la validation du modèle de charge proposé, visant à représenter quatre activités rythmiques pratiquées dans des conditions proches de la réalité. Des méthodes de calcul de la réponse vibratoire des planchers soumis à de telles activités ont ensuite été établies sur la base d'un modèle de charge équivalent de la foule. Après concertation sur les critères d'acceptabilité des vibrations par les parties prenantes, ces méthodes peuvent être adoptées pour l'évaluation du confort des occupants d'une large gamme de planchers concernés.

Des perspectives pour de futures recherches, élargies ou complémentaires, sur le sujet, sont également suggérées, dont :

- Des essais de vibration avec des paramètres complémentaires (taille de groupe plus large, densité de personnes plus élevée, participants plus expérimentés aux activités rythmiques, structures variées) ;
- Un « monitoring » des personnes en conditions réelles de mouvement moyennant des mesures d'accélération pendant une longue période ;
- L'analyse des activités aléatoires de foule (marche, course) fréquemment rencontrées en différents lieux (hôpitaux, gares, centres commerciaux, etc.) ;
- L'étude de l'interaction homme-structure, provoquant une variation des propriétés modales du plancher en présence des personnes, ainsi qu'un changement du rythme de mouvement des personnes dans le cas d'une structure oscillante.

Contents

List of Figures

List of Tables

General notations

Notational conventions

[ ]	Matrix
{ }	Vector
$[\ ]^T$	Transpose of a matrix
$\{\ \}^T$	Transpose of a vector
$E[\ ]$	Mathematical expectation
$\bar{x}$	Mean value of the real number x
$\bar{y}$	Complex conjugate of the complex number y
$\dot{x}$	First order time derivative of x
$\ddot{x}$	Second order time derivative of x
x^*	Generalized force of the input force x
$X(\omega)$	Fourier transform of the time-varying function $x(t)$
$S_x(\omega)$	Power Spectral Density of the time-varying function $x(t)$

Subscripts

i	Load harmonic
k	First individual
l	Second individual
n	First natural mode
m	Second natural mode
M	Number of natural modes
N	Crowd size
p	Load
r	Response
s	Activity window
w	Response parameter

1 Introduction

1.1 Research problem and motivation

In recent years, structures designed for human occupation (building floors, footbridges, staircases, grandstands, etc.) have experienced a rapid development due to the increasing demands of performance and economic efficiency. This includes [93]:

- The use of materials having high strength properties but low weight, giving rise to more lightweight structures;
- The growing design of long-span structures (such as open-plan offices) resulting in the elimination of non-structural partitions;
- The trends for more aesthetic and architectural requirements, leading to novel structural forms and increased slenderness.

These improvements yield floors having appropriate strength behaviour against static loads, fulfilling Ultimate Limit State requirements. However, these structures are characterized by low natural frequencies and low damping ratios, which makes them more sensitive to vibrations induced by human occupants. Their design is thus governed by the Serviceability Limit State. The resulting vibration may cause discomfort or even panic to occupants.

In 1999 and 2000, vibration issues occurred at two footbridges: the Paris Solférino Bridge and the London Millennium Bridge [51]. Both bridges swayed in the lateral direction due to walking of a group of people just after their inauguration [94]. Moreover, since 1889, a significant number of demountable grandstands excited by jumping crowds collapsed [21]. These unexpected incidents triggered researchers to work on better understanding of the behaviour of such structures when subjected to human-induced excitation.

Building floors are one of the structures most sensitive to excessive vibrations. Depending on the usage of the floor, several activities may take place such as walking, running, jumping, skipping, bouncing, etc. However, the worst load case corresponds to rhythmic excitation in the vertical direction, especially in presence of a coordinated group of people on the floor ([50], [71]).

An et al. [4] put in evidence this phenomenon by conducting an experimental investigation on an innovative composite floor subjected to human-induced vibrations. Among investigated rhythmic activities, they confirmed that crowds jumping synchronously produced the greatest acceleration responses. De Silva and Thambiratnam [23] analysed a multi-panel composite floor devoted to a high-rise office, and found that the floor accelerations due to normal jumping could exceed the allowable limits for human comfort. The impact of these actions could be even more pronounced. Lee et al. [53] investigated a 39-storey steel building in Seoul, South-Korea, whose upper floors shaked vertically for 10 min causing panic to occupants. The authors demonstrated that this abnormal vibration was produced by crowd rhythmic movements in a fitness centre located at the 12^{th} floor of an adjacent complex service (see Figure 1.1). In addition, a temporary grandstand in Bastia, Corsica, collapsed under the rhythmic jumping of the audience during a sports match [50], which resulted in the injury and even the death of several persons [21]. As a conclusion, floor structures must be accurately designed so that vibrations caused by rhythmic activities would be acceptable to occupants. This requires two keys elements to be provided:

- The establishment of a reliable load model for crowd-rhythmic activities;
- The development of a serviceability assessment method of floors against human-induced vibrations.

These points are discussed in detail in Chapter 2 but are briefly pointed out here.

Figure 1.1: 39 storey building and an adjacent 12 storey complex service [53]

- **Crowd-rhythmic load models**

Several attempts are made in order to develop accurate load models for rhythmic activities. Crowd models proposed in the literature were at first based on a single person practicing rhythmic movements on the floor. The developed analytical load models were either expressed as a Fourier series with harmonics having frequencies that are multiples of the excitation frequency [33], or a combination of series of identical jumping pulses each given by a pulse model [7]. These load models were characterized by parameters obtained analytically, but they do not reflect experimental findings in terms of amplitude and frequency [50]. To overcome this issue, measurements have been conducted on floors subjected to jumping in order to determine Dynamic Load Factors (DLFs) characterizing Fourier series load [3], or a modified half-sine model to be used for jumping pulses [15].

However, those load models, having constant parameters, did not include the variability observed during human motion. In fact, each person cannot maintain a constant frequency and amplitude during movement (called "intra-subject variability") and has a specific motion different from another person (called "inter-subject variability") [50]. This leads to a total force produced by crowds which does not correspond to a simple multiplication of individual loads. Some standards dealing with the subject, such as ISO 10137 [45], proposed using coordination factors to attenuate the total force induced by crowds due to group effect. A review of existing coordination factors in the literature can be found in [57]. On the other hand, many studies have been undertaken in order to characterize load variability based on a jumping pulse formulation

and a sample of individual force measurements ([58], [71], [80]). Randomness of load parameters is described by fitted probability distributions for a single person. Next, Monte Carlo simulations have been used to generate loads for a given group of people. Although it provided a more realistic jumping load model for multiple persons, this method did not consider crowd effects observed in real situations due to physical constraints, visual cues from crowd movement, stimulation from near environment [18], etc.

An experimental investigation of the crowd size effect is then essential in order to derive an appropriate model for crowd rhythmic loads. A straightforward method consists of conducting direct force measurements induced by a group of people on the floor [73]. This could be done either by force plates placed at each excitation position ([39], [65], [67]) or by load cells located at the corners of the floor [27]. Alternatively, force parameters could be determined from measured vibrations by means of indirect identification techniques. This includes collected responses on the floor ([31], [34]) or gathered accelerations of the human body at specific locations [54]. The resulting crowd model usually comprises a load model for a single person exciting the floor, in which experimentally determined coordination factors are appended to reflect the lack of synchronization between participants.

Most of the load models representing rhythmic activities are expressed in the time domain, characterized by sharp peaks at each harmonic. In reality, there is a spread of energy near each harmonic of the load due to "intra-subject variability" [71]. Assuming the same load energy as for real cases, these load models have larger amplitudes at the peaks of each harmonic and lower amplitudes at their vicinity. This leads to an overestimation of the floor response when resonance occurs and the inverse effect in non-resonant cases [88]. In addition, the response of structures when using time domain load models would be dominated by only one mode of vibration at resonance. Many building floors encountered in real life have multiple dominant modes in general, and some have closely-spaced modes as for multi-span or multi-panel floors ([20], [22], [75]), indicating that the previously mentioned load models would not provide accurate results for these structures. Frequency domain modelling is a suitable alternative to circumvent these limitations, as it offers an excitation frequency window that could excite multiple close modes simultaneously. This was initially done for walking excitation in terms of Power Spectral Density functions ([12], [42], [95]), but only a few proposals of such model have been made for rhythmic activities, especially in a random field approach ([89], [90]).

- **Response prediction of floors subjected to human activities**

Despite being an issue of concern nowadays, human-induced vibrations in building floors are poorly treated in the Eurocodes, which are the official design codes of practice in Europe. Indeed, Eurocode 3 [37] admits that the vibrations of floors subjected to human activities could result in significant discomfort to users, but only refers to the National Annex of each country to specify limits for such vibrations. For instance, in the French National Annex of Eurocode 3 [6], floors are assumed acceptable with regard to vibration if the natural frequency of the fundamental mode exceeds some frequency limits depending on the type and usage of the floor. The same procedure was also adopted by the Comité Euro-International du Béton (CEB) [19] with different limiting values. However, this condition is not always sufficient in practice, especially when the floor is subjected to rhythmic activities [56]. In fact, other modal properties (modal mass, damping ratio, modal shape) must be considered as they affect the vibrational behaviour of floors.

To this end, guidelines presenting methodologies for the serviceability assessment of floors against human discomfort were established. Some design recommendations were based on the results of European projects [77], such as HiVoSS guideline [40] for walking activity. This guideline provides a simplified calculation method for the response of floors by means of charts depending on damping ratio (see Figure 1.2). Other guidelines were drawn by technical and scientific centres for steel construction around the world. Two of them are commonly used for rhythmic activities: SCI P354 guideline [81] and AISC DG11 guideline [63]. Nevertheless, Royvaran et al. [76] found critical differences in terms of floor responses using the last three guidelines for a large number of investigated floors. This was also confirmed by Muhammad et al. [62], who attributed that to different estimation methods of modal properties along with the unrepresentative character of vibration descriptors. On the other hand, SCI P354 and AISC DG11 guidelines are majorly based only on the rhythmic excitation of a single person. They provide no explicit guidance about calculating the response of floors induced by a crowd-rhythmic load, although this case is quite common in many structures (stadiums, fitness centres, sports halls, etc.). Vijayan et al. [86] pointed out the considerable impact of the group effect on floors (especially for slender ones) and invited to take it into account in their serviceability design.

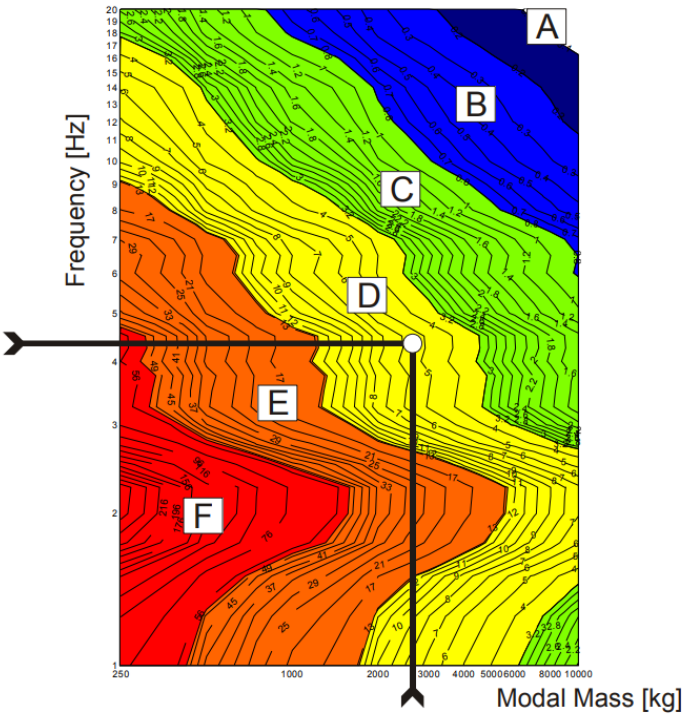

Figure 1.2: Example of a chart for the calculation of floor response [40]

1.2 Scope and objectives

Structures covered by this research are building floors expected to be excited by humans performing rhythmic activities. This includes various facilities such as sports venues, fitness centres, gymnasiums, grandstands, etc.

This work aims to establish a load modelling strategy in the frequency domain which could reproduce two particular types of rhythmic activity induced by a single person or a group of people. The proposed model comprises a Power Spectral Density (PSD) function for a single

person, combined with coordination factors for multiple individuals. This formulation overcomes the issues of time domain load models cited above and provides a simpler representation of crowd loads compared to random field technique. For that purpose, test campaigns involving four rhythmic activities (two jumping and two skipping actions) were carried out. In these experiments, conditions close to real life situations were adopted for rhythmic activities, as individuals were moving comfortably while exposed to audible and visual stimulus. Parameters of the PSD load model are identified by means of a least-squares procedure, whilst coordination factors are obtained from best-fit functions describing the variation of crowd forces against group size. In addition, methods for predicting the response of floors subjected to crowd-rhythmic activities are suggested, based on the developed spectral load model and the random vibration theory. After choosing a vibration acceptability criterion with the stakeholders, these methods could be used by engineers to assess such floor structures against human discomfort. The outcomes of this work might be a first step of a procedure to be implemented in future Eurocodes editions for practical application.

1.3 Thesis outline

The research work outlined in this thesis is divided in seven chapters. Chapter 1 introduces the context of the research and highlights the main objectives and the organisation of the work.

Chapter 2 presents a literature review about the vibration of floors subjected to rhythmic activities. The state-of-the-art starts with a presentation of the analytical rhythmic load models, followed by the available official documents dealing with the subject of floor vibrations due to rhythmic activities. These include standards characterizing the human exposure to vibrations along with design guidelines for the serviceability assessment of floors against human discomfort. Subsequently, the main research findings about crowd-rhythmic load models are highlighted, including single person models and crowd size effect. The chapter concludes with the presentation of methods for the response calculation of floors subjected to rhythmic activities.

Chapter 3 describes an experimental campaign carried out on a laboratory floor subjected to multiple rhythmic activities. At first, the presentation of the floor specimen used for that purpose is made. This includes numerical modelling and final configuration design of the structure. First experiments conducted on the floor specimen are then introduced, comprising deflection tests along with Experimental Modal Analysis. Vibration tests under crowd-rhythmic activities for up to 16 individuals are presented afterwards, by giving details about adopted instrumentation and experimental setup.

Chapter 4 is dedicated to the proposition of a load model for crowd-rhythmic activities. A simplified PSD load model for a single person is established first, followed by the presentation of a direct identification method to determine load parameters based on force measurements on the floor. Coordination factors are then obtained via optimal functions describing the variation of crowd forces against the number of participants. The total crowd load model is formulated using the PSD load model together with coordination factors, and the procedure for the verification of such model using response measurements on the floor is detailed. The experimental results from vibration tests described in Chapter 3 are used to identify the above rhythmic load models for each investigated activity. Results of identification of the PSD load model are presented for the case of a single person, followed by obtained coordination factors

for the case of crowds. Finally, the predicted response using the proposed crowd-rhythmic load models is compared against displacement measurements on the floor.

Chapter 5 focuses on experiments realized on a full-scale floor in order to verify the crowd-rhythmic load models established in Chapter 4. The floor structure is first presented together with the conducted tests. The proposed load models are then verified by means of acceleration responses with an extension of their scope to a maximum number of 32 individuals. Subsequently, the verified load models are compared against existing literature in terms of forces. The proposed and existing load models are also used to compute floor accelerations and compared against each other for three different floor structures. In the last part of this chapter, an equivalent crowd load model is established, based on the observation of experimental loads and responses against crowd size. Indeed, instead of applying the PSD load model at each of the excitation positions, the equivalent model is concentrated at a single specific location.

Chapter 6 is devoted to propose methods for the prediction of the response of floors against crowd-rhythmic activities, accounting for the crowd load models established in the previous chapters. The equivalent load model formulation detailed in Chapter 5 enables a more direct response prediction of floors compared to the exact model developed in Chapter 4. Based on that model together with the random vibration theory, a general method for the response evaluation of multi-modal floors is established and a sensitivity study is conducted in order to analyse and validate the proposed method. The last part of this chapter presents a simplified method for the response calculation of single-mode floors which is applied to an existing floor structure.

Chapter 7 summarizes the main conclusions of the present work and proposes recommendations for further research on the subject.

2 Literature review

2.1 Introduction

Human-induced actions exciting floor structures are divided into two major categories ([3], [64]). In the first category, loss of contact of the individual with the structure does not occur resulting in a continuous loading [7] (see Figure 2.1(a)). Corresponding activities include walking, some aerobic exercises, bobbing or bouncing [26]. The second category comprises a phase when the person loses contact with the structure (being in the air for a few moments), leading to a discontinuous loading [7] (see Figure 2.1(b)). Activities producing such a loading include running, jogging [72], distinctive styles of jumping and skipping. The vast majority of structures are designed to resist vertical loads whereas the magnitude of loads in other directions are far below and have a little effect [50].

Among these vertical loads, rhythmic exercises with loss of contact are likely to produce the most significant loads and responses ([50], [71]). This is more pronounced when a group of people performs such activities with a certain degree of synchronization. Discomfort or even panic of occupants could result from such a load case [50]. The present review is focused on this type of activity. According to ISO 10137 [45], the key elements of the vibration problem to be defined are the vibration source (load model), the transmission path (floor response) and the vibration receiver (acceptability limits).

Following the above rationale, this review begins with a presentation of the analytical rhythmic load models, followed by the available guidance documents dealing with the subject of floor vibrations due to rhythmic activities. These include standards characterizing the human exposure to vibrations along with design guidelines for the serviceability assessment of floors against human discomfort. Subsequently, the main research findings about crowd-rhythmic load models are highlighted, including single person models and crowd size effect. Methods for the response calculation of floors subjected to rhythmic activities are then detailed.

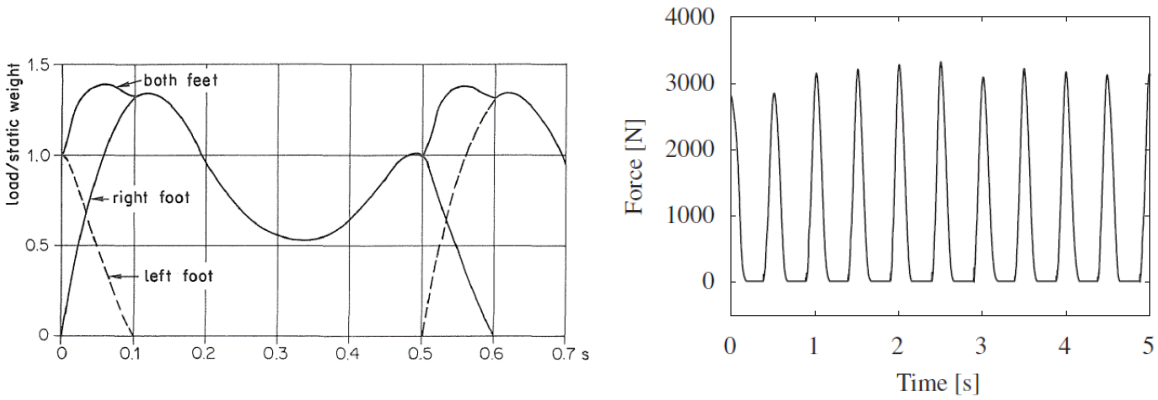

(a) Walking [7] (b) Jumping [50]

Figure 2.1: Human load records

2.2 Analytical rhythmic load models

This section presents the approaches aiming to describe load models representing a single person performing rhythmic activities (with loss of contact). This includes the rhythmic pulse model characterized by a combination of series of identical jumping pulses and the Fourier series model with harmonics having frequencies that are multiples of the excitation frequency.

2.2.1 Rhythmic pulse model

When an individual practices a rhythmic activity, successive impacts are recorded on the structure. A first modelling approach is to characterize each pulse of the load, and then reconstruct the entire signal using successive pulses.

A jumping pulse (see Figure 2.2) is characterized by a landing phase when the person is in contact with the floor, and an aerial phase when the person leaves the floor in the air.

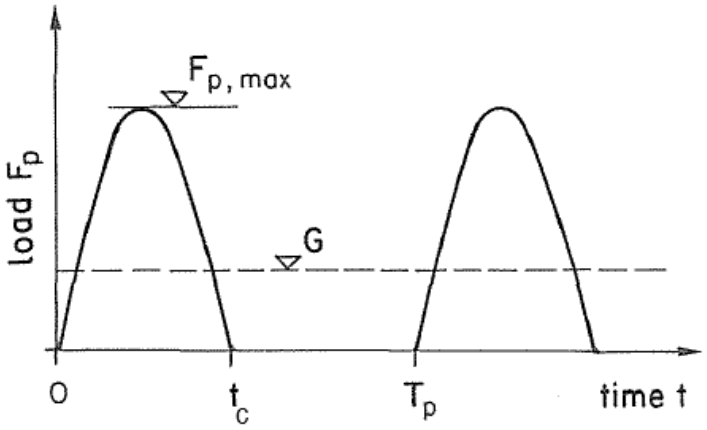

Figure 2.2: Idealized jumping pulses (modified from [7])

Bachmann and Ammann [7] used the following half-sine expression to model a jumping pulse impact $P(t)$:

$$P(t) = \begin{cases} K_p G \sin\left(\dfrac{\pi t}{t_c}\right), & 0 \le t \le t_c \\ 0, & t_c \le t \le T_p \end{cases} \tag{2.1}$$

Here, G is the weight of the jumper, with three major parameters defined below for each pulse:

- The impact factor K_p, which is the ratio of the maximum force to the weight of the individual;
- The pulse period T_p, which is the time comprising the landing and the aerial phase;
- The duration of the landing phase t_c.

By assuming conservation of momentum, the following relation is obtained [50]:

$$\int_0^{t_c} P(t)dt = GT_p \tag{2.2}$$

The impact factor is then expressed by:

$$K_p = \frac{\pi}{2\alpha_c} \tag{2.3}$$

where α_c is the contact ratio, which is the ratio between the landing phase time t_c and the pulse period T_p.

2.2.2 Fourier series model

In this modelling approach, rhythmic excitation is considered as a periodic signal $P(t)$, which can be decomposed in Fourier series as follows:

$$P(t) = G\left[1 + \sum_{i=1}^{H} DLF_i \sin(2\pi i f_p t + \phi_i)\right] \tag{2.4}$$

where G is the individual's weight, f_p the excitation frequency, H the number of considered harmonics, DLF_i the Dynamic Load Factor (DLF) of the i^{th} harmonic and ϕ_i the phase lag of the i^{th} harmonic.

Parameters characterizing the load model are f_p, DLF_i and ϕ_i. As can be seen in Figure 2.3, this load model simulates jumping pulses with a non-zero component between two successive pulses. However, in the frequency range of human excitation, it is considered that this component has a negligible amplitude when three harmonics of the load are used [32].

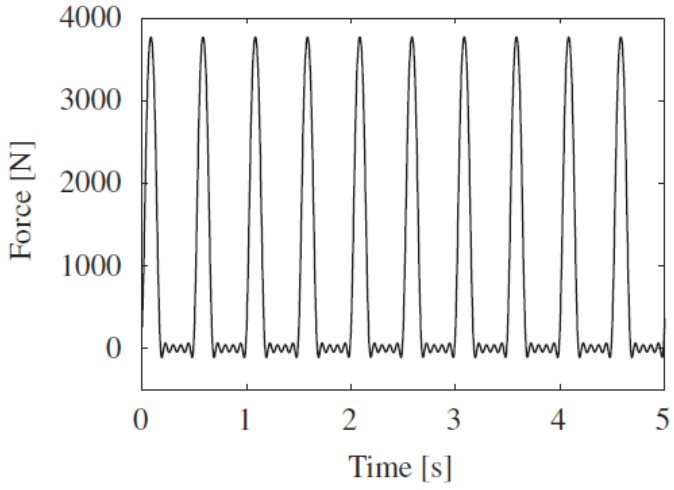

Figure 2.3: Fourier series load model [50]

The excitation frequency depends on each rhythmic activity and the training level of each individual. Low frequencies are encountered for activities like low-impact aerobics, whilst high frequencies are observed in activities close to running-on-the-spot. However, the most frequent frequency range for such activities is between 1.5 and 3.5Hz, as stated by several guidelines ([45], [81]). Based on half-sine approximation ([33], [50]), it was possible to determine analytically DLF_i and ϕ_i by the following equation:

$$\begin{cases} DLF_i = \sqrt{a_i^2 + b_i^2} \\ \phi_i = \tan^{-1}\left(\dfrac{a_i}{b_i}\right) \end{cases} \tag{2.5}$$

$$a_i = \begin{cases} 0, & i\alpha_c = 0.5 \\ \dfrac{1+\cos(2i\pi\alpha_c)}{1-4i^2\alpha_c^2}, & i\alpha_c \neq 0.5 \end{cases}$$

$$b_i = \begin{cases} \dfrac{\pi}{2}, & i\alpha_c = 0.5 \\ \dfrac{\sin(2i\pi\alpha_c)}{1-4i^2\alpha_c^2}, & i\alpha_c \neq 0.5 \end{cases}$$

Here, $\alpha_c = t_c/T_p$ is the contact ratio as defined for the jumping pulse model.

Another alternative is to use the Fourier series model with a cosine function instead of sine [65]:

$$P(t) = G\left[1 + \sum_{i=1}^{H} DLF_i \cos(2\pi i f_p t - \phi_i)\right] \tag{2.6}$$

2.3 Human exposure to vibrations

When a floor structure is excited by a dynamic load (inside or outside the building), occupants may be affected by the resulting vibrations of the structure. This effect ranges from just a perception of the vibration to a certain degree of discomfort or even panic [50]. In particular, human-induced excitation on the floor is one of the most encountered vibration sources in buildings which increasingly caused such effects to the floor users. Vibration acceptability limits regarding human response are then a key element for a convenient serviceability assessment of such floors. This section presents common standards dealing with the subject of human response to vibrations, providing recommendations about response parameters to be calculated along with limit values for human comfort [29]. The objective is to address the comfort of the users of a structure exposed to human-induced vibrations, by assessing its acceptability for the intended use.

ISO 2631 provides values, expressed in terms of acceleration, to assess comfort taking into account the direction of vibration, the frequency sensitivity and the effects of duration of vibrations. ISO 10137 suggests acceptability criteria and comfort limits based on the quantities from the above mentioned standard. Finally, DIN 4150-2 proposes performance criteria for vibration comfort, no longer based on acceleration, but on velocity.

2.3.1 ISO 2631 standard

2.3.1.1 Overview

The international standard ISO 2631 ([46], [48]) provides a detailed procedure for the analytical determination of characteristic parameters for the human-induced vibration response (mainly in terms of acceleration). These parameters are used in the evaluation of the impact of vibrations on the human body (for receivers) with respect to certain criteria (health, motion sickness, perception, comfort). Focus here is on the criterion of vibration comfort.

The effect of vibrations depends on both the direction of incidence and the position of the human body, which may be standing, sitting or lying. The standard coordinate system is shown in Figure 2.4; human perception is generally more important for vibrations in the *x* or *y* direction.

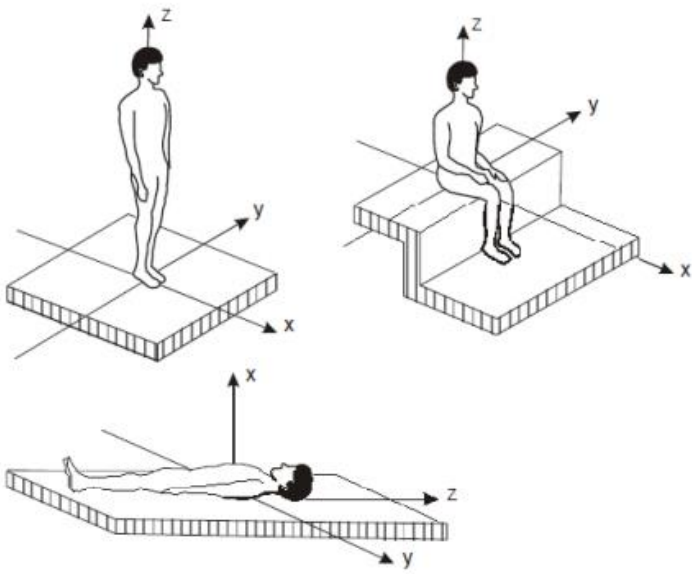

Figure 2.4: Coordinate system according to human body positions [46]

2.3.1.2 Frequency weighting

The impact of vibration on the occupants of a structure depends on their sensitivity to vibrations, strongly related to its frequency of incidence. In general, there are frequency ranges not very perceptible to humans, where the received response is attenuated by means of so-called frequency weighting factors *W*, presented in the form of curves (expressed in dB) shown in Figure 2.5. These factors are applied to the response terms (presented in Section 2.3.1.3). The choice of frequency weighting curves is made according to Table 2.1, depending on the direction of vibration shown in Figure 2.4. The frequency weighting depends on the axes of incidence since the user perceives vibrations more easily along the *x* and *y*-axes than along the *z*-axis.

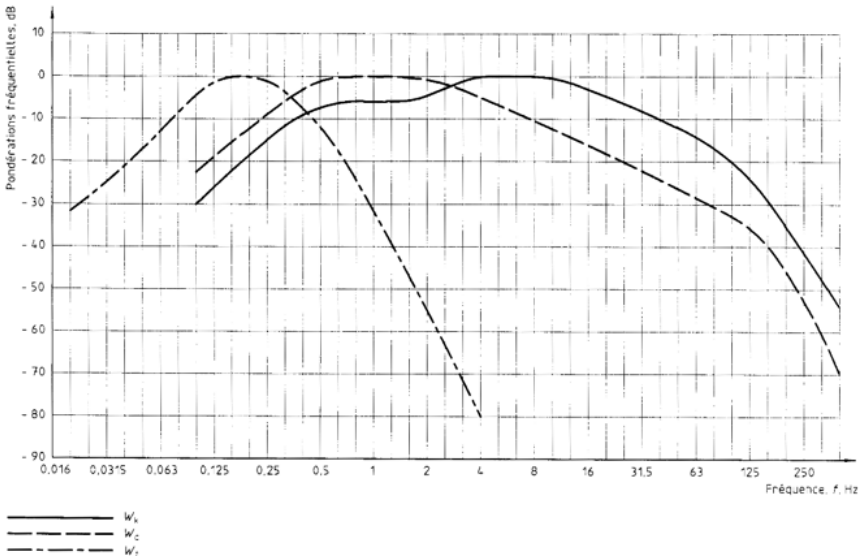

(a) W_k, W_d and W_f [46]

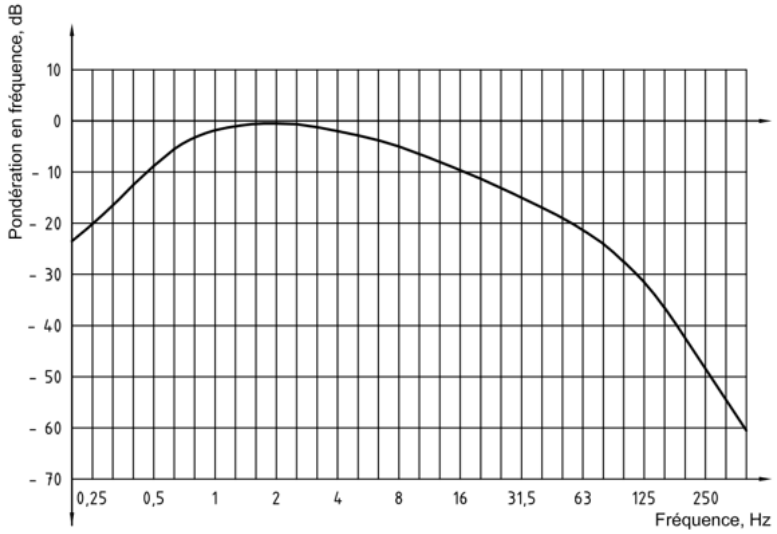

(b) W_m [48]

Figure 2.5: Frequency weighting curves from ISO 2631

Axis	Frequency weighting	
	Known body position	Unknown body position
x	W_d	W_m
y	W_d	W_m
z	W_k	W_m

Table 2.1: Choice of frequency weighting curves from ISO 2631 ([46], [48])

According to the previous curves, the most perceptible frequency range to humans is between 4 and 8Hz for the z direction (W_k) as well as between 0.5 and 2Hz for x and y directions (W_d).

An equivalent calculation of the frequency weighting factors can be made using four transfer functions presented next:

- High pass:

$$H_h(f) = \sqrt{\frac{f^4}{f^4 + f_1^4}} \tag{2.7}$$

- Low pass:

$$H_l(f) = \sqrt{\frac{f_2^4}{f^4 + f_2^4}} \tag{2.8}$$

- Acceleration-velocity transition:

$$H_t(f) = \sqrt{\frac{f^2 + f_3^2}{f_3^2}} \sqrt{\frac{f_4^4 Q_4^2}{f^4 Q_4^2 + f^2 f_4^2 (1 - 2Q_4^2) + f_4^4 Q_4^2}} \tag{2.9}$$

- Upward step:

$$H_s(f) = \begin{cases} \dfrac{Q_6}{Q_5} \sqrt{\dfrac{f^4 Q_5^2 + f^2 f_5^2 (1 - 2Q_5^2) + f_5^4 Q_5^2}{f^4 Q_6^2 + f^2 f_6^2 (1 - 2Q_6^2) + f_6^4 Q_6^2}} & \text{for } W_k \text{ and } W_f \\ 1 & \text{for } W_d \end{cases} \tag{2.10}$$

The total frequency-weighting factor is then obtained by:

$$W(f) = H_h(f)\,H_l(f)\,H_t(f)\,H_s(f) \tag{2.11}$$

Parameters of the previous transfer functions f_i ($1 \leq i \leq 6$) and Q_i ($4 \leq i \leq 6$) are given for each weighting curve (see Figure 2.5(a)) in Table 2.2.

Weighting	High pass	Low pass	Acceleration-velocity transition			Upward step			
	f_1 (Hz)	f_2 (Hz)	f_3 (Hz)	f_4 (Hz)	Q_4	f_5 (Hz)	Q_5	f_6 (Hz)	Q_6
W_k	0.4	100	12.5	12.5	0.63	2.37	0.91	3.35	0.91
W_d	0.4	100	2	2	0.63	-	-	-	-
W_f	0.08	0.63	∞	0.25	0.86	0.0625	0.8	0.1	0.8

Table 2.2: Parameters of transfer functions [46]

2.3.1.3 Basic method (weighted RMS acceleration)

The basic method is applied in the case of continuous vibrations. It consists of calculating a weighted RMS acceleration, which takes into account the reduction of response in the frequency ranges of low human perception. This acceleration is calculated per direction of vibration according to two cases:

- If N_f discrete values of acceleration over time are available, a cumulative acceleration calculation is performed using the following expression:

$$a_{w,d} = \sqrt{\sum_{i=1}^{N_f} (W_i a_i)^2} \tag{2.12}$$

- If a continuous acceleration record is available, an integral is made over the recording time T as follows:

$$a_{w,d} = \sqrt{\frac{1}{T}\int_0^T a_{w,d}^2(t)\,dt} \tag{2.13}$$

The total acceleration is then obtained as:

$$a_v = \sqrt{k_x^2 a_{w,x}^2 + k_y^2 a_{w,y}^2 + k_z^2 a_{w,z}^2} \tag{2.14}$$

In the previous equations, $a_{w,d}$ is the RMS acceleration calculated for each direction d (x, y or z), W_i a frequency weighting factor (see Section 2.3.1.2), a_i the incident acceleration in the direction of the human body (see Figure 2.4), $a_{w,d}(t)$ the weighted acceleration at time t, k_x, k_y and k_z are multiplying factors depending on the studied effect of vibration and the position of the receiver (taken equal to 1 for comfort assessment).

2.3.1.4 Additional methods

A first method consists of determining a running acceleration (Maximum Transient Vibration Value - *MTVV*), in order to take into account the transient effects of the response, by calculating a RMS acceleration noted $a_{w,d}(t_0)$ for small time intervals τ along the entire signal as follows:

$$a_{w,d}(t_0) = \sqrt{\frac{1}{\tau}\int_{t_0-\tau}^{t_0} a_{w,d}^2(t)dt} \tag{2.15}$$

Here, $a_{w,d}(t)$ is the weighted time-dependent acceleration for each direction of vibration.

Subsequently, the maximum value of these accelerations is evaluated by:

$$MTVV = \max_{t_0}\left[a_{w,d}(t_0)\right] \tag{2.16}$$

A second method considers the intermittent nature of the loading: for occasional vibrations, the level of time domain accelerations is generally low over a certain duration. Instead, a response parameter called Vibration Dose Value (*VDV*, in $ms^{-7/4}$) is adopted, allowing considerable responses for limited durations of vibration. It is calculated using the following expression:

$$VDV = \left[\int_0^T a_{w,d}^4(t)dt\right]^{1/4} \tag{2.17}$$

2.3.2 ISO 10137 standard

ISO 10137 standard [45] suggests serviceability acceptance criteria for vibration loading applied to buildings and footbridges, using the characteristic parameters of ISO 2631-1 [46] (weighted RMS acceleration, *VDV*). This standard is limited to the analysis of the occupant vibration comfort.

2.3.2.1 Basic method (RMS acceleration)

The basic method is mainly used for continuous vibrations, defined as excitations lasting more than 30 minutes per day. For each excitation frequency, the standard presents basic acceptability curves, showing the acceleration limits beyond which the vibration is perceived by the receiver, depending on the excitation frequency and the direction of vibration shown in Figure 2.4. These curves are presented in Figure 2.6.

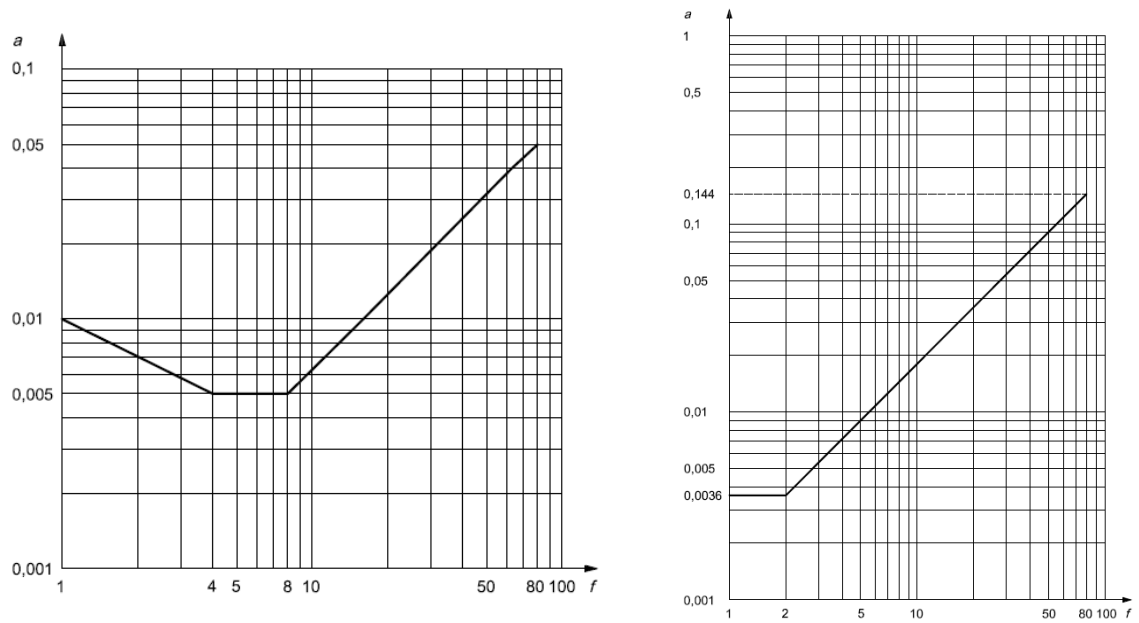

(a) Along z-axis (b) Along x and y-axis

Figure 2.6: Basic acceptability curves from ISO 10137 [45]

In order to assess the acceptability of vibration, a response factor evaluating the degree of exceedance to the vibration perception limit is adopted. This factor is based on the determination of the weighted RMS acceleration $a_{w,rms}$ according to ISO 2631 (see Section 2.3.1.3) and calculated as follows:

$$R = \begin{cases} \dfrac{a_{w,rms}}{a_z} & \text{for } z \text{ axis} \\ \dfrac{a_{w,rms}}{a_{x,y}} & \text{for } x \text{ and } y \text{ axis} \end{cases} \tag{2.18}$$

Here, the limits of perception are $a_z = 0.005\text{m/s}^2$ and $a_{x,y} = 0.00357\text{m/s}^2$. The response factor R must remain below the values provided in Table 2.3 to ensure an acceptable level of comfort for the occupants.

Use	Time	Continuous(1) / Repetitive(2) vibration	Occasional vibration
Critical working areas	Day	1	1
	Night	1	1
Residential	Day	2 to 4	30 to 90
	Night	1.4	1.4 to 20
Quiet offices	Day	2	60 to 128
	Night	2	60 to 128
General offices, schools	Day	4	60 to 128
	Night	4	60 to 128
Workshops	Day	8	90 to 128
	Night	8	90 to 128

(1) Continuous vibration: lasts more than 30 minutes per day.
(2) Repetitive vibration: occurs more than 10 times per day.

Table 2.3: Response factor limits according to ISO 10137 (modified from [45])

2.3.2.2 *VDV* method

For the case of repetitive vibrations (recurring more than 10 times per day), limit values are also given for the Vibration Dose Value (see Section 2.3.1.4), as a function of the duration of exposure and the probability of occurrence of the events acceptable by the client. Depending on the latter probability of occurrence, the *VDV* limits are provided in Table 2.4.

Residential buildings	Probability of occurrence		
Duration	Low	Possible	Probable
16h day	0.2 to 0.4	0.4 to 0.8	0.8 to 1.6
8h night	0.13	0.26	0.51

Table 2.4: VDV limits in $ms^{-7/4}$ (modified from [45])

The major shortcoming of this method is its limited usage on floor areas likely to be subjected to walking action (notably corridors) which are supposed to be known in advance and well defined by the stakeholders.

2.3.3 DIN 4150-2 standard

The German standard DIN 4150-2 [25] proposes a method for assessing the vibration comfort level of building occupants subjected to continuous or non-continuous vibrations with an excitation frequency ranging between 1 and 80Hz. This standard is not generally used in comfort assessment guidelines ([63], [81]), because it is based on velocity, which is more difficult to measure in practice than acceleration.

2.3.3.1 Vibration velocity

The velocity characterizes the vibration response of the structure and is directly related to the vibration energy produced by the human activity over the time. It should be measured at the points where vibrations are occurring most of the time. The frequency domain vibration velocity $KB(f)$ is determined as follows:

$$KB(f) = \frac{V(f)}{\sqrt{1+\left(\frac{f_0}{f}\right)^2}} \tag{2.19}$$

where $V(f)$ is the Fourier transform of the velocity response, f the frequency of the input signal and f_0 a reference frequency equal to 5.6Hz.

The weighting of $V(f)$ is performed to account for the range of vibration frequencies perceived by humans. By performing the inverse Fourier transform of $KB(f)$, the time-dependent vibration velocity $KB(t)$ is obtained which constitutes the basis of the acceptability assessment parameters presented below.

2.3.3.2 Basic method

This method aims to determine the transient effective vibration amplitude $KB_\tau(t_0)$ obtained by:

$$KB_\tau(t_0) = \sqrt{\frac{1}{\tau}\int_0^{t_0} e^{-\frac{t_0-t}{\tau}} KB^2(t)dt} \tag{2.20}$$

where τ is the integration time window (taken as 0.125s) and $KB(t)$ the vibration velocity at time t.

The maximum transient effective velocity is then computed by:

$$KB_{F\max} = \max_{t_0}\left[KB_\tau(t_0)\right] \tag{2.21}$$

This value should be compared against the values noted A_u and A_o given in Table 2.5.

Class	Zone	Day		Night	
		A_u	A_o	A_u	A_o
1	Exclusively commercial area	0.4	6	0.3	0.6
2	Mainly commercial area	0.3	6	0.2	0.4
3	Mixed zone	0.2	5	0.15	0.3
4	Residential area	0.15	3	0.1	0.2
5	Protected area	0.1	3	0.1	0.15

Table 2.5: Limits of KB_{Fmax} [25]

Three cases are possible:

- If $KB_{Fmax} \leq A_u$, the vibration is acceptable;
- If $KB_{Fmax} > A_o$, the vibration is not acceptable;
- If $A_u < KB_{Fmax} \leq A_o$, then the additional method, described below, must be used.

2.3.3.3 Additional method

When $A_u < KB_{Fmax} \leq A_o$, an alternative method is to determine a velocity for an oscillatory vibration evaluation denoted $KB_F(T_r)$, which takes into account the accumulation of vibration doses throughout the vibration period. More severe excitation for a shorter period of time can then be allowed. This velocity is determined by the following equation:

$$KB_F(T_r) = \sqrt{\frac{1}{N_c}\sum_{i=1}^{N_c} KB_{F\max}^2(T_i)}\sqrt{\frac{T_e}{T_r}} \tag{2.22}$$

where T_r is the total time of vibration, T_e the total time of evaluation (from 6 a.m. to 10 p.m. during the day and 10 p.m. to 6 a.m. at night), $KB_{Fmax}(T_i)$ the maximum transient effective value during a 30s cycle and N_c the number of 30s cycles during T_e.

The velocity $KB_F(T_r)$ is then compared to a limiting value noted A_r, given in Table 2.6.

Class	Zone	Day	Night
		A_r	A_r
1	Exclusively commercial area	0.2	0.15
2	Mainly commercial area	0.15	0.1
3	Mixed zone	0.1	0.07
4	Residential area	0.07	0.05
5	Protected area	0.05	0.05

Table 2.6: Limits of $KB_F(T_r)$ [25]

2.4 Design guidelines of floors against human discomfort

The application of the standards described in Section 2.3 is not at the reach of all stakeholders participating in the building process, but rather at that of the specialists in the field of structural dynamics. In order to bring the verification of the comfort of floors to the greatest possible number of the persons involved, various design recommendations were drafted in order to provide guidelines for the assessment of floors against human discomfort, yet with verifications not necessitating a complex structural dynamics analysis.

In these guidelines, investigated floors are not only characterized by their natural frequencies as was proposed previously in terms of frequency limitations ([6], [19]), but also by other modal properties affecting their vibrational performance (modal masses, damping ratios, modal shapes). They are all based on the key elements of the vibration problem as presented in ISO 10137 [45], which are the vibration source (load model), the transmission path (floor response) and the vibration receiver (acceptability limits). Since this research is limited to rhythmic activities, this section presents the two commonly used guidelines for this type of activity, which are SCI P354 guideline and AISC DG11 guideline [29].

***Note**: A uniform notation for the parameters used by the two design guidelines has been adopted in this section. Therefore, slight differences in notation may be encountered while consulting the official versions of these documents.*

2.4.1 SCI P354 guideline

SCI P354 guideline was developed by the British Steel Construction Institute. In 1989, a simplified method, based on a brief analysis of the vibration properties of the structure, was proposed in SCI P076 guideline [87]. In order to take into account the major advances in vibration analysis of floors (mainly provided in the European RFCS research project "Vibrations of Floors" [77]), a new guideline, SCI P354, was published in 2007 by Smith et al. and revised in 2009 [81]. The proposed general method is applicable to all types of floors subjected to the action of a single person (walking or rhythmic activities). This method should be favoured when the analysis of the vibration properties of the floor is performed using a Finite Element Model. The comfort evaluation method for rhythmic activities is presented in this section, where the response study is carried out using weighted RMS accelerations.

2.4.1.1 General considerations

If a floor subjected to rhythmic activities has a fundamental natural frequency exceeding 24Hz, it is considered that serviceability conditions are fulfilled. Below this limit, the response evaluation must be carried out. In this case, the vibrational response is considered as stationary, due to the continuous nature of the applied loading. A gradual increase in response is perceived during the application of the loading until its stabilization (resonance), as illustrated in Figure 2.7.

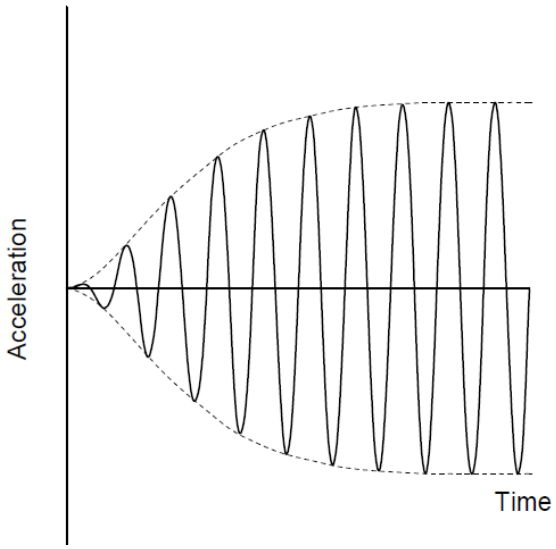

Figure 2.7: Stationary response [81]

The adopted load model for rhythmic activities is the Fourier series model given by Eq. (2.4). Numerical parameters are obtained by Eq. (2.5) for three rhythmic activities and summarized in Table 2.7.

α_c	Type of activity	Parameter	i=1	i=2	i=3
2/3	Low impact aerobics	DLF_i	9/7	9/55	2/15
		ϕ_i	-π/6	-5π/6	-π/2
1/2	High impact aerobics	DLF_i	π/2	2/3	0
		ϕ_i	0	-π/2	0
1/3	Normal jumping	DLF_i	9/5	9/7	2/3
		ϕ_i	π/6	-π/6	-π/2

Table 2.7: Fourier series load parameters proposed by SCI P354 guideline [81]

For the case of multiple individuals, the guideline proposes DLFs for the case of a group performing "normal jumping" activity based on the crowd size relation proposed by Ellis and Ji [31]. For the first three harmonics, DLFs are expressed as a function of the crowd size N by the following equation:

$$\begin{cases} DLF_1(N) = 1.61N^{-0.082} \\ DLF_2(N) = 0.94N^{-0.24} \\ DLF_3(N) = 0.44N^{-0.31} \end{cases} \quad (2.23)$$

2.4.1.2 Weighted RMS acceleration

The weighted RMS acceleration $a_{w,rms,e,r,i,n}$ for a natural mode n depends on the excitation point e, the response point r and the excitation harmonic i, and is expressed as:

$$a_{w,rms,e,r,i,n} = \mu_{e,n}\mu_{r,n}\frac{\alpha_i Q}{\sqrt{2}M_n}D_{n,i}W_i \quad (2.24)$$

where $\mu_{e,n}$ is the amplitude of the normalized modal shape of the n^{th} mode at the excitation point e, $\mu_{r,n}$ the amplitude of the normalized modal shape of the n^{th} mode at the response point r, α_i the DLF of the i^{th} harmonic of the load (depending on the considered activity as listed in Table 2.7), Q the weight of the individual (usually taken as 746N), M_n the modal mass of the n^{th} mode, W_i the frequency weighting factor corresponding to if_p and $D_{n,i}$ the dynamic magnification factor applied to the acceleration response (with $\beta_n = f_p / f_n$), given by:

$$D_{n,i} = \frac{(i\beta_n)^2}{\sqrt{(1-(i\beta_n)^2)^2 + (2\xi_n i\beta_n)^2}} \quad (2.25)$$

When amplitudes of modal shapes are unknown, $\mu_{e,n} = \mu_{r,n} = 1$ are conservatively taken. The damping ratio ξ depends on the type of the floor finishes and is given in Table 2.8.

Type of floor finishes	Damping ratio
Fully welded steel structures (staircases)	0.5%
Completely bare floors or floors when only a small amount of furnishings is present	1.1%
Fully fitted-out and furnished floors in normal use	3%
Floors with partitions interrupting the relevant mode(s) of vibration	4.5%

Table 2.8: Floor damping ratio according to SCI P354 guideline [81]

The frequency weighting W_i is obtained from one of the weighting curves of BS 6841 [11] (see Figure 2.8) according to Table 2.9.

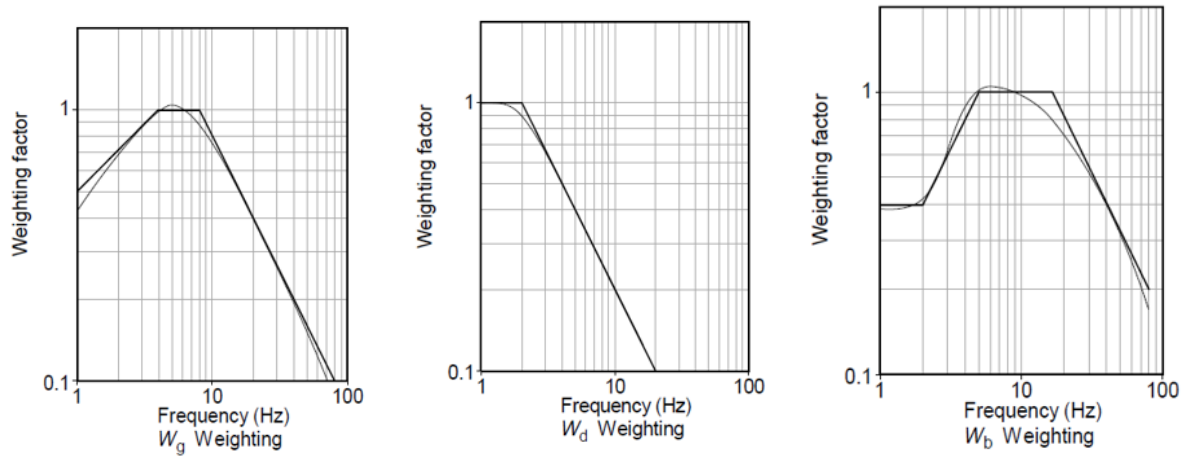

(a) W_g (b) W_d (c) W_b

Figure 2.8: Frequency weighting curves from BS 6841 [11]

Type of use	Vibration axis	Category	Weighting curve
Critical working areas (hospital operating theatres, precision laboratories)	z	Vision - hand control	W_g
	x-y	Perception	W_d
Residential, offices, wards, general laboratories, consulting rooms	z	Discomfort	W_b
	x-y	Discomfort	W_d
Workshops and circulation spaces	z	Discomfort	W_b
	x-y	Discomfort	W_d

Table 2.9: Choice of frequency weighting curves according to SCI P354 guideline [81]

The above calculation should be made with respect to the dominant modes of vibration, the natural frequency of which is lower than 26Hz. The weighted RMS acceleration for all dominant natural modes is then calculated by combining the responses of H harmonics according to M dominant modes of vibration as follows:

$$a_{w,rms,e,r} = \sqrt{\sum_{i=1}^{H}\left[\sum_{n=1}^{M} a_{w,rms,e,r,i,n}\right]^2} \tag{2.26}$$

2.4.1.3 Acceptability check

In accordance with BS 6472 [10], which is quite close to ISO 10137 [45], a response factor R is determined with respect to the perception base curve along the vibration axis by:

$$R = \begin{cases} \dfrac{a_{w,rms,e,r}}{a_z} & \text{for } z \text{ axis} \\ \dfrac{a_{w,rms,e,r}}{a_{x,y}} & \text{for } x \text{ and } y \text{ axis} \end{cases} \tag{2.27}$$

Here, the limits of perception are $a_z = 0.005\text{m/s}^2$ and $a_{x,y} = 0.00357\text{m/s}^2$. The response factor R should be lower than the values given in Table 2.10.

Place	Response factor limit
Office	8
Shopping mall	4
Dealing floor	4
Stairs – light use (e.g. Offices)	32
Stairs – heavy use (e.g. public buildings, stadia)	24
Car parks	65
Floors subjected to crowd rhythmic movements	120

Table 2.10: Response factor limits according to SCI P354 guideline [81]

2.4.2 AISC DG11 guideline

AISC DG11 guideline is applicable to floor vibrations under the action of walking or rhythmic activities of a single person. It was established in collaboration between the American Institute of Steel Construction and the Canadian Institute of Steel Construction in 1997 and revised in 2003 [63]. Similarly to SCI P354 guideline, modal Finite Element Analysis of floors is also favoured in this guideline.

The procedure for the comfort assessment of floors subjected to rhythmic activities is detailed in this section. The adopted load model for this type of activity is the Fourier series model given by Eq. (2.6). Corresponding DLFs are provided for three rhythmic activities in Table 2.11.

Activity	DLF_1	DLF_2	DLF_3
Jumping exercises	1.5	0.6	0.1
Sports event	0.25	0.05	-
Bouncing	0.5	-	-

Table 2.11: Dynamic Load Factors proposed by AISC DG11 guideline [63]

2.4.2.1 Natural frequency limitation

For each harmonic excitation, it must be checked that the maximum acceleration remains below a given value of a_0/g (presented in Section 2.4.2.2). This check is expressed as a condition on the natural frequency f_1 of the fundamental mode, given by:

$$f_1 \geq f_p \sqrt{1+\frac{k}{\frac{a_0}{g}}\frac{\alpha_i w_p}{w_t}} \tag{2.28}$$

where α_i is the DLF of the i^{th} harmonic (depending on the considered activity given in Table 2.11), w_p the maximum surface weight of individuals (related to their occupied surface) and w_t the surface weight of the floor including the weight of people. The excitation frequency f_p and weight w_p are provided in Table 2.12. The latter parameter was based on the maximum density of participants on the occupied area of the floor for "commonly encountered conditions", which could be greater for special events. Parameters k and a_0/g are given by:

- $k = 2$; $a_0/g = 5\%$ for jumping and aerobics;
- $k = 1.3$; $a_0/g = 2\%$ for bouncing;
- $k = 1.7$; $a_0/g = 5\%$ for sports event.

Harmonic	Jumping or aerobics		Bouncing		Sports event	
	f_p (Hz)	w_p (kPa)	f_p (Hz)	w_p (kPa)	f_p (Hz)	w_p (kPa)
1	2-2.75	0.2	1.5-3	0.6	1.5-3	1.5
2	4-5.5	0.2	-	-	3-5	1.5
3	6-8.25	0.2	-	-	-	-

Table 2.12: Parameters f_p and w_p for various rhythmic activities [63]

2.4.2.2 Response evaluation

As the frequency limitation given in Section 2.4.2.1 may be quite conservative, a response analysis can be conducted, in particular, when the criterion of the previous method is not verified for some harmonics.

For a natural mode n (frequently the fundamental one), three possible cases should be considered for each harmonic i (with frequency $f_i = if_p$):

- If $0.83f_i \leq f_n \leq 1.2f_i$, the response is resonant, and the maximum acceleration is:

$$\frac{a_{p,i}}{g} = \frac{k}{2\xi_n}\frac{\alpha_i w_p}{w_t} \tag{2.29}$$

- If $f_n > 1.2f_i$, the response is transient, and the maximum acceleration is:

$$\frac{a_{p,i}}{g} = \frac{k}{\left(\frac{f_n}{f_i}\right)^2 - 1}\frac{\alpha_i w_p}{w_t} \tag{2.30}$$

- If $f_n < 0.83f_i$, the following equation is applied:

$$\frac{a_{p,i}}{g} = \frac{k\frac{\alpha_i w_p}{w_t}}{\sqrt{\left[\left(\frac{f_n}{f_i}\right)^2 - 1\right]^2 + \left[2\xi_n\left(\frac{f_n}{f_i}\right)\right]^2}} \tag{2.31}$$

The damping ratio ξ is taken equal to 6%. The peak accelerations determined for H harmonics are then combined to give the total acceleration as follows:

$$\frac{a_m}{g} = \left[\sum_{i=1}^{H}\left(\frac{a_{p,i}}{g}\right)^{1.5}\right]^{1/1.5} \tag{2.32}$$

This acceleration should be compared with the acceleration limit a_0/g, obtained using the acceptability curves of ISO 2631-2:1989 [47], illustrated in Figure 2.9.

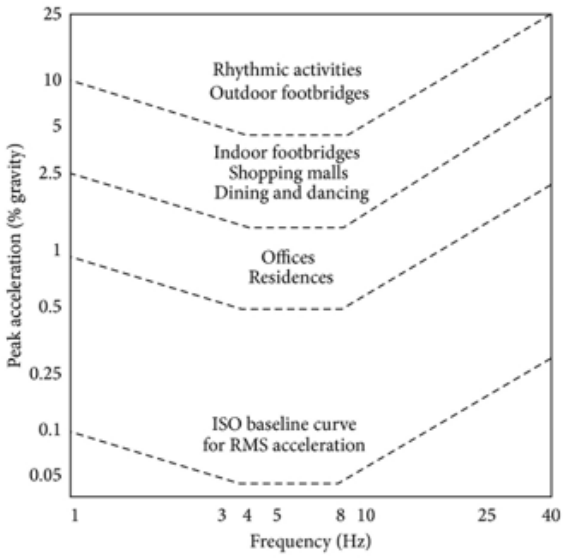

Figure 2.9: Acceptability curves for peak acceleration from ISO 2631-2:1989 [47]

The values of a_0/g are conservatively taken by extending the horizontal line of each of the above curves for all frequencies, resulting in the following values:

- Bouncing: 1.5%;
- Jumping / sports event: 5%.

2.4.3 Common limitations of guidelines

Although widely used for the assessment of floors against human discomfort around the world, the two presented design guidelines have technical and usage limitations.

The first common limitation is the assumption that the floor is loaded by a single person in service conditions, which is only the case for a limited category of floors (some gymnasiums and residential spaces). In spite of being very frequent in many structures (sports venues, fitness centres, grandstands, etc.), the case of crowd loading is not explicitly considered by these guidelines. In fact, the SCI P354 guideline proposes DLFs for the case of a group performing "normal jumping" activity (see Section 2.4.1.1). However, no detail is provided about the implementation of that model for the response calculation of floors. On the other hand, it is not clear whether or not AISC DG11 guideline allows evaluating the comfort of a floor subjected to crowd loads, as stated by Jones et al. [50]. The unique provided information is that the maximum density of participants on the occupied area of the floor corresponds to “commonly encountered conditions”. Vijayan et al. [86] confirm the impact of the group effect on floors (especially for slender ones) and invite to take it into account in their serviceability design.

The second limitation is that both guidelines consider the human load as a deterministic periodic action, which is far from being the case in reality, as highlighted by Muhammad et al. [62]. Indeed, there are other load models in the literature accounting for the realistic behaviour of human motion which will be presented in the next section.

2.5 Rhythmic load models reported in literature

This section presents several models in the literature aiming at characterizing rhythmic activities. This includes loads produced by either a single person or a group of people, considering the coordination between individuals during movement.

Note: *A comprehensive comparison of the load models detailed in this section (for a single person and crowds) against the proposed load models is given in Chapter 5.*

2.5.1 Single person load models

Rhythmic excitation resulting from the performance of a single person on a structure can be modelled either in the time domain or in the frequency domain. The two modelling strategies are presented in the next sub-sections.

2.5.1.1 Time domain load models

- **Rhythmic pulse model**

As outlined in Section 2.2.1, the analytical definition of the rhythmic pulse model assumes constant jumping pulse parameters during the activity. However, this may not correspond to jumps encountered in real life, where jumpers cannot maintain a constant frequency and amplitude during the activity. This phenomenon is called “intra-subject variability”.

Further works based on experimentally recorded jumps attempted to define an appropriate function for the jumping pulse shape. Corresponding parameters were considered as random variables characterized by fitted probability distributions, and Monte Carlo simulations were used to generate successive jumps based on these parameters.

Chen et al. [15] compared the model given by Eq. (2.1) with measured jumps, and confirmed that the half-sine pulse model is not appropriate for this activity. Instead, a modified half-sine-squared model has been suggested along with a Gaussian distribution for the model parameters. Sim et al. [80] proposed a cosine-squared function for the pulse profile, whose parameters were characterized by a beta distribution. Martinez et al. [58] modified the latter model and suggested to use a double cosine-squared function with a normal distribution to generate pulse parameters. Racic and Pavic [71] considered that the real jumping pulse has an asymmetric morphology. A double Gaussian function was then proposed for the pulse model, whilst peak-to-peak time intervals were assumed to follow a normal distribution. The same distribution was considered by Li et al. [55] for jumping pulse parameters. However, they analysed the shape of measured jumping pulses and proposed a jumping pulse model with three different patterns depending on the excitation frequency (double-peaked, merged and single-peaked pattern) as illustrated in Figure 2.10.

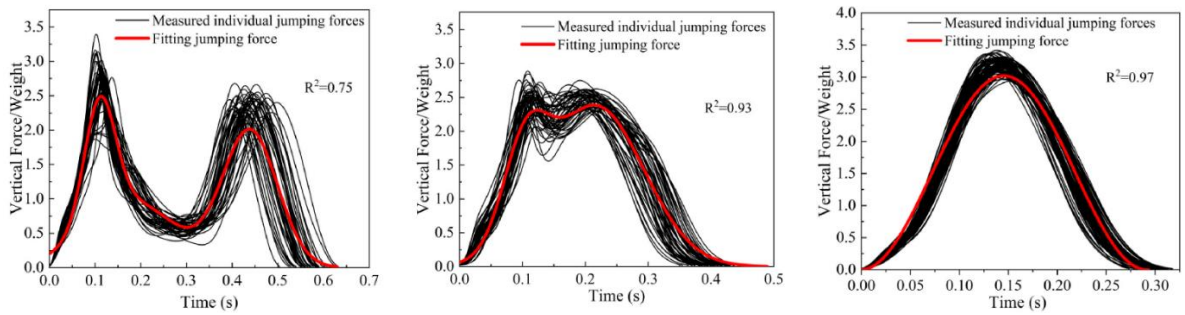

(a) Double-peaked (b) Merged (c) Single-peaked

Figure 2.10: Illustration of jumping pulse patterns [55]

Table 2.13 summarizes jumping pulse models proposed by different authors.

Reference	Normalized jumping pulse model ($P(t)/G$)
Chen et al. [15]	$\begin{cases} K_p \sin\left(\frac{\pi t}{t_c}\right), & f_p < 2\text{Hz} \\ K_p \sin^2\left(\frac{\pi t}{t_c}\right), & f_p \geq 2\text{Hz} \end{cases}$
Sim et al. [80]	$K_p \cos^2\left(\frac{\pi t}{t_c}\right)$
Martinez et al. [58]	$\sum_{i=1}^{2} A_i \cos^2\left(\omega_i \left(t - t_i\right)\right)$
Racic and Pavic [71]	$\sum_{i=1}^{2} a_i \exp\left(-\frac{\left(t-t_i\right)^2}{2b_i^2}\right)$
Faisca [39]	$0.5K_p\left[1-\cos\left(\frac{2\pi t}{t_c}\right)\right]$

Table 2.13: Normalized jumping pulse models

All models cited above correspond to "normal jumping" only, where an individual is launching himself in the vertical direction and returning to the ground with an impact. However, this behaviour may differ from other rhythmic activities. Faisca [39] analysed two different rhythmic activities (aerobics, audience motion) and concluded that the Hanning window function best fitted their resulting impacts (see Table 2.13). Corresponding parameters were found to be normally distributed, with mean and standard deviations given in Table 2.14.

Activity	t_c (s)	T_p (s)	K_p
Free jumps	0.32 ± 0.09	0.44 ± 0.15	3.17 ± 0.58
Aerobics	0.34 ± 0.09	0.44 ± 0.09	2.78 ± 0.60
Audience motion	0.33 ± 0.09	0.37 ± 0.03	2.41 ± 0.51

Table 2.14: Jumping pulse parameters proposed by Faisca [39]

- **Fourier series model**

As previously stated for the pulse model, analytical parameters of the Fourier series model (presented in Section 2.2.2) may not reflect experimental findings especially in terms of

rhythmic load amplitudes [50]. Consequently, several experiments have been conducted in order to determine corresponding load parameters.

Ellis and Ji [31] characterized individual normal jumping loads, whereas Alves et al. [3] determined DLFs for jumping and running activities. DLFs for various activities (normal and high jumping, running) had been suggested by CEB (Comité Euro-International du Béton) based on a previous experimental research [19]. Pernica [67] also determined maximum DLFs for three rhythmic activities (jumping, stride jumps, running-on-the spot). Table 2.15 summarizes DLFs proposed in the previously mentioned references.

Reference	Activity	DLF_1	DLF_2	DLF_3
Ellis and Ji [31]	Jumping	1.61	0.94	0.44
Alves et al. [3]	Jumping	1.8	1.19	0.51
	Running	1.35	0.25	0.13
CEB [19]	Normal jumping	1.8	1.3	0.7
	High jumping	1.9	1.6	1.1
	Running	1.6	0.7	0.2
Pernica [67]	Jumping	1.8	1.1	0.47
	Stride jumps	1.75	1.1	0.42
	Running-on-the-spot	1.57	0.58	0.26

Table 2.15: Various Dynamic Load Factors (DLFs)

All research mentioned earlier considered that DLFs are independent of the excitation frequency. However, observations in real situations highlighted that people have difficulties to maintain the same amplitude for usual frequencies when they are subjected to higher excitation frequencies [49]. This was taken into account by ISO 10137 [45], which proposed a Fourier series load model for coordinated jumping having DLFs inversely proportional to excitation frequency. Other rhythmic activities were also considered (vertical actions for seated audience, running) as can be found in Table 2.16.

Activity	DLF_1	DLF_2	DLF_3
Coordinated Jumping	$2.1-0.15f_p$	$1.9-0.34f_p$	$1.25-0.33f_p$
Vertical actions for seated audience	0.5	0.25	0.15
Running	1.4	0.4	0.1

Table 2.16: Dynamic Load Factors proposed by ISO 10137 [45]

In all Fourier series load models, when the phase lag is not provided, it is recommended to take a value equal to zero because it has in general a little effect on the floor response [50].

2.5.1.2 Frequency domain load models

As stated previously, each individual cannot maintain the same amplitude and frequency when performing a rhythmic activity ("intra-subject variability"). While this is not taken into account in Fourier series loads, this variability is simulated in jumping pulse models by a random generation of load parameters (see Section 2.5.1.1). In this way, each pulse would have a set of parameters different from the others along the activity duration. However, this method would not capture variabilities as observed in real situations, which are dependent on several conditions (audible stimulus, visual cues, etc.) [50]. Furthermore, the response of floors when using time domain load models would be dominated by only one mode of vibration at

resonance, which is not convenient for many building floors having multiple closely spaced modes such as multi-span or multi-panel floors ([20], [22], [75]).

For these reasons, it is more common to consider the rhythmic load as a near-periodic narrowband process [71], which is characterized in the frequency domain by its Power Spectral Density function (PSD) [70]. If the time-varying load $p_T(t)$ is assumed to be a stationary stochastic process, then its PSD $G_p(f)$ is calculated by [88]:

$$G_p(f) = \lim_{T \to +\infty} \frac{1}{2T} E\left[\left| P(f,T) \right|^2 \right] \tag{2.33}$$

where f is the frequency, T the duration of the excitation and $P(f,T)$ the Fourier transform of $p_T(t)$, which can be computed by:

$$P(f,T) = \int_{-\frac{T}{2}}^{\frac{T}{2}} p_T(t) e^{-2j\pi ft} dt \tag{2.34}$$

where j stands for the imaginary unit. For practical applications in which the frequency f does not take negative values, the one-side Power Spectral Density $S_p(f)$ (called PSD in the rest of the manuscript for simplicity) is often used, as defined by [88]:

$$S_p(f) = \begin{cases} 2G_p(f), & f > 0 \\ G_p(f), & f = 0 \\ 0, & f < 0 \end{cases} \tag{2.35}$$

This type of model was first used to simulate walking excitation especially on footbridges. Several authors proposed PSD load models based on experimental tests (e.g. Brownjohn et al. [12], Zivanovic et al. [93], etc.). Moreover, the frequency domain approach was first partially adopted by Racic and Pavic [71] in order to characterize the variability of pulse amplitudes in their proposed time domain jumping model (see Table 2.13). A PSD function was established for the peak amplitudes, from which a complex Fourier transform can be derived. Using the inverse Fourier transform, a random set of pulse amplitudes can then be obtained assuming randomly generated phases between $-\pi$ and π.

However, little experimental research has been carried out to determine complete frequency domain load models for rhythmic activities. The major contribution in this line was made by Xiong and Chen [88]. They measured individual jumps at various excitation frequencies, and fitted experimental PSDs using a bilinear symmetrical model (see Figure 2.11) given by:

$$S_{p,i}(f) = \begin{cases} \dfrac{\rho A_i}{0.1\Delta f_i}(0.1\Delta f_i - |f - f_i|), & |f - f_i| \in \left[0, 0.1\Delta f_i \left(1 - \dfrac{C_i}{0.9\Delta f_i A_i} \right) \right] \\ \dfrac{\rho C_i A_i (\Delta f_i - |f - f_i|)}{(0.9\Delta f_i)^2 A_i + 0.1 C_i \Delta f_i}, & |f - f_i| \in \left[0.1\Delta f_i \left(1 - \dfrac{C_i}{0.9\Delta f_i A_i} \right), \Delta f_i \right] \\ 0, & \text{otherwise} \end{cases} \tag{2.36}$$

where

$$C_i = S_i - 0.1\Delta f_i A_i \tag{2.37}$$

For each harmonic i: $S_{p,i}(f)$ is the PSD function (normalized by the weight of the individual), f_i the excitation frequency (if_p), A_i the PSD amplitude and Δf_i the frequency bandwidth defining the spread range of energy ($i\Delta f$).

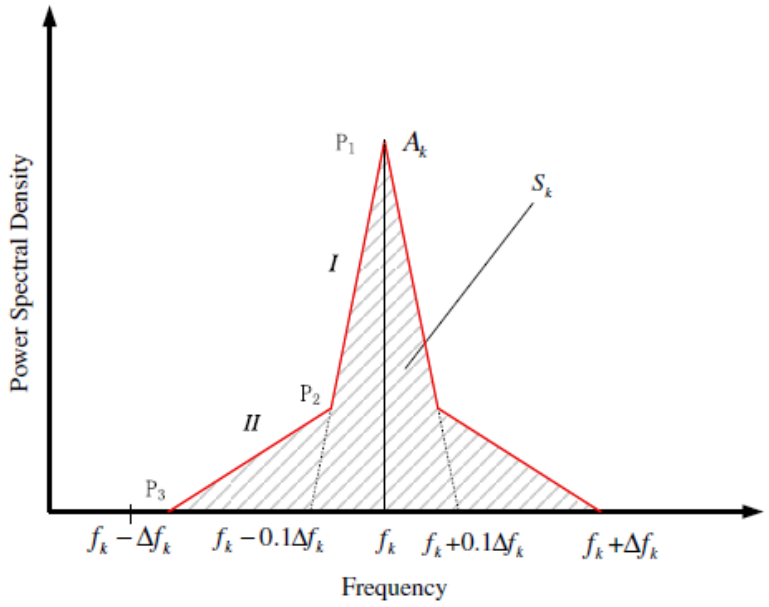

Figure 2.11: Bilinear symmetrical PSD model (k is the considered harmonic) [88]

The energy correction factor ρ accounts for the difference between the total energy of the analytical and experimental PSDs by the following expression:

$$\rho = \frac{S_0}{\sum S_i} \tag{2.38}$$

where:

$$\begin{cases} S_0 = \int_0^{+\infty} S_p(f)df \\ S_i = \int_{f_i-\Delta f_i}^{f_i+\Delta f_i} S_{p,i}(f)df \end{cases} \tag{2.39}$$

The final mass-normalized PSD load model is then given by:

$$S_p(f) = \sum S_{p,i}(f) \tag{2.40}$$

The definition of such a load model depends on five parameters: f_p, S_i, A_i, ρ and Δf. Table 2.17 provides corresponding parameters obtained for the first three harmonics at various excitation frequencies.

f_p (Hz)	1.5	2	2.67	3.5
S_0	0.88	1.27	1.39	1.19
S_1	0.53	0.90	0.78	0.89
S_2	0.066	0.13	0.12	0.10
S_3	0.031	0.011	0.010	0.0029
A_1	21.38	26.00	23.72	28.55
A_2	0.45	1.43	2.40	1.01
A_3	0.23	0.064	0.052	0.013
ρ	1.40	1.22	1.51	1.19
Δf (Hz)	0.15	0.15	0.15	0.15

Table 2.17: PSD jumping load parameters proposed by Xiong and Chen [88]

2.5.2 Crowd size effect

When a floor structure is subjected to rhythmic activities performed by a group of people (see Figure 2.12), the corresponding load is not a simple summation of the individual loads. In fact, each individual has a specific motion different from that of another person, resulting in different amplitudes and frequencies during movement. This is called "inter-subject variability" [50]. This effect was initially taken into account in jumping pulse models, by randomly generating the load parameters as described in Section 2.5.1.1 to have specific parameters for each individual in the group. Combination of random loads have then been made to have the total crowd load. Although it provides a more realistic jumping load model for multiple persons, this method is quite laborious in terms of implementation and does not consider crowd effects observed in real situations due to physical constraints, visual cues from crowd movement, stimulation from near environment, etc. [18]. This section discusses several propositions to characterize crowd size effect based on experimental observations.

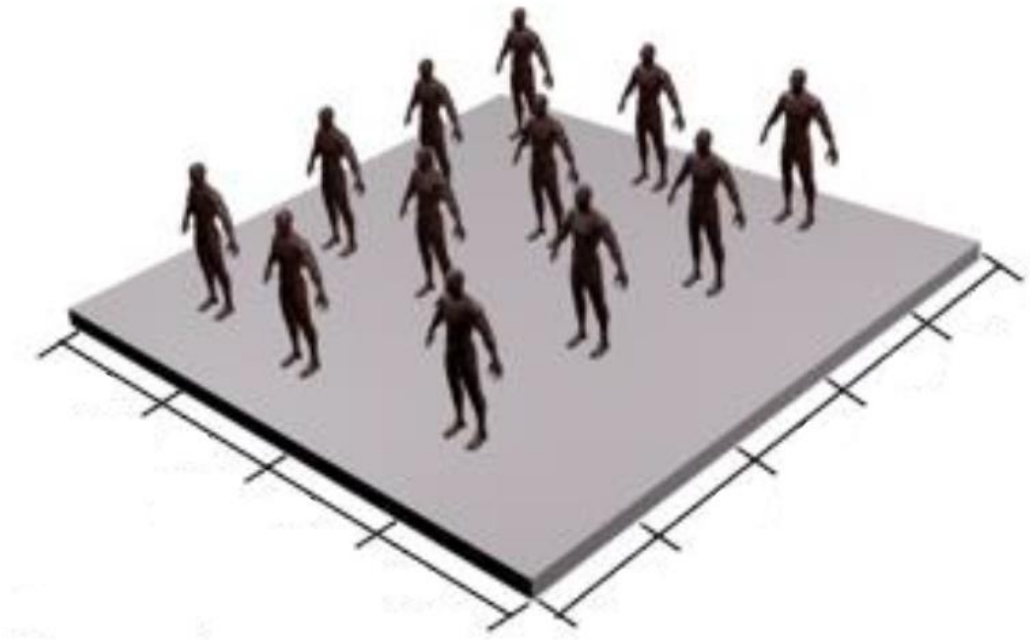

Figure 2.12: A group of individuals on a floor structure (modified from [75])

2.5.2.1 Deterministic crowd models

Deterministic load models are established by multiplying the time domain crowd model by a reduction parameter (called coordination factor) to take into account the lack of synchronization between individuals resulting from inter-variability effects. This reduction is expressed by the following relation:

$$P_N(t) = C(N)P(t) \tag{2.41}$$

where $P(t)$ is the force due to a single person present on the floor, $C(N)$ the coordination factor and $P_N(t)$ the equivalent force of an individual in a group of N participants defined by [31]:

$$P_N(t) = \frac{P_{crowd}(t)}{N} \tag{2.42}$$

where $P_{crowd}(t)$ is the total force produced by the group of N individuals.

A unique coordination factor was first proposed, such as 0.75 by Bachmann and Ammann [57] and 0.67 by BS 6399-1 [9]. These coefficients allow only a first approximation of the actual load since the variation of crowd size is not considered in the final load. This variation was analysed by ISO 10137 which suggested the following crowd size relation for walking and running activities [45]:

$$C(N) = \frac{\sqrt{N}}{N} \tag{2.43}$$

where N is the number of individuals. Costa-Neves et al. [20] determined numerical coefficients by crowd size based on experimental measurements made by Faisca [39] for two rhythmic activities (see Table 2.18).

N	Aerobics	Free jumps
1	1	1
3	1	0.88
6	0.97	0.74
9	0.96	0.70
12	0.95	0.67
16	0.94	0.64
24	0.93	0.62
32	0.92	0.60

Table 2.18: Coordination factors by crowd size N from Faisca experiments [20]

Further research was intended to determine crowd size relations dependent on each harmonic of the load, defined by:

$$P_{N,i}(t) = C_i(N)P_i(t) \tag{2.44}$$

where $P_{N,i}(t)$ is the i^{th} harmonic of the equivalent force related to a single person in a group of N individuals (given by Eq. (2.42)), $P_i(t)$ the i^{th} harmonic of the force due to one person present on the floor and $C_i(N)$ the coordination factor dependent on the i^{th} harmonic.

The reduction was applied to the corresponding Dynamic Load Factors (DLFs) for the first three harmonics. This was initially done by Ebrahimpour and Sack [27] for a jumping group of up to 40 persons, and DLFs were expressed as a function of the crowd size N by:

$$\begin{cases} DLF_i(N) = \dfrac{A_i - B_i N}{w_p}, & 1 \le N \le 10 \\ DLF_i(N) = \dfrac{C_i}{w_p}, & N > 10 \end{cases} \tag{2.45}$$

where A_i, B_i and C_i are reduction parameters of the i^{th} harmonic (see Table 2.19) and w_p the load intensity per person (weight by occupied surface).

Ellis and Ji [31] examined crowd loads produced by up to 64 persons jumping and suggested DLF relations for a group size N given by Eq. (2.23).

Parkhouse and Ewins [65] analysed squared DLFs of jumping activity simulated for a group of up to 200 persons and proposed the following model for each group size N:

$$DLF_i^2(N) = r_\infty^2 + \frac{r_{ST}^2}{N} \tag{2.46}$$

where r_∞ is the DLF of the synchronized component of the load and r_{ST} the DLF of the stochastic component of the load (see Table 2.19).

Reference	Parameter	1st harmonic	2nd harmonic	3rd harmonic
Ebrahimpour and Sack [27]	A_i (psf)	50.89	20.89	4
	B_i (psf)	1.89	0.89	0
	C_i (psf)	32	12	4
Parkhouse and Ewins [65]	r_∞	1.09	0.29	0.024
	r_{ST}	1.07	0.62	0.22

Table 2.19: Parameters for various crowd size relations

Two major developments have been performed regarding crowd size effect models. The first one consists of the derivation of various relations depending on the coordination degree among participants. This was done in ISO 10137 [45], which proposed coordination factors for three levels of synchronization:

- High: all individuals are well trained and are experienced to coordinate the motion in a group;
- Medium: only some individuals are well trained, but most individuals are experienced to coordinate the motion in a group;
- Low: only some individuals are well trained, and most individuals are not experienced to coordinate the motion in a group.

Table 2.20 presents coordination factors for more than 50 persons. A coordination factor of 1 is considered for a group of 5 persons or less. A linear interpolation should be made between 5 and 50 individuals.

Coordination	1st harmonic	2nd harmonic	3rd harmonic
High	0.8	0.67	0.5
Medium	0.67	0.5	0.4
Low	0.5	0.4	0.3

Table 2.20: Coordination factors for more than 50 persons according to ISO 10137 [45]

The second proposition was to characterize each excitation frequency by an appropriate group reduction, assuming that people have difficulties to coordinate their motion at higher frequencies [18]. Li et al. [54] suggested such crowd relations for frequencies ranging between 1.5 and 3.5Hz and a group of up to 48 persons jumping, which have the following form:

$$\begin{cases} RDLF_i(N) = a_i N^{b_i} + c_i, & 2 \le N \le N_{\max} \\ RDLF_i(N) = RDLF_i(N_{\max}), & N > N_{\max} \end{cases} \tag{2.47}$$

where $RDLF_i$ is the ratio of DLF for a person in a group of N individuals to the DLF of a single person on the floor for the i^{th} harmonic. Table 2.21 illustrates obtained parameters a_i, b_i, and c_i for an excitation frequency of 2Hz (with N_{max}=45).

Parameter	1st harmonic	2nd harmonic	3rd harmonic
a_i (2Hz)	0.48	0.90	0.90
b_i (2Hz)	-1.06	-0.59	-0.55
c_i (2Hz)	0.52	0.08	0.10

Table 2.21: Illustration of crowd size relation parameters proposed by Li et al. [54]

2.5.2.2 Random field models

Individual spectral load models can be extended to crowds by means of a random field approach. For walking excitation, this was initially done by Piccardo and Tubino [68] for the case of unrestricted traffic on footbridges. The model was then generalized by Ferrarotti and Tubino [42] for any traffic situation, and numerically validated by Venuti and Tubino [85].

Concerning rhythmic activities, Xiong and Chen [89] proposed a random field model based on two major components:

- An auto-spectral model $S_p(f)$ for the case of a single person;
- A coherence function $\gamma_{kl}(f)$ defining the degree of coordination between every couple of persons in the group, given by the following expression:

$$\gamma_{kl}(f) = \frac{S_{kl}(f)}{\sqrt{S_k(f) S_l(f)}} \tag{2.48}$$

In the above equation, $S_k(f)$ and $S_l(f)$ are the PSD load models for the individual k and l, respectively, and $S_{kl}(f)$ the cross-PSD between the two persons, obtained by random field theory ([84], [89]). The spatial variation of $S_{kl}(f)$ was not considered because individuals do not change their position during movement.

For a single person, Xiong and Chen [89] updated the mass-normalized PSD load model presented in Section 2.5.1.2 (expressed by Eq. (2.36)), by replacing the bilinear function with Gaussian functions. The resulting model has the following expression for each harmonic i:

$$\bar{S}_{p,i}(\bar{f}) = \frac{\rho S_i}{i f_p} \left[p_5 \exp\left(-\left(\frac{\bar{f} - 1}{p_6} \right)^2 \right) + p_7 \exp\left(-\left(\frac{\bar{f} - 1}{p_8} \right)^2 \right) \right] \tag{2.49}$$

Here, $\bar{S}_{p,i}(\bar{f})$ is the mass-normalized PSD load of the i^{th} harmonic, f_p the excitation frequency, $\bar{f} = f / i f_p$ the normalized frequency, S_i the load energy of the i^{th} harmonic and ρ an energy-compensation factor expressed by:

$$\rho = \frac{S_0}{\sum_{i=1}^{3} S_i} \tag{2.50}$$

where

$$S_i = p_1 f_p^{\,3} + p_2 f_p^{\,2} + p_3 f_p + p_4 \tag{2.51}$$

p_k ($1 \le k \le 8$) are model coefficients which were determined using experimental records and summarized in Table 2.22 for the first three harmonics.

Parameter	p_1	p_2	p_3	p_4
S_0	0.21	-1.92	5.62	-3.96
S_1	0.21	-1.84	5.23	-3.77
S_2	0.035	-0.36	1.17	-0.99
S_3	-0.018	0.14	-0.35	0.31
Parameter	p_5	p_6	p_7	p_8
-	2.80	0.079	29.27	0.012

Table 2.22: PSD load model parameters proposed by Xiong and Chen [89]

The mass-normalized PSD load model is then given by:

$$\bar{S}_p(f) = \sum_{i=1}^{3} \bar{S}_{p,i}(\bar{f}) \tag{2.52}$$

Figure 2.13 displays a log-plot of the PSD load model obtained by Eq. (2.52) for an excitation frequency of 2Hz, where the three harmonic peaks are clearly visible.

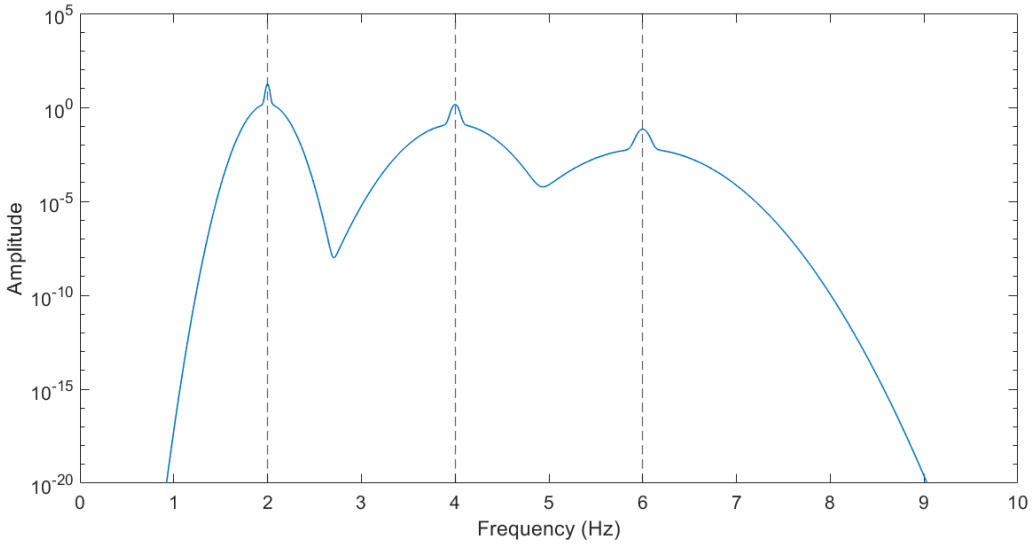

Figure 2.13: Normalized PSD load model proposed by Xiong and Chen [89] for an excitation frequency of 2Hz (log-plot)

The coherence function $\gamma_{kl}(f)$ equals one for a perfectly synchronized group and zero for a totally uncoordinated group. The realistic case is somewhere in between. Experimental tests were conducted for up to 48 individuals jumping and correlation parameters were then suggested to simulate crowd-rhythmic activities [89].

2.6 Response of floors subjected to rhythmic loads

Consider a floor structure having a number of *M* dominant natural modes where a single person or a group of individuals ($N \geq 1$) performs rhythmic movements at fixed positions, as shown in Figure 2.14. The floor is assumed to represent a linearly elastic system. The objective of this section is to present the major steps to calculate the response of the floor due to this load case, either in the time domain or in the frequency domain.

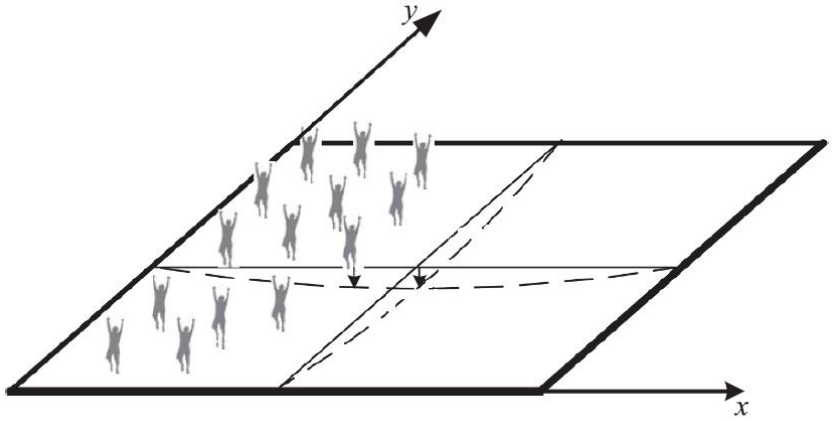

Figure 2.14: Floor subjected to crowd-rhythmic loads (modified from [89])

2.6.1 Response in time domain

The *N* loads exciting the floor are collected in a force vector noted $\{p(t)\}$.

Using the modal decomposition method, the equations of motion for the *M* natural modes are uncoupled, which gives for each mode *n* [17]:

$$\ddot{q}_n(t) + 2\xi_n\omega_n\dot{q}_n(t) + \omega_n^2\, q_n(t) = \frac{1}{M_n}\, p_n^*(t) \tag{2.53}$$

where ω_n, M_n, ξ_n, and $p_n^*(t)$ are the circular frequency, the modal mass, the damping ratio and the generalized force of the n^{th} mode, respectively, and $q_n(t)$, $\dot{q}_n(t)$ and $\ddot{q}_n(t)$ are the displacement, the velocity and the acceleration modal coordinates of the n^{th} mode, respectively.

The generalized force $p_n^*(t)$ is determined by the following expression:

$$p_n^*(t) = \left\{\Phi_{p,n}\right\}^T \left\{p(t)\right\} \tag{2.54}$$

where $\{\Phi_{p,n}\}^T$ is the transposed modal shape vector of the n^{th} mode at all excitation positions ($1 \times N$) and $\{p(t)\}$ the force vector applied at each excitation position ($N \times 1$).

Eq. (2.53) is solved using step-by-step numerical integration methods. The most common ones are the Wilson-θ method and the Newmark-β method [66]. Parameters of such methods should be chosen so that the integration process could be unconditionally stable, which results in accurate modal coordinates $q_n(t)$, $\dot{q}_n(t)$ and $\ddot{q}_n(t)$.

The displacement response of the floor could then be calculated as follows:

$$d(t) = \sum_{n=1}^{M} \Phi_{r,n} q_n(t) \tag{2.55}$$

where $\Phi_{r,n}$ is the modal shape amplitude of the n^{th} mode at the response position.

The acceleration response is also computed by:

$$a(t) = \sum_{n=1}^{M} \Phi_{r,n} \ddot{q}_n(t) \tag{2.56}$$

For a given response parameter w (displacement or acceleration), the Root Mean Square (RMS) value w_{rms} was adopted as the main parameter in response prediction. Indeed, it takes into account the variation of the whole signal such that parasite peaks would have a limited effect on the resulting amplitude. This explains its wide use in the definition of vibration acceptability limits against human discomfort ([45], [46], [81]).

The RMS response is computed for a duration T by:

$$w_{rms} = \sqrt{\frac{1}{T}\int_0^T w^2(t)dt} \tag{2.57}$$

2.6.2 Response in frequency domain

The crowd load model is considered as a stationary stochastic process. It contains an auto-spectral density defining each individual load k (noted $S_{p,k}(f)$) and a cross-spectral density defining correlation between each two persons k and l (noted $S_{p,k,l}(f)$), as defined in Section 2.5.2.2.

Applying Fourier transform to Eq. (2.54) for all natural modes results in:

$$\left\{P^*(f)\right\} = \left[\Phi_p\right]^T \left\{P(f)\right\} \tag{2.58}$$

where $\{P^*(f)\}$ is the Fourier transform vector of generalized forces ($M \times 1$), $\left[\Phi_p\right]^T$ the transpose of the modal shape matrix at all excitation positions ($M \times N$) and $\{P(f)\}$ the Fourier transform of the load vector $\{p(t)\}$.

Using the definition of Power Spectral Density provided in Section 2.5.1.2, the PSD matrix of generalized forces $\left[S_{p^*}(f)\right]$ ($M \times M$) is then calculated from $\{P^*(f)\}$ by [70]:

$$\left[S_{p^*}(f)\right] = \left[\Phi_p\right]^T \left[S_p(f)\right] \left[\Phi_p\right] \tag{2.59}$$

Here, $\left[S_p(f)\right]$ is the PSD matrix of crowd loads ($N \times N$) defined by:

$$\left[S_p(f)\right]_{k,l} = \begin{cases} S_{p,k}(f), & k = l \\ S_{p,k,l}(f), & k \neq l \end{cases} \tag{2.60}$$

The Fourier transform of Eq. (2.53) for all natural modes gives:

$$\left\{Q(f)\right\} = \left[H(\omega)\right] \left\{P^*(f)\right\} \tag{2.61}$$

where $\{Q(f)\}$ is the Fourier transform vector of modal coordinates ($M \times 1$) and $[H(\omega)]$ the Frequency Response Function matrix ($M \times M$) defined by:

$$\left[H(\omega)\right]_{n,n} = \frac{1}{M_n(\omega_n^2 - \omega^2 + 2j\xi_n\omega_n\omega)} \tag{2.62}$$

The PSD matrix of modal coordinates $\left[S_q(f)\right]$ ($M \times M$) is then:

$$\left[S_q(f)\right] = \left[H(\omega)\right]\left[S_{p^*}(f)\right]\left[\bar{H}(\omega)\right]^T \tag{2.63}$$

Here, $[\bar{H}(\omega)]^T$ is the transpose conjugate matrix of $[H(\omega)]$.

Performing Fourier transform to Eq. (2.55) leads to:

$$D(f) = \{\Phi_r\}\{Q(f)\} \tag{2.64}$$

where $D(f)$ is the Fourier transform of the displacement response and $\{\Phi_r\}$ the modal shape vector at the response position ($1 \times M$).

This results in the PSD of displacement response $S_d(f)$ given by:

$$S_d(f) = \{\Phi_r\}\left[S_q(f)\right]\{\Phi_r\}^T \tag{2.65}$$

The PSD of acceleration response $S_a(f)$ is obtained by:

$$S_a(f) = \omega^4 S_d(f) \tag{2.66}$$

For a given parameter w (displacement or acceleration), the RMS response is then deduced by:

$$w_{rms} = \sqrt{\int_0^{+\infty} S_w(f)df} \tag{2.67}$$

The resulting responses (in time or frequency domain) could be used to perform the serviceability assessment of floors against human discomfort based on one of the standards detailed in Section 2.3 agreed by the stakeholders.

2.7 Conclusions

This review was intended to present the principal findings dealing with the topic of vibrations of floors subjected to rhythmic activities. It was found that the modelling of the human motion is a rather complex task because of many variabilities coming into play. The key outcomes of the state-of-the-art can be summarized as follows:

2.7.1 Load models

- For a single person, rhythmic activities are generally modelled in the time domain. Both modelling strategies (Fourier series, jumping pulses) do not account for "intra-subject variability" (the variation of load parameters during movement) observed experimentally. Time domain load models also cannot excite multiple dominant natural modes simultaneously. Few frequency domain models were developed to overcome these issues.

  In this research, a simplified spectral load model for rhythmic activities will be proposed, and corresponding parameters identified using force measurements.

- For a group of people, the lack of synchronization due to "inter-subject variability" was modelled either by deterministic coordination factors in time domain models or by correlation functions in a random field model.

The load modelling strategy proposed in this research will adopt coordination factors to be added to the spectral load model, which is simpler to manage compared to a random field approach.

- The majority of research reported in the literature focused on "normal jumping" activity (corresponding to a regular vertical jumping) since it produces the greatest loads among rhythmic actions. However, there are other rhythmic activities taking place at many locations (such as fitness centres, sports venues, gymnasiums, etc.) which could have larger loads than "normal jumping" [67].

  Four common rhythmic activities will be investigated in this work by conducting experiments on two floors where individuals are moving under controlled conditions.

2.7.2 Response of floors subjected to rhythmic loads

The two comfort evaluation guidelines investigated in this review (SCI P354 and AISC DG11) exhibit some limitations. Firstly, both guidelines consider the human load as a deterministic periodic action, which is far from reality as explained previously. Secondly, they are primarily applied to floors loaded by a rhythmic activity produced by a single person in service conditions. The case of rhythmic activities performed by groups of people is not explicitly studied by the guidelines, although quite frequent in many structures (sports venues, fitness centres, grandstands, etc.).

In that context, response prediction methods for floors subjected to crowd-rhythmic activities will be derived using the developed spectral crowd models.

3 Design and vibration testing of a laboratory floor

3.1 Introduction

Human-induced vibrations, especially due to crowd-rhythmic activities, are a complex random phenomenon observed on full-scale floor structures such as sports venues, gymnasiums, grandstands, etc. ([50], [82]). Thus, experiments on small-scale floor structures are a first step paving the way for characterizing loads and responses due to such activities.

In the vast majority of tests carried out for that purpose, the analysed activity was "normal jumping" and the movement of individuals was controlled by a metronome, which does not reflect real situations where people are free to perform such activities while subjected to various audible and visual stimulus. Therefore, four different rhythmic activities are investigated in this study. The scope corresponds to situations close to reality (without metronome), with a low density of participants (below 0.3 person/m² [42]).

This chapter begins with the presentation of a laboratory floor representing steel-concrete building floors. This includes numerical modelling and final configuration design of the structure. First experiments carried out on the floor specimen are then introduced, comprising deflection tests along with Experimental Modal Analysis. Vibration tests under various crowd-rhythmic activities are described afterwards, by providing details about instrumentation and experimental setup.

3.2 Design of the floor specimen

Several tests have been conducted on small-scale structures in order to investigate human rhythmic activities. Alves et al. [3] used a 4×1.15m² floor to measure loads due to a single person jumping, without studying crowd effects due to limited floor surface. These effects were analysed by Pernica [67] on a 17.04×2.13m² floor, allowing to measure the loads for up to 8 persons performing three rhythmic activities (jumping, running-on-the-spot, stride jumps). Ebrahimpour and Sack [27] worked on a 4.57×3.66m² laboratory floor and recorded loads and responses produced by up to 40 persons jumping. A 12.2×2.2m² floor specimen was designed by Faisca [39] where loads induced by up to 20 persons were measured. In that case, various rhythmic activities have been studied (jumping, aerobics, audience motion) but in a quite crowded situation (density of 2 persons/m² [42]). The above tested structures had a beam shape in general (length much larger than width) or considerably small dimensions, far from floors commonly encountered in practice.

For that reason, the floor specimen designed for vibration experiments within this study has comparable dimensions in plan (representing existing floors) in order to allow a uniform distribution along with a low density of individuals while performing rhythmic activities. Considerations related to the design of the laboratory floor are first presented. A parametric study of the main floor characteristics is undertaken based on a numerical model developed using ANSYS. From this analysis, the final configuration of the floor is defined, and both static and dynamic design are carried out.

3.2.1 General considerations

3.2.1.1 Area constraints

The structure is a typical steel-concrete composite floor, comprising a reinforced concrete slab with steel-decking profile, steel primary and secondary beams and steel columns. The connection between the slab and the beams is achieved by welded shear studs.

The floor was constructed at the FCBA technical centre in Bordeaux, France. The available area was about 60m² (see Figure 3.1(a)). A floor area of 8×7m² was then chosen, accommodating a maximum of 16 individuals with a density of 1 person/3m² (approximately 0.35 person/m²). As the area had an inclined bituminous ground, variable column heights were adopted to compensate the lack of horizontality of the floor specimen (see Figure 3.1(b) for ground altitudes).

(a) Front view

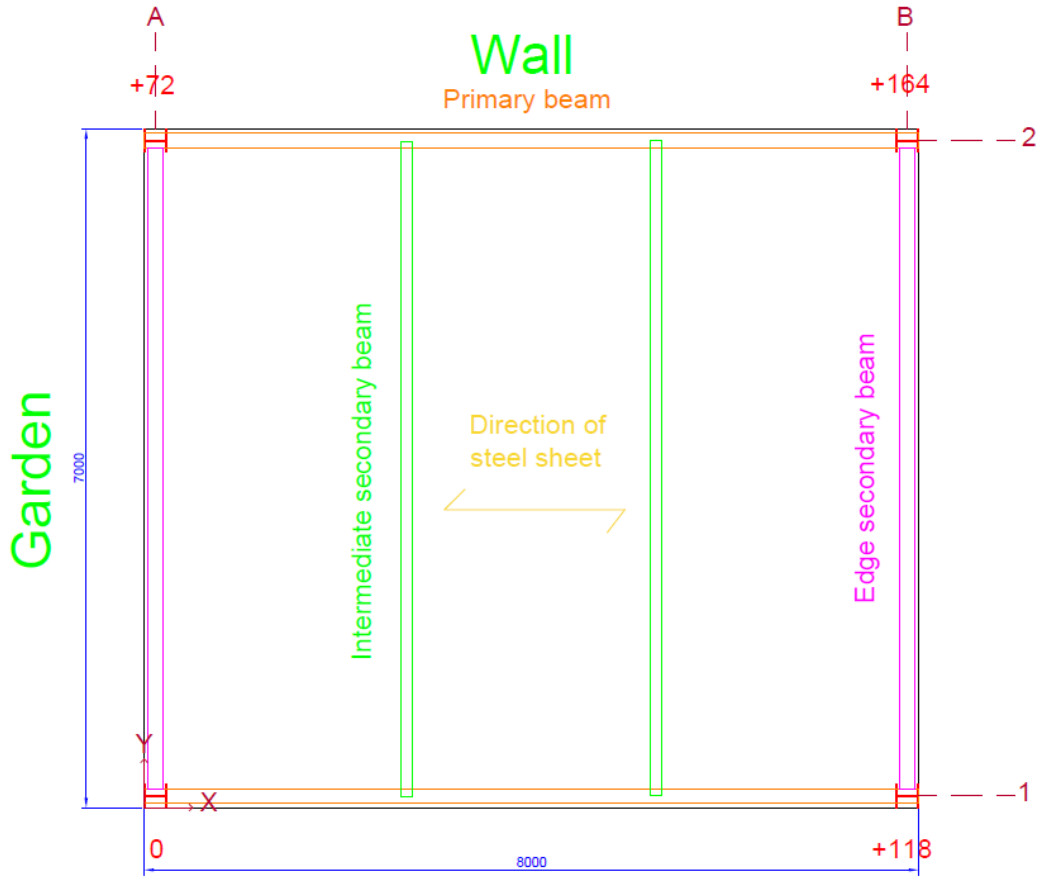

(b) Initial plan view with ground altitudes (dimensions in mm)

Figure 3.1: Laboratory floor area

The heights of the four floor columns are given in Table 3.1. As columns could not be anchored in the bituminous ground, the stability of the structure must then be ensured by two conditions:

- All column base horizontal displacements are restrained;
- Beam to column connections are rigid in bending.

Column	A1	A2	B1	B2
Height (mm)	594	522	476	430

Table 3.1: Columns heights

3.2.1.2 Floor requirements

The floor specimen should meet two major requirements in order to be suitable for the investigation of crowd-rhythmic activities. First of all, the floor should have an adequate strength [27] so that the safety of the participants could be guaranteed [31]. Moreover, the response of the floor should be dominated by its fundamental mode only, so that the interaction between higher modes in terms of the floor response could be avoided. The fundamental frequency should also be below 10Hz, which is the maximum expected frequency for human excitation [31]. This leads to a low-frequency floor where the response is likely to be stationary ([61], [81]). The above conditions were fulfilled by an adequate modelling and design of the floor as presented in the next sections.

3.2.1.3 Typical floor characteristics

The composite slab characteristics are in line with current practice. Indeed, reinforcements were composed of steel mesh ST25C of 7mm diameter and 150mm spacing. Cofraplus 60 steel-decking profile having 0.75mm thickness was selected, with the ribs perpendicular to secondary beams. The shear studs were TRW Nelson KB 3/4"-125, with 19mm diameter and 125mm height. They had a 207mm spacing (between steel profile ribs) for 7m span secondary beams and 200mm spacing for 8m span primary beams (see Figure 3.1(b)). Remaining characteristics to be determined are slab thickness, concrete strength, profile types (beams and columns), number and connection type of intermediate beams as well as number of columns.

3.2.2 Numerical modelling of the floor

A parametric study has been performed with a Finite Element Model (FEM) varying the remaining characteristics provided earlier. These parameters should contribute to the fulfilment of the second requirement presented in Section 3.2.1.2.

3.2.2.1 Description of the numerical model

The numerical model of the floor has been implemented using ANSYS largely used to model steel-concrete composite floors by the Finite Element Method [8]. The mesh has a density of 200mm, made up of the following element types:

- Shell elements with 8 nodes and 6 degrees of freedom per node (SHELL 281) for the concrete slab, with a layer to model reinforcements at the appropriate height;
- Beam elements with 2 nodes and 7 degrees of freedom per node (BEAM 188) for beams and columns.
- Beam elements with 2 nodes and 6 degrees of freedom per node (BEAM 188) for shear connectors and steel-decking profile.

An equivalent stiffness for shear studs EI_{eq} is considered as follows:

$$\frac{EI_{eq}}{e} = \frac{EI_s}{d} \tag{3.1}$$

where EI_s is the initial stiffness of shear studs, e the mesh density and d the actual spacing of studs. This corresponds to an equivalent diameter for shear studs ϕ_{eq} determined by:

$$\phi_{eq} = \phi_s \sqrt[4]{\frac{e}{d}} \tag{3.2}$$

where ϕ_s is the actual stud diameter. Figure 3.2 provides a general view of the FEM model.

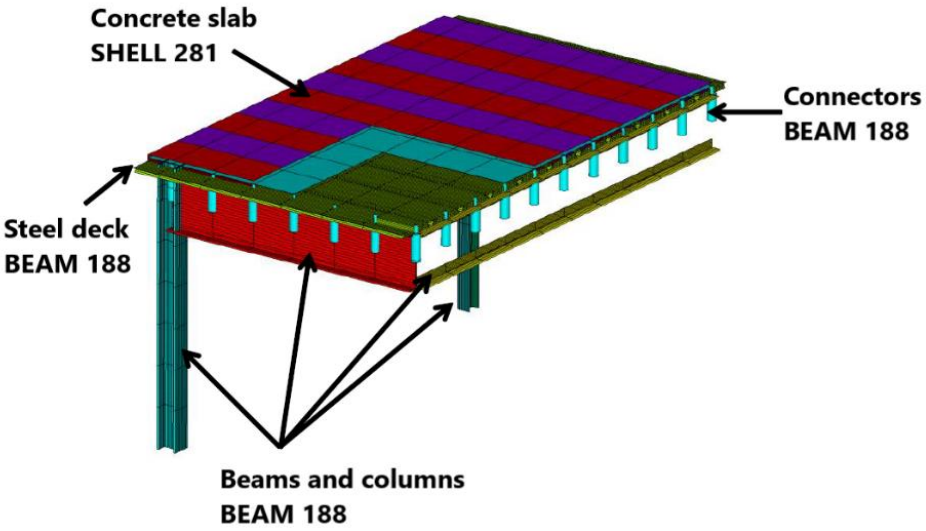

Figure 3.2: FEM model with element types (modified from [8])

Regarding boundary conditions, translation in the three directions along with rotation about the vertical direction were restrained at column bases (see Section 3.2.1.1). Rigid connections were considered between primary beams and columns and between edge secondary beams and primary beams, whilst intermediate secondary beams were considered simply supported (see Figure 3.1(b)). Vertical restraints were positioned in the middle of the primary beams to account for the presence of intermediate columns.

The specific weight was considered equal to 2.4t/m^3 for concrete and 7.85t/m^3 for steel. Steel tensile strength was taken as 275MPa for hot-rolled profiles, 355MPa for welded I-members, and 350MPa for shear studs [38]. Young's modulus was 210GPa for all steel members. For concrete, Young's modulus has been determined according to Eurocode 2 [36] as follows:

$$E_c = 22\left(\frac{f_{ck}+8}{10}\right)^{0.3} \tag{3.3}$$

where E_c is Young's modulus of concrete (in GPa) and f_{ck} the nominal compressive strength of a concrete cylinder (in MPa).

3.2.2.2 Parametric study

A parametric study was performed in order to assess the influence of floor characteristics on the natural frequencies of the dominant natural modes. The study was applied to the first four modes to cover a frequency range exceeding 10Hz (maximum for human activities) [31].

- **Initial floor configuration**

An initial set of floor characteristics was selected, representing one of the most common situations for steel-concrete floors. The composite deck was 15cm thick (11cm height for reinforcements) with a compressive concrete strength of 25MPa (class C25/30). IPE200 profile was chosen for secondary beams spaced at 2.6m (resulting in two intermediate beams). In addition, IPE400 and HEB240 profiles has been selected for primary beams and columns, respectively. The latter members were placed at the floor corners. Figure 3.3 presents a perspective view of the floor model with and without slab.

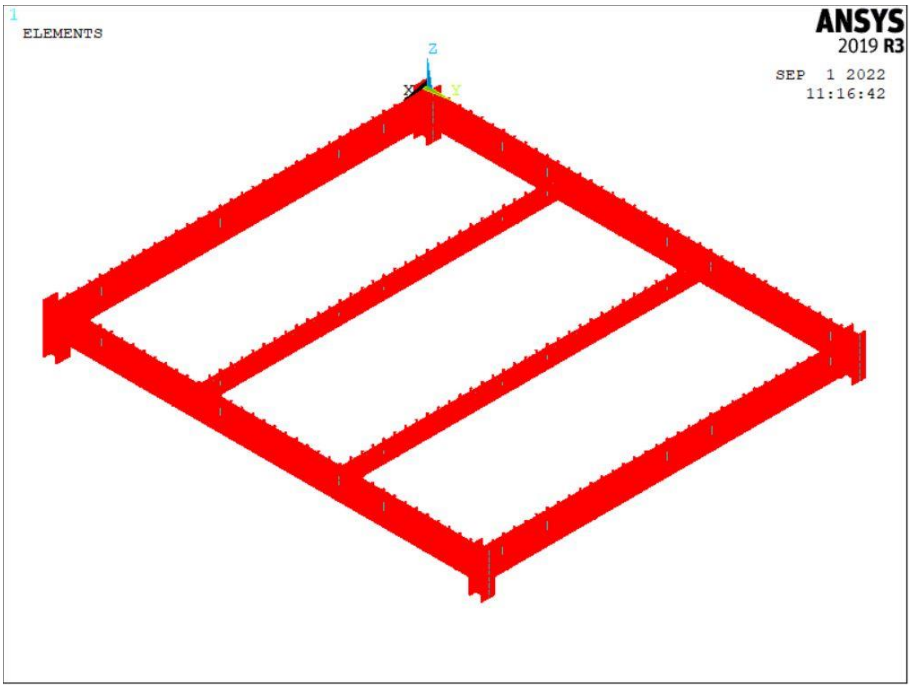

(a) Without slab

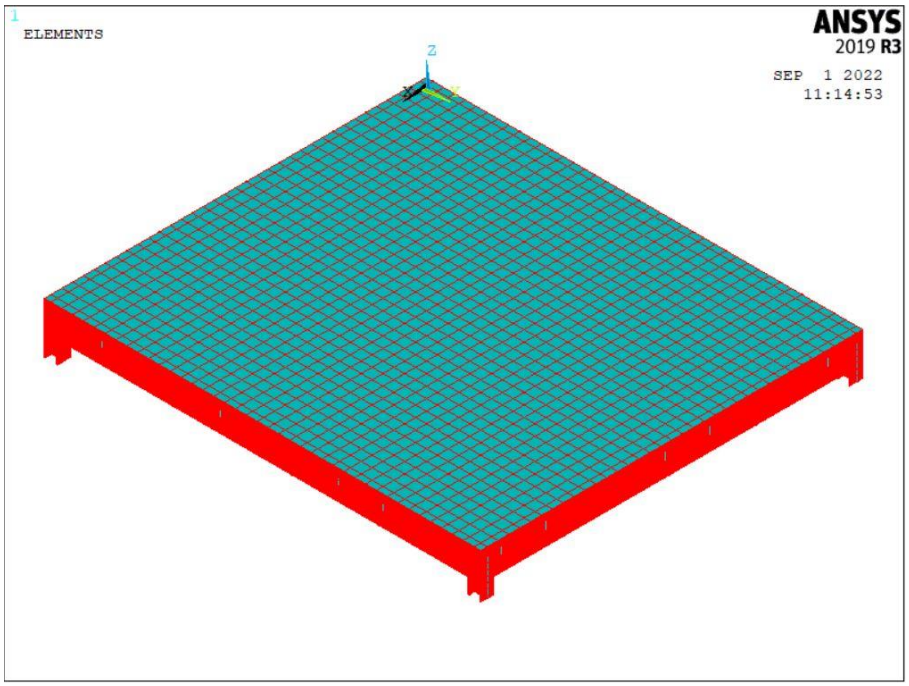

(b) With slab

Figure 3.3: FEM model of the floor specimen

Modal analysis was performed using Block-Lanczos eigenvalue extraction method for the first four natural modes. Obtained natural frequencies for the initial floor configuration are given in Table 3.2.

Mode	1	2	3	4
Natural frequency (Hz)	5.96	9.85	13.58	15.29

Table 3.2: Natural frequencies for the initial floor configuration

- **Variation of floor characteristics**

Each of the above characteristics was varied and natural frequencies of the four dominant natural bending modes were computed. Table 3.3 summarizes obtained frequencies for each investigated parameter.

Parameter	Value	Natural frequency (Hz)			
		f_1	f_2	f_3	f_4
Slab's thickness	13cm	5.96	9.9	13.71	15
	17cm	6.02	9.98	13.55	15.65
Concrete strength	20MPa	5.91	9.77	13.48	15.13
	30MPa	6.01	9.92	13.67	15.43
Columns	HEB180	5.76	9.35	12.83	14.63
	HEB300	6.05	10.05	13.97	15.56
Primary beams	IPE300	5.68	9.81	11.75	14.84
	IPE500	6.11	9.87	14.81	15.52
Edge secondary beams	IPE180	5.8	9.21	13.51	14.68
	IPE400	6.72	13.63	14.82	20.36
Intermediate secondary beams	IPE180	5.8	9.81	13.35	15.28
	IPE300	6.86	10.19	14.56	15.28
Intermediate beams	Rigid connection	6.06	9.88	13.69	15.29
Intermediate beams	1 beam	5.6	9.62	13.14	15.24
	3 beams	6.25	10.06	13.88	15.37
Intermediate columns	1 beam	5.94	9.63	15.94	16.64
	2 beams	8.91	12.62	19.09	21.74

Table 3.3: Floor natural frequencies for each parameter variation

- **Discussion**

To satisfy the second requirement presented in Section 3.2.1.2, the fundamental mode of vibration should have a natural frequency below 10Hz whereas higher modes should have a natural frequency exceeding 10Hz. As can be noticed from Table 3.3, characteristics that had negligible effect on natural frequencies are slab thickness, concrete strength, column profile, primary beam profile, intermediate beam profile and number of intermediate beams. When varying these characteristics, the second mode of vibration had a natural frequency near 10Hz, relatively close to the fundamental frequency.

However, when the edge secondary beams were of IPE400 profile (same as primary beams), the fundamental frequency was 6.72Hz, well-separated from the second natural frequency of 13.63Hz. The same remark is made for the case when two intermediate columns were considered at the middle of the floor, where the floor was much stiffer, leading to a fundamental frequency of 8.91Hz and a second natural frequency of 12.62Hz. Among these two situations,

the first is more economical (four columns instead of six) and provides more convenient results in terms of natural frequency.

3.2.3 Final floor configuration and design

3.2.3.1 Final floor configuration

Remaining characteristics of the floor were chosen according to the parametric study presented in Section 3.2.2. Composite slab properties were the same as for the initial floor configuration (see Section 3.2.2.2), with a thickness of 15cm and a concrete class of C25/30. Reinforcements were placed at 40mm below the upper portion of the slab thickness. Four columns consisting of HEB240 profiles were positioned at the corners. Two simply-supported intermediate secondary beams were considered (with 2.6m spacing). However, the profile was taken as IPE240 to meet connection requirements. For primary and edge secondary beams (having rigid connections), the steel construction company proposed to build-up welded I-members with a web of 400×6 and flanges of 150×15. This profile had a moment of inertia for the strong axis of about 22584cm^4, close to that of IPE400 profile (23130cm^4).

Modal analysis was performed using the FEM model presented in Section 3.2.2.1. Natural frequencies of the four natural modes are provided in Table 3.4. The modal shape of the fundamental mode is illustrated in Figure 3.4. It can be seen that the second requirement of Section 3.2.1.2 (dominant fundamental mode with natural frequency below 10Hz) is well satisfied with the proposed configuration.

Mode	1	2	3	4
Natural frequency (Hz)	7.02	14.05	14.88	23.80

Table 3.4: Natural frequencies of the final configuration

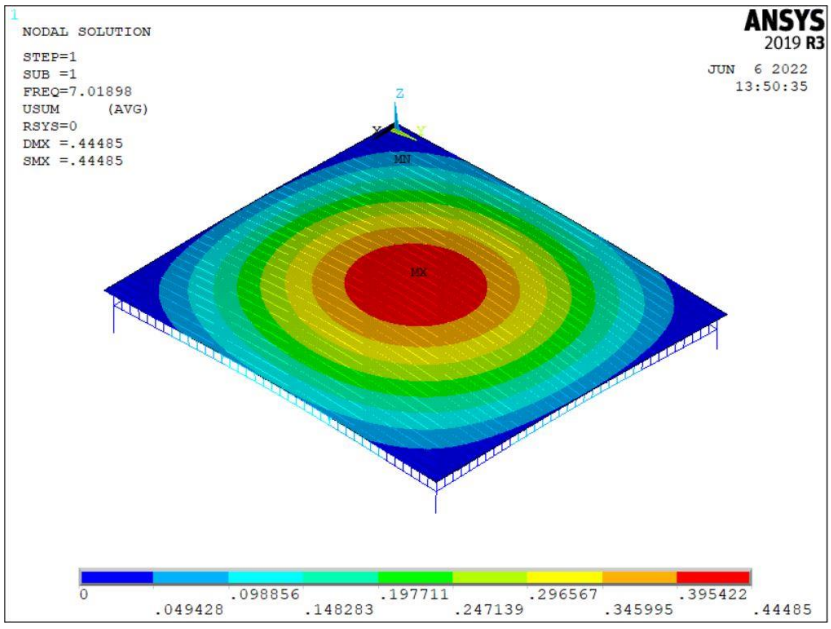

Figure 3.4: Modal shape of the fundamental mode

Various drawings of the final configuration of the floor are presented in Figure 3.5. Further details regarding connection between steel members are provided in Appendix A.1.

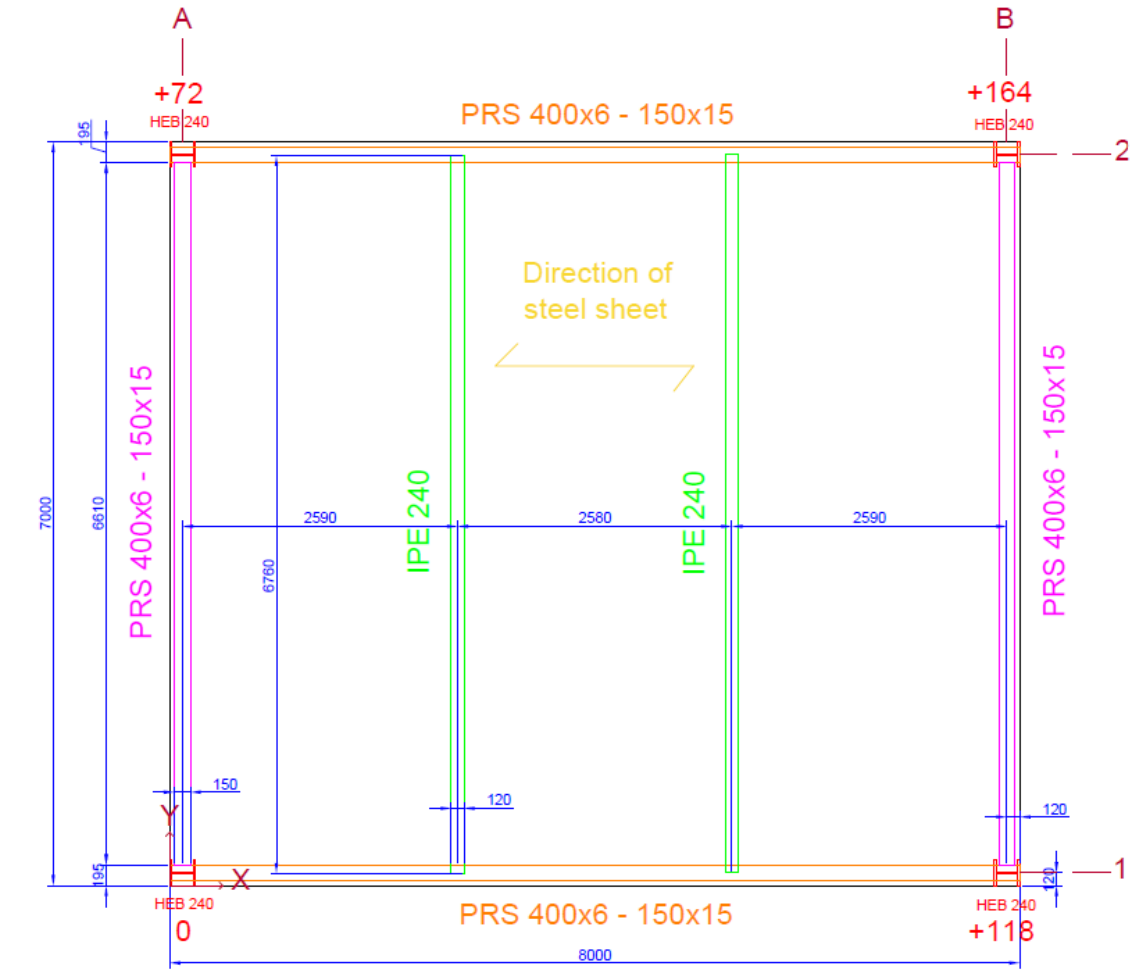

(a) Plan view

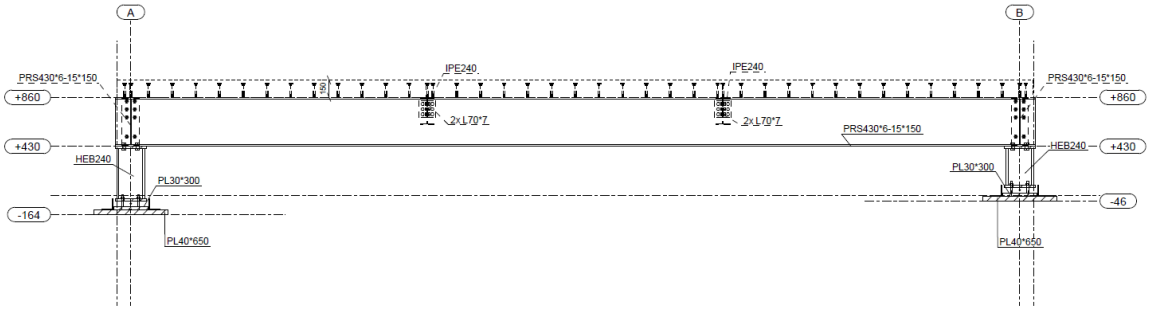

(b) Front view (columns A1 and B1)

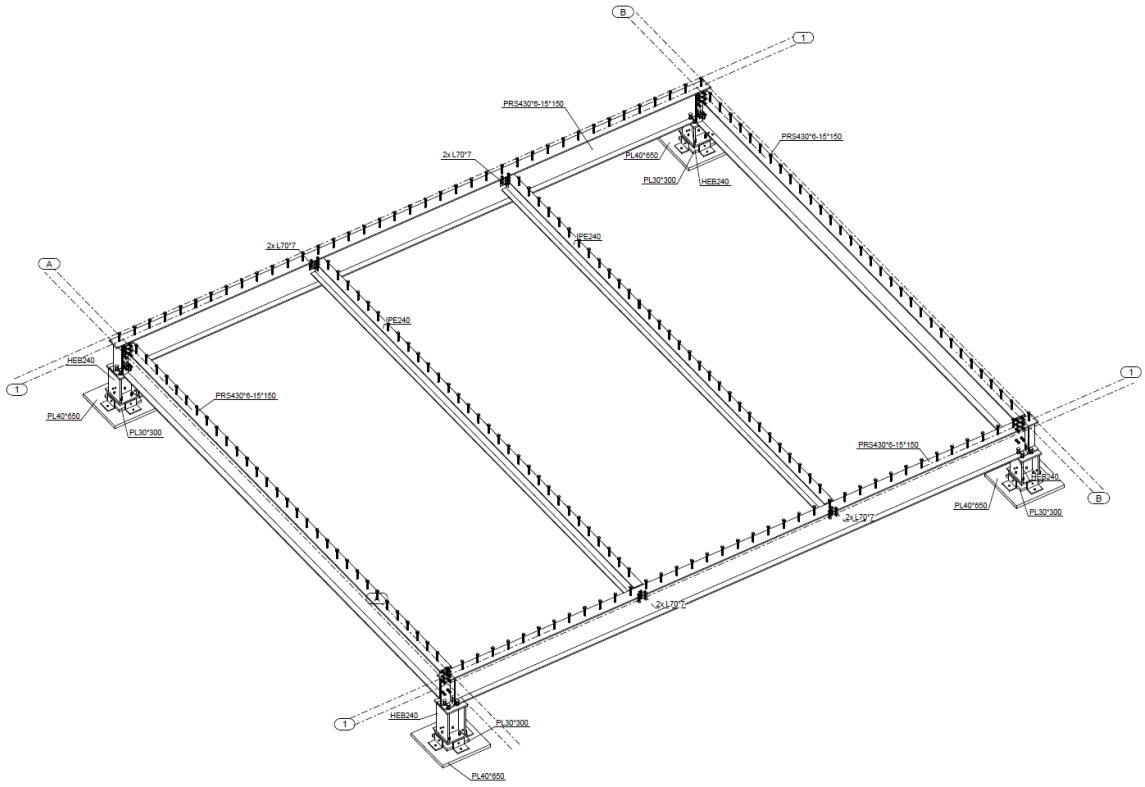

(c) Perspective view

Figure 3.5: Final floor specimen layout (dimensions in mm)

3.2.3.2 Design under static loads

In order to meet the first requirement presented in Section 3.2.1.2 (adequate floor strength to ensure the safety of participants), the floor was designed to support the following static loads:

- The self-weight of the floor (total mass of 18.64t): G = 3.33kN/m²;
- The weight of 16 participants for the worst load case. In fact, the weight of each individual was considered equal to 100kg, amplified by a factor of 1.8, which is the first Fourier coefficient related to "normal jumping" activity proposed by SCI P354 guideline [81]. This gives a live load Q_1 = 0.52kN/m²;
- Equipment live loads: Q_2 = 0.48kN/m², which results in a total live load applied to the floor $Q = Q_1 + Q_2$ = 1kN/m².

The floor elements were designed at the Ultimate Limit State (ULS) according to Eurocode prescriptions (Eurocode 2 [36] for reinforced concrete slab, Eurocode 4 [38] for composite beams and Eurocode 3 [37] for columns and connections) with a load combination of $1.35G+1.5Q$. Composite beams were also designed at the Serviceability Limit State (SLS) according to Eurocode 4 with a load combination of $G+Q$, considering a shrinkage of about 170µm/m for the concrete slab (60 days after the slab pouring). Details regarding the static design of the floor are presented in [30].

3.2.3.3 Floor response simulation

When rhythmic activities are performed on the floor, the total applied force F is given by:

$$F = M(a - g) \tag{3.4}$$

Here, M is the mass of the floor, g the gravity acceleration and a the acceleration of the floor due to rhythmic excitation. This force is directed downwards in major cases, but this direction could change if the acceleration a exceeds g (causing an uplift of the floor). To verify that such phenomenon will not take place, the floor response under crowd loads was investigated.

Calculation has been made considering only the fundamental mode of vibration having a natural frequency of 7.02Hz and a modal shape presented in Figure 3.4. Remaining modal parameters were determined according to HiVoSS guideline [40]. The damping ratio was taken equal to 1% as proposed by this guideline for bare steel-concrete composite floors. Given rigid connections between edge beams, the modal mass of the floor was considered equivalent to that of a double-clamped beam, expressed as follows [40]: $M_1 = 0.41M$. With a total floor mass of 18.64t, the obtained modal mass was then $M_1 = 7.64$t.

The loading scenario corresponds to 16 individuals jumping on the floor according to a uniform distribution as presented in Figure 3.6. The load model used to simulate jumping activity has been proposed by Ellis and Ji [31], including individual model and crowd size relations (given by Eq. (2.23)). The load parameters were chosen to represent the worst possible case (see Table 2.15). Each individual's mass was taken equal to 100kg and the excitation frequency equal to 2.4Hz, causing resonance at the third harmonic of the load (7.2Hz). The floor response was calculated at the centre, for a duration of 60s and a time step of 0.005s.

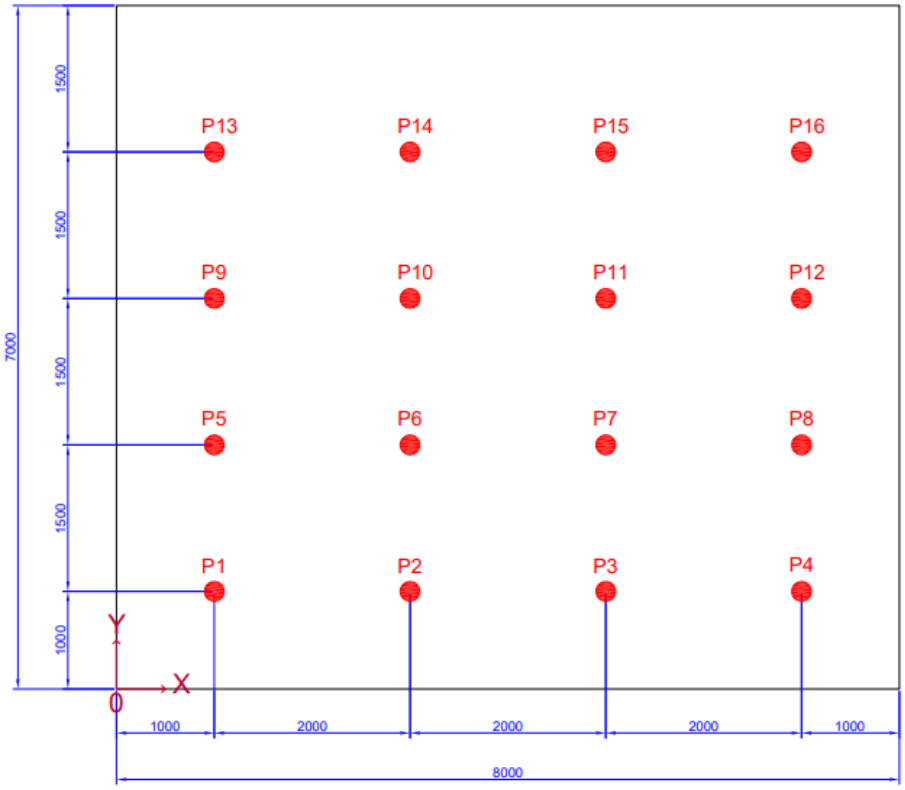

Figure 3.6: Positions of 16 individuals for response calculation (dimensions in mm)

A MATLAB script was written to calculate the time domain response of the floor using Newmark-β method (see Section 2.6.1). The resulting acceleration is plotted against time in Figure 3.7. The computed peak acceleration was 5.21m/s², below the gravity acceleration (9.81m/s²). Therefore, the floor is well secured against uplift risk for all possible rhythmic load cases.

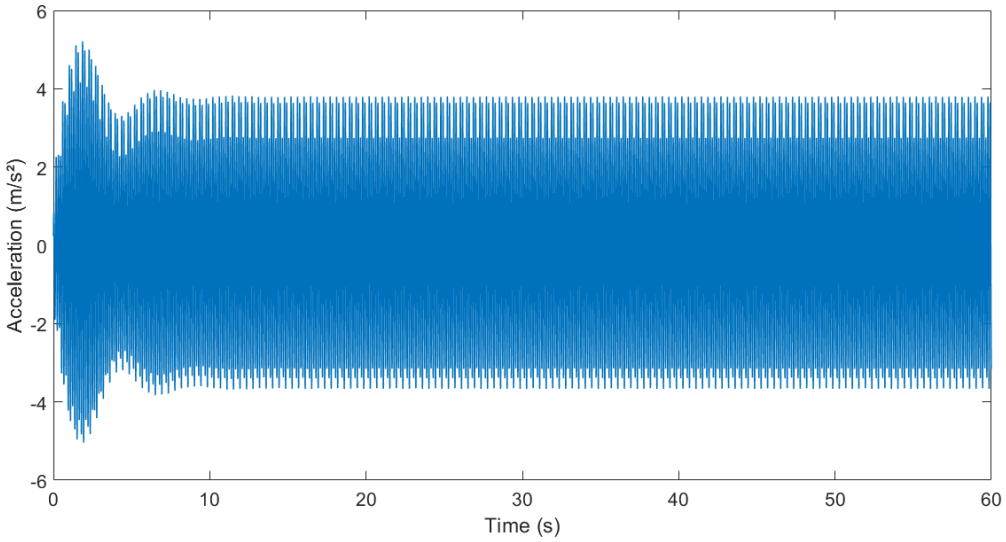

Figure 3.7: Simulated floor acceleration at centre

3.3 First experiments on the constructed floor

After the construction of the floor specimen, experiments were carried out at the structural mechanics laboratory of FCBA technical centre in order to verify the quality of the modelling presented in Section 3.2. Deflection tests along with Experimental Modal Analysis on the structure are first described. Resulting modal parameters are then compared against Finite Element Analysis.

3.3.1 Construction and deflection tests

The steel-concrete composite floor was erected according to the steps described in Appendix A.2. A side view of the floor 28 days after erection is shown in Figure 3.8. At that time, measured compressive strength and Young's modulus of the concrete slab (see Appendix A.3) were 29.8MPa and 28.1GPa, respectively.

Figure 3.8: Side view of the floor specimen

The first field tests on the floor aimed at determining the floor's stiffness. For that purpose, deflections have been measured using comparator devices labelled C1 to C4 (see Figure 3.9(a)) located at four positions below the floor, two at each intermediate secondary beam (at 1/3 and 2/3 of the span), as can be seen in Figure 3.9(c). The floor was loaded using plumb bags having pre-determined masses (see Figure 3.9(b)). The total masses applied on the floor were 550kg and 1050kg, respectively [13].

(a) Comparator

(b) Plumb bags

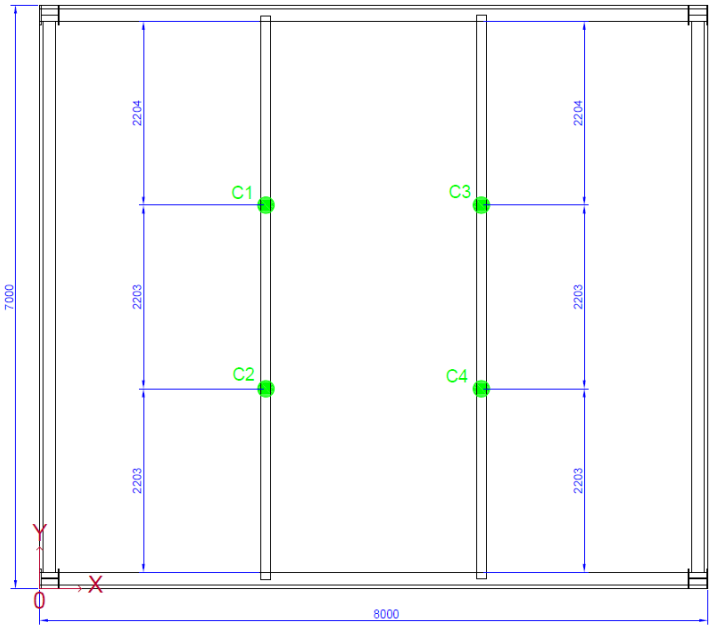

(c) Location of measuring points (dimensions in mm)

Figure 3.9: Deflection test setup

Resulting deflections are plotted as a function of the applied mass in Figure 3.10. A different quasi-linear tendency exists between the four points (maximum relative difference is 42% between C2 and C3). This may be caused by the imperfections of the structure resulting from construction circumstances. However, the difference between deflections gradually decrease for higher applied masses, indicating a limited influence of the imperfections at this load range.

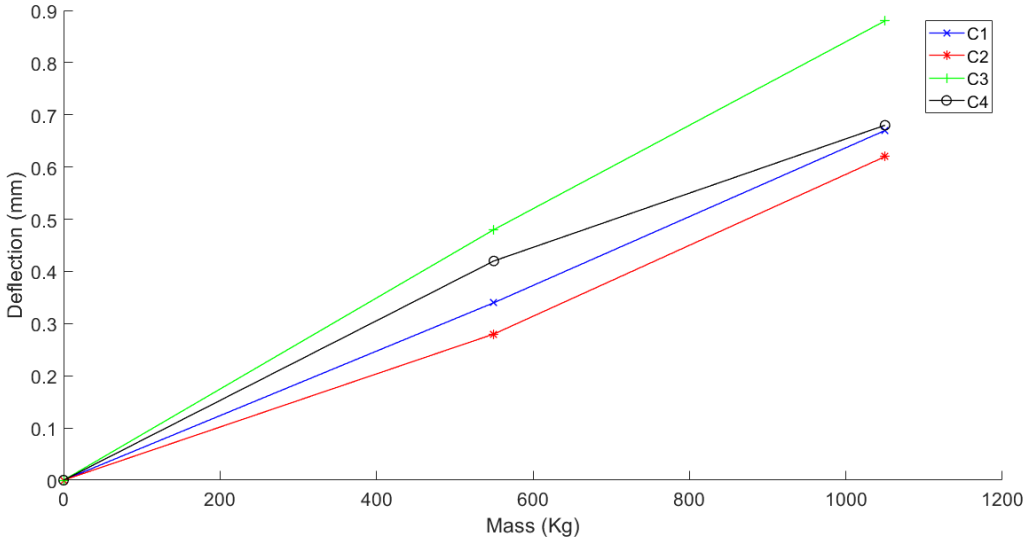

Figure 3.10: Experimental deflection against applied mass

The FEM model of the floor presented in Section 3.2.2 was updated to take into account concrete parameters measured experimentally (compressive strength of 29.8MPa, Young's modulus of 28.1GPa). Simulations were performed to calculate the deflections at the four points presented in Figure 3.9(c) using the two previous loads (550kg and 1050kg). Resulting deflections-mass curves are plotted in Figure 3.11. The deflection of the modelled structure increases linearly with respect to the mass as expected. Closer values between the investigated points are also noticed compared to measured deflections (with a maximum relative difference of 5% between C2 and C3) since experimental imperfections are not considered in the FEM model.

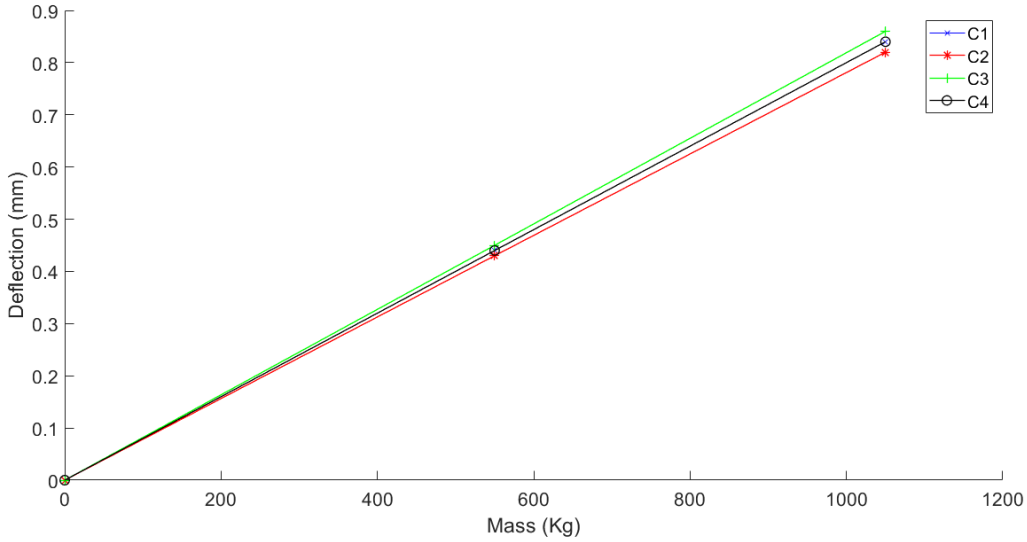

Figure 3.11: Numerical deflection against applied mass

Based on the previous results, the experimental and numerical stiffness are summarized in Table 3.5.

Point	C1	C2	C3	C4
Experimental stiffness (N/mm)	15376	16537	11690	14929
Numerical stiffness (N/mm)	12263	12559	11980	12263

Table 3.5: Floor stiffness by deflection point

The experimental and numerical stiffness have the same order by measuring points, indicating that the updated FEM model is appropriate for deflection calculations. It was found that the mean experimental and numerical stiffness are equal to about 14700N/mm and 12300N/mm, respectively. This difference can be attributed to the fact that connections of intermediate beams are modelled pinned whereas they are actually semi-rigid (see Appendix A.1).

3.3.2 Experimental Modal Analysis

In order to verify whether the built structure was in accordance with the design, modal parameters were determined by means of Experimental Modal Analysis (EMA) [69]. The setup of this campaign is first described and corresponding results are presented.

3.3.2.1 Experimental setup

- **Instrumentation**

Since the floor configuration is rather classical yet with a limited floor surface, the floor excitation was performed using an instrumented hammer [2] (see Figure 3.12(a)). The hammer model is PCB 086D20, which could produce up to 22.5kN of impulsive load amplitude within a wide frequency range. The response of the floor due to these impacts was measured by PCB 3711 accelerometers (see Figure 3.12(b)) having a frequency limit of 1000Hz. Acquisition was made by a Bruël & Kjaer Lan XI data acquisition system.

(a) Instrumented hammer (b) Accelerometer

Figure 3.12: Hammer EMA equipment

- **Test procedure**

First of all, the floor surface was meshed with 121 points (12 points along each line parallel to a longer span, 10 points along each line parallel to a shorter one, and the floor's centre). The distance between points was taken equal to 70cm in both directions, as shown in Figure 3.13(a). Accelerometers were placed at 10 locations over the floor (noted A1 to A10 in Figure 3.13(a)) and fixed on the floor using adhesive tape (see Figure 3.13(b)).

At each mesh point, an impact was performed by the hammer (see Figure 3.13(c)), and the corresponding load and acceleration responses were measured. The Frequency Response Function (FRF) $H(\omega)$ was then calculated for each response point by:

$$H(\omega) = \frac{A(\omega)}{F(\omega)} \tag{3.5}$$

where $A(\omega)$ is the Fourier transform of the acceleration and $F(\omega)$ the Fourier transform of the load. The impact was applied three consecutive times and the average of FRFs was then computed.

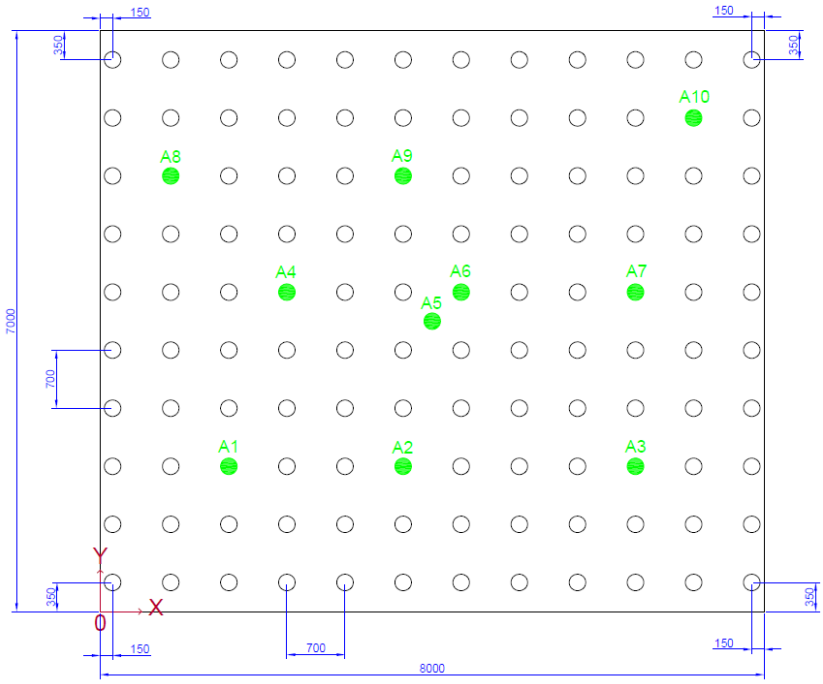

(a) Mesh and response points (dimensions in mm)

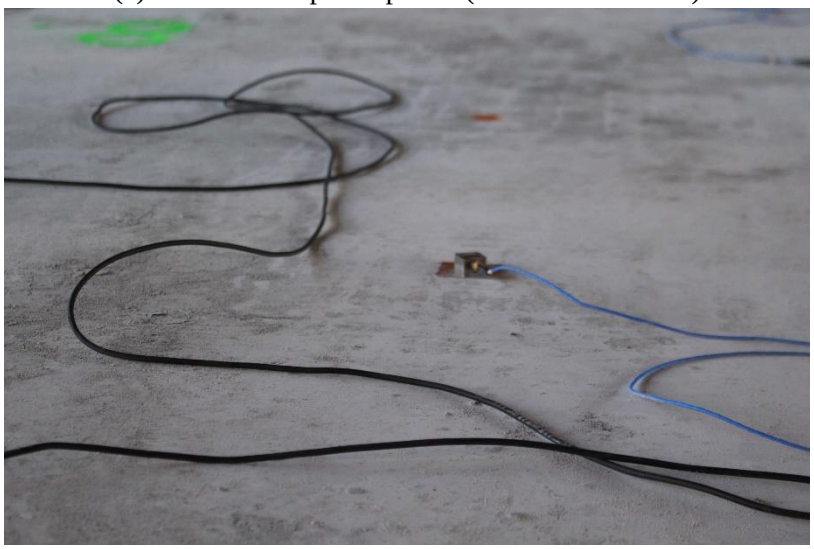

(b) Accelerometer placed on the floor

(c) Hammer impact on the floor

Figure 3.13: Hammer EMA setup

Successive impacts at all points of the mesh allow constructing a FRF matrix with dimensions 10×121 (10 response points, 121 excitation points) for each frequency. Since the FRF matrix is symmetric for linear systems due to Maxwell's Reciprocity Theorem [2], the transpose of FRF matrix (121×10) was used in modal extraction.

3.3.2.2 Experimental results

The floor modal parameters were extracted using BK Connect [13]. First, FRFs determined previously were condensed to obtain a function called Complex Mode Indication Function (CMIF), characterizing the dynamic behaviour of the structure [79]. An initial curve fitting of the plotted CMIF as a function of frequency was then performed (see Figure 3.14). A stability diagram was built-up afterwards using Rational Fraction Polynomial Method [74], where each mode was characterized by a vertical line illustrating successive iterations related to modal parameters (red diamonds in Figure 3.14). Identified natural modes were those presenting stable results after a certain number of iterations. Subsequently, natural frequencies, damping ratios and modal shapes could be determined using the first stable results (white circles with black contours in Figure 3.14).

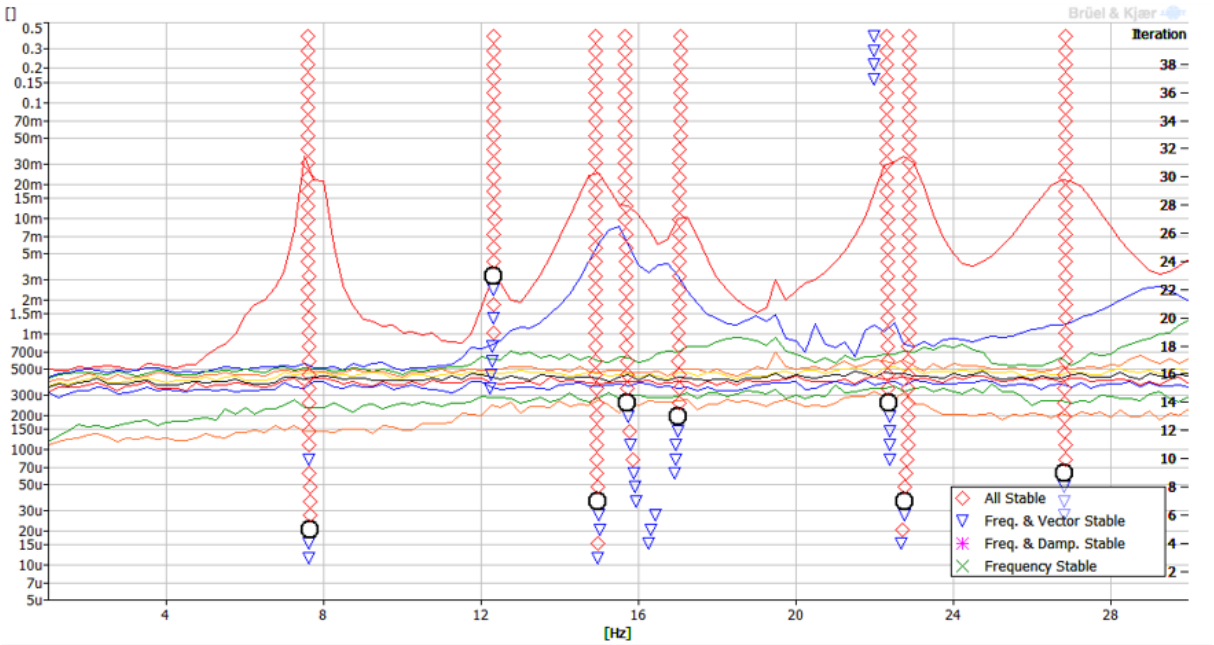

Figure 3.14: CMIF plot and stability diagram after modal extraction [13]

Modal extraction was done for frequencies ranging between 0 and 20Hz, which resulted in five natural modes. Table 3.6 summarizes associated natural frequencies and damping ratios, and Figure 3.15 illustrates modal shapes of the first four modes.

Mode	Natural frequency (Hz)	Damping ratio (%)
1	7.65	2.92
2	12.33	1.90
3	14.98	3.42
4	15.74	3.95
5	17.02	2.96

Table 3.6: Experimental modal properties

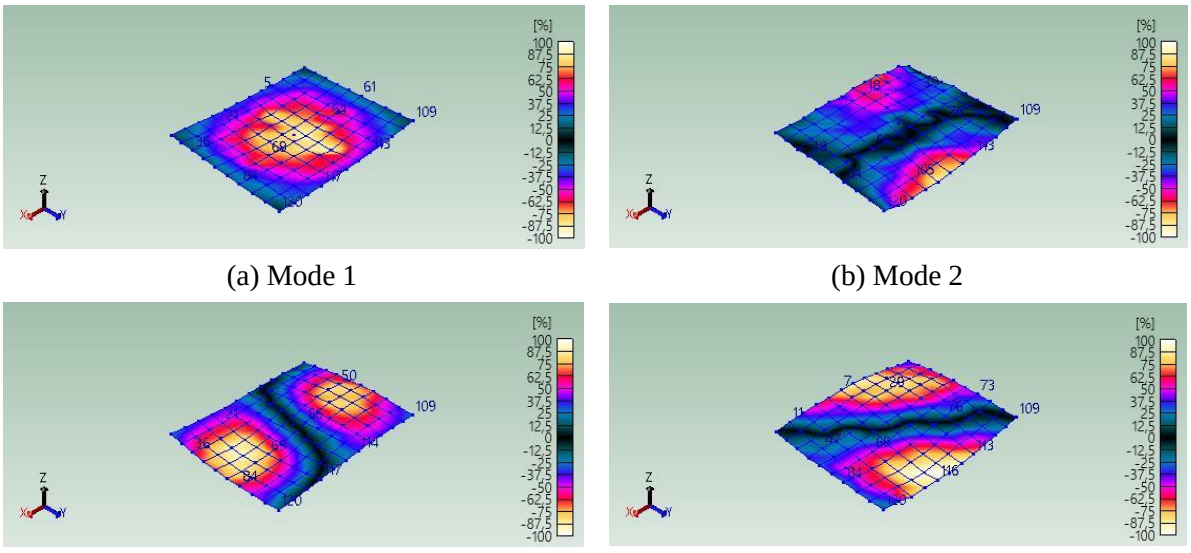

(a) Mode 1 (b) Mode 2

(c) Mode 3 (d) Mode 4

Figure 3.15: Experimental modal shapes

3.3.3 Comparison against numerical results

For comparison purposes, numerical modal analysis of the floor was performed using the updated FEM model (see Section 3.3.1). However, since concrete becomes stiffer when subjected to dynamic loads ([40], [63], [81]), the corresponding Young's modulus was increased by 35% ([16], [63]). Obtained natural frequencies of the first four modes are given in Table 3.7 and corresponding modal shapes are presented in Figure 3.16.

Mode	1	2	3	4
Natural frequency (Hz)	7.30	14.38	15.42	24.51

Table 3.7: Natural frequencies from the updated FEM model

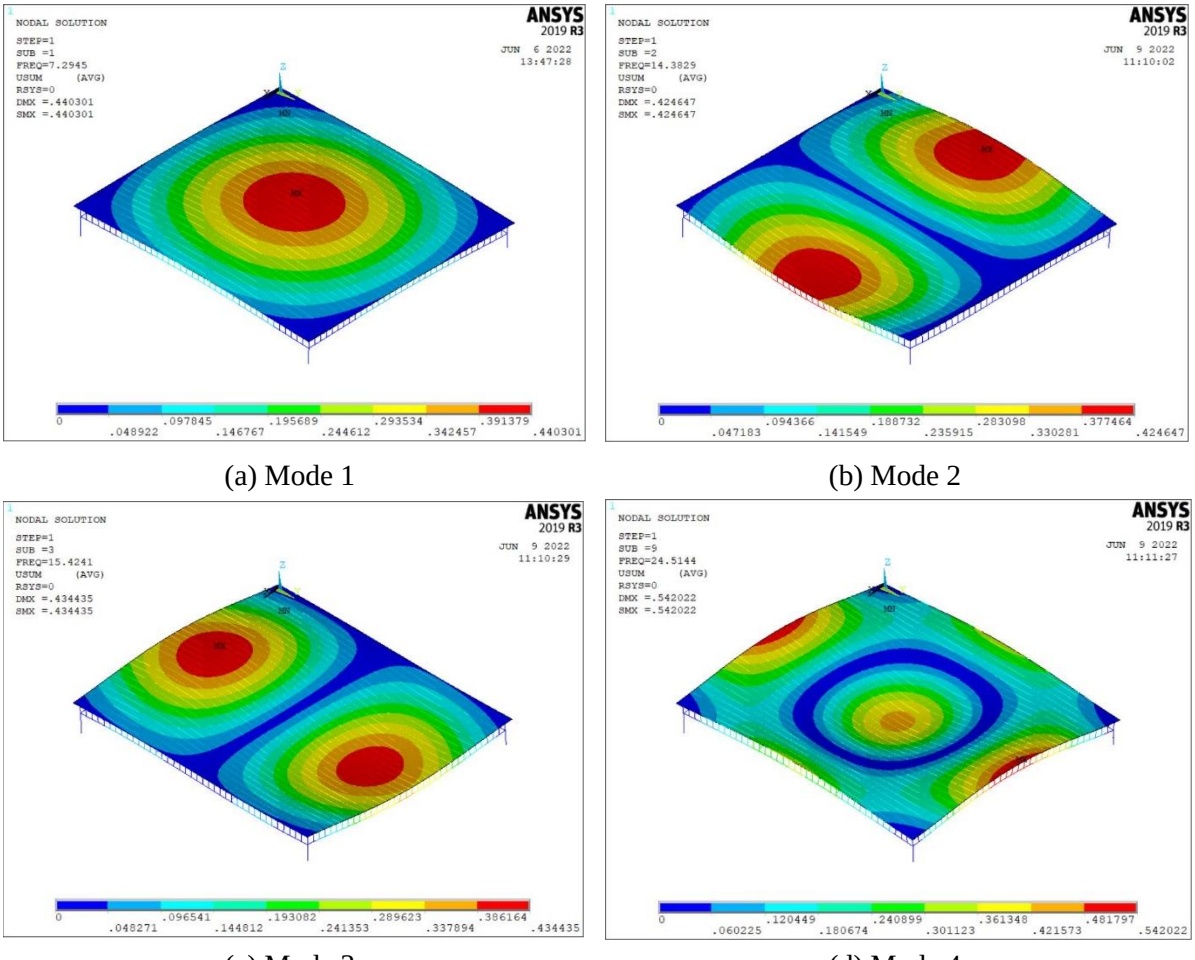

(a) Mode 1 (b) Mode 2

(c) Mode 3 (d) Mode 4

Figure 3.16: Numerical modal shapes

Experimental Modal Analysis resulted in only one mode having natural frequency below 10Hz, clearly distinct from higher natural modes. This corresponds to what was expected by the numerical model and satisfies the second requirement of Section 3.2.1.2 (dominant fundamental mode with natural frequency below 10Hz). Furthermore, the experimental and numerical fundamental modal shapes are similar, with a maximum amplitude near the floor centre. However, the fundamental frequency obtained experimentally (7.65Hz) is 5% higher than its numerical counterpart (7.30Hz). This is probably due to the lower stiffness in the FEM model compared to the actual floor as concluded from deflection analysis (see Section 3.3.1).

Differences are especially noticeable for higher modes, but their influence is overlooked since they would not be excited by human activities.

3.4 Vibration tests under crowd-rhythmic activities

Vibration tests were performed at the structural mechanics laboratory of FCBA technical centre on the floor specimen presented in Section 3.2 involving crowd-rhythmic activities. Adopted instrumentation for the test campaign is described first, followed by a presentation of the experimental setup. This includes involved rhythmic activities, crowd sizes and positions, type of coordination stimulus, timing and repetitions. Characteristics of the individuals participating in the tests are also provided.

3.4.1 Instrumentation

3.4.1.1 Force measurements

When a group of people performs rhythmic excitation, corresponding forces are mainly acting vertically on the floor structure. Direct measurement of such forces can be accomplished by two principal techniques [73]. The first one consists of placing force plates (see Figure 3.17(a)) on each position of the participants. Individual loads are then measured while performing rhythmic excitations. This method was implemented by Parkhouse and Ewins [65] who measured individual jumping loads produced by 60 different participants one after another. Pernica [67] also used force plates to record loads for up to 8 persons performing rhythmic excitations. Although this technique allows to investigate experimental group effects for each person and trigger its variation during motion, it is not practical for a large crowd size. In fact, the maximum number of individual force plates used for crowd experiments as stated by Comer et al. [18] corresponds to 15 individuals jumping simultaneously. Moreover, the motion of each individual is restricted by the area of the force platform, such that he could not freely practice the activity which is characterized by a forward-backward and sideway movements.

Alternatively, human-induced forces can be measured by setting load cells (see Figure 3.17(b)) at specific locations on the floor. The total load produced by large crowds could then be measured without restricting their motion. This device was used by Alves et al. [3] to measure individual loads for various activities (involving jumping) and by Ebrahimpour and Sack [27] to record jumping forces for up to 40 individuals.

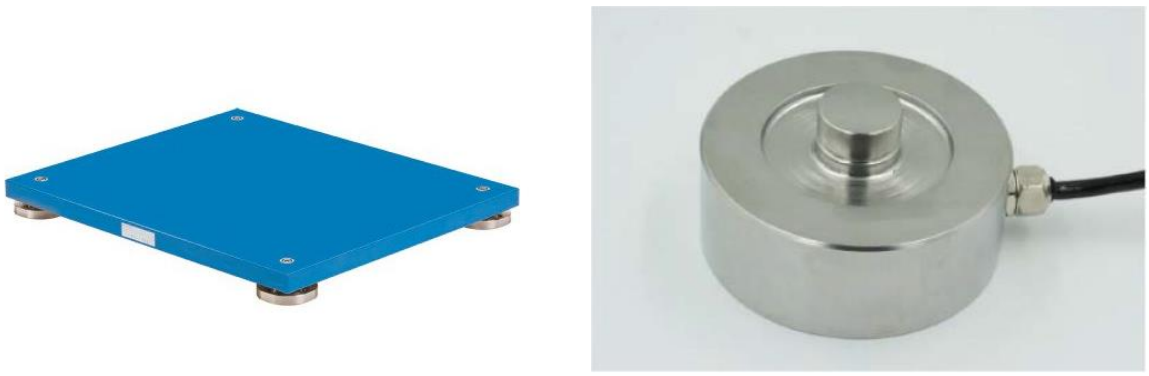

(a) Force plate (b) LC-C110C load cell

Figure 3.17: Force measurement devices

For the previous reasons, load cells were selected to measure vertical crowd-rhythmic loads. Effectively, four load cells were placed at the bottom of each floor column, and the total group-induced loading applied on the floor during rhythmic activities could be obtained by summing the four measured loads after eliminating the floor inertial force. The principal requirement to select the device model to be used is the maximum load to be measured. The total expected static load was 6kN/m² (see Section 3.2.3.2), which gives 8.5t supported by each column. Instrumentys LC-C110C load cells (see Figure 3.17(b)) with a capacity of 10t have then been adopted for safety considerations. These devices were tested for loads between 1 and 90kN, providing a measurement with a discrepancy of ±3%. Calibration has been made to have balanced measurements over the floor. The four load cells approximately measured the same load (25% of the weight of the floor) at the bare state of the floor.

After summing these loads, the total mass of the floor was equal to 18.85t. The modal mass of the fundamental natural mode of the floor could then be determined by the same method as presented in Section 3.2.3.3, considering the actual mass of the floor determined above, which gives: $M_1 = 0.41M = 7.73$t.

3.4.1.2 Response measurements

The response of the floor specimen subjected to crowd-rhythmic activities was measured. The aim was to investigate response amplitudes and to validate the associated load models. Proposed response parameter was the vertical displacement of the floor. One response point was assumed sufficient to capture the vibrational behaviour of such a classical structure. This practice has been made by Ellis and Ji [31], who measured displacements at the centre of two laboratory floors subjected to crowd-jumping loads.

Maximum expected displacement has been determined from the analysis carried out in Section 3.2.3.3, according to the worst possible floor loading scenario. It resulted in a displacement of 3.1mm. Linear Variable Differential Transformer (LVDT) device was adopted for such measurements. Associated model is ACT1000C transducer having a measurement range of ±25mm. The LVDT was placed below the floor at the mid-span of an intermediate beam (see Figure 3.18), which is considered as a fixed reference support.

Figure 3.18: LVDT device placed below the floor

3.4.1.3 Auxiliary instruments

The load cells and the LVDT transducer were connected to a Bruël & Kjaer Lan XI data acquisition system for signal conditioning and digitalization. The adopted sampling frequency was 128Hz for both measurement devices. Furthermore, a lightweight barrier was placed along three edges of the floor to ensure the safety of participants (see Figure 3.19).

Figure 3.19: Floor with edge barriers

3.4.2 Description of crowd-rhythmic tests

3.4.2.1 Investigated rhythmic activities

There are several rhythmic activities in which people stay at a fixed position and lose contact with the ground. The most classical one is normal jumping ([33], [50]), where an individual is launching himself in the vertical direction and returning to the ground with an impact. This activity has been widely studied by several authors for either individual ([3], [65]) or crowd cases ([18], [27], [31]). However, other jumping-type activities are commonly encountered in some usages (such as fitness centres). These activities could also produce higher loads, as found by Pernica [67] for stride jumps, which had greater Dynamic Load Factors (DLFs) than normal jumping for the case of 4 persons.

Among these activities, two jumping-type ones were investigated in this research. The first is jumping jack, where the arms move up with the outward movement of the legs and down with their inward movement for each jumping cycle. The second is quick jumping, similar to normal jumping, but the individual returns quickly to the ground due to a more limited duration of the launching phase. These activities are performed in sport venues, fitness centres, stadiums, etc. and illustrated in Figure 3.20.

(a) Jumping jack (b) Quick jumping

Figure 3.20: Jumping activities

Moreover, apart from jumping-type loads, there is a category of rhythmic activities where people practice running while remaining approximately at the same location. This type of activity is called running-on-the-spot [67], stepping [4], or skipping [7], and is likely to occur in gymnasiums, sports halls and other facilities. In this research, skipping (the adopted term in the rest of the manuscript) was investigated in terms of two contact modes with the ground: on feet toes and on feet soles as shown in Figure 3.21.

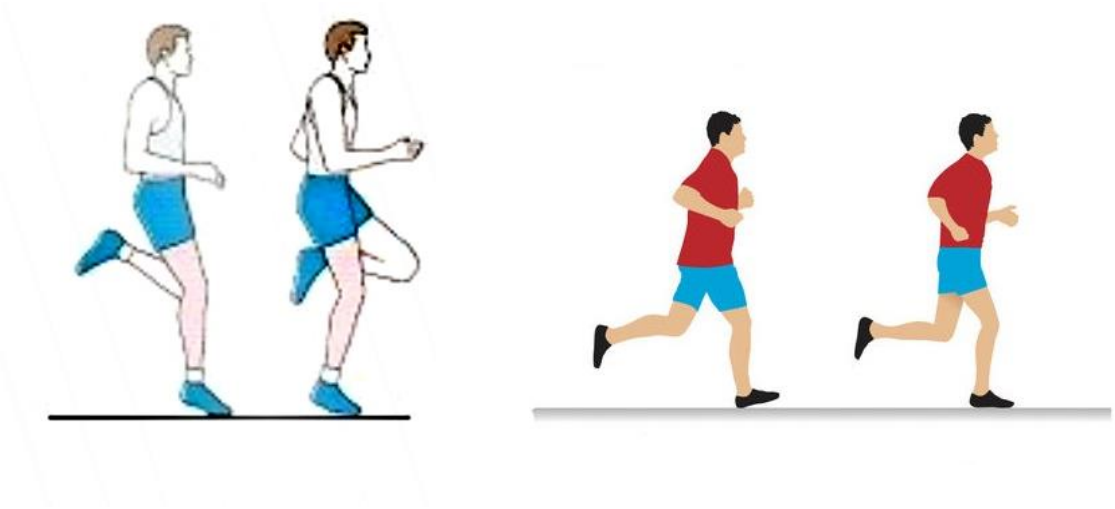

(a) Skipping on feet toes (b) Skipping on feet soles

Figure 3.21: Skipping activities

In general, skipping loads have higher frequencies but lower amplitudes than jumping loads [4]. The adopted terminology for the investigated activities (throughout all chapters) is presented in Table 3.8.

Activity	Terminology
Jumping jack	Jumping 1
Quick jumping	Jumping 2
Skipping on feet toes	Skipping 1
Skipping on feet soles	Skipping 2

Table 3.8: Adopted terminology for rhythmic activities

3.4.2.2 Experimental setup

- **Crowd sizes and positions**

It was considered that substantial effects on loads and responses would be observed through stepwise changes of group size [31]. In general, such activities are performed in well-spaced environments, resulting in reduced load densities ([44], [50]). The maximum crowd size allowed by the floor surface to have a limited density (1 person/3m²) was 16 individuals. Therefore, tests were carried out with numbers of 1, 2, 4, 8 and 16 participants. Figure 3.22 illustrates one performed activity for each investigated crowd size.

(a) 1 participant

(b) 2 participants

(c) 4 participants

(d) 8 participants

(e) 16 participants

Figure 3.22: Examples of rhythmic activities by crowd size performed on the laboratory floor

The participants were uniformly distributed over the floor according to positions shown in Figure 3.23. This corresponds to a spacing between individuals equal to 2.1m in the direction parallel to a longer span and 1.4m in the direction parallel to a shorter one. Table 3.9 indicates adopted positions for each group size.

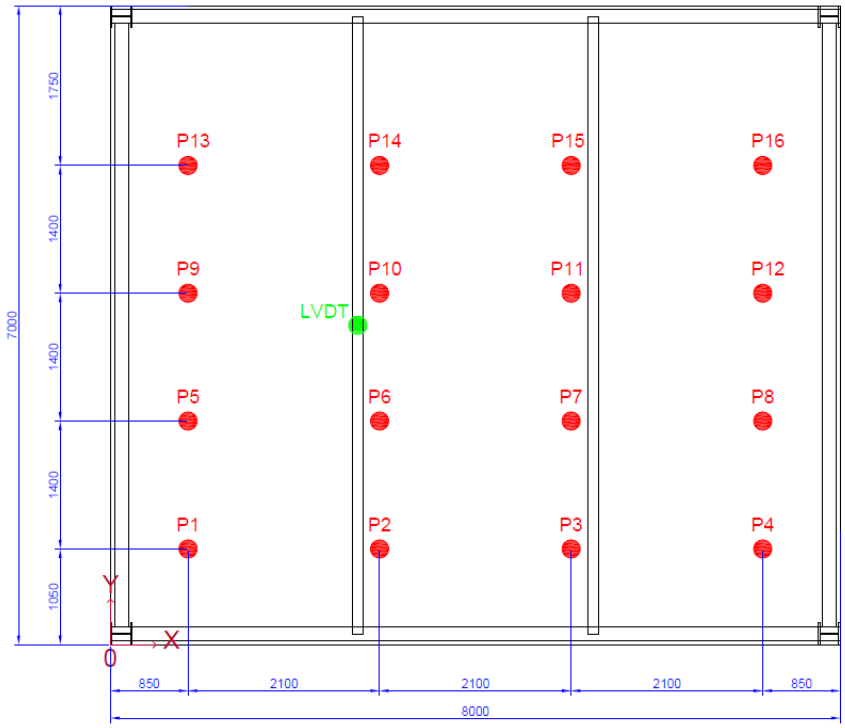

Figure 3.23: Positions of individuals in red circles and LVDT in green circle (dimensions in mm)

Crowd size	Positions
1	P11
2	P6, P11
4	P6, P7, P10, P11
8	from P5 to P12
16	from P1 to P16

Table 3.9: Positions of individuals by crowd size

- **Coordination stimulus**

The degree of coordination between individuals in rhythmic activities varies [45]. In order to achieve a high coordination degree, various external stimulus are possible. The first stimulus type is audible, which could be realized either by a metronome set at different frequencies ([3], [18], [27], [31], [65], [67]), or by a rhythmical song [34]. The second stimulus type is visual, ensured by following the movement of a person coaching away from the floor [39] or by watching a video of the performed activity displayed on a front screen [65].

The stimulus leading to a coordination which is the most likely to occur in real life situations are a rhythmical song (audible), combined with the movement of a person outside the floor surface (visual). Both stimulus were used in the performed tests. The visual stimulus was made by an experienced sports coach standing in front of the participants (see Figure 3.24). Moreover, participants were requested to perform rhythmic activities at their comfortable pace.

Figure 3.24: Sports coach in front of participants

- **Timing and repetitions**

Before each activity, a preliminary test was made during 30s so that participants could warm-up and get used to the activity movements. Then, individuals performed continuous movements during 45s, since people are likely to be tired after this duration [18]. For each investigated crowd size and rhythmic activity, the sequence was repeated three times, and the whole set was repeated two times, as noted in Table 3.10. Repetitions were adopted in order to take into account variabilities observed during motion [71] and to have a statistically representative sample of records. In total, experimental testing lasted about one and a half day.

Set 1		Set 2	
Preliminary test	Rhythmic test	Preliminary test	Rhythmic test
30s	45s × 3	30s	45s × 3

Table 3.10: Duration of sets for each activity and crowd size

3.4.2.3 Characteristics of the participants

A group of 33 individuals (all volunteers) participated in crowd-rhythmic tests, comprising 18 men and 15 women. Participants were majorly post-graduate students or staff of FCBA technical centre. Prior to starting experiments, the test protocol was briefly described to all involved persons. Data related to participants included sex, weights, ages and birth countries and are summarized in Table 3.11.

Individual	Sex	Age	Birth country	Body mass (kg)
1	Male	29	France	85
2	Female	31	Algeria	63.9
3	Female	28	France	63
4	Male	30	France	82.5
5	Male	39	Algeria	79.7
6	Male	24	France	84.7
7	Male	30	Morocco	72.5
8	Female	27	Algeria	58.8
9	Female	25	Morocco	66.1
10	Male	30	Congo	65
11	Female	24	France	64.4
12	Female	54	France	66
13	Male	52	France	78.3
14	Female	46	France	70
15	Female	50	France	60
16	Male	42	France	78.3
17	Male	32	France	80.5
18	Female	32	France	76.2
19	Male	48	France	86.6
20	Female	55	France	58.8
21	Female	53	France	67.7
22	Male	60	Yugoslavia	78.4
23	Female	43	France	58.6
24	Male	19	France	73
25	Male	55	Morocco	92.8
26	Female	47	France	65.6
27	Male	23	Réunion, France	108
28	Female	30	France	66
29	Male	29	France	61
30	Male	31	France	105.3
31	Male	31	Nigeria	70.3
32	Female	23	France	61
33	Male	43	France	78.6

Table 3.11: Collected data related to test participants

According to Table 3.11, 24 participants were born in European countries whereas 9 participants came from African ones. Their ages ranged between 19 and 60 years (mean: 37 years, standard deviation: 12 years) and their body masses varied from 58.6 to 108kg (mean: 73.5kg, standard deviation: 12.4kg). The mean mass is close to the nominal body mass suggested by several design recommendations (SCI P354 guideline [81] for example). Figure 3.25 illustrates body mass and age distributions, indicating that the sample of participants is quite representative of the whole population.

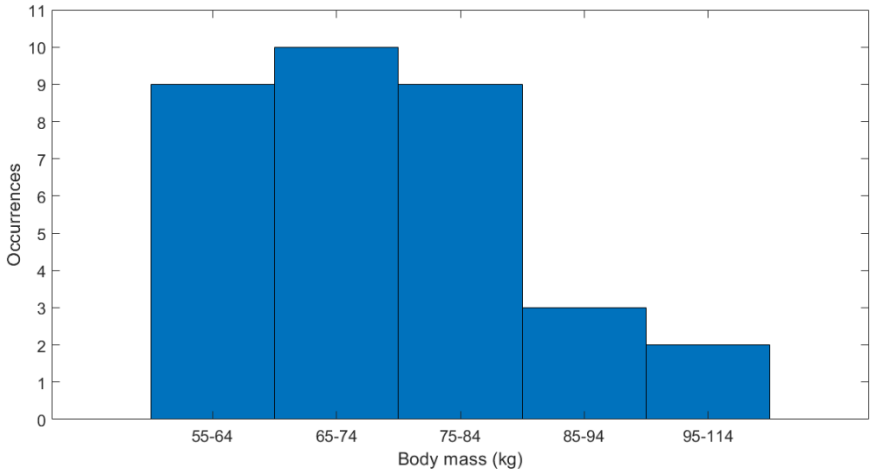

(a) Body mass

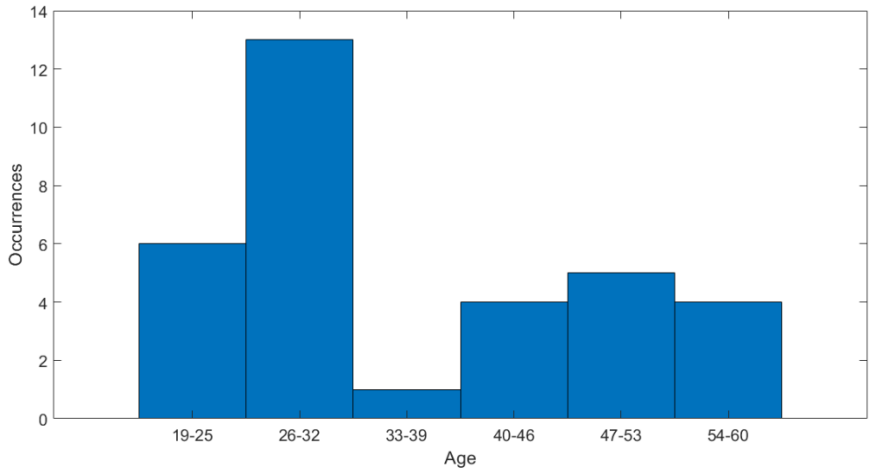

(b) Age

Figure 3.25: Distribution of parameters related to participants

3.5 Conclusions

This chapter describes a test campaign aiming to investigate the vibration of floors when subjected to crowd-rhythmic activities. A floor specimen representing steel-concrete composite floors was firstly designed to resist vertical loads and to have only one mode than can be excited by human-induced loads (with a natural frequency below 10Hz). After erection, deflection tests conducted on the floor specimen revealed that the numerical stiffness of the floor is lower than the experimental one. Experimental Modal Analysis carried out on the laboratory floor using hammer impacts confirmed the existence of one mode with a natural frequency below 10Hz. The obtained value is higher by 5% than its numerical counterpart, because more flexible connections were considered in the FEM model of the floor. Human-induced vibration tests were then realized involving four rhythmic activities usually encountered in practice (jumping jack, quick jumping, skipping on feet toes, skipping on feet soles). Groups of up to 16 individuals were uniformly distributed over the floor (with a density of 1 person/3m²). Participants were asked to move following audible and visual stimulus to be as close as possible to real life situations. Test results in terms of forces and displacements are dedicated to the identification of a load model characterizing crowd-rhythmic activities as will be presented in the next chapter.

4 Spectral load model identification for crowd-rhythmic activities

4.1 Introduction

Appropriate modelling of human-induced loads is a pre-requisite for the serviceability assessment of floors against human discomfort, especially when they are subjected to crowd-rhythmic activities with loss of contact [50]. As developed in Chapter 2, several models were established for such activities. Most of them were expressed in the time domain, which do not account for "intra-subject variability" as observed experimentally. Time domain load models are also unable to excite multiple dominant natural modes simultaneously. On the other hand, few frequency domain models were developed to circumvent these limitations.

This chapter has two main objectives. The first one is to present a load modelling approach in the frequency domain which is simple to handle yet appropriate for crowd-rhythmic activities. The proposed model is expressed as a Power Spectral Density (PSD) function for a single person, combined with coordination factors for multiple individuals. The second objective is to identify the parameters of the above established load model based on the vibration tests carried out on the laboratory floor described in Chapter 3. Two particular types of rhythmic activity (detailed in Section 3.4.2) are investigated, where corresponding load models are identified, and the model response is compared with measurements.

4.2 Rhythmic load model identification methods

The crowd-rhythmic load was modelled in the literature in two major ways. The first consists of a time domain load model for the case of a single person, with crowd size relations provided to take into account the reduction of the crowd load due to the lack of coordination between individuals in the group. The second was based on a random field approach, comprising a PSD function for one individual and a coherence function to consider the synchronization between multiple persons. This section presents a load modelling approach for crowd-rhythmic activities that combines the two previous procedures. A simplified PSD load model formulation is first established. A direct identification method is detailed in order to determine load parameters based on force measurements on the floor. Coordination factors are then obtained by size-dependent relations of crowd forces obtained for each number of participants. Finally, the total crowd load model is formulated using the PSD load model together with coordination factors, and the procedure for the verification of such model using response measurements on the floor is described.

4.2.1 Single PSD load model

4.2.1.1 Direct identification of individual load models

Based on direct force measurements on floor structures, load models for a single person performing rhythmic activities were identified by several authors. These models were generally expressed in the time domain, either as Fourier series decomposition or a succession of jumping pulses (see Section 2.2). For the first load model type, Dynamic Load Factors (DLFs) were identified based on the frequency domain representation of the measured forces. Pernica [67] and Yao et al. [92] determined DLFs from peaks of each harmonic component obtained by Fast Fourier Transform (FFT) of recorded loads (see Figure 4.1(a)). Alves et al. [3] used three methods for the identification of DLFs, which are Fast Fourier Transform (FFT), Discrete Fourier Transform (DFT), and step-by-step method (based on time convolution theorem). However, these methods do not consider the frequency content in the vicinity of each excitation frequency, thus leading to an underestimation of the load amplitude at these regions [90].

Ebrahimpour and Sack [27] as well as Parkhouse and Ewins [65] used PSD loads instead, and computed the energy content at each harmonic of the load (see Figure 4.1(b)). This resulted in an average peak used to obtain corresponding DLFs, but the concentration of the whole energy at the peaks could results in an overestimation of the load amplitude for each harmonic [90].

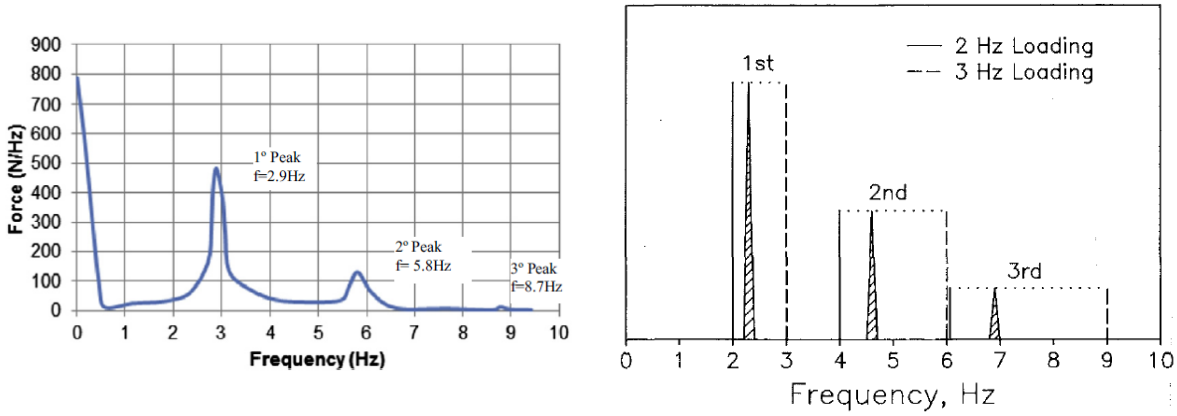

(a) Harmonic peaks by Fast Fourier Transform [20]

(b) Energy content by harmonic (shaded areas) [27]

Figure 4.1: Determination of Fourier series load model parameters

In what concerns the second load model type, each jumping pulse of the rhythmic action was isolated and associated parameters including landing phase time, pulse period and impact factor (see Section 2.2.1) were calculated (see Figure 4.2(a)). Parameters were obtained for successive jumps (see Figure 4.2(b)), and their variation was then characterized by probability density functions ([15], [39], [58], [80]).

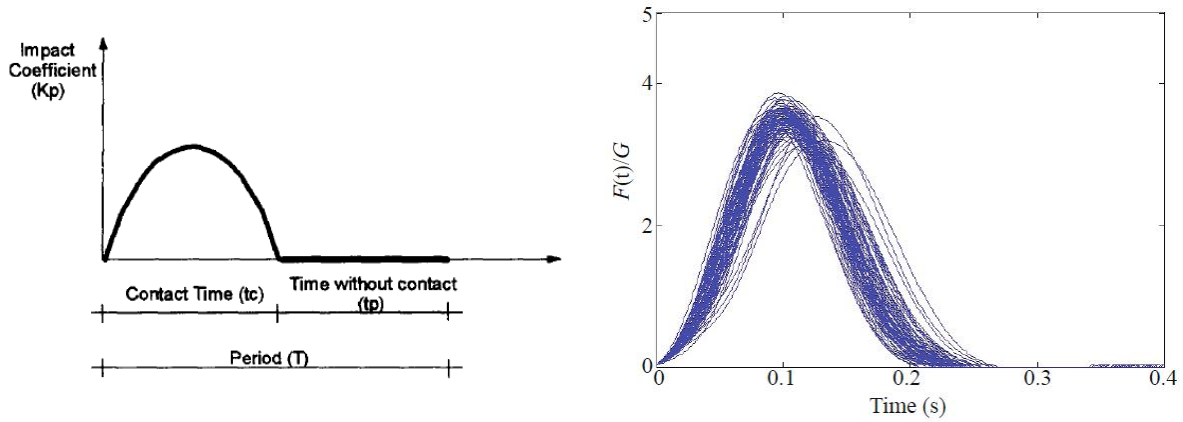

(a) Single pulse parameters [3]

(b) Consecutive jumping pulses [15]

Figure 4.2: Determination of jumping pulse load model parameters

All previous identification procedures are widely used in practice since they provide load parameters in a simple and straightforward way. However, time domain models are unlikely to represent the incapacity of each individual to keep the same frequency and amplitude during motion (called "intra-subject variability") [50], as encountered in real situations. For instance, Figure 4.3 illustrates the frequency content of a Fourier series load against an experimentally measured load. It can be seen that a large spread of energy, termed leakage [71], is present in the latter load, whereas energy is concentrated in the harmonics of the load for the time domain model. Furthermore, all previous methods used some parts of the recorded forces in order to

obtain load parameters. Hence, experimental observations related to the continuous motion over time could not be captured in these load models.

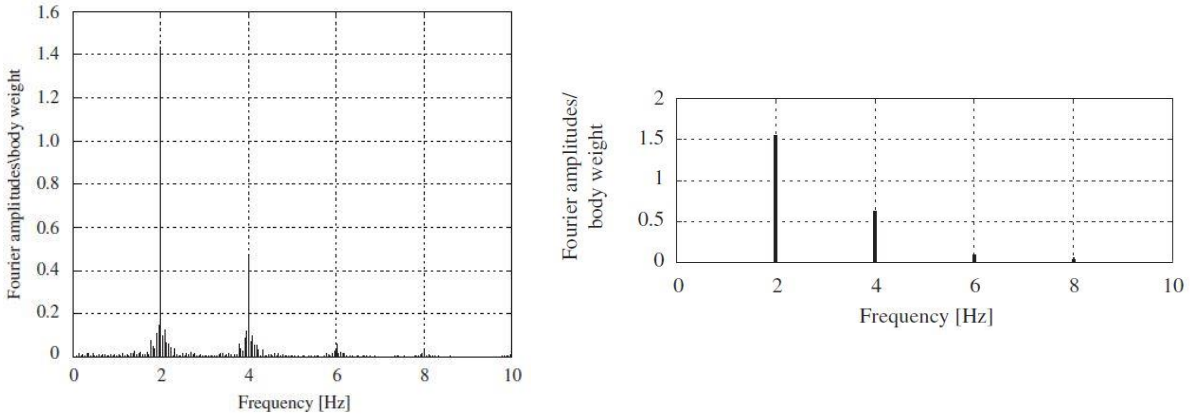

(a) Measured force (b) Synthetic force using Fourier series

Figure 4.3: Illustration of jumping loads in the frequency domain [71]

4.2.1.2 Proposed load model formulation

The frequency domain (PSD) modelling approach is adopted in order to consider randomness of the rhythmic action during time. Compared to time domain load models, PSD load models allow to have peak load amplitudes which gradually decrease for each harmonic, resulting in energy leakage. For that reason, time domain load models would overestimate structural response in a resonant case and underestimate this response in a non-resonant case [88].

The load model proposed by Xiong and Chen [89] is used for that purpose (see Section 2.5.2.2). Eq. (2.49) can be rewritten for each harmonic *i* by:

$$S_{p,i}(f) = (mg)^2 \left(\frac{\rho S_i}{if_p}\right)\left[p_5 \exp\left(-\left[\left(\frac{f/if_p - 1}{p_6}\right)\right]^2\right) + p_7 \exp\left(-\left[\left(\frac{f/if_p - 1}{p_8}\right)\right]^2\right)\right] \quad (4.1)$$

where m is the body mass of the individual and g the gravity acceleration (9.81m/s²). It is noticed that the exponential function accurately models the frequency content at each harmonic. In fact, it has a bell shape allowing a gradual decrease in amplitude, which represents the spread of energy (leakage) in the vicinity of the peak of each harmonic. Inspired by the time domain model proposed by Racic and Pavic [71] (see Table 2.13) characterizing jumping pulses (having also bell shapes), the proposed formulation simplifies Eq. (4.1) by assuming that each harmonic can be modelled by a unique exponential function given by:

$$S_{p,i}(f) = (mg)^2 \alpha_i^2 \exp\left(-\frac{(f - if_p)^2}{\delta_i^2}\right) \quad (4.2)$$

The total PSD load model is then obtained by:

$$S_p(f) = \sum_{i=1}^{3} S_{p,i}(f) \quad (4.3)$$

The proposed formulation was verified in comparison with the PSD load model developed by Xiong and Chen [89]. Both models were calculated using Eq. (4.3) (based on harmonic PSDs given by Eq. (4.1) and Eq. (4.2), respectively), for an individual having 75kg and an excitation

frequency of 2Hz. Both models are plotted in Figure 4.4, assuming equal load energy (variance of the PSD function). The two plots match well in general in terms of peaks for the three harmonics of the load. However, the proposed PSD model has a narrower bottom part than the model proposed by Xiong and Chen, which is compensated by a larger upper part. Hence, an equivalent energy content at each harmonic could be provided by the proposed load model.

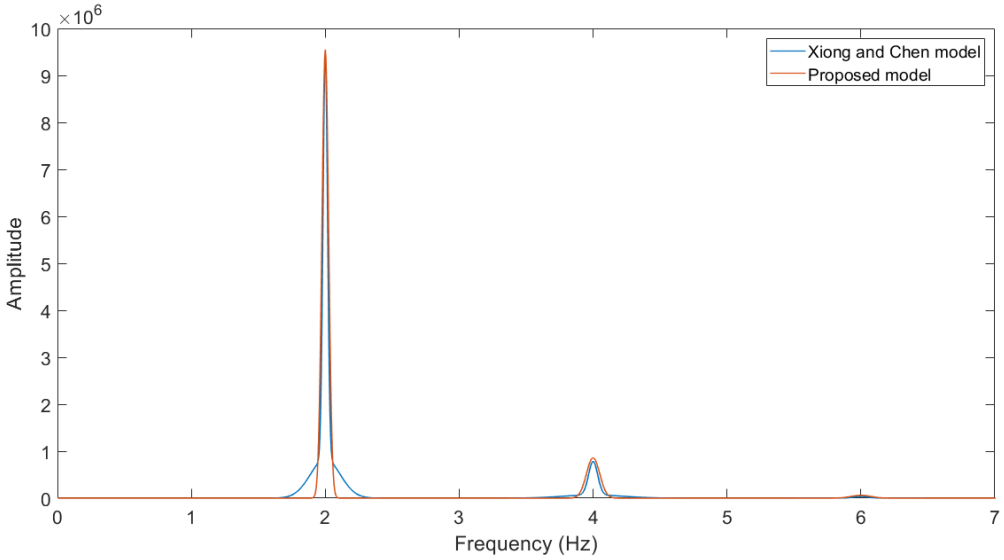

Figure 4.4: Comparison of PSD load models for an excitation frequency of 2Hz

The first three harmonics were considered because they represent most of the load energy in the frequency range of human excitation ([32], [89]). Parameters characterizing the proposed load model are then:

- The excitation frequency f_p;
- Parameter α_i (amplitude coefficient), which controls the load amplitude around the i^{th} harmonic;
- Parameter δ_i (bandwidth coefficient), which determines the range of the spread of energy in the vicinity of the i^{th} harmonic (depending only on the rhythm of motion).

In the frequency domain, the distribution range of energy becomes wider at higher harmonics [88], which is expressed in Eq. (4.1) by a linear increase in the denominator of each exponential. Hence, the variation of δ_i by harmonic i was taken as: $\delta_i = i\delta_1$.

In general, load amplitudes exhibit a decreasing trend by harmonic order ([3], [27], [65], [67], [92]). This is considered in Eq. (4.1) by a term inversely proportional to the harmonic frequency. Therefore, as DLFs could be directly obtained for a given rhythmic activity (from measurements or literature), it was assumed that the decreasing rate of the PSD load amplitude is equivalent to the same rate as these DLFs. In other words, the following relation applies:

$$\frac{\alpha_i}{\alpha_1} = \frac{DLF_i}{DLF_1} = a_i \tag{4.4}$$

Here, α_1 and α_i are amplitude coefficients of the PSD load model for the first and i^{th} harmonic, respectively, whilst DLF_1 and DLF_i are Dynamic Load Factors of the same activity for the first and i^{th} harmonic, respectively. Noting $\alpha_1 = \alpha$ and $\delta_1 = \delta$, the simplified PSD load model $S_p(f)$ is expressed by:

$$S_p(f) = (mg\alpha)^2 \sum_{i=1}^{3} \left[a_i^2 \exp\left(-\frac{(f - if_p)^2}{(i\delta)^2} \right) \right] \tag{4.5}$$

Load model parameters to be identified for each rhythmic activity are then reduced to f_p, α and δ. They are collected in a vector noted $\theta = \{ f_p, \alpha, \delta \}^T$.

4.2.2 Least-squares load model identification

4.2.2.1 Objective function

Consider $S_{p,exp}(f)$ as the experimental PSD load corresponding to a rhythmic activity performed by a single person and $S_{p,th}(f, \theta)$ the θ-dependent analytical PSD load model for the same activity (obtained by Eq. (4.5)). The objective is to determine the optimal parameters of vector θ (noted θ_{opt}), in order to have the closest analytical PSD model to its experimental counterpart.

This optimization problem is solved using the least-squares method for two main reasons:

- It is the most common and straightforward method for such problems [52];
- It allows the use of the complete signal record. Intra-variability effects are thus taken into account during the continuous rhythmic action.

Using the Euclidean 2-norm, an objective function representing the difference between analytical and experimental PSDs is formulated. The optimal vector θ_{opt} is then obtained by minimizing this function as follows [52]:

$$\theta_{opt} = \arg\min_{\theta} \left[\left\| S_{p,th}(f, \theta) - S_{p,\exp}(f) \right\|_2^2 \right] \tag{4.6}$$

From a practical point of view, the experimental load produced by one person is represented by a load vector noted $\{S_{p,exp}\}$. In this case, the θ-dependent analytical PSD load model is also a vector of the same length N_e noted $\{S_{p,th}(\theta)\}$. Eq. (4.6) is thus rewritten as:

$$\theta_{opt} = \arg\min_{\theta} \left[\sum_{i=1}^{N_e} \left| \left\{ S_{p,th}(\theta) \right\}_i - \left\{ S_{p,\exp} \right\}_i \right|^2 \right] \tag{4.7}$$

Optimal parameters were identified using *lsqnonlin* solver available in the Optimization toolbox of MATLAB [60]. This solver is convenient for most of the least squares problems. The optimal vector θ_{opt} is computed using Levenberg-Marquardt algorithm, adapted for nonlinear formulations [60]. Another advantage of this algorithm is that it finds the optimal solution even if it starts very far off the final minimum [1]. It requires two inputs: an initial estimation of vector θ (noted θ_0) and a difference function $f_d(\theta)$ in which the Euclidean 2-norm is applied: $f_d(\theta) = \{S_{p,th}(\theta)\} - \{S_{p,exp}\}$.

Corresponding options for the optimization process are:

- Maximum number of iterations: 400;
- Maximum number of evaluations of the objective function: 2000;
- Step tolerance: $\frac{|\theta_{i+1} - \theta_i|}{1 + |\theta_i|} \leq 10^{-10}$;
- Function tolerance: $\frac{|f_{d,i+1} - f_{d,i}|}{1 + |f_{d,i}|} \leq 10^{-10}$.

4.2.2.2 Parametric identification procedure

Consider a floor structure where a single person, having a known body mass m, performs a rhythmic activity. The associated force $P_{exp}(t)$ was assumed to be measured and provided in the time domain, along with the activity duration T and the time step dt. Because the signal has limited duration, the PSD of the experimental load $\{S_{p,exp,0}\}$ is calculated by the periodogram method using the rectangular window, which is implemented in MATLAB. The maximum investigated frequency is 10Hz, corresponding to the range of rhythmic excitation [31]. The frequency vector is resampled in order to provide more points near the peaks of each harmonic and less points away. Values of the experimental load $\{S_{p,exp}\}$ are then deduced by linear interpolation from the values of $\{S_{p,exp,0}\}$.

Load parameters to be determined are those collected in the vector $\theta = \{ f_p, \alpha, \delta\}^T$. First of all, initial parameters θ_0 should be provided, and the analytical PSD load model vector $\{S_{p,th}(\theta)\}$ is calculated by Eq. (4.5). Hence, the optimal vector θ_{opt} is obtained using least-squares technique by *lsqnonlin* solver (see Section 4.2.2.1).

In case successive forces are recorded for a given activity, the above procedure is applied for each force signal. The variability of all resulting optimal parameters f_p, α and δ is then characterized by their arithmetic mean values and standard deviations [39].

As stated earlier, the optimization algorithm requires initial parameters to be chosen in such a way that the obtained solution corresponds to the global minimum of the objective function. The variation range of such parameters is determined in the next section.

4.2.2.3 Synthetic study

Based on the proposed PSD load model, a synthetic study is conducted for two main objectives:

- Determine the range of initial conditions (see Section 4.2.2.2) leading to the optimal parameters of the identified PSD load model;
- Verify the robustness of the proposed model with regards to ambient noise.

To accomplish that, an initial case study is selected using the following parameters:

- A duration of 30s with a maximum frequency of 10Hz [31];
- A 75kg body mass, which is close to the nominal body mass recommended by design guidelines (SCI P354 for example [81]);
- An excitation frequency of 2.5Hz, which is the mean of the frequency range for rhythmic activities [1.5, 3.5Hz] ([45], [81]).

Remaining parameters (see Eq. (4.5)) are provided to have an appropriate RMS force and are presented in Table 4.1. Corresponding load model is plotted in Figure 4.5. It has an RMS force of 996N. This initial choice of parameters has no effect on the findings in this section (the same conclusions apply to other PSD load parameters).

Parameter	α	δ (Hz)	a_1	a_2	a_3
Value	3.5	0.05	1	0.5	0.25

Table 4.1: Parameters for the synthetic PSD load model

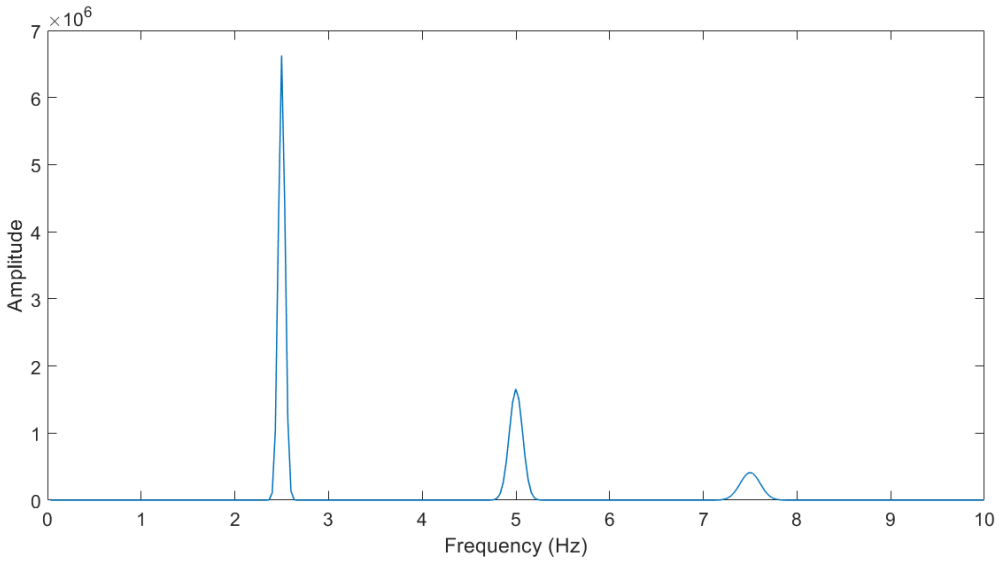

Figure 4.5: Synthetic PSD load model

- **Range of initial conditions**

The above developed load model is considered as a synthetic input signal for which load parameters are to be determined. Initial parameters (of vector θ_0) are then varied in order to examine their influence on the obtained solution. A multi-start optimization technique is adopted by determining successive optimal values for each set of initial conditions (using the method described in Section 4.2.2.2). The mean optimal parameters are then deduced as a representative solution to be compared with the PSD model input values of f_p, α and δ.

In general, a first approximation of f_p can be obtained from the frequency corresponding to the peak of the 1st harmonic of the load (termed peak picking). Therefore, the variation of f_p is considered by frequency increments close to $f_{p,0}$ = 2.5Hz, given by:

$$f_{p,\varepsilon} = f_{p,0} \pm \Delta f \tag{4.8}$$

where $f_{p,\varepsilon}$ is the perturbed parameter and Δf the frequency increment. However, there is no way to have a first approximation of parameters α and δ. The variation of human load parameters is generally assumed to follow a normal distribution ([32], [39]). Hence, a random perturbation using the Gaussian distribution is used for the latter parameters, expressed by:

$$p_\varepsilon = p_0 \left[\left| 1 + \varepsilon_p N(0,1) \right| \right] \tag{4.9}$$

Here, p_0 is the initial value of α or δ (see Table 4.1), p_ε the perturbed parameter, $N(0,1)$ a random number generated using the Gaussian distribution and ε_p the corresponding coefficient of variation.

100 increments are considered for each value of Δf (between $\Delta f/100$ and Δf) whilst 100 samples are generated for each value of ε_p. Table 4.2 summarizes obtained optimal parameters after the variation of initial conditions.

Parameter	Maximum Range	Optimal solution		
		f_p (Hz)	α	δ (Hz)
Initial	-	2.5	3.5	0.05
f_p	Δf = ±0.2Hz	2.5	3.5	0.05
	Δf = 0.3Hz	2.8	0.003	0.074
	Δf = −0.3Hz	2.2	0.003	0.075
α, δ	ε_p=1	2.5	3.5	0.05
f_p α, δ	Δf = ±0.1Hz ε_p=1	2.5	3.5	0.05
f_p α, δ	Δf = 0.2Hz ε_p= 0.5	2.57	3.18	0.048
f_p α, δ	Δf = −0.2Hz ε_p= 0.5	2.48	3.32	0.047

Table 4.2: Optimal solutions after the perturbation of initial conditions

When varying each parameter at once, the optimal solution is found for $\Delta f \leq 0.2$Hz with α=3.5 and δ=0.05Hz. The same result is noticed using ε_p=1 with f_p=2.5Hz. For Δf =±0.3Hz, the solution differs from the optimal one with a maximum relative difference of 12% for f_p, 99.9% for α and 50% for δ. On the other hand, when varying all parameters (which is the most common case), it is found that the optimal solution is reached with $\Delta f \leq 0.1$Hz and ε_p=1 for α and δ. This corresponds to a variation range of [1, 10] for α and [0.01, 0.2 Hz] for δ, respectively. However, using Δf =±0.2Hz and ε_p=0.5, discrepancies to the optimal values occur with a maximum relative difference of 3% for f_p, 9% for α and 6% for δ.

As a result, the initial conditions should be chosen for a given rhythmic activity as follows:

- The frequency peak of the 1st harmonic of the experimental PSD load is chosen for f_p with a tolerance range of ±0.1Hz;
- α is chosen in the interval [1, 10] and δ in the range [0.01, 0.2 Hz].

Using one set of the above parameters f_p, α and δ as initial conditions, the optimization method presented in Section 4.2.2.2 would lead to a solution corresponding to the global minimum of the objective function (given by Eq. (4.7)).

- **Load perturbation**

In order to verify the robustness of the PSD load model towards ambient noise, a second analysis is carried out considering a perturbation of the synthetic load, given by:

$$S_{p,\varepsilon}(f) = S_{p,0}(f)\left[\left|1+\varepsilon_s N(0,1)\right|\right] \tag{4.10}$$

where $S_{p,0}(f)$ is the initial (synthetic) PSD load, $S_{p,\varepsilon}(f)$ the perturbed PSD load, $N(0,1)$ a random number generated using the Gaussian distribution and ε_s the corresponding coefficient of variation. 100 samples were generated for each value of ε_s.

Using synthetic load parameters f_p, α and δ as initial conditions, identification is performed according to the instructions of Section 4.2.2.2 and mean optimal parameters are determined for four values of ε_s (0.02, 0.05, 0.1 and 0.2). Table 4.3 summarizes obtained results and Figure 4.6 illustrates the perturbed PSD load model using ε_s=0.1.

ε_S	Optimal solution		
	f_p (Hz)	α	δ (Hz)
0.02	2.5	3.53	0.051
0.05	2.49	3.47	0.044
0.1	2.52	3.34	0.051
0.2	2.51	2.9	0.06

Table 4.3: Optimal solutions after load perturbation

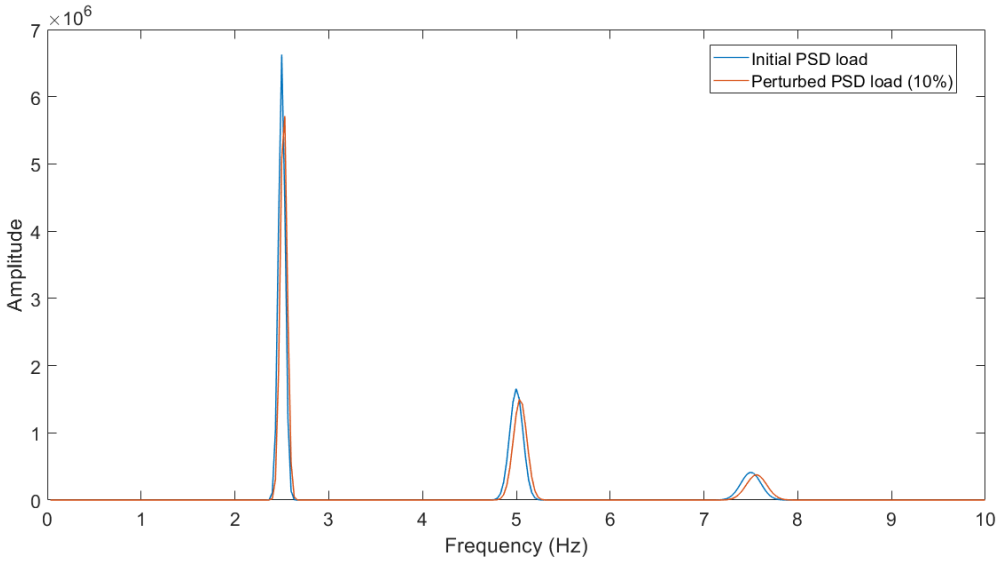

Figure 4.6: Comparison between synthetic and identified PSD load models after perturbation (with a coefficient of variation of 0.1)

It is noticed that the optimal parameters have a lower variation range than the load perturbation. Even for a coefficient of variation of 0.2, relative differences between the initial and identified parameters were 0.4% for f_p, 17% for α and 20% for δ. The general shape of the load is also barely affected (see Figure 4.6). Consequently, the PSD load model can be considered as robust towards ambient perturbation.

4.2.2.4 Equivalent DLF identification

In order to compare the proposed load amplitude with that of existing time domain load models associated to the same activity, equivalent DLFs should be determined from the PSD model $S_p(f)$, after identifying its optimal parameters f_p, α and δ.

For each harmonic i, the load energy is located in the frequency range between $(i\text{-}0.5)f_p$ and $(i\text{+}0.5)f_p$ [31] as can be seen in Figure 4.7. Hence, the RMS force of the i^{th} harmonic $F_{rms,i}$ is calculated by:

$$F_{rms,i} = \sqrt{\int_{(i-0.5)f_p}^{(i+0.5)f_p} S_p(f)df} \tag{4.11}$$

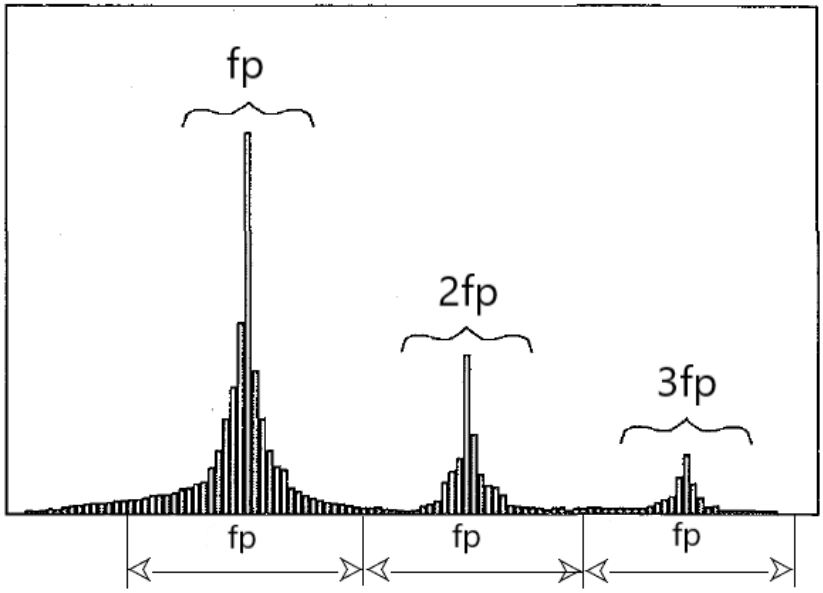

Figure 4.7: Load energy by harmonic (modified from [27])

An equivalent Fourier series load $P(t)$ is expressed as follows:

$$P(t) = mg\left[1 + \sum_{i=1}^{3} DLF_i \sin(2\pi i f_p t)\right] \tag{4.12}$$

where m is the body mass of the individual, g the gravity acceleration (9.81m/s²), f_p the excitation frequency and DLF_i the Dynamic Load Factor (DLF) of the i^{th} harmonic. An average peak amplitude for this load could then be obtained by multiplying $F_{rms,i}$ by $\sqrt{2}$ ([27], [65]). This amplitude takes into account the whole frequency content of each harmonic, not only the associated peak value. The equivalent DLF of the i^{th} harmonic is then deduced by:

$$DLF_i = \frac{\sqrt{2}F_{rms,i}}{mg} \tag{4.13}$$

In case multiple PSDs of the same activity are provided, the latter procedure is applied to each identified PSD. Resulting DLFs are then characterized by their mean values and standard deviations.

4.2.3 Crowd size effect

The common case of rhythmic activities on a floor consists of a group of individuals performing actions with a certain degree of synchronization. As outlined in Chapter 2, each individual has a specific motion different from other persons, resulting in different amplitudes and frequencies during movement. This effect is denoted "inter-subject variability", such that the total force would have a reduced amplitude compared to the sum of individual forces. This reduction is evaluated using experimental measurements of crowd forces for multiple group sizes.

4.2.3.1 Crowd size relation

For a given rhythmic activity, crowd forces are assumed to be measured for various numbers of individuals (each having a body mass m_k) for a number of S times (called windows) per crowd size. The RMS force is used as a representative load parameter since it covers all the frequency content of the measured load and allows to have more accurate evaluation of the amplitude (eliminating the effect of parasite peaks). As highlighted by Eq. (4.12), the rhythmic

load contains both a static part (weight of participants) and a dynamical part (load harmonics). However, since the weight of individuals is directly summed, the group effect must be investigated considering the dynamical part of the human loads (having a zero mean load).

For each crowd size, the dynamical load of the s^{th} activity window $F_s(t)$ is extracted and the corresponding RMS force $\hat{F}_{rms,s}$ is computed by:

$$\hat{F}_{rms,s} = \sqrt{\frac{1}{N_e}\sum_{m=1}^{N_e} F_s^2(t_m)} \tag{4.14}$$

Here, $F_s(t_m)$ is the time domain load amplitude of the s^{th} activity window at time t_m and N_e the number of time samples.

Eq. (4.12) indicates that the ratio of the rhythmic load to the body mass of the individual is constant for a given activity. In other words, two individuals having different weights but are performing a rhythmic activity in exactly the same way would have the same body acceleration (load to body mass ratio).

Hence, in order to eliminate the effect of variable body mass on the crowd load, RMS forces are normalized by the following expression:

$$F_{rms,s} = \frac{N\bar{m}}{\sum_{k=1}^{N} m_k}\hat{F}_{rms,s} \tag{4.15}$$

where $F_{rms,s}$ is the normalized RMS force of the s^{th} activity window, $\hat{F}_{rms,s}$ the initial RMS force, N the crowd size, m_k the body mass of the k^{th} individual and $\bar{m}$ a nominal body mass for all individuals (usually taken as 75kg [81]).The statistical variability of the resulting S RMS forces is then characterized by their mean values and standard deviations.

The variation of the mean RMS force $\bar{F}_{rms}(N)$ against crowd size N would exhibit a growth with a decreasing rate due to "inter-subject variability". This variation is fitted in order to obtain deterministic crowd size relations to be included in the total crowd load model. This was done by selecting an appropriate function that best describes this tendency, noted $F_{rms}(N, \lambda)$ (λ being the vector of function parameters). Corresponding optimal parameters λ_{opt} are then determined by means of curve fitting using *lsqcurvefit* function available in the Optimization toolbox of MATLAB [60]. This function calculates values of λ_{opt} that best fit the experimental data in a least-squares sense by:

$$\lambda_{opt} = \arg\min_{\lambda}\left[\left\|F_{rms}(N,\lambda) - \bar{F}_{rms}(N)\right\|_2^2\right] \tag{4.16}$$

4.2.3.2 Coordination factor

The coordination factor takes into account the lack of synchronization among participants, by applying a reduction coefficient to the individual load as follows [45]:

$$p_N(t) = C(N)\,p_1(t) \tag{4.17}$$

Here, N is the crowd size, $C(N)$ the coordination factor, $p_1(t)$ the load produced by a single person on the floor and $p_N(t)$ the equivalent load of a single person within the group of N individuals.

The coordination factor depends on the performed rhythmic activity (impact, style, etc.) and is usually determined by conducting vibration experiments on floors excited by the action of multiple groups of individuals.

Based on load measurements, this factor can be determined using RMS parameters by:

$$C(N) = \frac{F_{rms,eq}(N)}{F_{rms}(1)} \tag{4.18}$$

where $F_{rms}(1)$ is the RMS force corresponding to the case of a single person on the floor and $F_{rms,eq}(N)$ the equivalent RMS force for a single person within the group of N individuals.

The RMS force $F_{rms,eq}(N)$ can be obtained by [31]:

$$F_{rms,eq}(N) = \frac{F_{rms}(N, \lambda_{opt})}{N} \tag{4.19}$$

where $F_{rms}(N, \lambda_{opt})$ is the best-fit function for measured crowd RMS forces (see Section 4.2.3.1).

4.2.4 Final crowd-rhythmic load model

In the frequency domain, rhythmic activities practiced by a group of people (see Figure 4.8) are usually modelled by a random field approach (see Section 2.5.2.2), including an auto-spectral model for a single person and a coherence function to consider the interaction between two persons [84]. The same approach was used for the final crowd load model. However, since the positions of individuals are not variable during movement, a simplified coherence function was adopted.

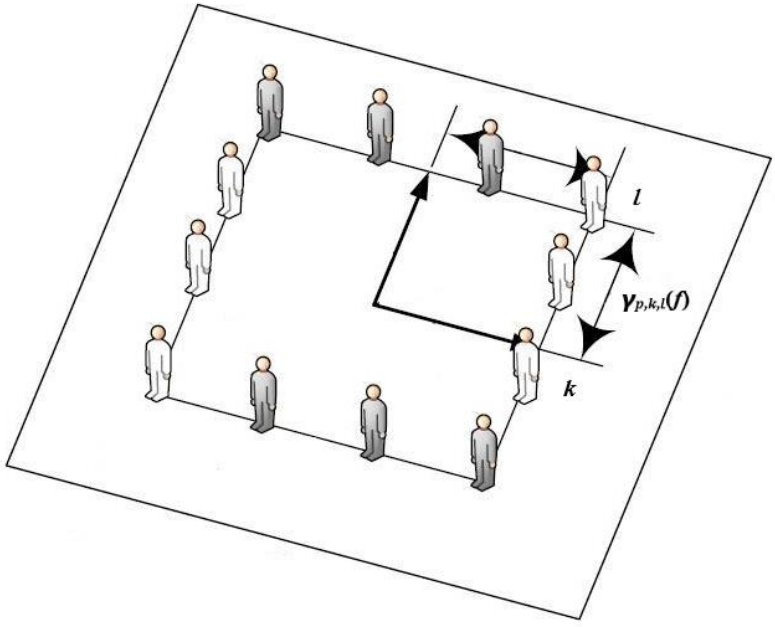

Figure 4.8: Interaction between individuals on a floor structure (modified from [43])

The Fourier transform of Eq. (4.17) expressed for each individual k gives:

$$P_{N,k}(f) = C(N)P_{1,k}(f) \tag{4.20}$$

where N is the number of individuals, $P_{N,k}(f)$ the Fourier transform of the time domain load $p_{N,k}(t)$ for the k^{th} individual and $P_{1,k}(f)$ the Fourier transform of $p_{1,k}(t)$.

Applying Eq. (2.33) to $P_{N,k}(f)$ results in the auto-spectral load $S_{p,N,k}(f)$ as follows:

$$S_{p,N,k}(f) = \left[C(N)\right]^2 S_{p,k}(f) \tag{4.21}$$

where $S_{p,k}(f)$ is the PSD load model of a single person given by Eq. (4.5). It could be noticed that the auto-spectral model is corrected by the coordination factor $C(N)$ to take into account "inter-subject variability" effects.

The cross-PSD between two individuals k and l $S_{p,N,k,l}(f)$ is calculated by:

$$S_{p,N,k,l}(f) = \sqrt{S_{p,N,k}(f) S_{p,N,l}(f)} = \left[C(N)\right]^2 \sqrt{S_{p,k}(f) S_{p,l}(f)} \tag{4.22}$$

Here, $S_{p,k}(f)$ and $S_{p,l}(f)$ are the PSD load models for the individual k and l, respectively. This leads to the coherence function $\gamma_{p,k,l}(f)$ obtained by:

$$\gamma_{p,k,l}(f) = \frac{S_{p,N,k,l}(f)}{\sqrt{S_{p,k}(f) S_{p,l}(f)}} = \left[C(N)\right]^2 \tag{4.23}$$

In the proposed crowd load model, the spatial coherence function was considered equal to 1. Indeed, the positions of individuals is assumed to be invariable during rhythmic motion and the density of occupants is at the low range (below 0.3 person/m² [42]). In that case, a global coherence is introduced using coordination factors in the auto-spectral model, providing a reduction of the single person model to simulate the level of synchronization as noticed experimentally (see Figure 4.8). This level begins with perfect coordination for a single person (γ=1), while a lack of synchronization is obtained as the number of individuals increases (until γ=0), thus confirming the formulation proposed in Eq. (4.23).

To conclude, the major steps to establish the crowd-rhythmic load model are presented next:

- Determine time parameters (duration, time step) and the body mass of each individual m_k (a nominal value of 75kg is adopted if unknown [81]);
- Identify load parameters f_p, α and δ for the PSD load model $S_p(f)$ given by Eq. (4.5), using the procedure detailed in Section 4.2.2;
- Establish the relation of coordination factors against the number of individuals based on crowd RMS forces as described in Section 4.2.3;
- Deduce the auto-spectral load model $S_{p,N,k}(f)$ using Eq. (4.21) and the cross-spectral load model $S_{p,N,k,l}(f)$ using Eq. (4.22).

A PSD matrix of the crowd load $\left[S_{p,N}(f)\right]$ ($N \times N$) could then be formulated as follows:

$$\left[S_{p,N}(f)\right]_{k,l} = \begin{cases} S_{p,N,k}(f), & \text{k=l} \\ S_{p,N,k,l}(f), & \text{k} \neq \text{l} \end{cases} \tag{4.24}$$

4.2.5 Evaluation of floor response

The crowd-rhythmic load model established in Section 4.2.4 could be verified for a rhythmic activity by conducting response measurements on the floor when subjected to crowd loads for various numbers of individuals. The response parameter w could be the dynamical displacement or acceleration of the floor. The RMS response is adopted as the main parameter in all calculations for the reasons highlighted in Section 2.6.1. The present section describes the method for performing such verification that is used in the upcoming investigations.

Each individual k is supposed to have a known position on the floor and body mass m_k, and the response measured at a number of r response points, with a duration T and a time step dt. The floor has known modal properties (natural frequencies, modal masses, damping ratios, modal shapes). Considered bending natural modes are those below 10Hz which is the maximum frequency reached by rhythmic excitations (at the third harmonic) [31].

4.2.5.1 Numerical RMS response for the proposed model

For each crowd size N, the PSD matrix of the crowd load model is formulated by Eq. (4.24). The response of the floor is then calculated in the frequency domain using the procedure detailed in Section 2.6.2 for a given response point r. Resulting parameter is the numerical RMS response $\hat{w}_{rms,r}$ (given by Eq. (2.67)). An alternative is to compute normalized RMS response in order to have a uniform body mass for all crowd sizes by:

$$w_{rms,r} = \frac{N\overline{m}}{\sum_{k=1}^{N} m_k} \hat{w}_{rms,r} \tag{4.25}$$

where $w_{rms,r}$ is the normalized RMS response at the r^{th} response point, $\hat{w}_{rms,r}$ the initial RMS response, m_k the body mass of the k^{th} individual and $\overline{m}$ a nominal body mass for all individuals (usually taken as 75kg [81]).

The mean and standard deviation (noted $\overline{w}_{rms,num}$ and $\sigma_{rms,num}$, respectively) are then computed for the r parameters ($\hat{w}_{rms,r}$ or $w_{rms,r}$) to represent the RMS response for the crowd size N [39].

4.2.5.2 Numerical RMS response for time domain load models

Time domain load models for crowd-rhythmic activities proposed in the literature usually comprise a single person model associated with coordination factors for multiple individuals. The equivalent load for each person within a group of individuals $p_N(t)$ is expressed by Eq. (4.17). For the studied activity, the excitation frequency used in $p_N(t)$ is the same as the adopted optimal f_p in the associated PSD load model (obtained by Eq. (4.5)).

For a given crowd size N, the auto-spectral load model $S_{p,N,k}(f)$ (obtained by Eq. (4.21)) is computed from $p_N(t)$ by means of the periodogram method with a rectangular window (using MATLAB). The PSD matrix of the crowd load $\left[S_{p,N}(f)\right]$ is then deduced by Eq. (4.24), after calculating the cross-spectral load model $S_{p,N,k,l}(f)$ by Eq. (4.22). The same procedure detailed in Section 4.2.5.1 is finally applied using $\left[S_{p,N}(f)\right]$ to determine RMS responses of the floor related to this load model (noted $\overline{w}_{rms,num}$ and $\sigma_{rms,num}$, respectively).

4.2.5.3 Experimental RMS response

For each crowd size N, the activity is assumed to be recorded at the r response points for a number of S times (called windows). Corresponding RMS response $\hat{w}_{rms,r,s}$ is calculated by:

$$\hat{w}_{rms,r,s} = \sqrt{\frac{1}{N_e}\sum_{m=1}^{N_e} w_{r,s}^2(t_m)} \tag{4.26}$$

Here, $w_{r,s}(t_m)$ is the response of the floor at time t_m for the r^{th} response point and the s^{th} activity window and N_e the number of time samples.

When a uniform body mass is required for all crowd sizes, the normalized RMS response could be obtained by:

$$w_{rms,r,s} = \frac{N\overline{m}}{\sum_{k=1}^{N} m_k} \hat{w}_{rms,r,s} \tag{4.27}$$

where $w_{rms,r,s}$ is the normalized RMS response for the r^{th} response point and the s^{th} activity window, $\hat{w}_{rms,r,s}$ the initial RMS response, m_k the body mass of the k^{th} individual and $\overline{m}$ a nominal body mass for all individuals (usually taken as 75kg [81]).

For each response point, the mean and standard deviation (noted $\overline{w}_{rms,r}$ and $\sigma_{rms,r}$, respectively) are calculated for the S RMS responses ($\hat{w}_{rms,r,s}$ or $w_{rms,r,s}$). To take into account the variability of activities in case of multiple response points, two values are generated per response point by adding and decreasing the standard deviation $\sigma_{rms,r}$ to the mean value $\overline{w}_{rms,r}$ [39]. From the $2r$ new samples associated to all response points, the mean and standard deviation (noted $\overline{w}_{rms,exp}$ and $\sigma_{rms,exp}$, respectively) could be deduced to represent the response of the floor at the crowd size N.

For verification purposes, comparison could then be made between numerical responses $\overline{w}_{rms,num}(N)$ computed using the load model related to each activity and corresponding experimental responses $\overline{w}_{rms,exp}(N)$ for all investigated group sizes.

4.3 Identification of rhythmic load models on the laboratory floor

The experimental results from vibration tests described in Section 3.4 are used to identify rhythmic load models for each investigated activity. Obtained records in terms of forces and displacements are first illustrated and pre-processing method is detailed. Results of identification of the PSD load model are presented for the case of a single person, followed by obtained coordination factors for the case of crowds. Finally, the response of crowd-rhythmic load models is compared against displacement measurements on the floor and results are discussed.

4.3.1 Test results and pre-processing

4.3.1.1 Test results

In the laboratory vibration tests, four rhythmic activities (see Section 3.4.2.1) along with five crowd sizes (see Section 3.4.2.2) were investigated. For each activity and crowd size, test results were the rhythmic forces and displacements measured while performing activities (see Section 3.4.1). Corresponding datasheets were imported using *readtable* function of MATLAB [59], in which signals were further pre-processed. The total number of records was 120 forces and 120 displacements (6 measurements × 4 activities × 5 crowd sizes per parameter).

Figure 4.9 displays force and displacement records in the time domain for the case of one person. Each record comprises a 45s window of rhythmic activity followed by a small signal (after 55s in Figure 4.9) representing walking of individuals on the floor. For each activity and crowd size, this force is obtained as the sum of the forces in the four columns. In the rest of the manuscript, it is assumed that the latter force corresponds to the applied rhythmic load, which actually differs due to the own dynamics of the floor specimen.

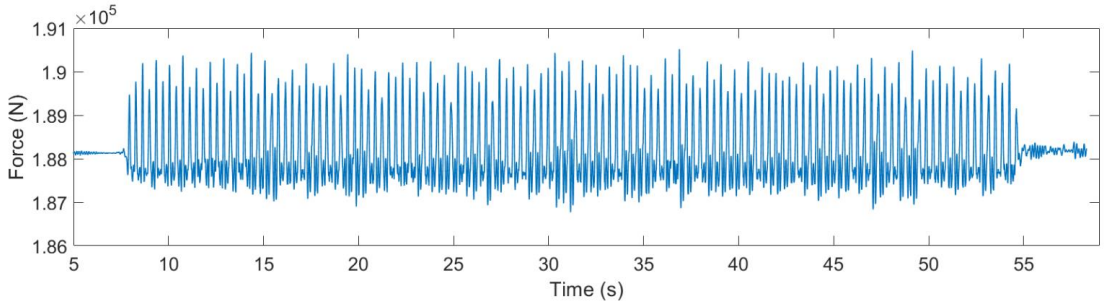

(a) Force signal

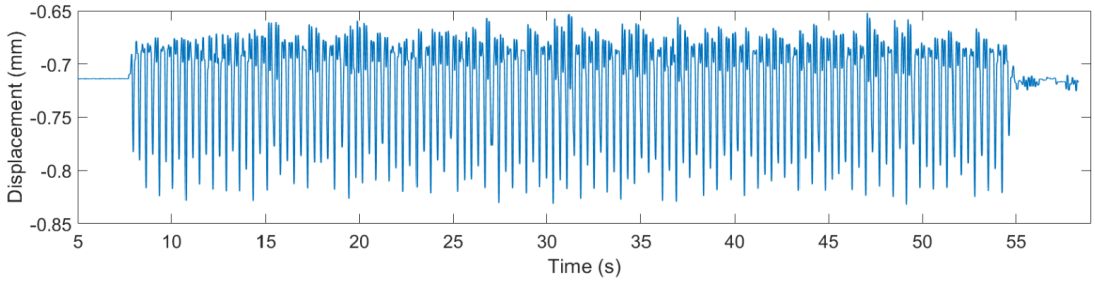

(b) Displacement signal

Figure 4.9: Example of raw test records for "skipping 2" activity

4.3.1.2 Pre-processing procedure

A pre-processing of test records is necessary to provide convenient signals that could be used for further analysis. Results for a single person performing "skipping 2" activity were selected to illustrate the procedure which is also applied to all other activities.

As can be seen in Figure 4.9, the records contain some parts which do not correspond to human activities (at the beginning and the end). Therefore, the relevant window during which participants performed rhythmic activities is to be determined. It was observed that this window began with a force amplitude higher than 0.5% of the mean force (corresponding to static loads), and lasted during 45s (see Table 3.10). This time window was extracted for both forces and displacements, as can be seen in Figure 4.10 for a force sample.

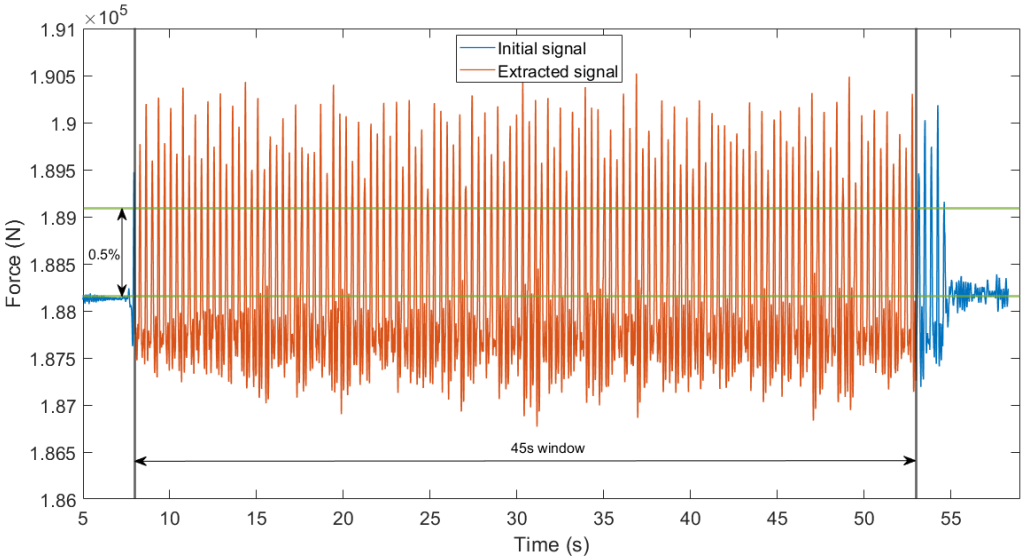

Figure 4.10: Illustration of force signal extraction

The mean force corresponds to the static load (self-weight of the floor, weight of participants) whereas the mean displacement corresponds to the static deflection under the weight of individuals only. Therefore, all mean values were removed from test records in order to keep only the dynamical contribution of forces and displacements useful for further analysis (see Section 4.2.3.1).

The next step is to filter all signals to meet the usual frequency range of human activities which lies between 0 and 10Hz [31]. This was done by removing all frequency content above 10Hz using Fast Fourier Transform (FFT) technique. Figure 4.11 illustrates a load signal before and after filtering (with elimination of the mean force).

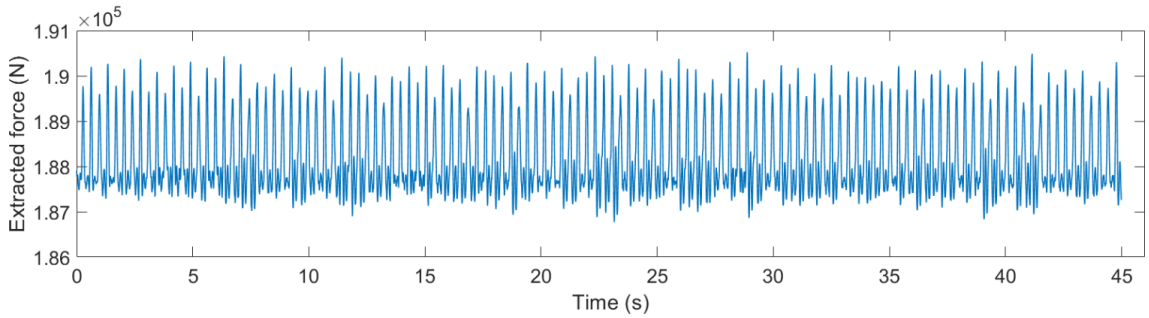

(a) Extracted force

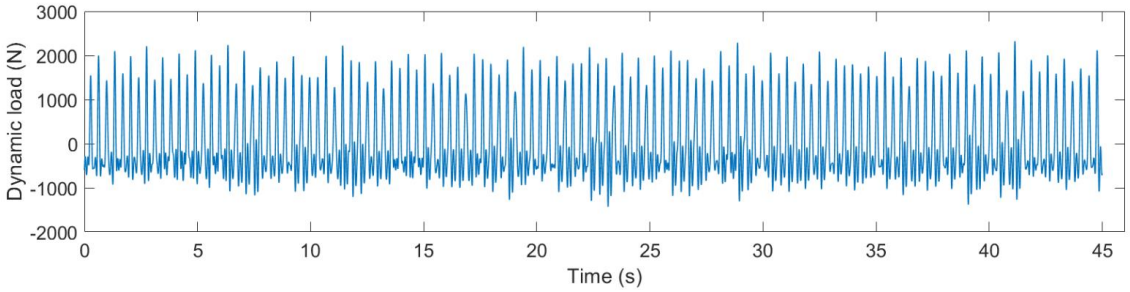

(b) Filtered dynamic load

Figure 4.11: Illustration of signal filtering

Filtered signals were finally truncated by removing 10s at the beginning and 5s at the end. The objective was to conserve the stationary response only and to match with the slot where all individuals were moving according to the protocol. An example of truncation of a load record for the case of a single person is presented in Figure 4.12.

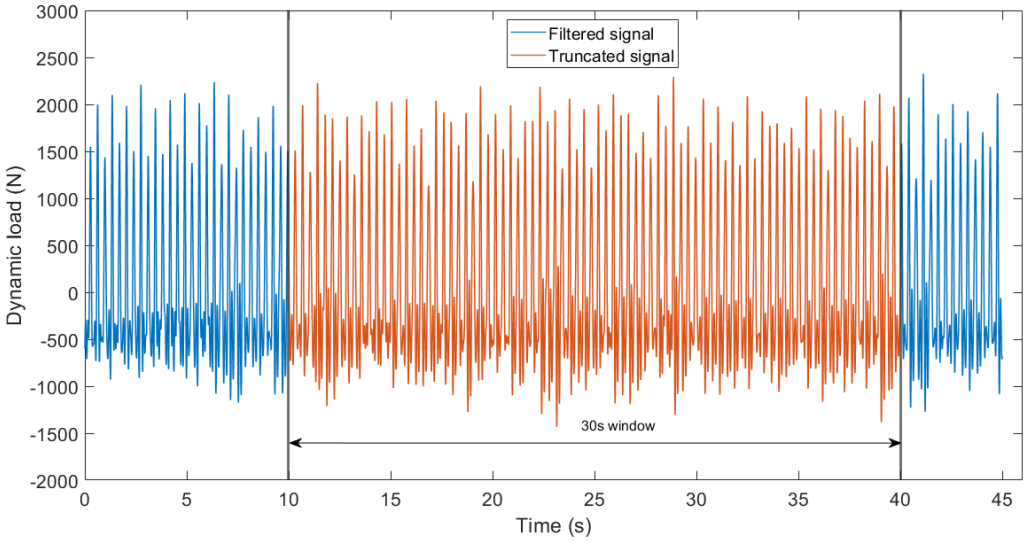

Figure 4.12: Illustration of load signal truncation

Figure 4.13 shows final load and displacement signals which were pre-processed from initial records of Figure 4.9 using the procedure detailed earlier. Resulting records have a duration of 30s and a time step of 0.0078s. This time frame is sufficiently long to allow post-processing in the frequency domain [77] and thus adequate for the next analysis.

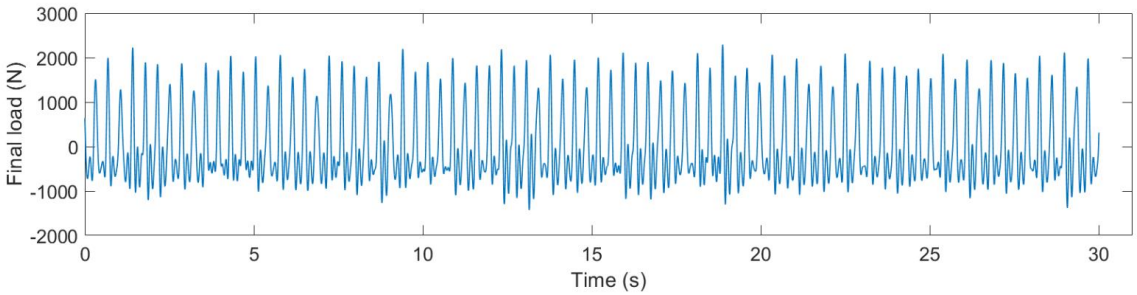

(a) Load signal

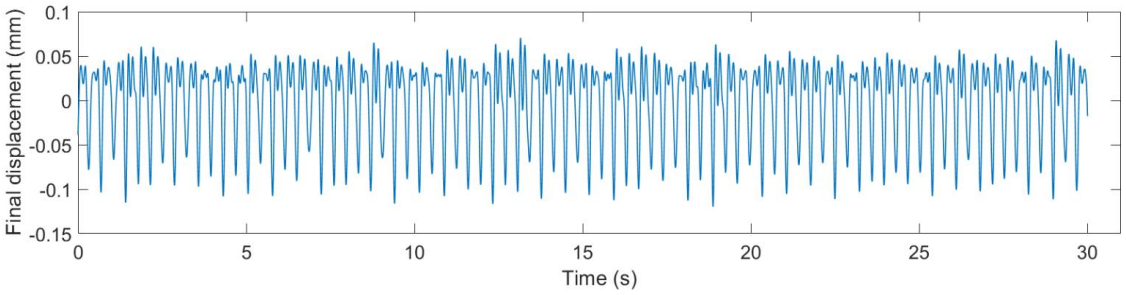

(b) Displacement signal

Figure 4.13: Example of pre-processed test records for "skipping 2" activity

4.3.2 Single person load model identification

4.3.2.1 Identified PSD load models

The PSD load model $S_p(f)$ established in Section 4.2.1.2 was adopted for both jumping and skipping activities (see Section 3.4.2.1). The related formulation is expressed by:

$$S_p(f) = (mg\alpha)^2 \sum_{i=1}^{3} \left[a_i^2 \exp\left(-\frac{(f - if_p)^2}{(i\delta)^2} \right) \right] \tag{4.28}$$

where m is the body mass of the individual, g the gravity acceleration (9.81m/s²), and for each activity: f_p is the excitation frequency, α the amplitude coefficient, δ the bandwidth coefficient.

This model requires the determination of coefficients a_i (i={1, 2, 3}) for each activity, controlling the variation of load amplitudes by harmonic (see Eq. (4.28)). Pernica [67] conducted an experimental study to extract Dynamic Load Factors (DLFs) for various human activities, including running-on-the-spot and stride jumps. These DLFs are presented in Table 4.4.

These findings lead to one of the most widely used models from the literature reproducing experimental activities (stride jumps for jumping jack, running-on-the-spot for skipping). Moreover, since activities of the same type (jumping or skipping) produce similar impacts on the floor, they were assumed to hold the same coefficients a_i (i={1, 2, 3}). Therefore, these coefficients were deduced by type of activity from associated DLFs obtained by Pernica (using Eq. (4.4)) and provided in Table 4.4.

Activity	DLF_1	DLF_2	DLF_3	a_1	a_2	a_3
Skipping / running-on-the spot	1.57	0.58	0.26	1	0.4	0.15
Jumping / stride jumps	1.75	1.1	0.42	1	0.6	0.25

Table 4.4: Dynamic Load Factors [67] and coefficients a_i for jumping and skipping activities

For each activity, six pre-processed load signal windows were available (see Section 4.3.1) for the case of a single person. The body mass of the individual performing these activities was 63kg. The PSD load parameters were then identified using the method detailed in Section 4.2.2. Both measured and identified PSD loads are represented by their amplitude envelopes at each frequency (between minimum and maximum values of the six activity windows). Results are plotted in Figure 4.14 for the four analysed activities.

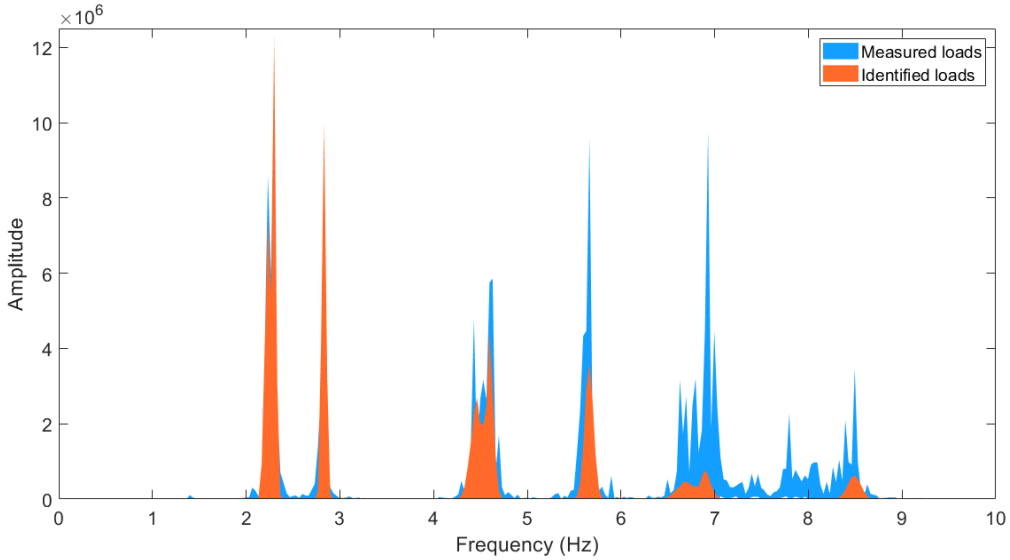

(a) Jumping 1

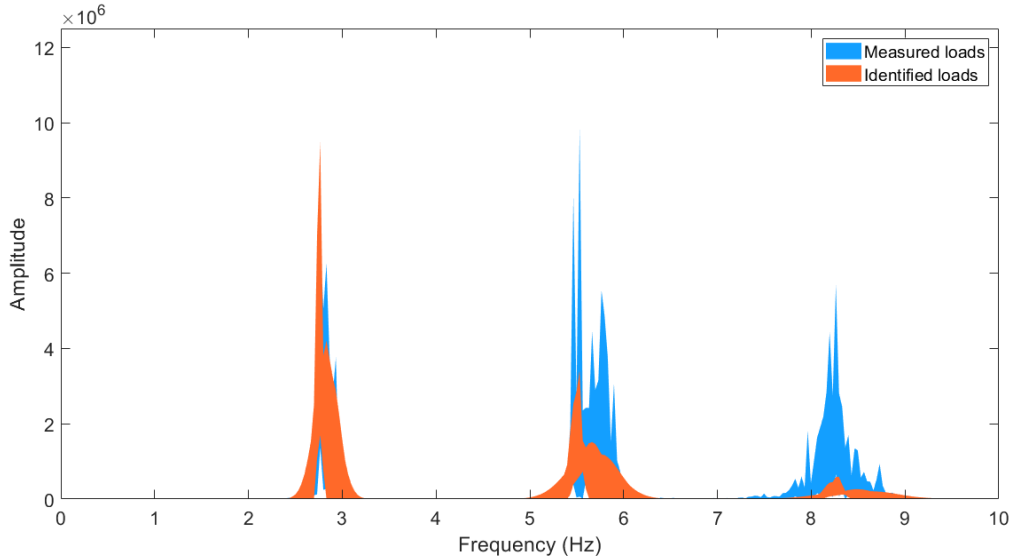

(b) Jumping 2

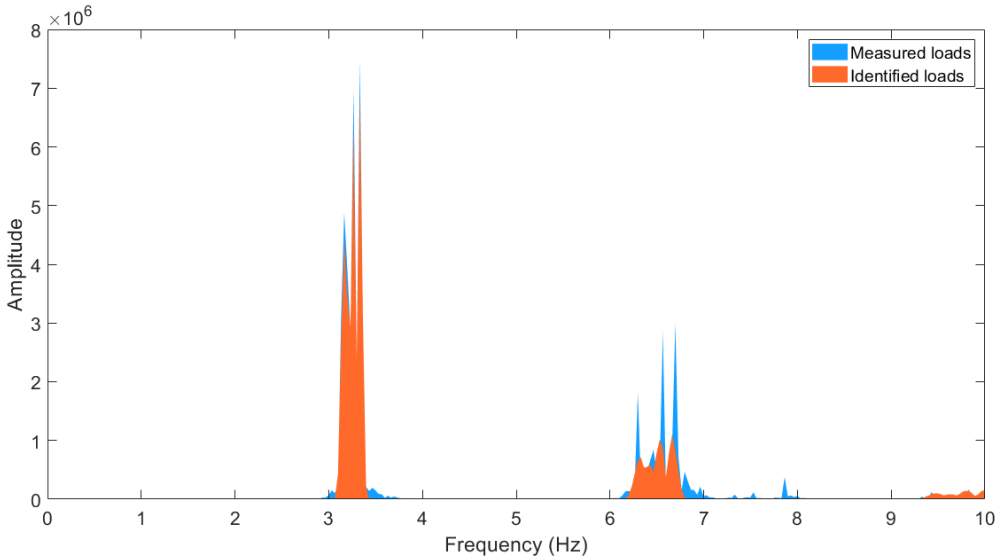

(c) Skipping 1

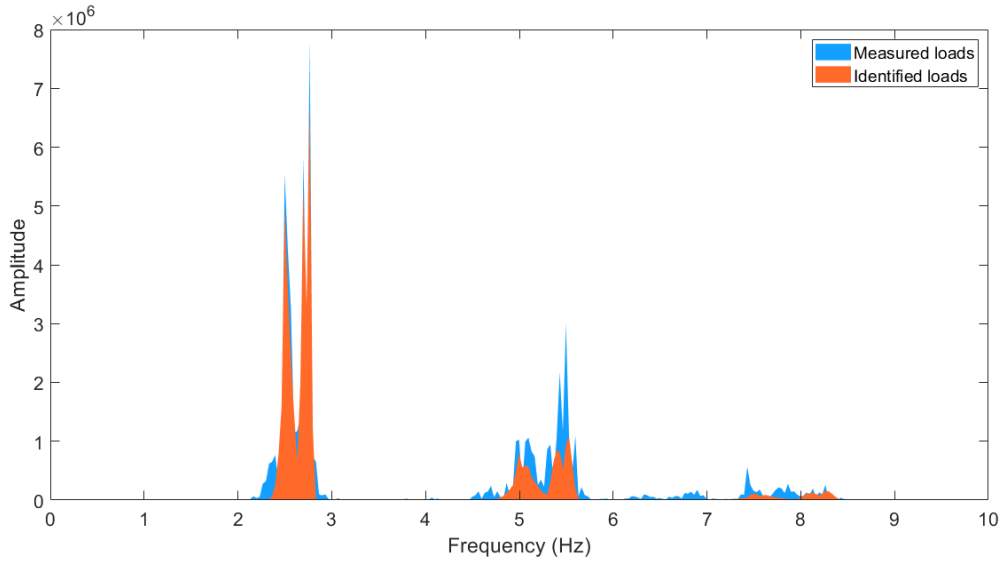

(d) Skipping 2

Figure 4.14: Measured and identified single person PSD loads

Overall, the experimental excitation frequency of each activity is well identified by the corresponding predicted PSD load model, and the mean relative difference between measured and numerical RMS forces ranges between 10.9% and 25.1% for the four investigated activities. This indicates that predicted PSDs are generally in good agreement with their experimental counterparts especially for the first load harmonic. The difference between the two PSDs is increasing with harmonic order. However, this has a little effect on the load amplitude since the energy of each activity is mainly concentrated at the first harmonic of the load. The experimental PSDs have the property of frequency content spreading for higher harmonics, which is well considered in the proposed PSD load model (see Section 4.2.1). Moreover, closer results between identified and measured PSDs are noticed for skipping activities compared to jumping activities. This is principally due to the wide energy band for "jumping 2" (see Figure 4.14(b)) and the great fluctuation of the excitation frequency for "jumping 1" (leading to two distinct peaks in Figure 4.14(a)). A probable reason for this could be that the individual lost

synchronization with the audible stimulus or that the latter has been changed in terms of frequency (beats per minute). This result reflects cases encountered in real life situations, which could not be captured using a metronome for the guidance of rhythmic activities as adopted by the vast majority of previous research.

4.3.2.2 Identified load model parameters

The previous results show that the identified load models depend to some extent on the type of coordination stimulus adopted in the experiments. However, the variability between activity windows allows to have a variation range (mean ± standard deviation) for each load parameter. The developed model could then be applied to similar situations encountered in real life.

Table 4.5 summarizes the mean and standard deviation of identified load parameters f_p, α and δ obtained from the six activity windows of each investigated activity. RMS forces were calculated using the mean load parameters for the four activities. Results by increasing order were 669N for "skipping 1" (on feet toes), 693N for "skipping 2" (on feet soles), 986N for "jumping 1" (jumping jack) and 1308N for "jumping 2" (quick jumping).

Activity	f_p (Hz)	α	δ (Hz)
Jumping 1	2.36 ± 0.21	4.64 ± 0.70	0.035 ± 0.01
Jumping 2	2.81 ± 0.05	3.64 ± 0.81	0.100 ± 0.05
Skipping 1	3.26 ± 0.06	3.80 ± 0.40	0.033 ± 0.01
Skipping 2	2.62 ± 0.10	3.53 ± 0.49	0.041 ± 0.02

Table 4.5: Identified parameters for individual PSD rhythmic loads

It can be seen from Table 4.5 that the PSD load parameters are different for each investigated activity. For jumping activities, the excitation frequency indicates that "jumping 1" is a low-frequency activity whereas "jumping 2" is a high-frequency one. The same remark is made for "skipping 2" and "skipping 1", respectively. All activities except "jumping 2" have similar values of α and δ, with differences attributed to the amplitude of each activity. This amplitude depends on the combination of both parameters. It is also noted that the signal energy (controlled by the bandwidth coefficient δ) is quite concentrated at each harmonic peak (see Figure 4.14(c) for example). However, "jumping 2" has the highest value of δ, indicating that this activity is characterized by a large spread of energy near the harmonic peaks (as noticed in Figure 4.14(b)).

The standard deviation results reveal that the parameter with the greatest fluctuation between the six activity windows is α, followed by f_p and then δ. This is due to the variable amount of energy produced by the individual at each rhythmic action. Activities were performed without pre-determined fixed frequency, which explains the variability in terms of f_p. It is observed that the frequency range is more limited for higher f_p since the choice of the excitation frequency by the participant is more restricted at that level. Maximum variation is found for "jumping 1" which copes well with the multiple peaks of Figure 4.14(a).

For design purposes, the choice of load parameters for the calculation of floor responses due to rhythmic activities (based on Table 4.5) depends on the comfort level agreed by the stakeholders. Therefore, recommendations are provided for each activity considering two principal load cases:

- **Usual/mean load case:** This is devoted to the most frequent and regular loads applied to a floor. Since human-induced load parameters are generally assumed to follow Gaussian distributions ([32], [39]), the mean of f_p, α and δ (see Table 4.5) are to be adopted for this load case as they represent the most probable values.
- **Occasional/maximum load case:** Corresponding rhythmic loads are likely to produce the maximum responses on a floor structure. Maximum values of α and δ (mean + standard deviation) are thus taken from Table 4.5. However, the excitation frequency should be chosen in order to cause resonance at one of the three harmonics of the load whenever possible. In other words, if an excitation frequency (or its integer multiples) in the interval provided in Table 4.5 (mean ± standard deviation) is equal to the natural frequency of the dominant natural mode of the floor, it is used for the considered load. Otherwise, the mean excitation frequency is selected because the floor response would be barely affected by this parameter due to the absence of resonant effects.

4.3.3 Crowd size effect

4.3.3.1 Coordination factors

Crowd size effect has been investigated for 1, 2, 4, 8 and 16 individuals. The procedure described in Section 4.2.3.1 was adopted to determine crowd size relations. For each activity and crowd size, the six pre-processed force records (see Section 4.3.1) were used to calculate RMS forces. Table 4.6 provides the mean and standard deviation of RMS forces for each crowd size. The variation of mean RMS forces by number of participants is displayed in Figure 4.15 for the four investigated activities. This variation is best described by a linear function for jumping activities and a power function for skipping activities.

Activity	RMS force (N)				
	1	2	4	8	16
Jumping 1	1536 ± 156	1899 ± 96	2992 ± 170	4470 ± 1382	9946 ± 1636
Jumping 2	1630 ± 79	2067 ± 259	2736 ± 398	4041 ± 857	8256 ± 1271
Skipping 1	871 ± 47	1338 ± 103	1474 ± 116	2223 ± 646	3181 ± 338
Skipping 2	958 ± 29	1643 ± 115	1763 ± 254	3135 ± 466	4565 ± 631

Table 4.6: Experimental RMS forces by crowd size

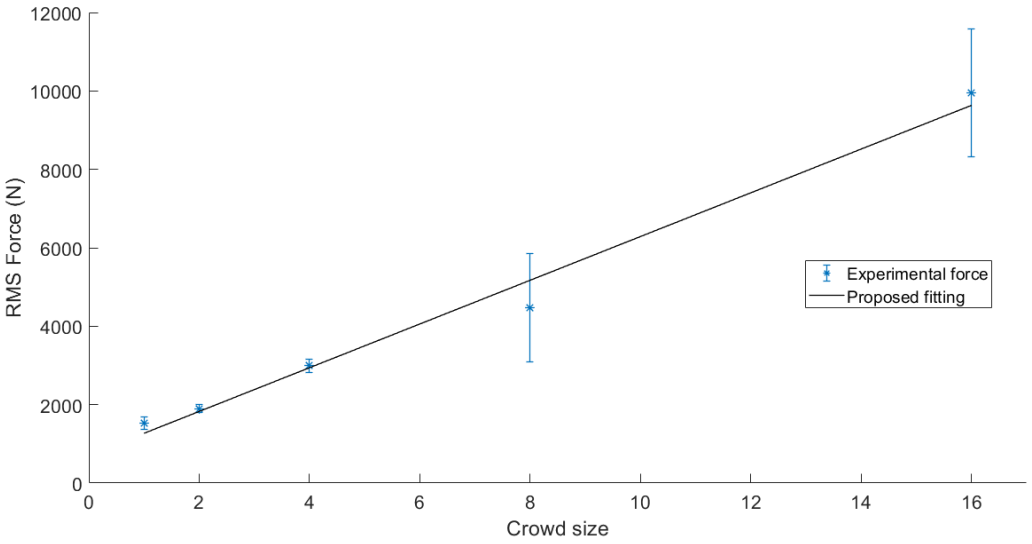

(a) Jumping 1

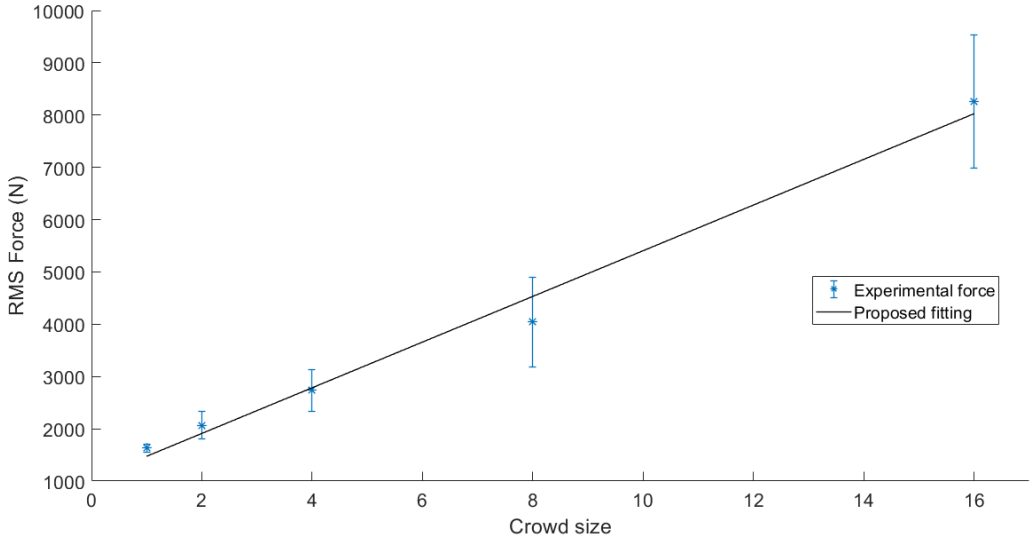

(b) Jumping 2

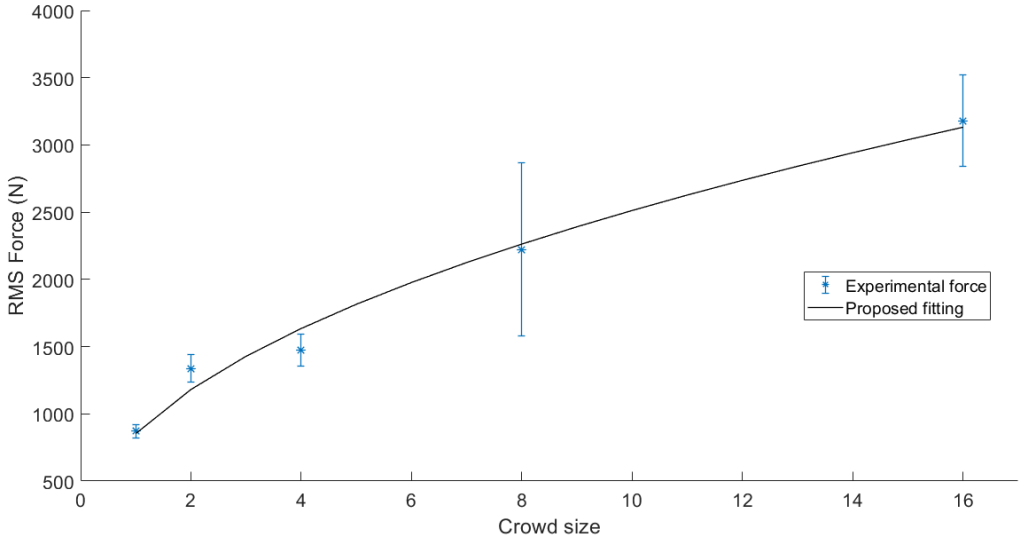

(c) Skipping 1

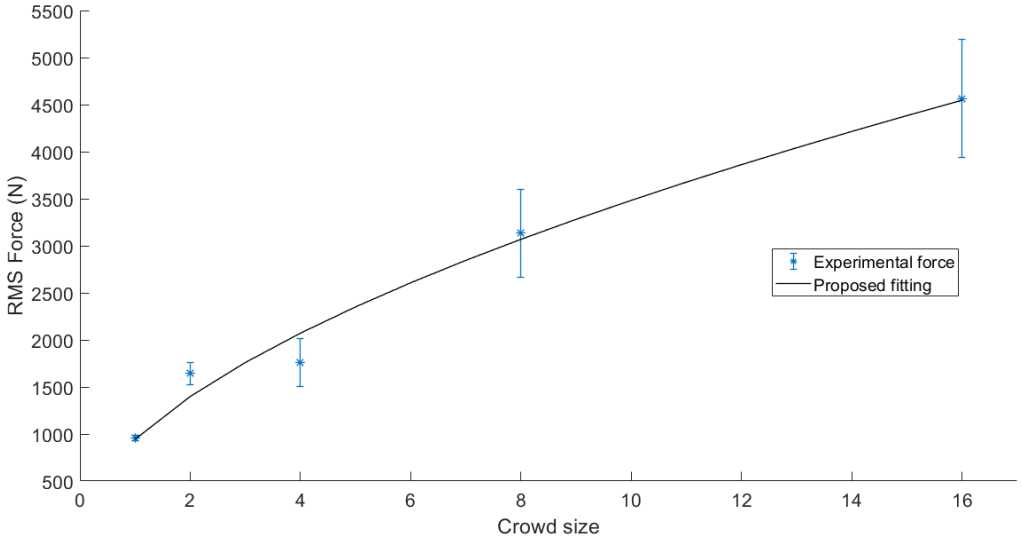

(d) Skipping 2

Figure 4.15: Experimental RMS forces against crowd size (mean in asterisk marks, standard deviation in error bars) and optimal curves (black lines)

The optimal parameters for the best-fit functions of RMS forces against crowd size are presented in Table 4.7 for a group size between 1 and 16. Regression has a high quality for all activities ($R^2 \geq 0.98$).

Activity	Best fit function	R^2
Jumping 1	$F_{rms}(N) = 558N + 711$	0.99
Jumping 2	$F_{rms}(N) = 437N + 1037$	0.99
Skipping 1	$F_{rms}(N) = 853N^{0.47}$	0.99
Skipping 2	$F_{rms}(N) = 944N^{0.57}$	0.98

Table 4.7: Variation of RMS force F_{rms} against crowd size N (R^2 is the determination coefficient)

Coordination factors were then deduced from crowd size relations by the method explained in Section 4.2.3.2. They are given in Table 4.8 and illustrated in Figure 4.16 for up to 16 individuals.

Activity	Coordination factor
Jumping 1	$C(N) = 0.44 + \frac{0.56}{N}$
Jumping 2	$C(N) = 0.30 + \frac{0.70}{N}$
Skipping 1	$C(N) = N^{-0.53}$
Skipping 2	$C(N) = N^{-0.43}$

Table 4.8: Coordination factors C(N) by crowd size N for investigated activities (up to 16 individuals)

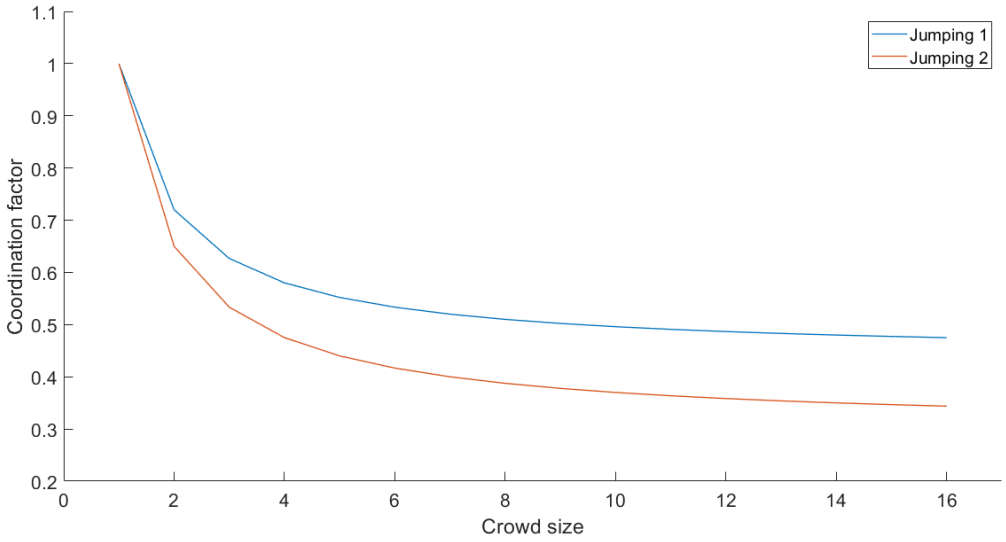

(a) Jumping activities

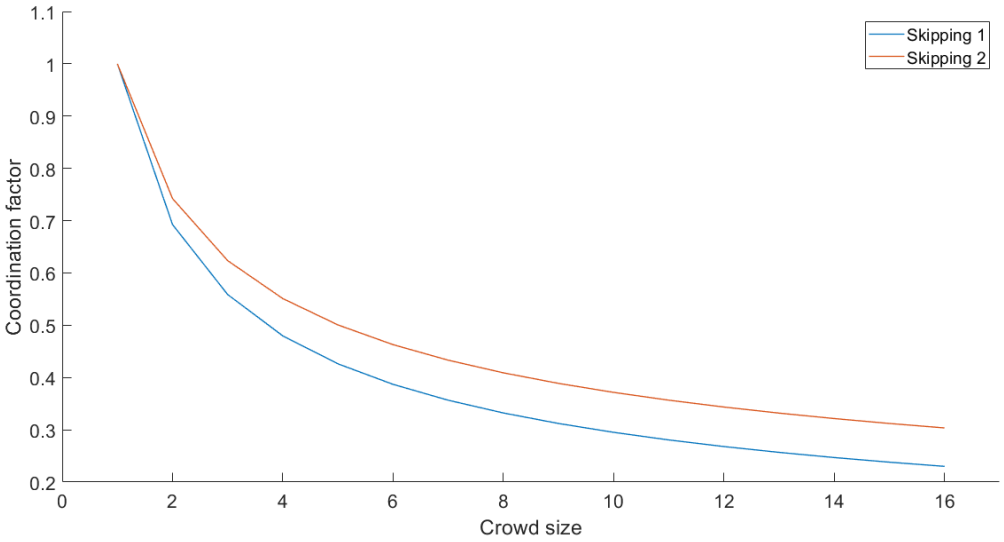

(b) Skipping activities

Figure 4.16: Coordination factors against crowd size (for up to 16 individuals)

4.3.3.2 Discussion

The standard deviation of RMS forces is more important for higher crowd sizes. This is due to the growing variability in the movement of individuals as their number increases, because each of them responds differently to audible and visual stimulus.

The coordination factor has a hyperbolic trend for jumping activities, which yields a stabilization of group effect for higher crowd sizes (see Figure 4.16(a)). However, lower coordination factors are observed for skipping activities, with a decreasing exponential trend providing a stronger decrease of these factors for larger groups (see Figure 4.16(b)). In fact, jumping activities are characterized by a longer aerial phase, enabling jumping pulses to be clearly distinguished. On the other hand, skipping activities are similar to running at a fixed place, exhibiting more randomness between impulses. Hence, participants have more chance to better synchronize their motion in the first category than in the second.

For jumping activities, the excitation frequency is higher for "jumping 2" than "jumping 1" (see Table 4.5). In that case, individuals find more difficulties to synchronize their action in response to audible and visual stimulus. This explains the lower coordination factors determined for the first activity compared to the second.

Concerning skipping activities, it can be concluded that the contact mode of the feet on the floor has an impact on the crowd synchronization. Indeed, the coordination factor corresponding to skipping on feet soles is slightly higher than skipping on feet toes. This may be due to the fact that the contact at soles is more comfortable and less dependent on the type of shoes worn by each participant, thus allowing more coordination than the other type of contact.

4.3.4 Evaluation of floor response due to rhythmic activities

For the analysed activities, the crowd-rhythmic load model is obtained in accordance with Section 4.2.4, by calculating the auto-spectral load model $S_{p,N,k}(f)$ using Eq. (4.21) and the cross-spectral load model $S_{p,N,k,l}(f)$ using Eq. (4.22). The response of these load models is compared against displacement measurements on the floor (see Section 3.4.1.2) for 1, 2, 4, 8 and 16 individuals. For both experimental and numerical cases, a nominal value of 75kg was considered for the mass normalization of responses (see Section 4.2.5), whereas the body mass of individuals was taken from Table 3.11.

4.3.4.1 Experimental RMS responses

Experimental RMS displacements were determined according to the method described in Section 4.2.5.3 using the pre-processed displacement signals (see Section 4.3.1). The variation of RMS response against crowd size was then fitted using the same procedure as for RMS forces (see Section 4.2.3.1) in MATLAB. Figure 4.17 illustrates experimental RMS responses along with the proposed fitting against the number of individuals for all activities.

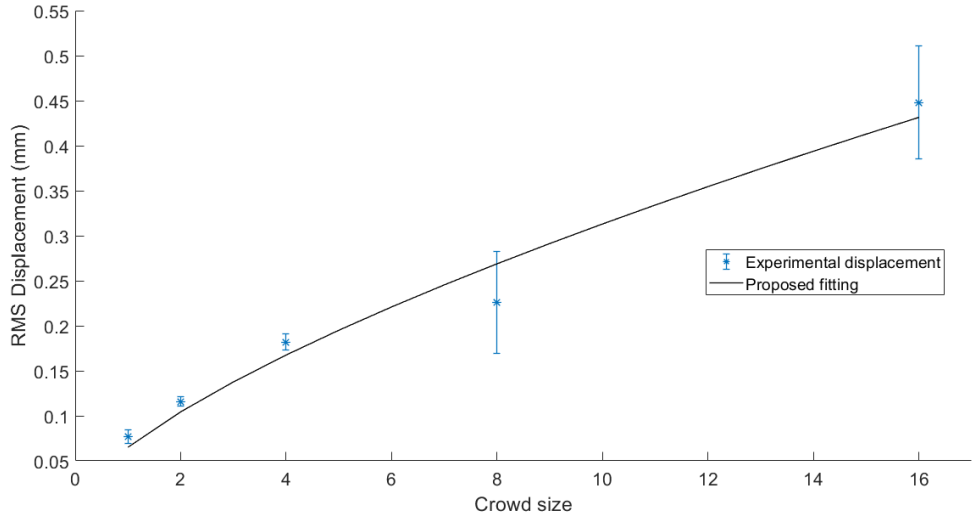

(a) Jumping 1

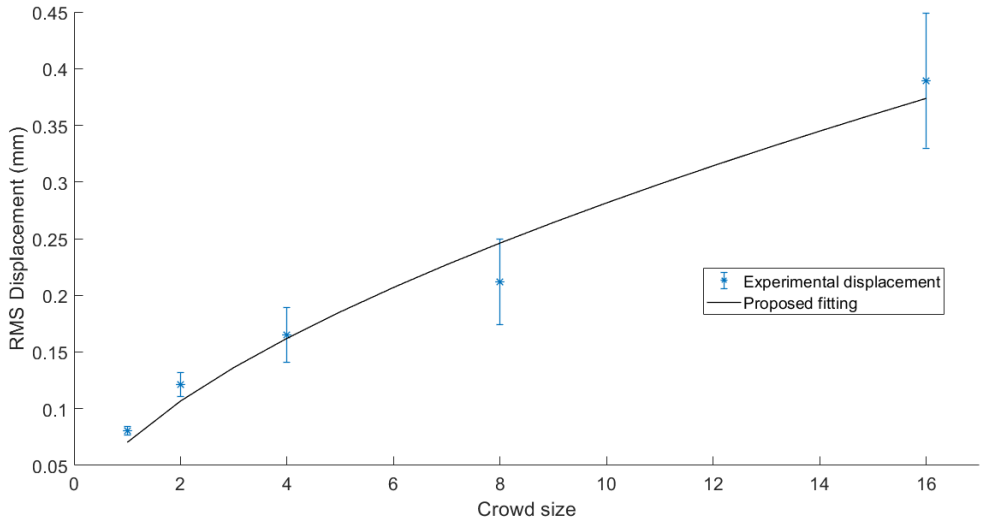

(b) Jumping 2

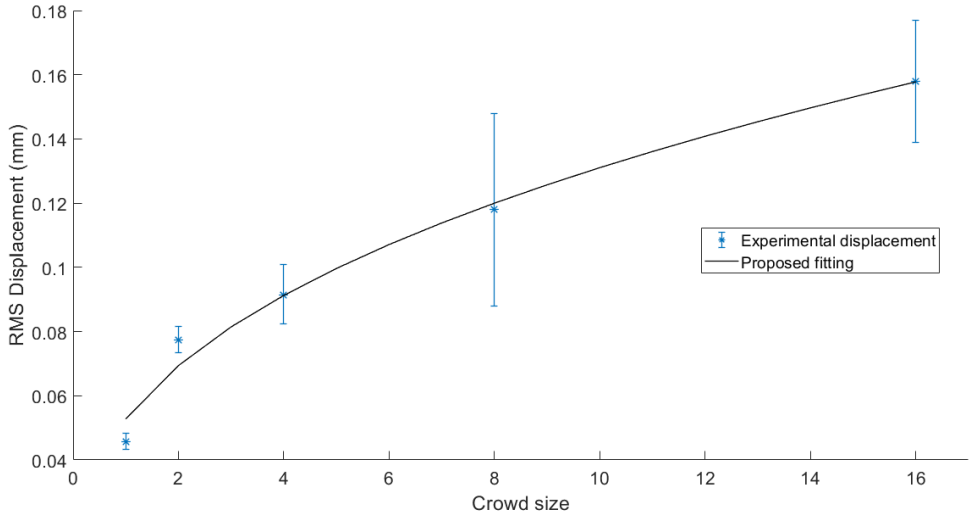

(c) Skipping 1

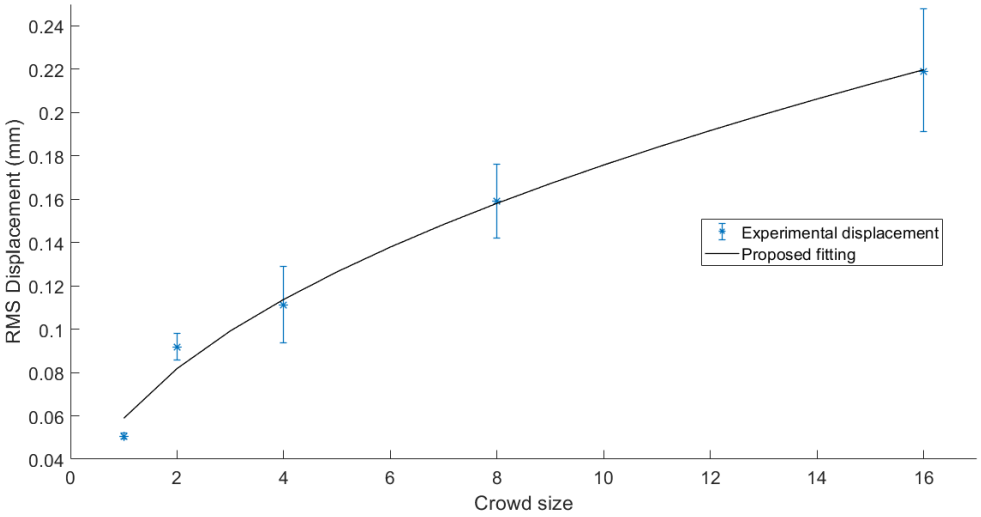

(d) Skipping 2

Figure 4.17: Experimental RMS displacements against crowd size (mean in asterisk marks, standard deviation in error bars) along with optimal curves (black lines)

Table 4.9 summarizes the corresponding best-fit functions for RMS displacements. It can be noticed that the variation of responses exhibits a power trend for all activities. Compared to RMS forces, the same order of amplitudes is found ("jumping 1" – "jumping 2" – "skipping 2" – "skipping 1"). A power trend was also observed for RMS forces related to skipping activities whereas a linear tendency was found for jumping activities (see Section 4.3.3).

Activity	Best fit function	R^2
Jumping 1	$d_{rms}(N) = 0.065N^{0.68}$	0.98
Jumping 2	$d_{rms}(N) = 0.0703N^{0.60}$	0.98
Skipping 1	$d_{rms}(N) = 0.0528N^{0.40}$	0.99
Skipping 2	$d_{rms}(N) = 0.0589N^{0.48}$	0.99

Table 4.9: Best fit functions for RMS displacement d_{rms} against crowd size N (R^2 is the determination coefficient)

However, the principal difference between the two parameters against crowd size is that RMS displacements are decreasing more severely than RMS forces. This can be directly observed for skipping activities for example, which have lower exponents in the power functions of RMS displacements (compared to those of Table 4.7 for crowd RMS forces). This is also noticed for jumping activities but for larger crowd sizes. The observed difference is due to the transition from forces to displacements using the modal properties of the floor.

4.3.4.2 Numerical RMS responses

All activities lasted 30s with a time step of 0.0078s. The positions of the individuals for each crowd size are given in Table 3.9 and illustrated in Figure 3.23. Modal properties of the fundamental mode of the floor (natural frequency, damping ratio, modal shape) are the result of Experimental Modal Analysis described in Section 3.3.2.2. The modal mass is the same as for Section 3.4.1.1.

According to the instructions detailed in Section 4.2.5.1, numerical RMS displacements were calculated for the investigated activities and crowd sizes using the PSD matrix of the crowd load model (using mean optimal parameters) computed with Eq. (4.24). Table 4.10 provides all resulting responses (numerical responses, mean and standard deviation values of experimental responses).

Activity	RMS Displacement (mm)				
	1	2	4	8	16
Jumping 1	0.0852 0.0767±0.007	0.112 0.116±0.005	0.185 0.182±0.009	0.243 0.226±0.057	0.392 0.448±0.063
Jumping 2	0.103 0.0807±0.004	0.122 0.121±0.01	0.183 0.165±0.024	0.224 0.212±0.038	0.344 0.389±0.059
Skipping 1	0.0485 0.0458±0.003	0.0612 0.0775±0.004	0.0868 0.0914±0.009	0.0899 0.118±0.03	0.108 0.158±0.019
Skipping 2	0.0752 0.0505±0.001	0.102 0.0918±0.006	0.155 0.111±0.018	0.172 0.159±0.017	0.221 0.219±0.029

Table 4.10: RMS displacements by crowd size (for each activity, upper line represents numerical results and lower line represents experimental results)

The variation of RMS displacements against crowd size is shown in Figure 4.18 for all analysed activities.

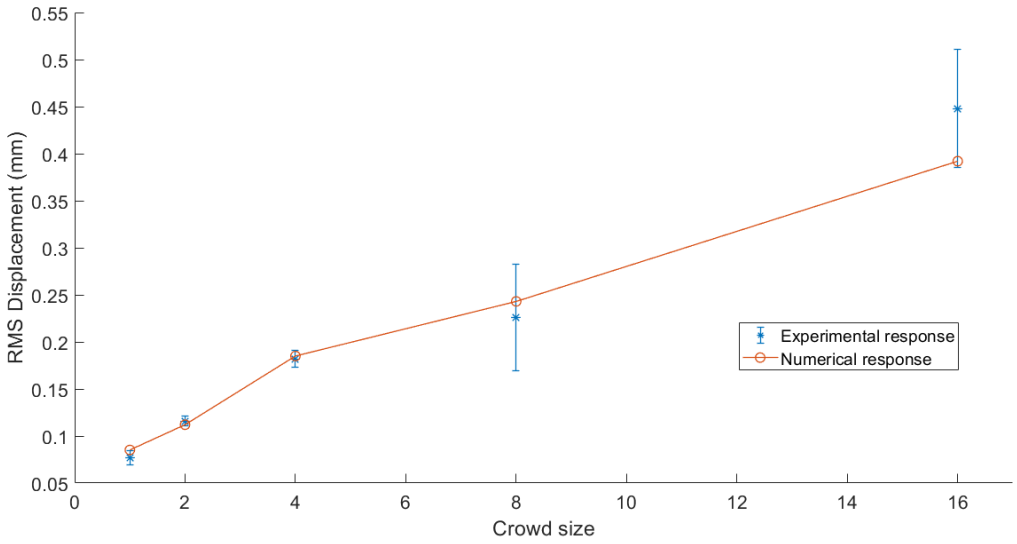

(a) Jumping 1

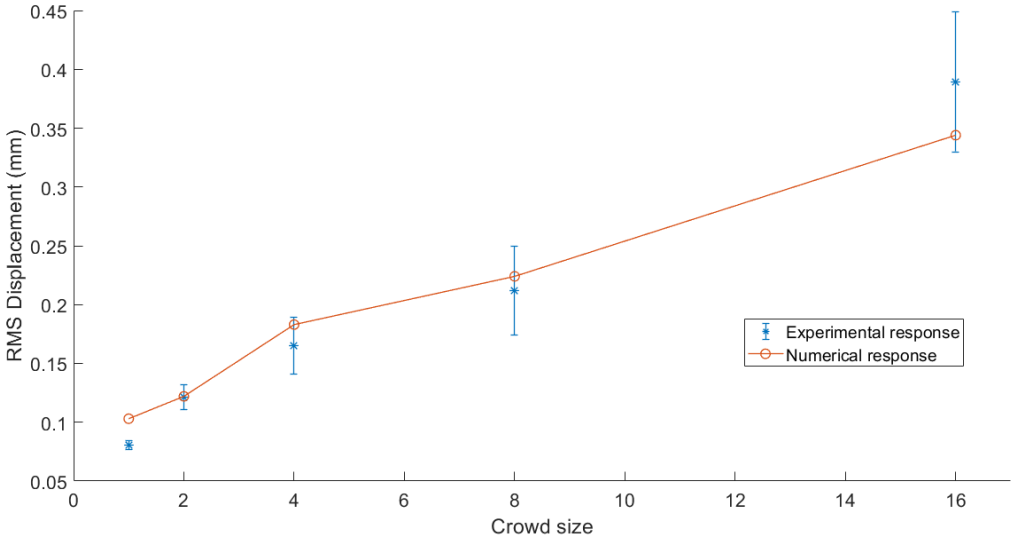

(b) Jumping 2

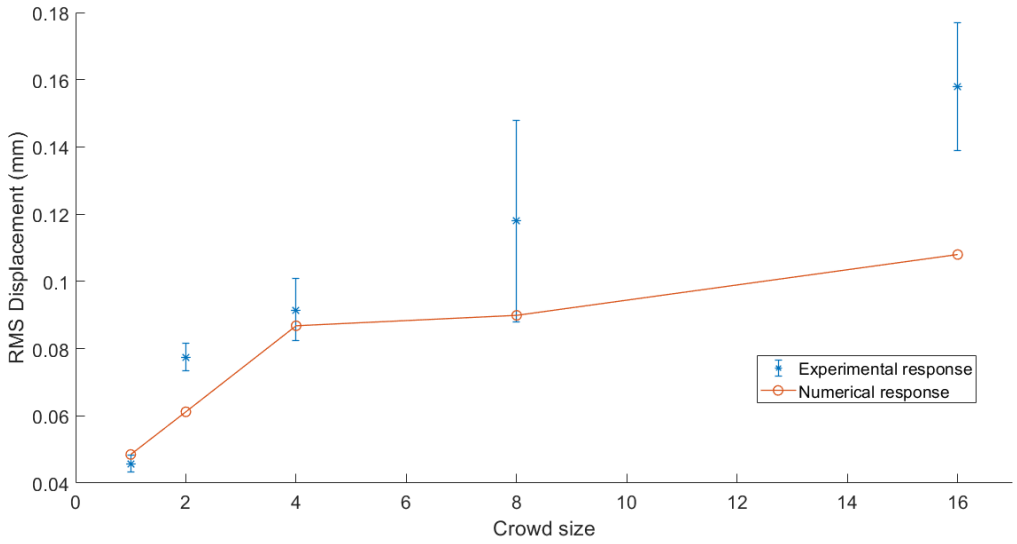

(c) Skipping 1

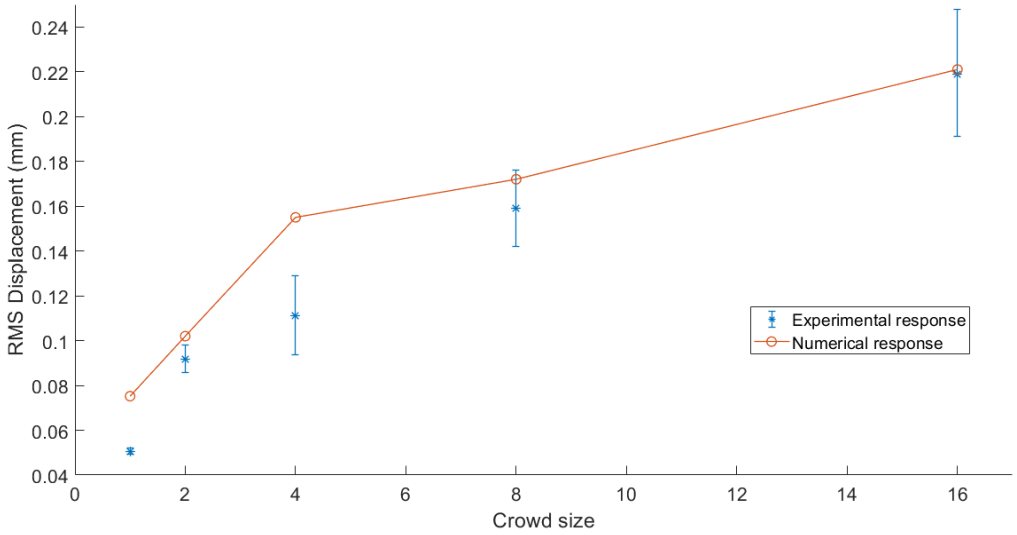

(d) Skipping 2

Figure 4.18: Comparison between numerical RMS displacements (round marks) and experimental RMS displacements (mean in asterisk marks, standard deviation in error bars) against crowd size

4.3.4.3 Discussion

The mean relative difference between numerical and mean experimental responses ranges between 7.2% and 21.8% for the four investigated activities. These differences are attributed to variabilities noticed while performing movements during experiments as well as the inevitable residue resulting from the load identification process. A similar result was obtained by Xiong and Chen [88], who calculated the enclosed area (variance) of the numerical and experimental PSD response curves for the case of a single person jumping. They found a lower relative difference ranging between 0.8% and 14%, probably due to the more complex characterization of the rhythmic load model as a random field.

Concerning jumping activities, numerical displacements are within the variation range of experimental ones ($d_{\mathrm{rms,exp}} \pm \sigma_{\mathrm{rms,exp}}$) for all considered crowd sizes. Differences are attributed

to the variation of excitation frequency and amplitude among activity windows [32]. However, in comparison with experimental responses, higher numerical responses are observed for small groups (up to 8 persons) against lower responses for large groups (16 persons). In fact, when the number of participants increases, the excitation frequency and amplitude become more variable from an activity window to another. In these activities, the excitation frequency is close to 2.55Hz, which matches the fundamental frequency of the floor at the third harmonic (7.65Hz) and causes resonance. This frequency is likely to be reached for larger crowds in vibration tests, thus resulting in higher experimental responses than numerical ones.

For skipping activities, a general tendency for higher RMS displacements is observed for "skipping 2" against lower RMS displacements for "skipping 1". This is concurrent with the higher coordination factors obtained for the first activity compared to the second. Greater differences are also noticed between numerical and experimental responses compared to jumping activities. Besides the variability in excitation frequency and amplitude, skipping exhibits more randomness than jumping. This is translated by a slight variation of excitation positions, which may affect the experimental responses especially for larger crowds.

4.4 Conclusions

A frequency domain modelling approach for rhythmic activities is proposed in this chapter. The single person model is expressed by means of Power Spectral Density (PSD) functions. The model has a bell shape allowing a spread of energy (leakage) in the vicinity of each harmonic peak. The identification of PSD load parameters from measured forces due to a single person is made by the least-squares method. This technique allows for the entire signal record to be used so that "intra-subject variability" observed during the rhythmic action could be considered. Coordination factors, taking into account "inter-subject variability", are derived from the best-fit curves describing the variation of crowd RMS forces against crowd size. The total spectral crowd load model is then obtained after combination of the two above mentioned elements.

Subsequently, the proposed rhythmic load model is identified using the results of vibration tests presented in Chapter 3. For the case of a single person, obtained parameters are quite different among the four rhythmic activities. The load energy is rather concentrated at the peaks of each harmonic, except for quick jumping where a spread of energy is noticed. The amplitude has the highest variability as the impact on the floor differs at each sequence of activity. Recommendations regarding the definition of load parameters for design purposes are provided afterwards depending on the considered comfort level (to be determined by the stakeholders). Furthermore, the variation of crowd RMS forces is more considerable for an increasing crowd size as larger groups of individuals find more difficulties to coordinate their motion compared to smaller groups. In terms of coordination factors, a hyperbolic decrease with respect to crowd size is found for jumping activities (see Figure 4.16(a)) against lower values for skipping activities characterized by an exponential decrease (see Figure 4.16(b)). The contact mode of the foot on the floor has an impact on the crowd synchronization as coordination factors are higher for skipping on soles compared to skipping on toes. The crowd PSD load models are then used to determine RMS displacements which were compared with their experimental counterparts (the mean relative difference ranged between 7.2% and 21.8%). Despite these satisfactory results, the proposed crowd-rhythmic load models need to be verified on existing real-life floor structures and their scope extended to higher crowd sizes, which is done in the next chapter.

5 Verification of rhythmic load models on a full-scale floor structure

5.1 Introduction

Compared to small-scale structures, building floors encountered in real life have geometrical properties that differ from a simple rectangular shape due to architectural considerations. When subjected to rhythmic activities, more than one dominant mode of the floor is usually excited in the frequency range of human excitation [20]. Therefore, experimental investigation of such floors is a key element in order to take into account these differences in the characterization of rhythmic activities performed by a single person or crowds. A first possible way to do this is by conducting rhythmic tests under controlled conditions in terms of frequency and crowd size. This was done by Fernández Martínez et al. [41] on a 36×12m² floor having a non-symmetric shape. Accelerations were recorded for various crowd sizes with a maximum of 30 individuals jumping with a controlled frequency. An et al. [4] carried out jumping tests on an innovative "Cable Supported Beam Structure-Concrete Slab Composite Floor System", having an area of 56×40m². Acceleration responses were measured for up to 64 persons performing jumping and stepping activities, for either random or controlled frequency by a metronome. Previous tests may not capture group effects as noticed in reality, where people practice activities in unrestricted conditions. Instead, a monitoring of floor structures was made under real-life events. Ellis and Littler [34] monitored a three-cantilever grandstand during sport events. The upper and lower cantilever tiers both support ten rows of seats and each main section supports approximately 280 persons. Ellis et al. [35] conducted detailed tests on 11 cantilevered stands during diverse public events. The capacities of the cantilevered tiers vary from 600 to over 10,000 seats. Most of the previous tests investigated "normal jumping" activity only as it has the maximum load amplitude among rhythmic activities. However, there are other activities which are likely to occur in several floors (such as aerobics in gymnasiums, other jumping styles in fitness centres, etc.) and could result in higher load magnitudes than "normal jumping" [67].

In that context, experiments were carried out on a full-scale floor in order to verify the crowd-load models established in Chapter 4 associated to multiple rhythmic activities. This multi-modal structure enables extending the range of crowd size to a maximum of 32 individuals uniformly distributed over the floor. This chapter begins with the presentation of the floor structure together with conducted tests (Experimental Modal Analysis, vibration tests under rhythmic actions). The crowd-induced load models are then verified (with an extension of their scope) by means of acceleration responses for two rhythmic activities. Subsequently, proposed load models are compared against existing literature in terms of forces and numerical responses for three different floor structures. An equivalent crowd load model formulation is finally proposed, based on the observation of experimental loads and responses against crowd size.

5.2 Experimental tests on a full-scale floor

An experimental program was designed in order to provide reliable data to be used in the verification of the load models characterizing rhythmic activities performed by groups of people. Two test campaigns have then been performed on a full-scale floor structure: Experimental Modal Analysis and human-induced vibration tests [28]. Both campaigns were conducted by the Structural and Stochastic Dynamics group of the University of Liège together with V2i Company.

5.2.1 Description of the structure

The tested building is an open car parking newly constructed by Briand CM Company at the time of experiments and located in Nantes, France (see Figure 5.1(a)). The structure has three storeys composed of composite steel and concrete floors with large dimensions (an area of about 4200m² per storey). The tested floor was located at the first storey (3m above the ground). A rectangular area of 22.5×15.785m² near the floor centre was selected for testing (see Figure 5.1(b)).

(a) 3-storey open car parking

(b) Tested floor area

Figure 5.1: Tested building

The tested area comprised a 130mm thick composite concrete deck, with 0.75mm thick profiled steel sheet of Cofraplus 60 type (see Figure 5.2(a)). The composite floor was supported underneath by welded I-members, and connection was achieved by shear studs with 19mm diameter and 100mm height. The secondary beams had a 500×5 web and 150×12 flanges. The primary beams had a 470×8 web and 200×15 flanges, except for two beams which had a 480×6 web and 150×10 flanges. The columns were made of HEB340. All beams were assumed simply supported.

Figure 5.2(b) illustrates a plan view of the tested floor. Concrete was of C30/37 class whereas steel beams and columns were of S355 and S275 grade, respectively. At the moment of tests, the structure was in a bare state and the existing non-structural elements were side partitions only.

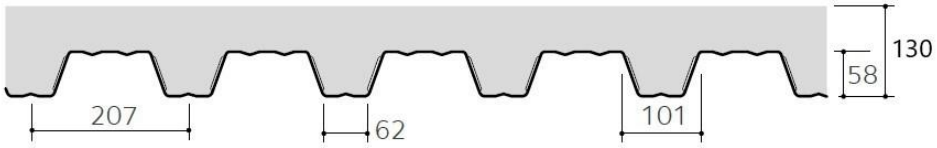

(a) Cofraplus 60 steel sheet

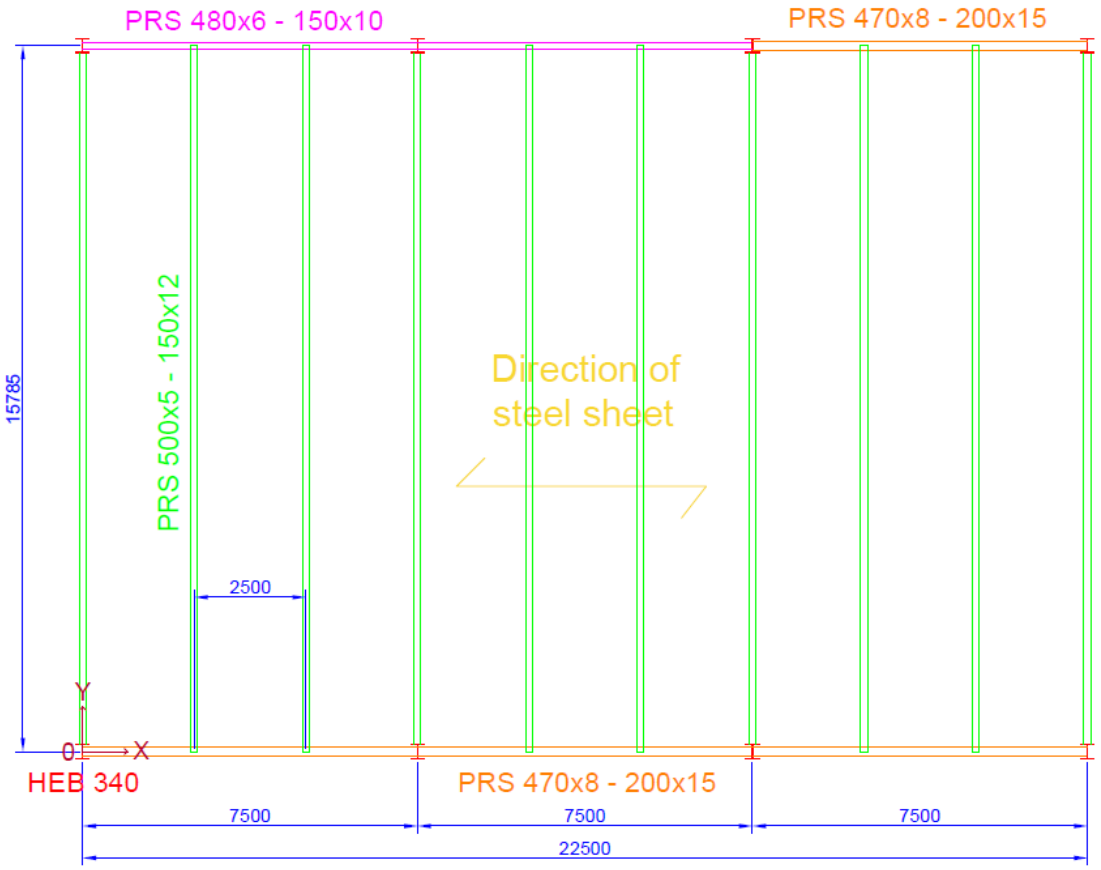

(b) Plan view of the floor

Figure 5.2: Tested floor layout (dimensions in mm)

5.2.2 Experimental Modal Analysis

In order to determine modal properties of the full-scale structure, Experimental Modal Analysis (EMA) [69] was conducted during the first day of experiments. Instrumentation and procedure for this test campaign are presented, followed by resulting modal parameters of the floor in the frequency range of interest.

5.2.2.1 Instrumentation

As the floor structure is of large mass and dimensions, modal testing was made using an electrodynamic shaker [2] (see Figure 5.3(a)) designed by the Structural and Stochastic Dynamics group of the University of Liège. The shaker system is digitally controlled (see Figure 5.3(b)) and equipped with a 230kg mass which moves vertically with an amplitude of

0.5 or 1mm [24]. This device can generate white noise excitation or a sinusoidal excitation in a wide range of frequencies. The response of the floor due to the shaker excitation was measured by G-link-200 wireless accelerometers (see Figure 5.3(c)). A synchronous measurement of the acceleration near the shaker was also made by PCB 3713B122G accelerometers (see Figure 5.3(d)).

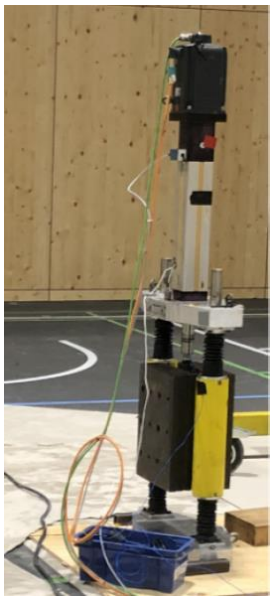

(a) Electrodynamic shaker [24]

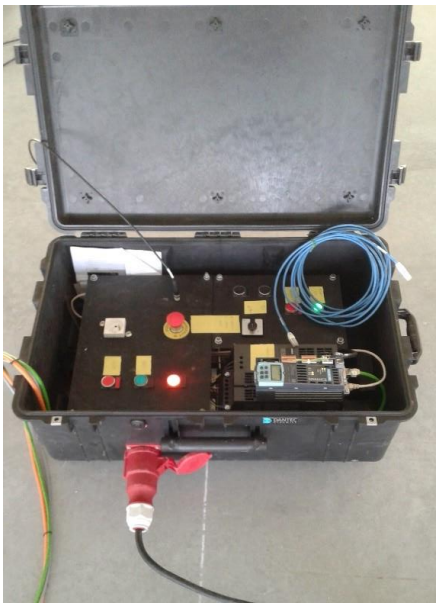

(b) Shaker controlling device

(c) G-link-200 accelerometer

(d) PCB 3713B122G accelerometer

Figure 5.3: Shaker EMA equipment

5.2.2.2 Experimental setup

The shaker was consecutively placed at two locations labelled Setup 1 and Setup 2 in Figure 5.4(a). An illustration of the shaker at one of these positions is shown in Figure 5.4(b).

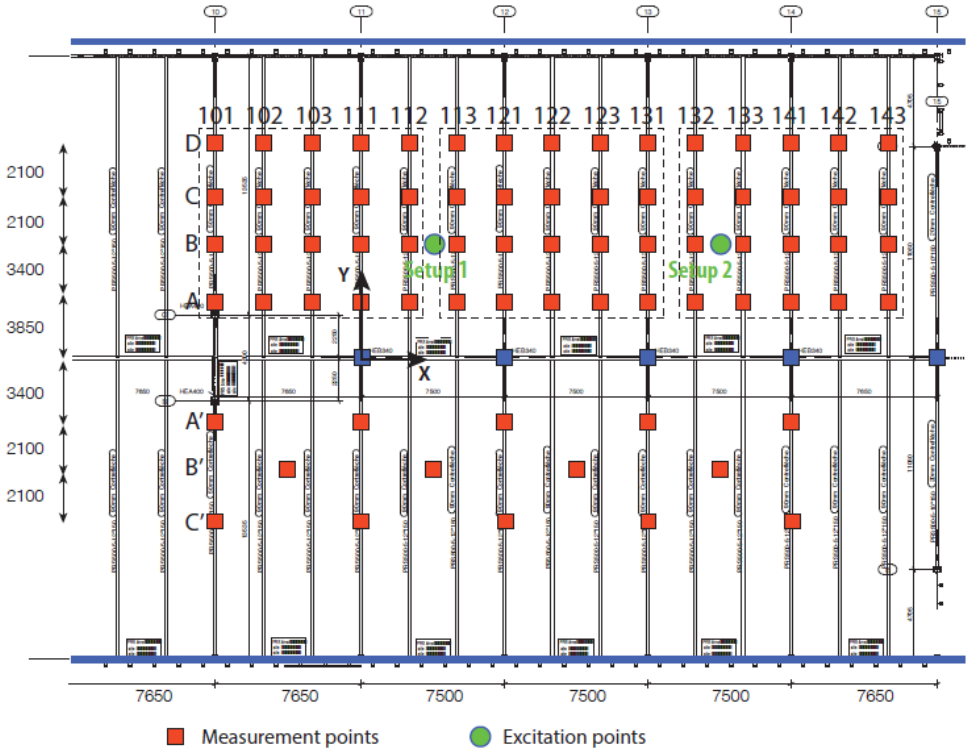

(a) Positions of the shaker and accelerometers [24] (dimensions in mm)

(b) Shaker exciting the floor

Figure 5.4: Shaker EMA setup

For each position of the shaker, a white noise excitation in the frequency range between 3 and 10Hz has been applied on the analysed floor [24]. The frequency of 3Hz is the minimum natural frequency recommended by several design guidelines for floor structures ([63], [81]), whilst the maximum frequency encountered for rhythmic activities is 10Hz [31]. Accelerations were measured on the moving mass (leading to shaker force) and near the shaker. This provides Frequency Response Functions (FRFs) (given by Eq. (3.5)) which allow the detection of natural frequencies at the time of excitation. The main objective is to identify the frequency bands that contain the major dominant natural modes of the structure in the frequency range of interest.

Figure 5.5 displays the obtained FRFs from the two setups. Major peaks are comprised in the frequency range of [3, 6.5Hz] and [7, 10Hz] for both setups. For both frequency bands, a sinusoidal excitation was applied by the shaker with a variable frequency and increasing variation step, leading to a more refined identification of resonant peaks.

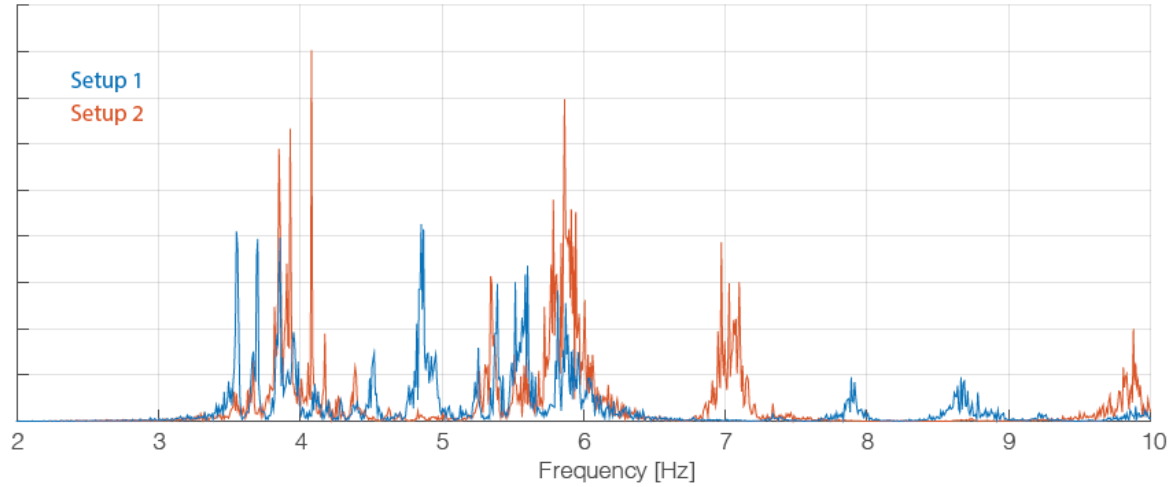

Figure 5.5: FRFs after white noise excitation for Setup 1 and 2 [24]

For each detected natural mode, harmonic excitation was applied using the associated natural frequency while accelerations were measured at different locations of the floor (see Figure 5.4(a)). These locations comprised the investigated area and its neighbourhood in order to account for boundary effects. These measures provided relative responses (to the maximum value), thus leading to the determination of corresponding modal shapes. Modal peaks were then obtained from resulting FRF plot against frequency. Figure 5.6 illustrates an FRF plot for Setup 1 and the first frequency band. A curve-fitting procedure was used at the local FRF of each mode to determine a first approximation of natural frequencies, damping ratios and modal masses. The latter could be determined due to the presence of the driving point response (same as excitation point) [2].

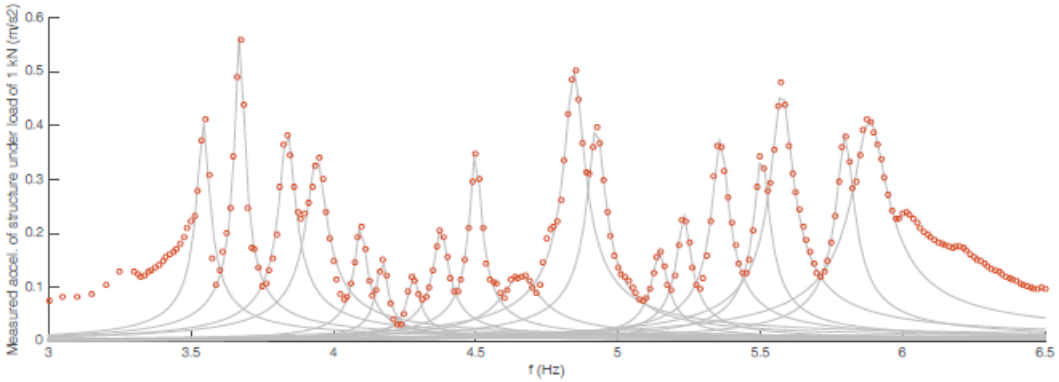

Figure 5.6: Mode-by-mode FRF for Setup 1 and frequency band between 3 and 6.5Hz [24]

A unique multi-modal FRF was then constructed based on the contributions of all extracted modes. Subsequently, a curve-fitting algorithm was applied to the resulting FRF to provide more precise values of modal parameters. Figure 5.7 shows a multi-modal FRF plot corresponding to the driving point for Setup 1 and the first frequency band. Finally, modal

results from the two setups were compared in order to deduce the most dominant modes in the common frequency range, along with natural modes detected by each setup only.

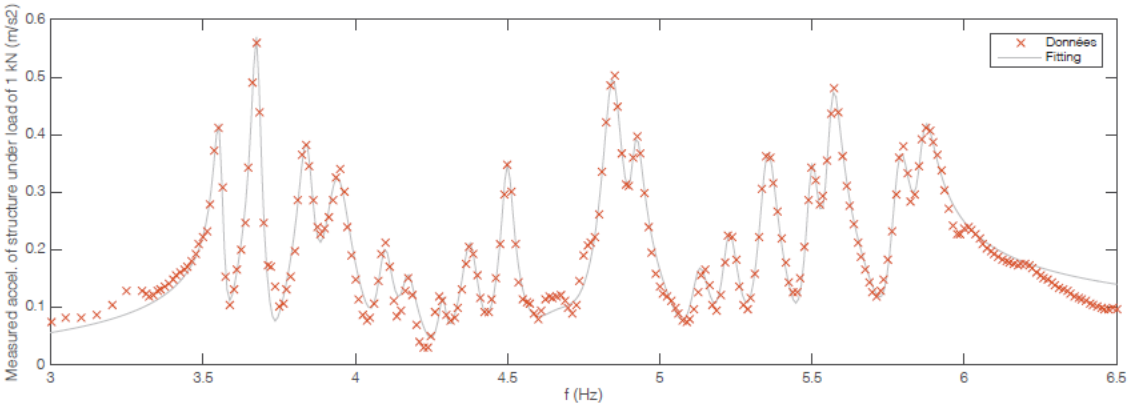

Figure 5.7: Multi-mode FRF for Setup 1 and frequency band between 3 and 6.5Hz [24]

5.2.2.3 Modal analysis results

Data analysis revealed the existence of 20 closely spaced bending modes whose natural frequencies range between 3 and 10Hz. Natural frequencies, modal masses and damping ratios of the floor are presented in Table 5.1. The floor is thus a multi-modal structure, due to the absence of a perfect symmetry in the tested area and the whole floor (non-uniform shape, side partitions, existence of multiple storeys, etc.). Furthermore, the fundamental natural frequency is 3.56Hz, indicating that the structure is a low-frequency floor ([61], [63], [81]). The low damping ratios of the natural modes (see Table 5.1) causes the floor to be more sensitive to human excitation.

Mode	Natural frequency (Hz)	Modal mass (t)	Damping ratio (%)
1	3.56	297	0.44
2	3.68	174	0.45
3	3.84	127	0.69
4	3.94	167	0.57
5	4.10	159	0.53
6	4.17	150	0.61
7	4.29	150	0.30
8	4.50	133	0.46
9	4.67	123	0.70
10	4.85	98	0.70
11	5.23	161	0.50
12	5.35	191	0.56
13	5.50	238	0.40
14	5.57	242	0.49
15	5.78	112	0.57
16	5.86	125	0.53
17	6.93	120	1.17
18	7.85	121	0.73
19	8.60	34	1.23
20	9.99	36	0.89

Table 5.1: Identified modal properties of the floor

An example of identified modal shapes is illustrated for four different modes in Figure 5.8.

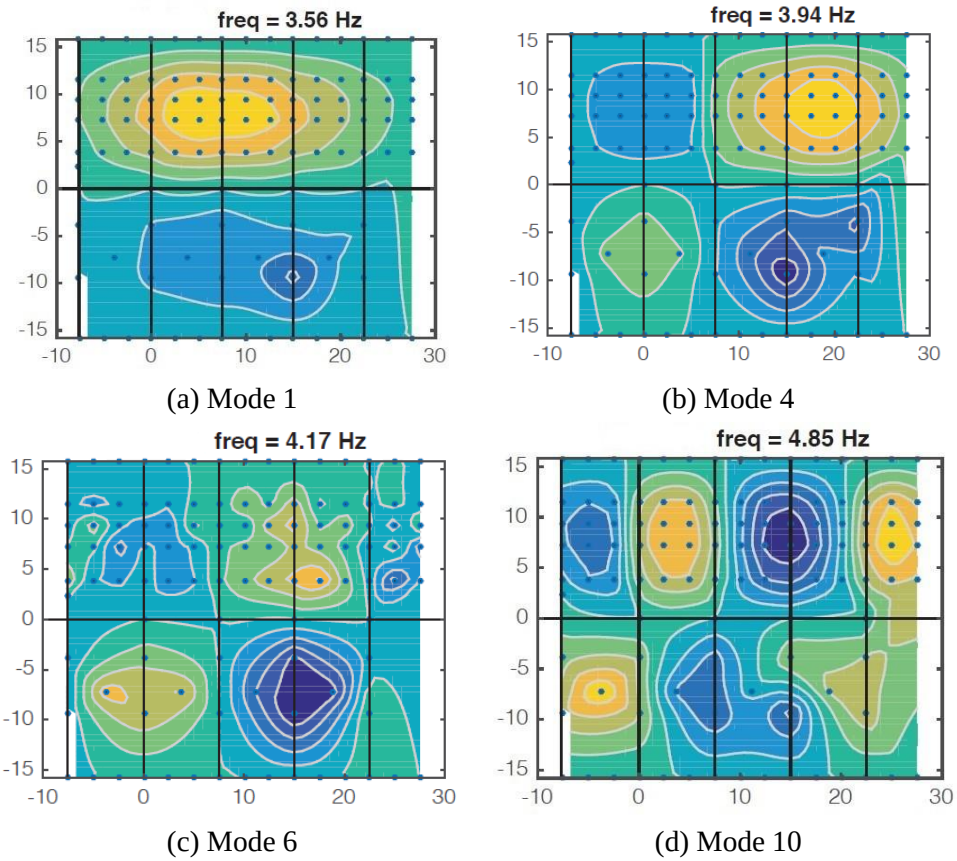

(a) Mode 1 (b) Mode 4

(c) Mode 6 (d) Mode 10

Figure 5.8: Identified modal shapes [24] (dimensions in m)

5.2.3 Vibration tests under crowd-rhythmic activities

5.2.3.1 Experimental protocol

A series of tests were conducted in order to measure the floor response under various human-induced rhythmic loads. It was intended to reproduce the same activities as performed in laboratory tests in order to accurately validate the associated load models. Each rhythmic category (jumping, skipping) described in Section 3.4.2.1 was represented by one activity, which were jumping jack and skipping on feet soles (termed “jumping 1” and “skipping 2”, respectively).

Similar to the laboratory tests, rhythmic excitation was carried out in multiple series of crowd size (with a minimum of 2 persons). However, the case of 32 persons was also considered since the floor offered a convenient area for such number of participants without safety issues. Figure 5.9 illustrates performed activities for all investigated crowd sizes.

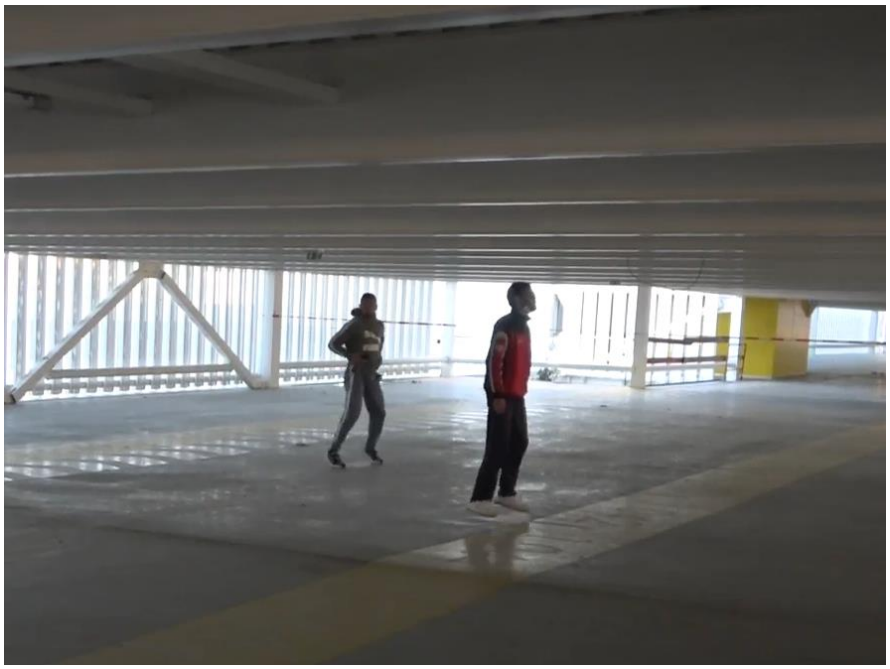

(a) 2 participants

(b) 4 participants

(c) 8 participants

(d) 16 participants

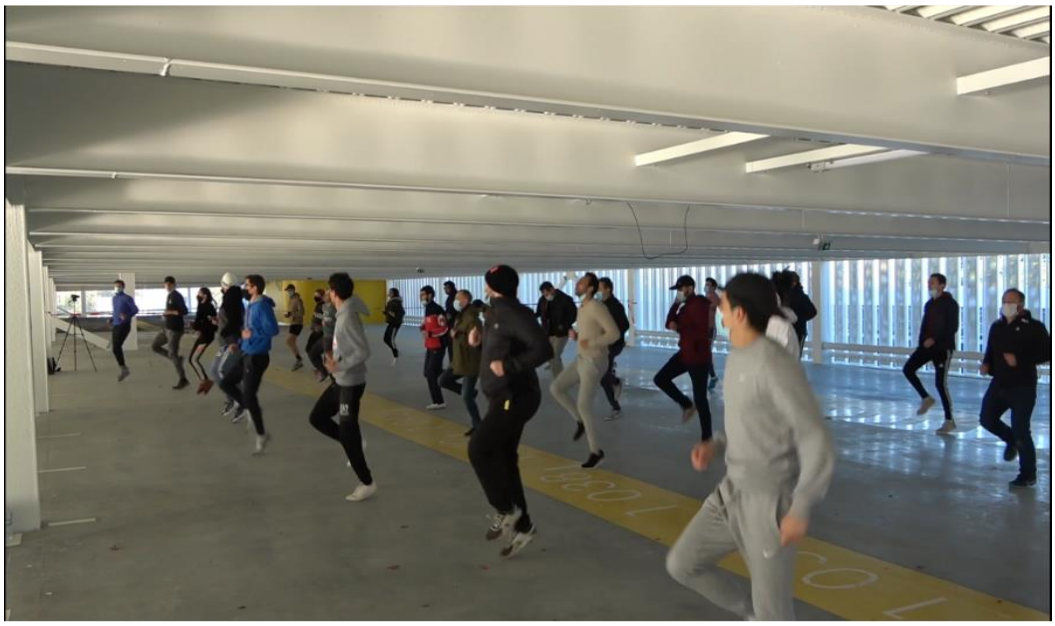

(e) 32 participants

Figure 5.9: Examples of rhythmic activities by crowd size performed on the full-scale floor

Individuals stayed at fixed positions uniformly distributed over the floor (see Figure 5.10). The distance between participants was 2.5m in both directions in plan, resulting in a density of 0.16 person/m², which belongs to the low range of density of occupants [42]. The adopted positions of participants by crowd size are presented in Table 5.2.

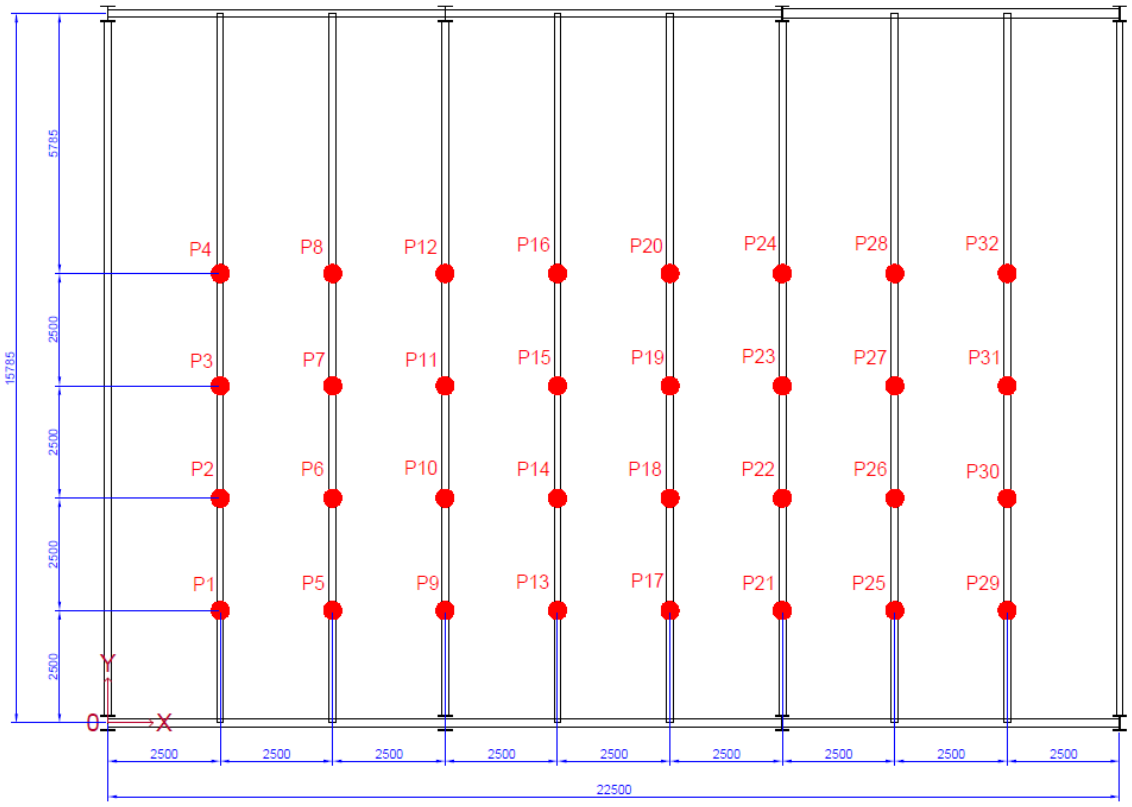

Figure 5.10: Positions of participants during rhythmic tests (dimensions in mm)

Crowd size	Positions
2	P14, P19
4	P14, P15, P18, P19
8	P10, P11, P14, P15, P18, P19, P22, P23
16	from P9 to P24
32	From P1 to P32

Table 5.2: Positions of participants by crowd size

The same coordination stimulus used in laboratory tests was adopted, which is a rhythmical song (audible), and the movement of an experienced sports coach away from the floor (visual). The latter was followed by the participants in order to achieve synchronization as close as possible to real life situations (see Figure 5.11).

Figure 5.11: Coach (at left) in front of participants

Tests have been divided into two sets, each having specific crowd size, duration and repetition of activities (called windows) as presented in Table 5.3. A duration of 1min was adopted for each window to have a full record of motion from the beginning to tiring of participants (longer than 45s used in laboratory tests). More repetitions were also considered to take into account the variability of rhythmic actions, which were reduced from 9 to 6 because fatigue of individuals was noticeable after the first two series of crowd sizes.

Set	Crowd size	Duration	Repetition (windows)
1	16, 32	1 minute	9 times
2	2, 4, 8	1 minute	6 times

Table 5.3: Vibration test sets

5.2.3.2 Characteristics of the participants

A total of 35 participants (all volunteers) were involved in this campaign, including 26 men and 9 women. The test procedure was shortly explained to all participants at their arrival. The collected data from this group (sex, weights, ages and birth countries) is provided in Table 5.4.

Individual	Sex	Age	Birth country	Body mass (kg)
1	Male	27	France	79.6
2	Male	24	Morocco	66.6
3	Male	58	Yugoslavia	79.1
4	Male	36	France	91.5
5	Male	54	Morocco	92.7
6	Male	42	Belgium	88.6
7	Male	37	France	94.5
8	Male	23	Morocco	61.4
9	Male	18	France	72.9
10	Male	24	Morocco	76.2
11	Male	20	France	96.7
12	Male	21	France	74.8
13	Female	21	France	59.2
14	Female	22	Morocco	63.4
15	Female	22	Morocco	56.7
16	Female	23	Morocco	56.7
17	Male	23	Morocco	126.6
18	Male	24	France	80.7
19	Male	21	France	71.2
20	Male	55	France	99.6
21	Male	21	France	96
22	Male	22	Morocco	58.8
23	Male	21	France	70.6
24	Male	23	Morocco	73.8
25	Male	20	France	81.8
26	Female	22	France	61.8
27	Male	20	France	73
28	Male	23	Morocco	72.2
29	Male	21	France	75.7
30	Male	20	France	72.3
31	Female	21	France	52.3
32	Male	54	France	86.5
33	Female	53	France	63
34	Female	21	France	58.9
35	Female	21	France	67.9

Table 5.4: Collected data for involved individuals in vibration tests

24 participants were born in European countries whilst 11 participants came from African ones. The age of volunteers ranged between 18 and 58 years (mean: 28 years, standard deviation: 12 years) and their weight varied from 52.3 to 126.6kg (mean: 75.8kg, standard deviation: 15.4kg). The distribution of weight and age for all participants is presented in Figure 5.12. It reveals that participants have a mean body mass of nearly 75kg (close to the nominal body mass suggested by SCI P354 guideline [81]) and most of them were aged below 24 years, indicating a rather young sample of individuals.

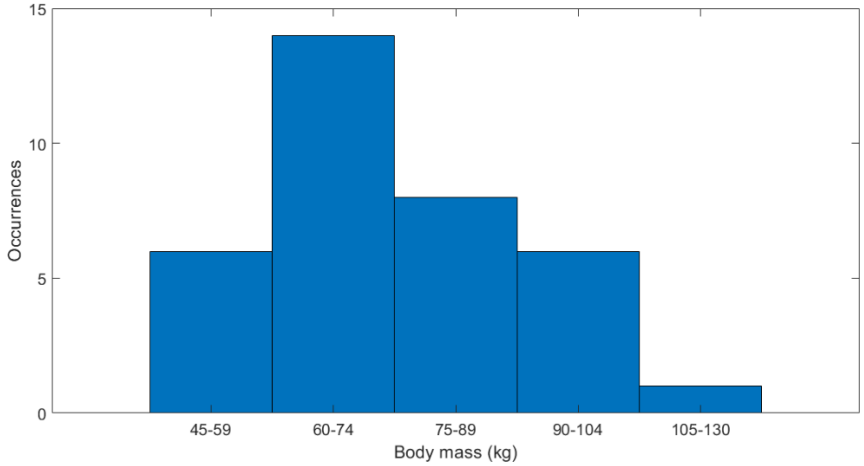

(a) Body mass

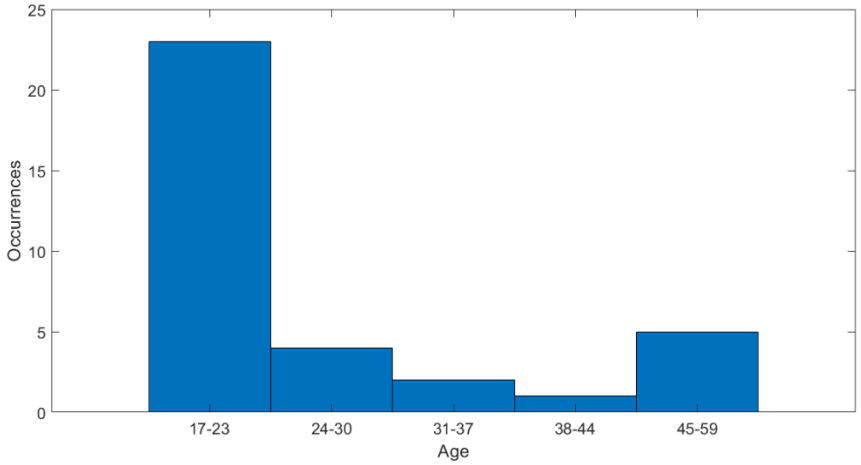

(b) Age

Figure 5.12: Distribution of parameters associated to participants

5.2.3.3 Response measurements

Since the structure has large dimensions along with multiple natural modes, the most suitable response parameter to be investigated was acceleration (conversely to displacement for the laboratory floor). It is also the easiest response parameter to be measured on floors, which supports its wide usage in vibration serviceability assessment against human discomfort ([45], [63], [81]).

Floor accelerations induced by human activities were measured using 10 cabled PCB 3713B122G accelerometers, having a sampling frequency of 256Hz and a measurement range of ±2 g. They were placed at different positions over the investigated area, as shown in Figure 5.13(a). Mounting of accelerometers was made on the secondary beams below the floor by means of magnets (see Figure 5.13(b)).

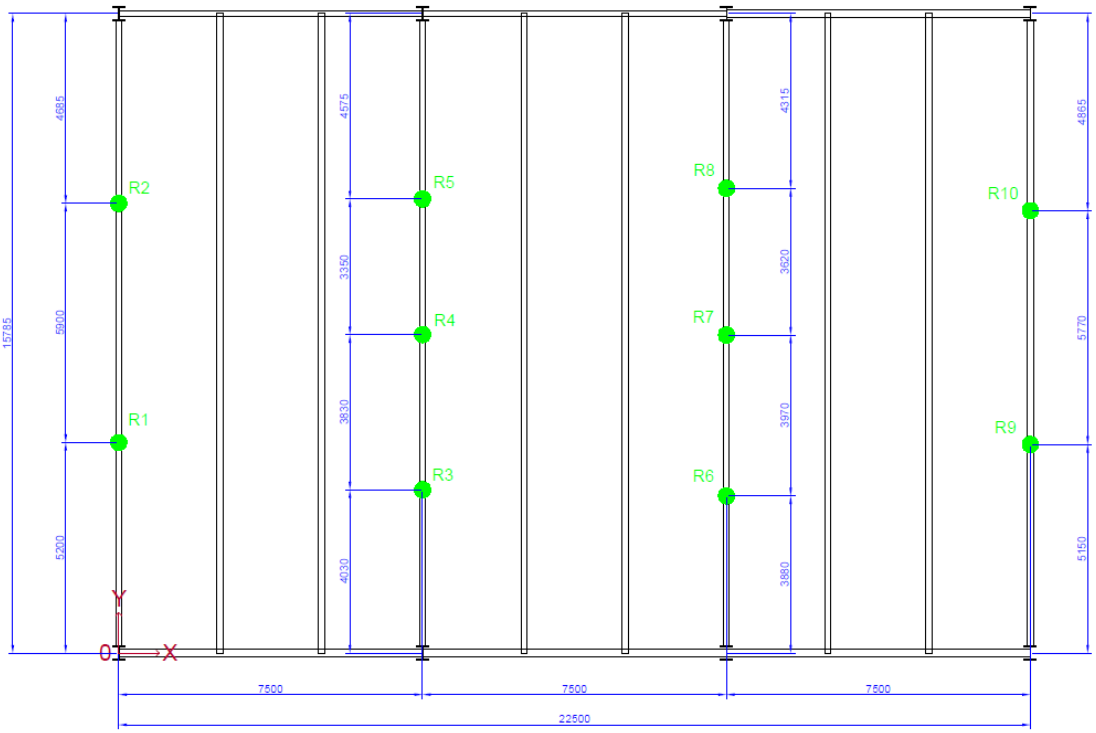

(a) Positions of accelerometers (dimensions in mm)

(b) Accelerometer R9 placed on a secondary beam

Figure 5.13: Configuration of response measurements

A total of 2 hours of response data was recorded during this campaign. For the investigated rhythmic activities, accelerations were measured for each activity window (see Table 5.3) as illustrated in Figure 5.14.

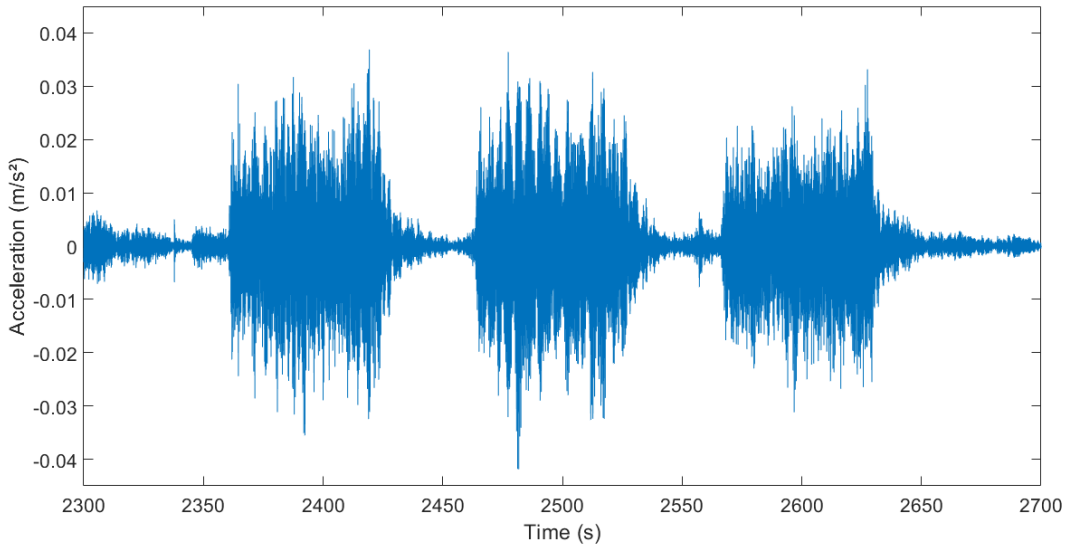

(a) Jumping 1

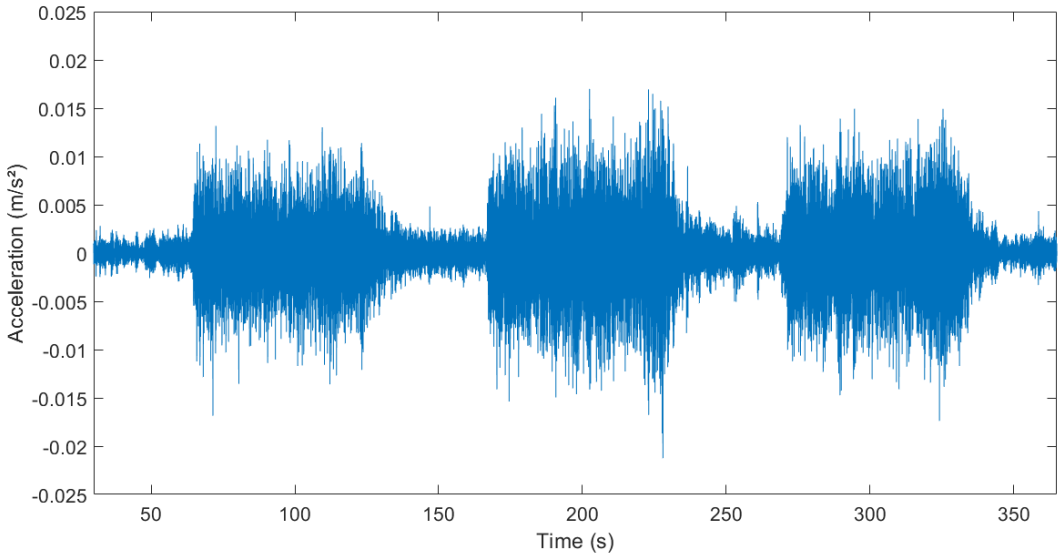

(b) Skipping 2

Figure 5.14: Illustration of rhythmic activity windows performed by 4 persons

5.3 Full-scale verification of rhythmic load models

5.3.1 Pre-processing

Acceleration records due to rhythmic activities were processed using MATLAB. Illustration is made in the following text for the case of 4 persons performing "skipping 2" activity. The same pre-processing procedure was applied to all measured signals. For each activity, crowd size and accelerometer, structural responses were extracted based on an automatic envelope detection implemented with a Hilbert transform. Using this envelope, activity windows having an acceleration exceeding the value of ambient noise (between windows) by 50% were conserved. Figure 5.15 displays an activity window after extraction.

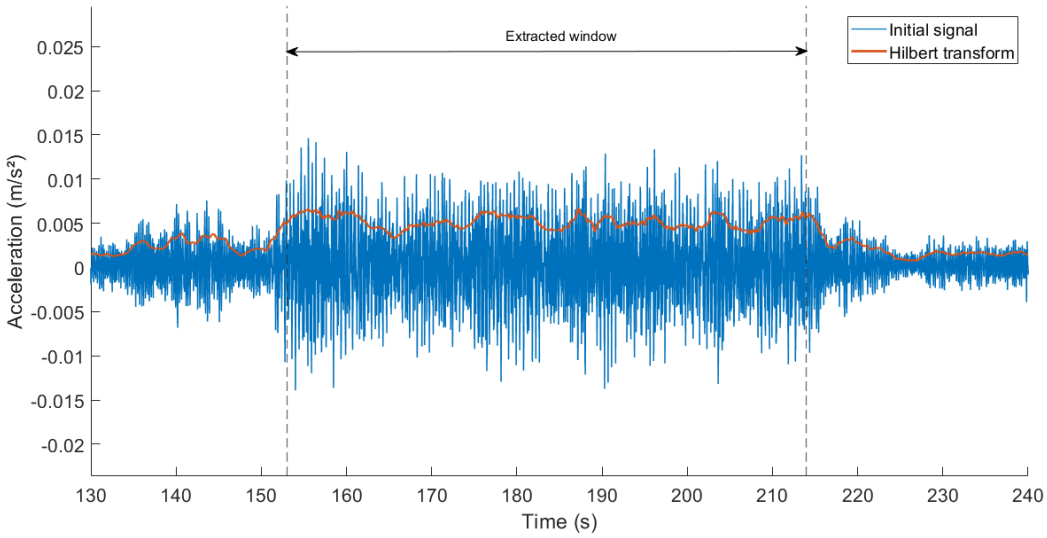

Figure 5.15: Activity window extracted using Hilbert transform

The latter extraction method eliminated a small part of the signal on both ends. In addition, the envelope corresponding to each time window was truncated by 5s at the beginning and at the end of each record to keep the stationary response only and to match with the slot where all individuals were moving according to the protocol (see Figure 5.16).

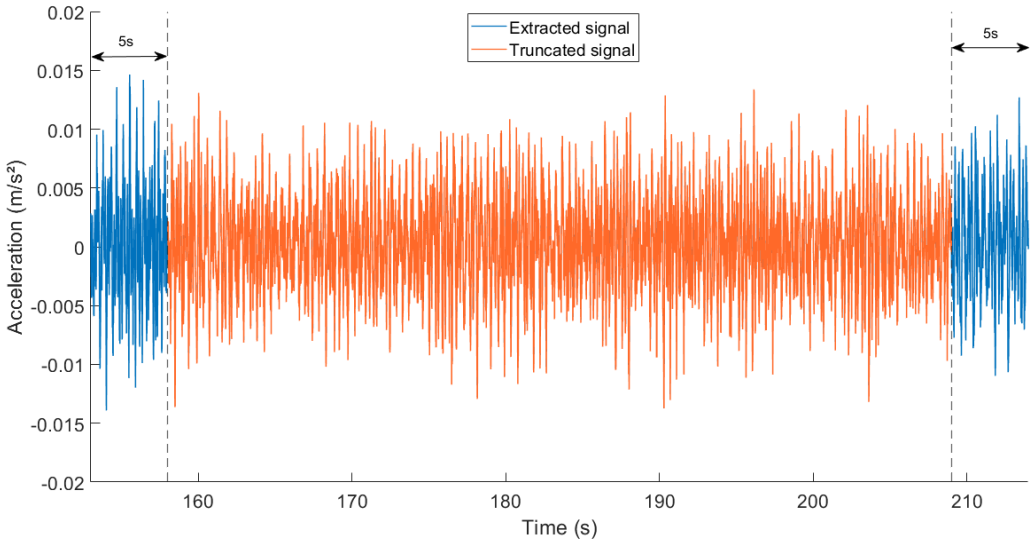

Figure 5.16: Example of a truncated response signal

Each record was then filtered within the frequency range between 0 and 10Hz via Fast Fourier Transform (FFT). An example of filtered acceleration extracted from the complete record of Figure 5.14(b) is shown in Figure 5.17, where the associated PSD response (and all PSDs presented in this chapter) was calculated using the periodogram method (with a rectangular window). The case of 2 persons was removed for "jumping 1" activity due to irregularities detected in corresponding activity windows after pre-processing.

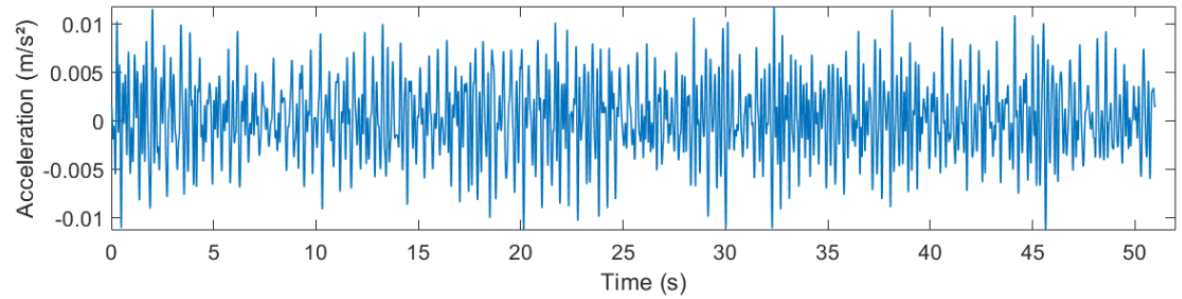

(a) Time domain signal

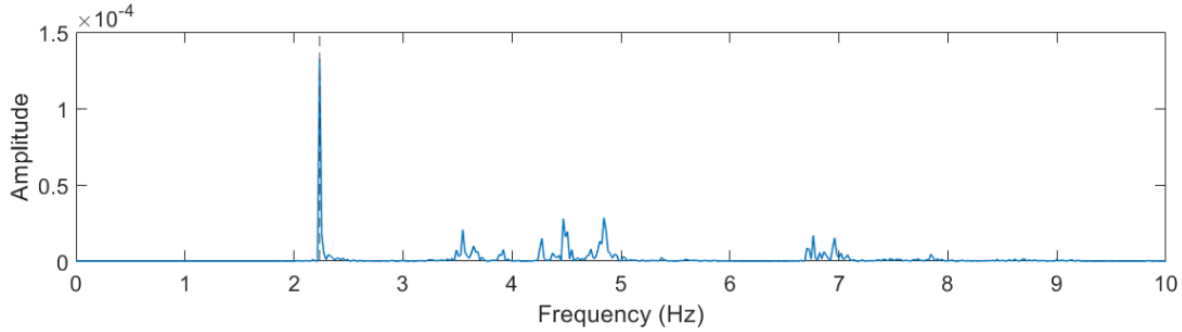

(b) Frequency domain signal (the vertical line represents the excitation frequency)

Figure 5.17: Illustration of a filtered signal

5.3.2 Determination of RMS responses

RMS responses were calculated for "jumping 1" and "skipping 2" activities. All resulting records from Section 5.3.1 lasted nearly 50s with a time step of 0.0039s. The body mass of individuals is given in Table 5.4 and their positions taken from Table 5.2 and shown in Figure 5.10. The 10 response points presented in Figure 5.13(a) were adopted for the investigation of floor vibration. Experimental PSD responses are characterized by various dominant peaks in the frequency range between 0 and 10Hz, depending on the response point as well as the considered activity and crowd size. However, since analysed activities have an excitation frequency (see Figure 5.17(b)) near the fundamental frequency of the floor (3.56Hz), it was assumed that the response of the structure would be majorly governed by that mode. Hence, the floor response was calculated using this single mode with modal parameters resulting from Experimental Modal analysis (see Section 5.2.2.3).

The method described in Section 4.2.5 was adopted for all response calculations made for each activity and crowd size (2 to 32 persons for skipping, 4 to 32 persons for jumping). Numerical RMS responses were calculated for the 10 response points using the crowd load model identified in Section 4.3. Although investigated for up to 16 persons for laboratory tests in Chapter 3, the scope of crowd size relations was extended between 16 and 32 persons and this extension was further verified by response comparison. On the other hand, experimental RMS accelerations were computed for all activity windows and response points using the pre-processed records resulted from Section 5.3.1. Table 5.5 summarizes the mean and standard deviation of RMS accelerations for investigated rhythmic activities.

Activity	Case	RMS acceleration (mm/s²)				
		2	4	8	16	32
Jumping 1	Numerical	-	7.8±2.8	11.8±4.2	17.8±6.3	33.2±11.8
	Experimental	-	9.3±2.3	10.4±2.3	18.3±3.2	31.0±4.9
Skipping 2	Numerical	2.8±1.0	4.5±1.6	5.7±2.0	6.9±2.5	10.0±3.6
	Experimental	2.7±0.7	3.5±0.8	4.8±1.1	8.2±2.1	12.6±2.0

Table 5.5: Numerical and experimental RMS accelerations for jumping and skipping activities

For illustration purposes, the mean values of numerical RMS accelerations were plotted along with the variation range of experimental responses against crowd size in Figure 5.18.

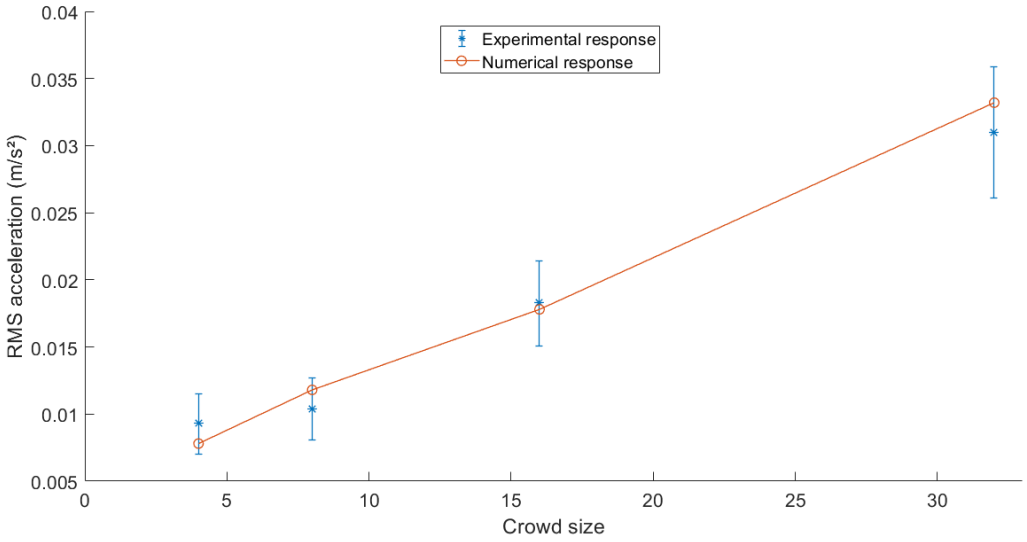

(a) Jumping 1

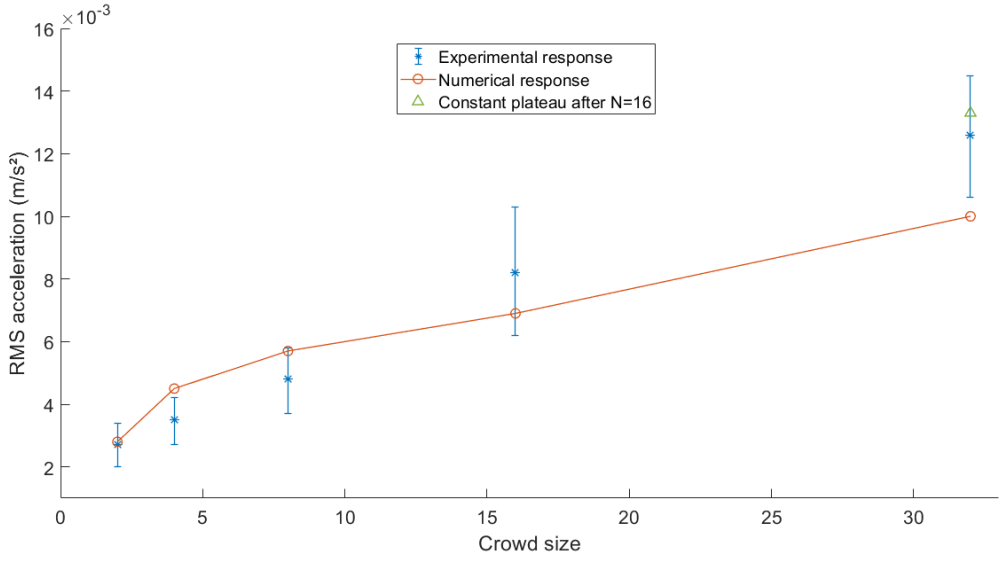

(b) Skipping 2

Figure 5.18: Comparison between numerical RMS accelerations (round marks) and experimental RMS accelerations (mean in asterisk marks, standard deviation in error bars) against crowd size

5.3.3 Discussion

In a global sense, numerical RMS accelerations are close to their experimental analogues (see Figure 5.18). The mean relative difference was 9.8% and 17.5% for jumping and skipping, respectively. This validates the fact that the structure is solely excited by the fundamental mode when subjected to investigated rhythmic activities. Differences could come from the variation of motion of each participant from an activity window to another. This is confirmed by Ellis and Ji [32], who carried out tests for jumping activities performed by up to 64 individuals. They also noticed differences between experimental and predicted responses computed with a Fourier series load. This was attributed to the variation of three major parameters, which are the excitation frequency, the contact ratio (see Section 2.2.1) and the phase lag between individuals. The slight differences between coordination stimulus adopted for the laboratory tests (from which the PSD model is derived) and the full-scale tests could also be a possible reason behind these discrepancies.

Moreover, the standard deviation of all RMS responses has an increasing trend against crowd size. This is due to the rising variabilities encountered in crowd movements in terms of frequency, amplitude, excitation positions, etc., resulting in more fluctuated accelerations for the 10 response points. However, higher standard deviations were noticed for calculated responses compared to measured ones especially for higher crowd sizes. The existence of one excited mode may result in near-resonant effects on computed responses, which highly differ from a response point to another. In that context, Xiong and Chen [89] performed measurements on an existing floor structure under various jumping test conditions. Experimental responses were compared with those calculated using a random field jumping model. They came up with a mean relative difference of about 23% between simulated and measured RMS accelerations.

Concerning "jumping 1" (jumping jack), it can be seen from Figure 5.18(a) that the mean value of numerical RMS responses lies in the variation range of experimental responses for all crowd sizes. It has a higher value than the mean measured acceleration for 8 and 32 persons and a lower value for 4 and 16 persons. Close RMS accelerations for the case of 32 persons confirm that the scope of coordination factors for this activity could be extended to a crowd size between 16 and 32 individuals. This was also assumed for "jumping 2" (quick jumping) belonging to the same category of activity (having also a hyperbolic function for the coordination factor).

For "skipping 2" (on feet soles), higher differences are found between the mean values of predicted and measured responses than for jumping. Higher RMS responses were observed for lower crowd sizes (up to 8 persons) against lower responses for higher crowd sizes (16 and 32 persons). This is due to the more randomness in this activity, whose effects appear for more and more people as stated in Section 4.3.3.2. Numerical RMS accelerations are close to the range of experimental ones for up to 16 persons (see Figure 5.18(b)). However, the predicted response for 32 persons was notably lower than its measured counterpart, indicating that the extension of the crowd size relation results in lower coordination factors than reality. When the coordination factor of 16 persons (0.3 for "skipping 2") was used for 32 persons, calculated RMS acceleration was 13.3 ± 4.7 mm/s², which is within the range of experimental values on the conservative side (green triangle in Figure 5.18(b)). Therefore, it is suggested to adopt the same coordination factor related to this activity as determined in Chapter 4 until 16 individuals, but with a constant plateau for the extension between 16 and 32 persons. This was also

considered for "skipping 1" (on feet toes) due to similarities between activities and coordination factors (both are decreasing exponential functions).

Consequently, final coordination factors for the analysed activities are given in Table 5.6 for up to 32 individuals.

Activity	Coordination factor
Jumping 1	$C(N) = 0.44 + \frac{0.56}{N}$
Jumping 2	$C(N) = 0.30 + \frac{0.70}{N}$
Skipping 1	$C(N) = \begin{cases} N^{-0.53}, & 1 \le N \le 16 \\ 0.23, & 16 \le N \le 32 \end{cases}$
Skipping 2	$C(N) = \begin{cases} N^{-0.43}, & 1 \le N \le 16 \\ 0.3, & 16 \le N \le 32 \end{cases}$

Table 5.6: Coordination factors C(N) by crowd size N for investigated activities (up to 32 individuals)

5.4 Comparison with existing load models

The spectral crowd load models for investigated rhythmic activities obtained in Chapter 4 and validated in Section 5.3 were compared against load models from the literature. Comparison was made in terms of forces first, either for one person or for a group of people. In sequence, responses due to the proposed model along with various existing crowd load models were calculated for three distinct floor structures and results were discussed.

5.4.1 Comparison of rhythmic force models

5.4.1.1 Single person load models

As highlighted in Section 2.5.1.1, most of existing load models for rhythmic activities are expressed in Fourier series in the time domain. Hence, equivalent Dynamic Load Factors (DLFs) were calculated for spectral models in order to have an equivalent amplitude for comparison purposes. This was done by following the instructions provided in Section 4.2.2.4 for the identified PSD load models (see Section 4.3.2). Resulting DLFs for the three harmonics are summarized in Table 5.7 for the four investigated activities.

Activity	DLF_1	DLF_2	DLF_3
Jumping 1	1.60 ± 0.10	1.35 ± 0.08	0.69 ± 0.04
Jumping 2	1.93 ± 0.30	1.64 ± 0.26	0.84 ± 0.13
Skipping 1	1.27 ± 0.04	0.72 ± 0.02	0.33 ± 0.01
Skipping 2	1.28 ± 0.13	0.72 ± 0.07	0.33 ± 0.04

Table 5.7: Equivalent Dynamic Load Factors (DLFs) from the identified PSD load models

The same procedure was applied to have equivalent DLFs for the spectral jumping load model proposed by Xiong and Chen [89]. Existing load models for a single person were taken from Section 2.5.1. Frequency-dependent DLFs were calculated with mean excitation frequencies (2.36Hz for "jumping 1", 2.81Hz for "jumping 2"). Table 5.8 summarizes several existing DLFs for jumping activities.

Reference	Activity	DLF_1	DLF_2	DLF_3
SCI P354 [81]	Normal jumping	1.8	1.29	0.67
Ellis and Ji [31]	Jumping	1.61	0.94	0.44
Alves et al. [3]	Jumping	1.8	1.19	0.51
CEB [19]	Normal jumping	1.8	1.3	0.7
	High jumping	1.9	1.6	1.1
Pernica [67]	Jumping	1.8	1.1	0.47
	Stride jumps	1.75	1.1	0.42
AISC DG11 [63]	Jumping exercises	1.5	0.6	0.1
ISO 10137 [45]	Jumping (2.36Hz)	1.75	1.1	0.47
	Jumping (2.81Hz)	1.68	0.94	0.32
Xiong and Chen [89]	Jumping (2.36Hz)	1.54	0.65	0.12
	Jumping (2.81Hz)	1.52	0.65	0.08

Table 5.8: Existing Dynamic Load Factors (DLFs) for jumping-type activities

DLFs corresponding to "Jumping" and "Normal jumping" activities lie in general between equivalent DLFs obtained for "jumping 1" and "jumping 2", respectively. Furthermore, DLFs decrease for an increasing frequency of "jumping" activities as proposed by ISO 10137 as well as Xiong and Chen, whereas the inverse occurs for investigated jumping activities. This is due to the distinction between the mode of motion and the type of contact to the ground for these activities. The nearest activities from Table 5.8 to the analysed ones are "stride jumps" (to jumping jack) and "high jumping" (to quick jumping). A similar amplitude is noticed for these activities for DLF_1 whilst DLF_2 and DLF_3 are higher for suggested load models. This is because the energy content within harmonic peaks is characterized by a larger width by harmonic order ([88], [89]), leading to greater DLFs than peak DLFs proposed in the literature.

On the other hand, "Running" is the only activity in the literature resembling to skipping activities. Table 5.9 presents some associated DLFs.

Reference	Activity	DLF_1	DLF_2	DLF_3
Alves et al. [3]	Running	1.35	0.25	0.13
CEB [19]	Running	1.6	0.7	0.2
Pernica [67]	Running-on-the-spot	1.57	0.58	0.26
ISO 10137 [45]	Running	1.4	0.4	0.1

Table 5.9: Existing Dynamic Load Factors (DLFs) for running-type activities

A lower value of DLF_1 is observed for proposed skipping activities probably due to the variation of configuration between the two activities (variable position in running, fixed position in skipping). However, larger DLF_2 and DLF_3 occur because of the spread of energy at higher harmonics as found for jumping activities.

5.4.1.2 Coordination factors

Proposed coordination factors given in Table 5.6 are compared against existing factors suggested by the literature. These factors were obtained from deterministic crowd size relations presented in Section 2.5.2.1.

Coordination factors for jumping-type activities were confronted to "Jumping" factors against crowd size for a maximum number of 32 persons. A medium synchronization degree (similar

to experimental conditions) was assumed for ISO 10137 coordination factors [45] (see Table 2.20), whereas the DLF ratios from Li et al. [54] (calculated by Eq. (2.47)) were computed for each mean excitation frequency (2.36Hz for "jumping 1", 2.81Hz for "jumping 2"). Figure 5.19 illustrates coordination factors against group size for the proposed models compared to existing literature for jumping activities.

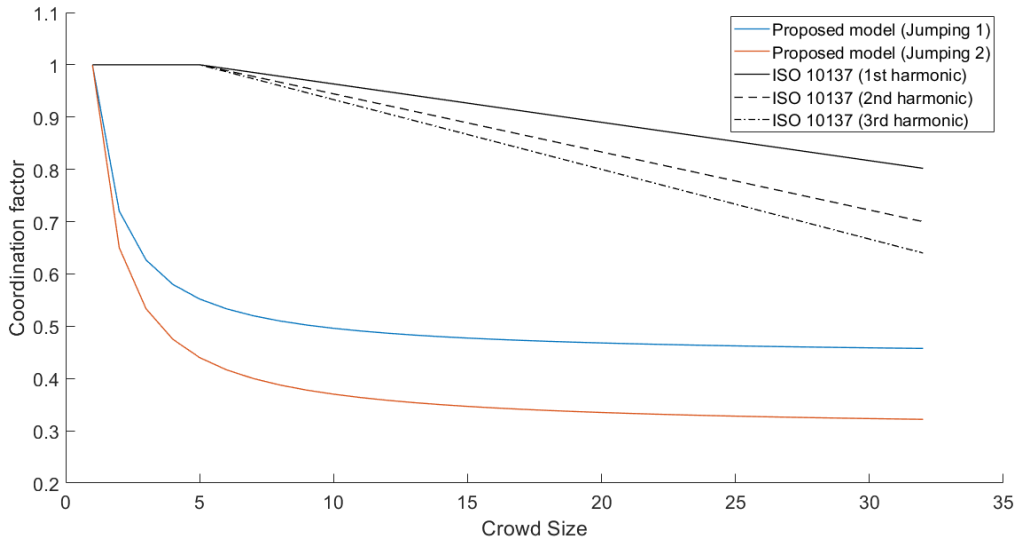

(a) ISO 10137 [45]

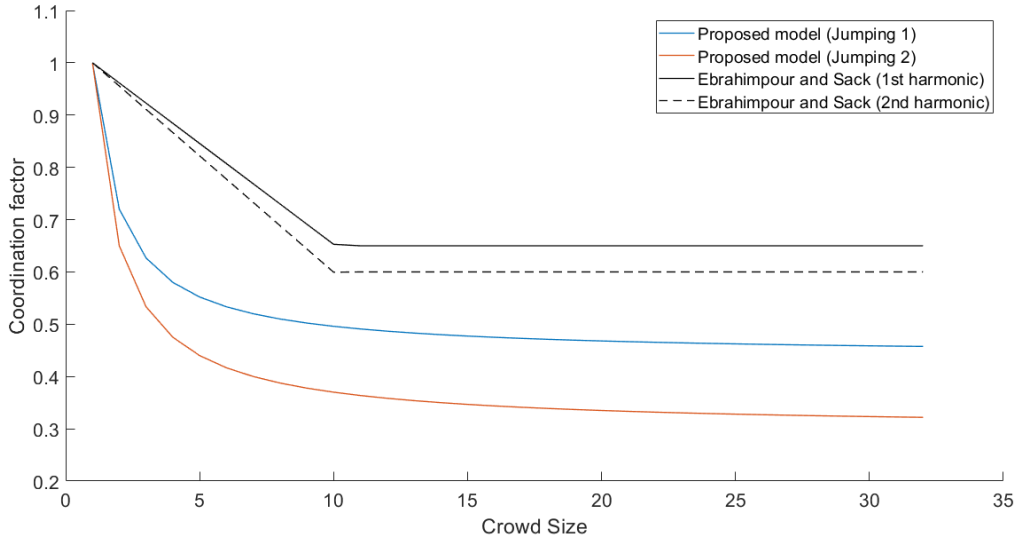

(b) Ebrahimpour and Sack [27]

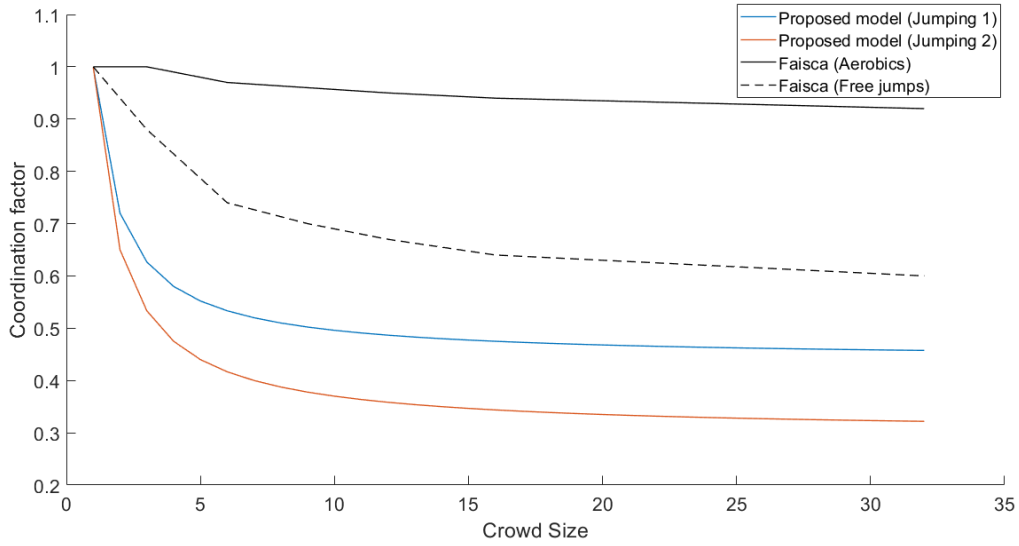

(c) Faisca [39]

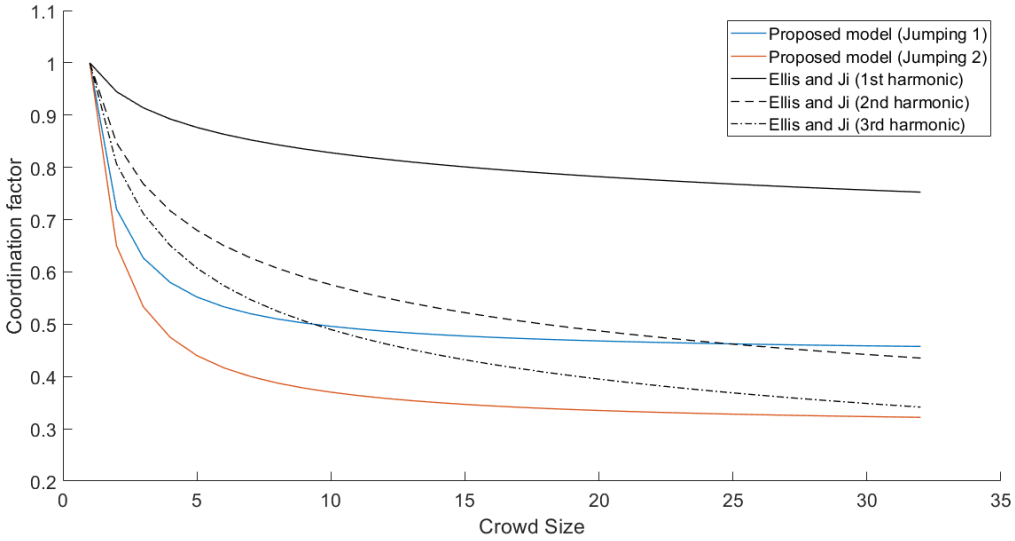

(d) Ellis and Ji [31]

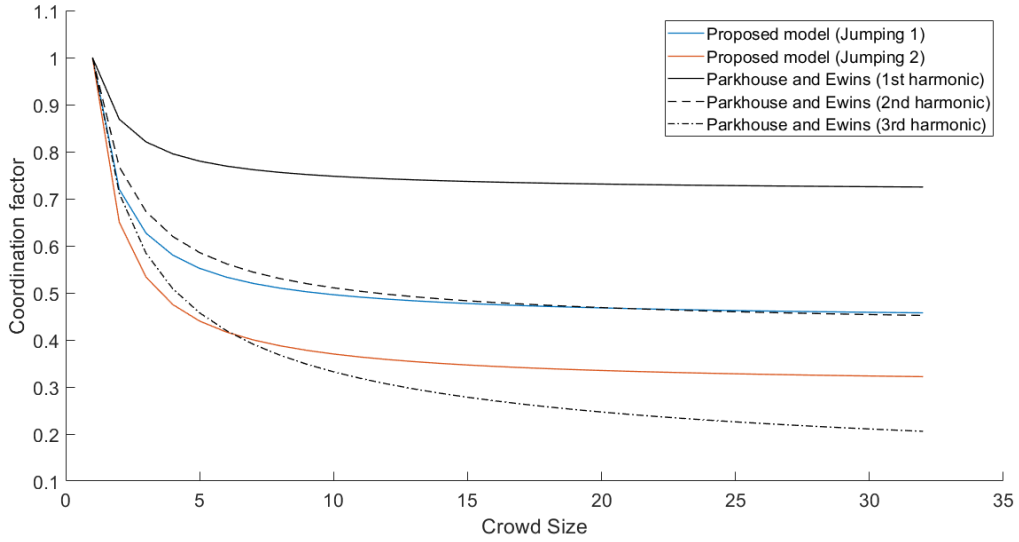

(e) Parkhouse and Ewins [65]

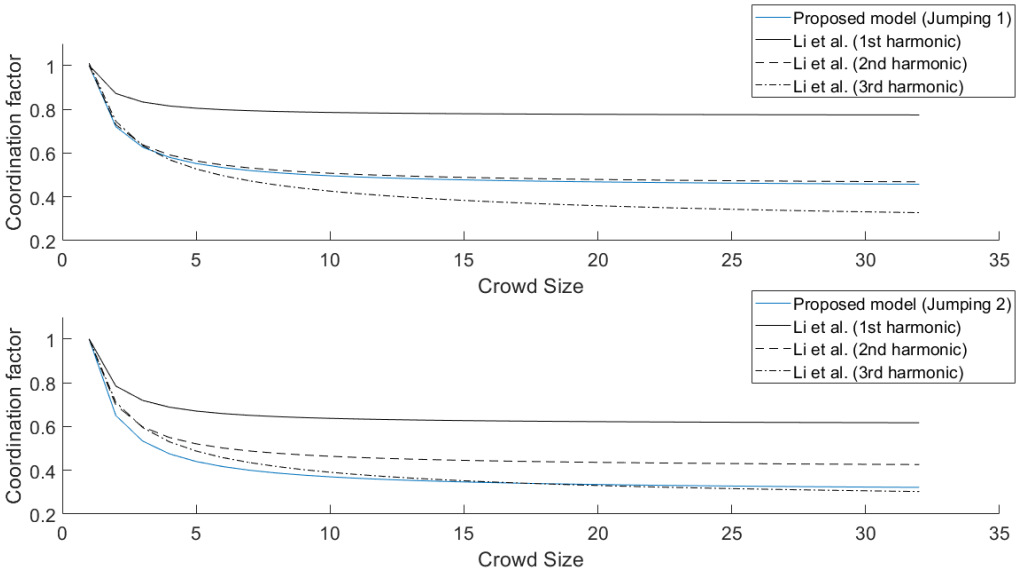

(f) Li et al. [54]

Figure 5.19: Comparison of coordination factors by crowd size for jumping-type activities proposed by several models

Three principal groups appear for the existing coordination factors:

- A first group assumes a linear tendency against crowd size with a constant plateau after a given number of individuals. This is the case for coordination factors suggested by ISO 10137 [45] as well as Ebrahimpour and Sack [27]. These coefficients are more conservative than the proposed ones for all considered harmonics especially for ISO 10137, which assumes no group effect for crowd sizes lower than 5 and constant coordination factors starting from 50 persons against 10 persons suggested by Ebrahimpour and Sack.
- A second group considers a decreasing exponential trend against crowd size. Models given by Faisca [39] together with Ellis and Ji [31] are within this group. The proposed models have a closer trend to this group compared to the first group but with less-

conservative factors. However, differences still exist especially for larger groups where coordination factors are still decreasing. It is noted that the model proposed by Faisca is applied to the whole load as is the case for suggestion relations.

- A third group has a decreasing trend which gradually stabilizes for larger crowd sizes. It comprises models proposed by Parkhouse and Ewins [65] in addition to Li et al. [54]. These relations are the closest ones to the hyperbolic tendency obtained for the investigated jumping activities. Furthermore, both activities have coordination factors which lie within the three harmonic values for Parkhouse and Ewins model. The lower values for "jumping 2" related to "jumping 1" is effectively reproduced by Li et al., which provides slightly greater coordination factors especially for the high-frequency jumping.

For skipping activities, the only relation available in the literature is that proposed by ISO 10137 [45] for running (given by Eq. (2.43)) which belongs to the same rhythmic category. Figure 5.20 displays related coordination factors along with the proposed ones against crowd size for up to 32 persons. The same power trend exists for these models with coordination factors for running lying between those of "skipping 1" and "skipping 2". This indicates that investigated activities present upper and lower levels of synchronization between participants for this category of action. However, the existence of a constant plateau for the proposed models leads to higher coordination factors for "skipping 1" compared to running starting from 20 individuals. The response of floors for the case of higher group sizes might then be underestimated if the existing running model is used.

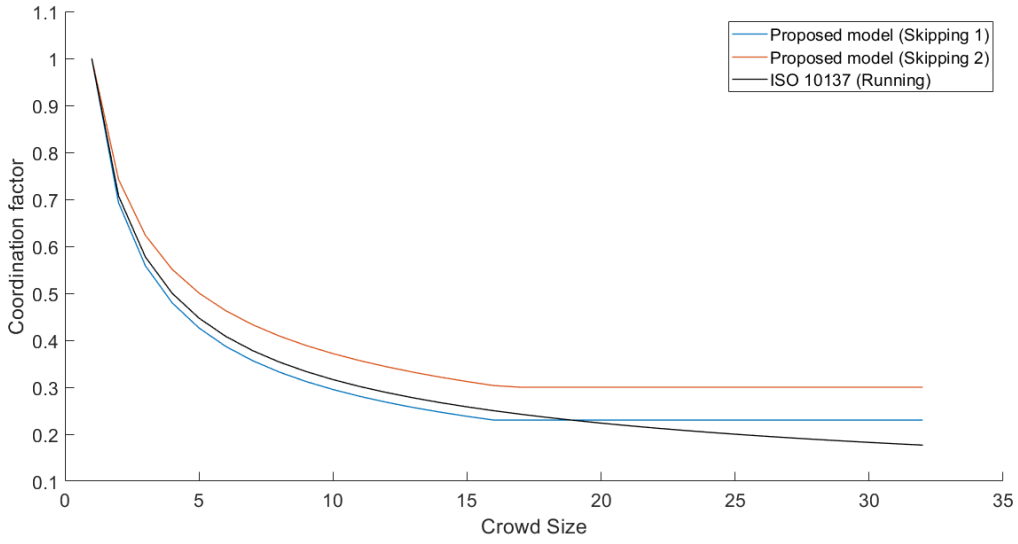

Figure 5.20: Comparison of coordination factors by crowd size for running-type activities

Overall, proposed coordination factors are different from existing factors in the literature due to the difference between activities for each rhythmic category (style, floor impact, etc.) and the variable configuration used in vibration experiments for each research (especially coordination stimulus, leading to higher factors when using metronome).

5.4.2 Comparison of responses from existing time domain models

Among time domain load models proposed in the literature, three of them assume a complete presentation of rhythmic actions. Indeed, they propose a load model for a single person, which is associated to crowd size relations considering synchronization between individuals. These models were presented in Chapter 2 and are reminded below:

- Ellis and Ji load model [31] (jumping): a Fourier series model with DLFs presented in Table 2.15 and variation of DLFs by group size given by Eq. (2.23);
- Faisca load model [39] (jumping): a jumping pulse model taken from Table 2.13 (with parameters from Table 2.14) along with coordination factors from Table 2.18;
- ISO 10137 load model [45] (jumping and skipping): a Fourier series model with DLFs from Table 2.16 as well as coordination factors given by Eq. (2.43) for skipping and Table 2.20 for jumping (assuming medium coordination degree).

The proposed spectral crowd load models were compared to the latter models by calculating RMS accelerations using both configurations of floors tested in this research (laboratory/"single-mode" floor, parking/"multi-modal" floor). For each investigated activity and crowd size, numerical RMS accelerations were calculated with the related PSD crowd load model (see Section 4.2.4) with mean optimal parameters from Table 4.5 using the procedure detailed in Section 4.2.5.1. The same response parameter was also computed for the three existing load models described earlier by following the instructions detailed in Section 4.2.5.2. The mean and standard deviation of RMS accelerations by crowd size obtained from the PSD load models along with existing models are summarized in Appendix B.

5.4.2.1 Response of single-mode floor

The response of the single-mode floor described in Chapter 3 is investigated for the four analysed activities for 1, 2, 4, 8 and 16 individuals. A time duration of 30s was considered for each activity with a maximum frequency of 10Hz. The body mass of individuals was obtained from Table 3.11. Their positions for each crowd size are given in Table 3.9 and shown in Figure 3.23. Modal properties of the fundamental mode of the floor (natural frequency, damping ratio, modal shape) are the result of Experimental Modal Analysis described in Section 3.3.2.2, whereas the modal mass was taken from Section 3.4.1.1. Ten response points over the floor were considered as illustrated in Figure 5.21.

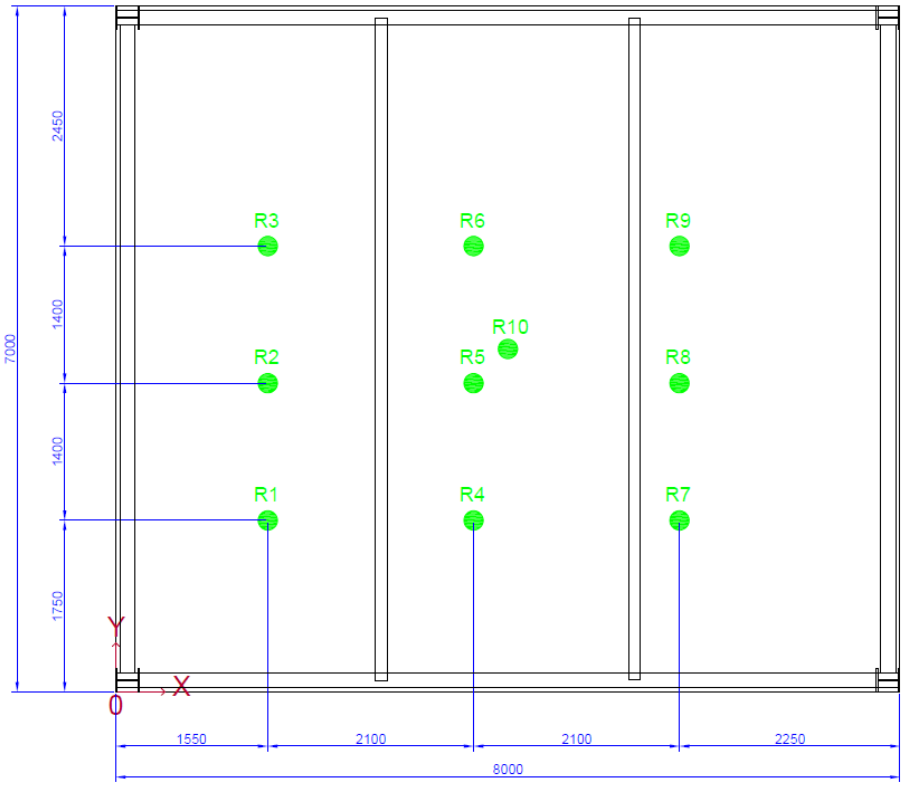

Figure 5.21: Response points for the single-mode floor (dimensions in mm, R10 is the centre of the floor)

- **Jumping activities**

For jumping activities, the variation of mean RMS accelerations by crowd size for the PSD load models along with existing models is shown in Figure 5.22.

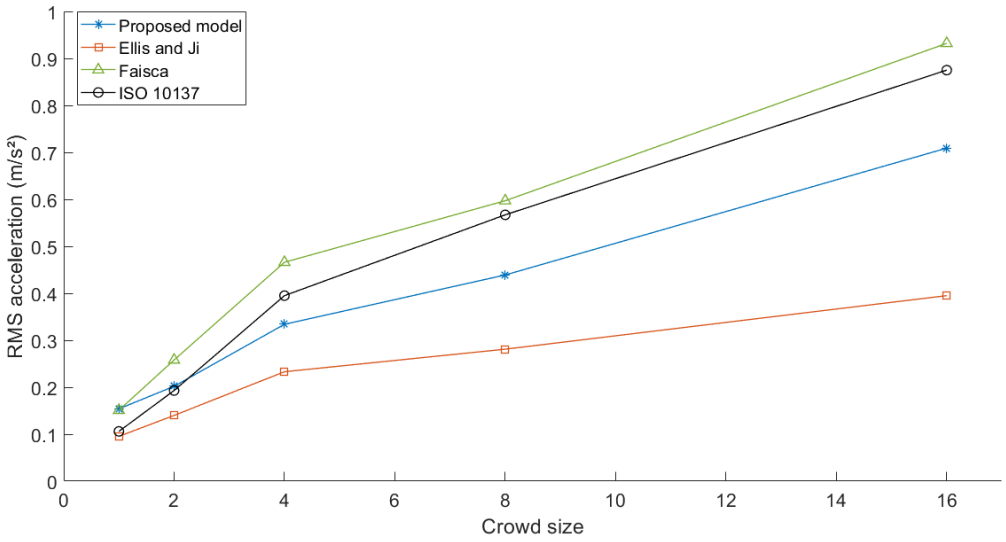

(a) Jumping 1

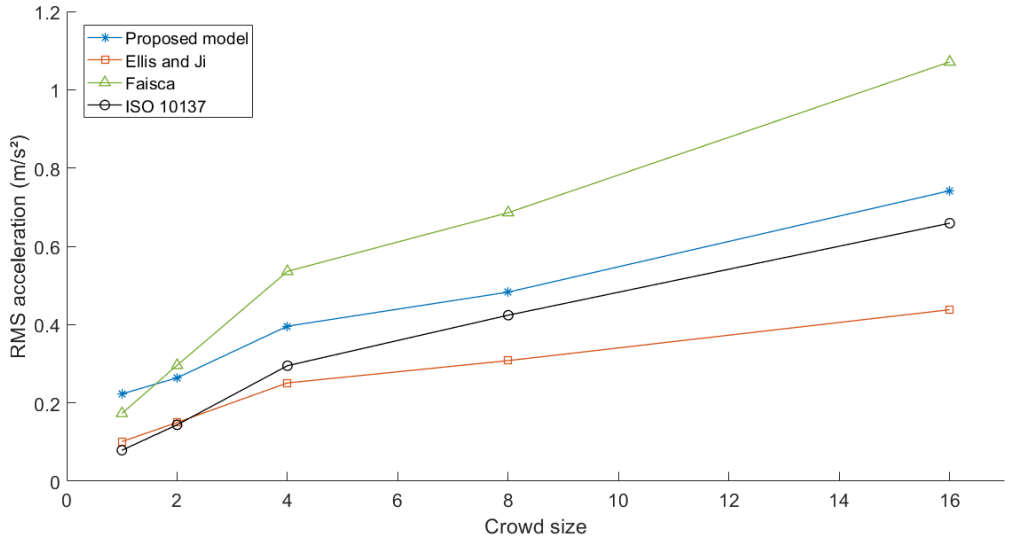

(b) Jumping 2

Figure 5.22: Mean RMS accelerations against crowd size for single-mode floor (jumping)

RMS accelerations of the two proposed models have an amplitude which lies within those obtained by the three existing load models for both jumping activities. The difference of RMS responses between load models is more pronounced for larger groups. This is attributed to the distinction of motion between "normal jumping" and experimentally analysed jumping activities. The most excited harmonic for all load models is the third harmonic (close to the natural frequency of 7.65Hz). The lowest RMS responses are those from Ellis and Ji load model, since coordination factors have a strong decreasing tendency against crowd size. Compared to this load model, ISO 10137 proposes slightly lower DLFs but greater coordination factors, which leads to higher RMS responses especially for larger crowds. RMS responses belonging to Faisca model are the most conservative, because of high coordination factors and contact ratio (nearly 0.3).

The switch from "jumping 1" to "jumping 2" implies an increase of excitation frequency in all load models (from 2.36Hz to 2.81Hz). Higher RMS responses occur in the proposed PSD load model principally because of the amplitude difference between the two activities. Given that DLFs proposed by ISO 10137 are inversely proportional to the excitation frequency, RMS responses are lower for the second activity compared to the first. RMS accelerations for other load models (suggested by Ellis and Ji as well as Faisca) are higher for "jumping 2" compared to "jumping 1" although there was no change in the amplitude of the analytical load. This indicates a dependence of these loads on the frequency of each investigated activity.

- **Skipping activities**

Figure 5.23 presents RMS responses against the number of individuals computed from the proposed models and ISO 10137 model for skipping activities.

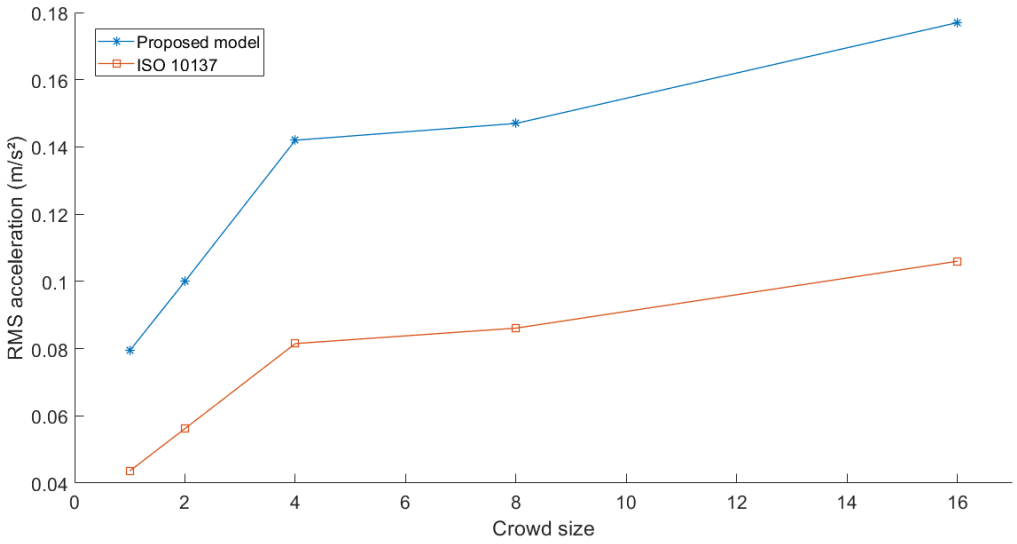

(a) Skipping 1

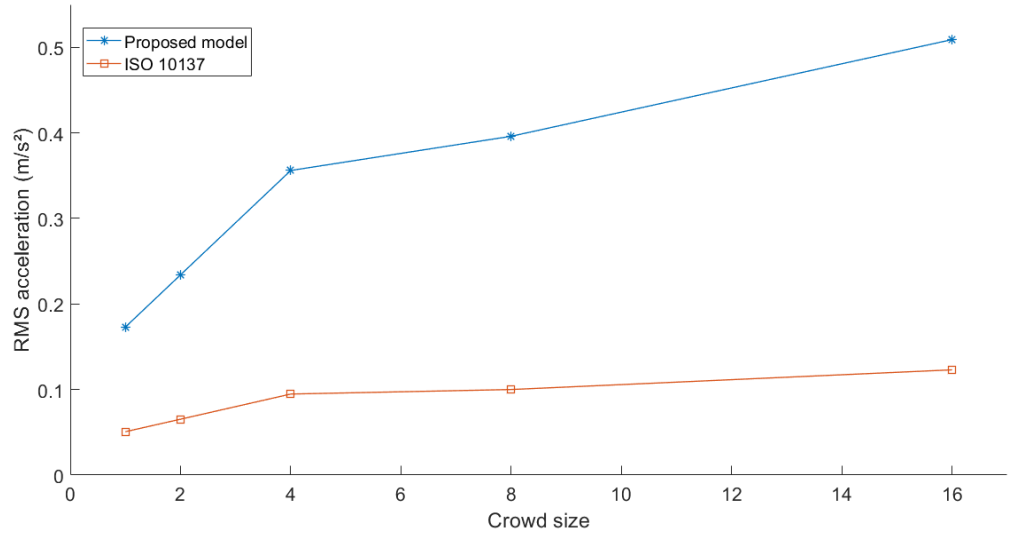

(b) Skipping 2

Figure 5.23: Mean RMS accelerations against crowd size for single-mode floor (skipping)

Higher RMS responses occur for both skipping activities due to the greater load amplitudes than DLFs proposed by ISO 10137 for higher harmonics (see Table 5.7 and Table 5.9 for comparison). Larger responses are noticed in both models when switching from 3.26Hz ("skipping 1") to 2.62Hz ("skipping 2"). However, the difference between RMS accelerations is more accentuated in the latter case due to greater coordination factors for "skipping 2" than for "skipping 1" in the proposed model, whereas the same relation is proposed by ISO 10137 for both activities.

- **Conclusion**

Compared to existing load models, it is concluded that the PSD load models are less-sensitive to the excitation frequency for single-mode floors. In particular, time domain load models would result in overestimated responses for resonant cases, which highly decrease for non-resonant cases.

5.4.2.2 Response of multi-modal floor

The response of the multi-modal floor presented in this chapter is analysed for both jumping and skipping activities. The investigated crowd sizes are 1, 2, 4, 8, 16 and 32 individuals. The duration of activities was taken as 60s with a time step of 0.005s. The body mass of participants is given in Table 5.4. Their positions for each group size are provided in Table 5.2 and illustrated in Figure 5.10. The twenty natural modes of the floor were used in response calculation. Their modal properties (natural frequency, modal mass, damping ratio, modal shape) are those resulting from Experimental Modal Analysis described in Section 5.2.2. The response points illustrated in Figure 5.13(a) were also adopted in this study.

- **Jumping activities**

Concerning jumping activities, Figure 5.24 illustrates mean RMS responses against crowd size computed for the PSD load models in conjunction with existing models.

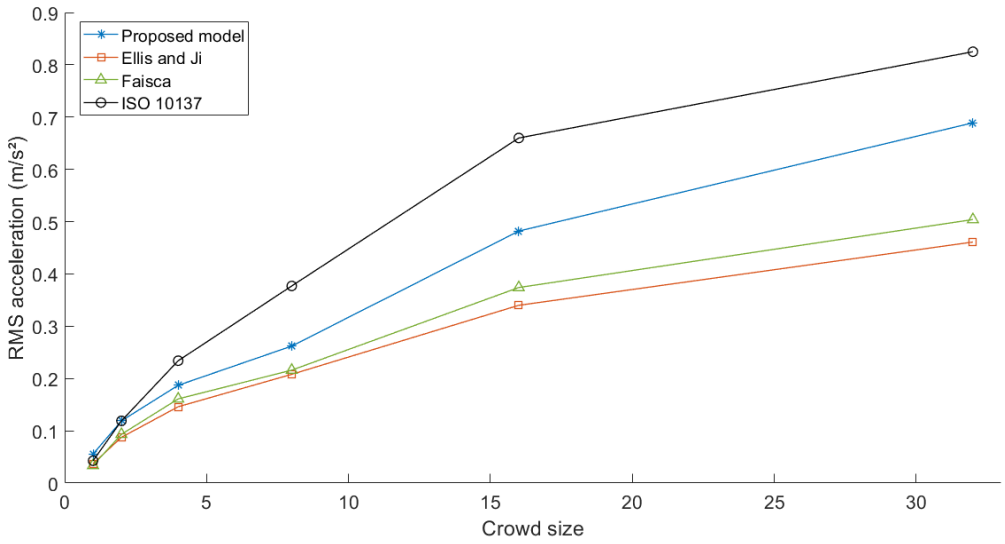

(a) Jumping 1

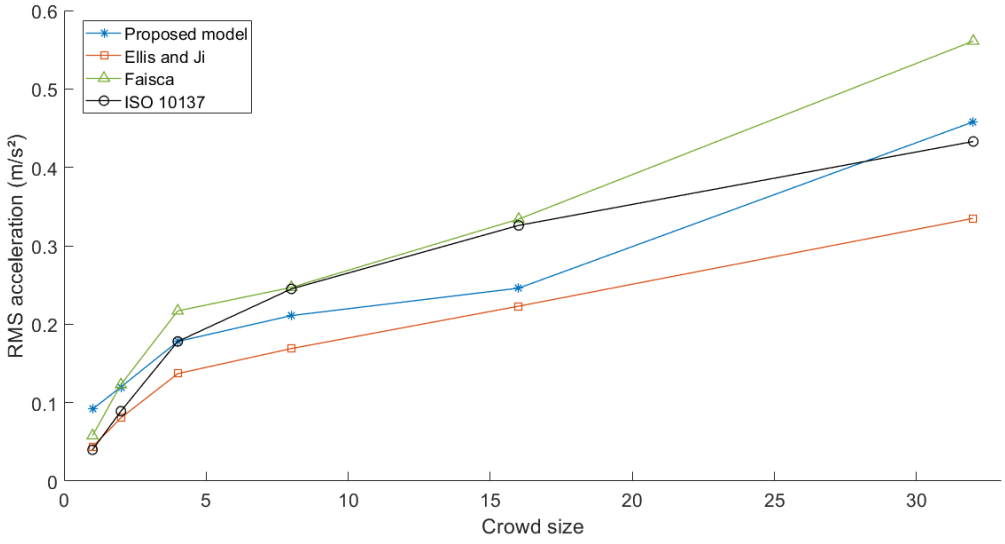

(b) Jumping 2

Figure 5.24: Mean RMS accelerations against crowd size for multi-modal floor (jumping)

"Jumping 1" has an excitation frequency of 2.36Hz. The PSD load model has a narrow energy band for that activity (see Section 4.3.2.2), which allows to excite only the 9th and 10th natural modes (having natural frequencies of 4.67Hz and 4.85Hz, respectively) as can be seen in the PSD response of Figure 5.25. These modes are highly dominant and lead to RMS responses greater than those obtained by Ellis and Ji as well as Faisca models, which are dominated by their second harmonic in terms of PSD response (see Figure 5.25). The same remark applies to ISO 10137 model, but its largest coordination factor contributes to the highest RMS response among investigated load models (as found by Gaspar and da Silva [44]).

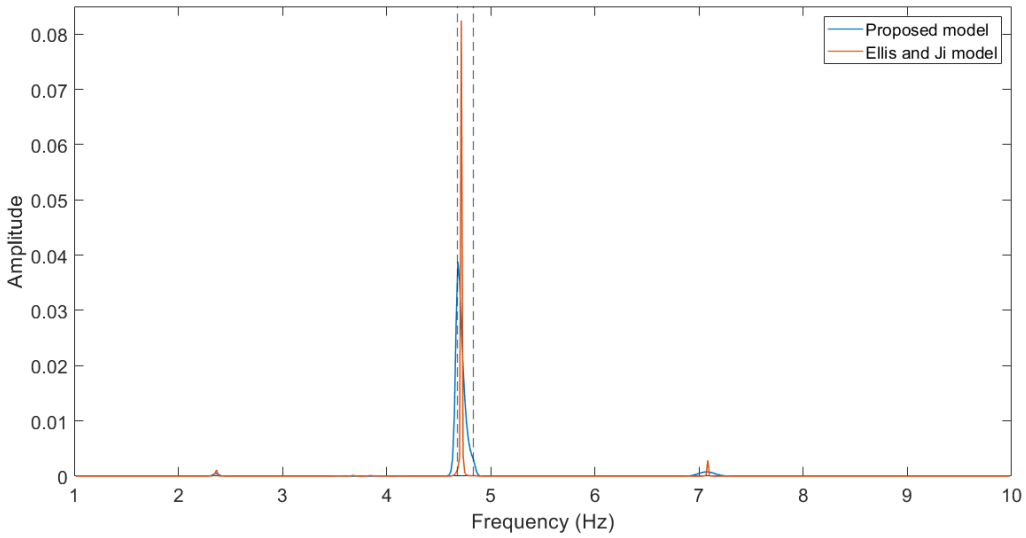

Figure 5.25: Mean PSD responses for a single person performing "jumping 1"

On the other hand, "jumping 2" is assumed to have an excitation frequency of 2.81Hz. Owing to the large energy band of the associated PSD load model (see Section 4.3.2.2), more natural modes are expected to be involved in the floor response. In this particular case, five natural modes are simultaneously excited as shown in the PSD response of Figure 5.26. They have natural frequencies of 5.5, 5.57, 5.78, 5.86 and 8.6Hz (see Table 5.1). Conversely, the only dominant peaks in the PSD responses for time domain loads are those of the second and third harmonics (see Figure 5.26). Nevertheless, proposed coordination factors are lower for "jumping 2" than "jumping 1". This results in an amplitude of RMS responses lying between those obtained by existing models. Almost the same order of accelerations by load model resulting from the single-mode floor analysis (see Section 5.4.2.1) is reproduced here.

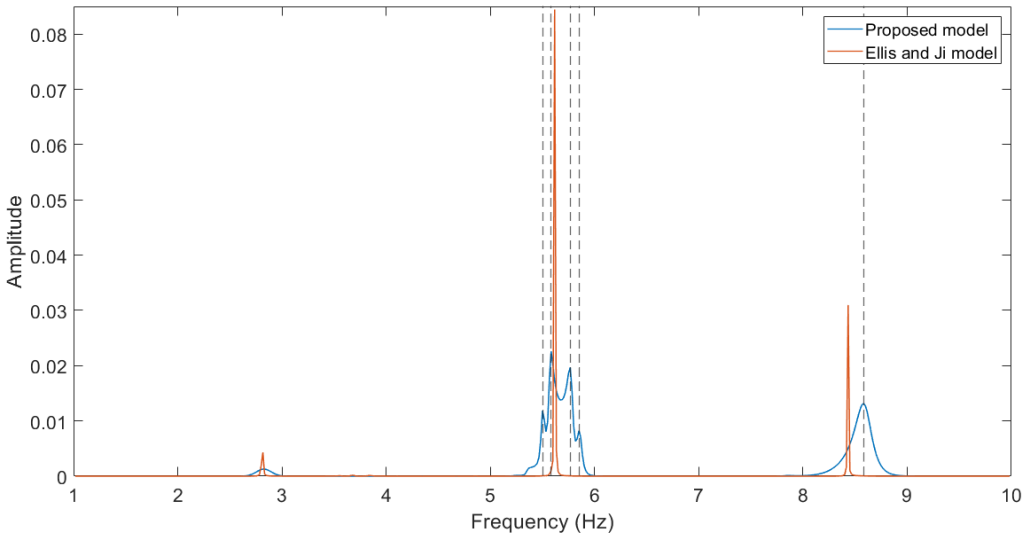

Figure 5.26: Mean PSD responses for a single person performing "jumping 2"

- **Skipping activities**

The variation of RMS responses against crowd size is presented in Figure 5.27 for the suggested PSD load models together with ISO 10137 load model.

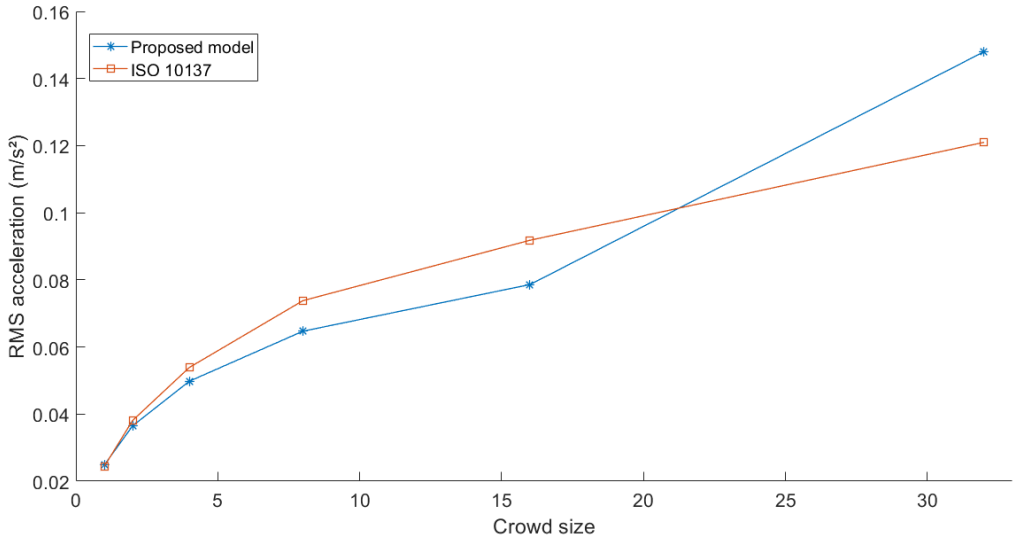

(a) Skipping 1

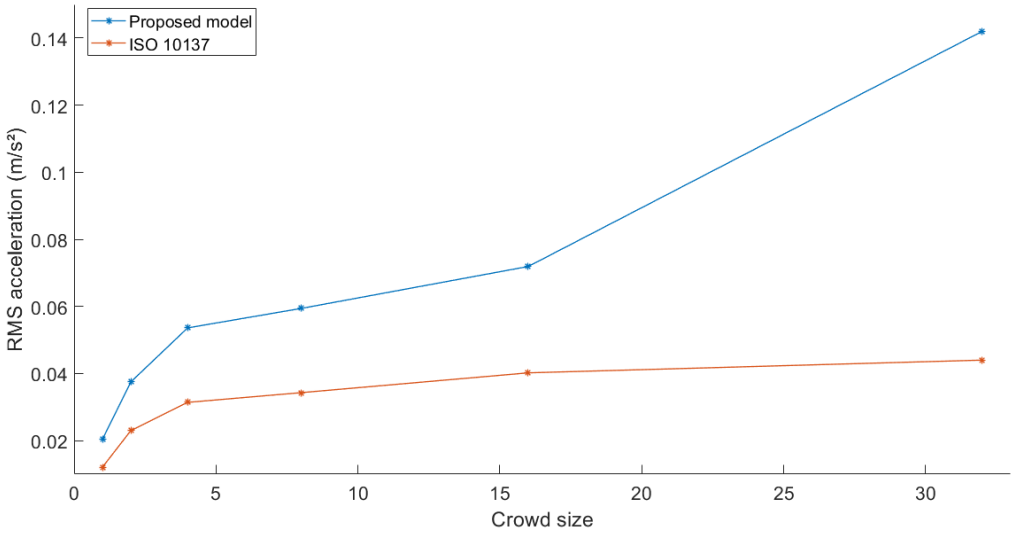

(b) Skipping 2

Figure 5.27: Mean RMS accelerations against crowd size for multi-modal floor (skipping)

For "skipping 1", lower RMS responses are noted for the proposed model compared to ISO 10137. Besides lower coordination factors, the high excitation frequency of this activity (3.26Hz) makes no dominant mode to be excited as shown in Figure 5.28. The only dominant peak occurred at the first harmonic for both models. However, the existence of constant plateau beyond 16 persons in the coordination factor of this activity allows to have higher responses due to the PSD model for 32 individuals.

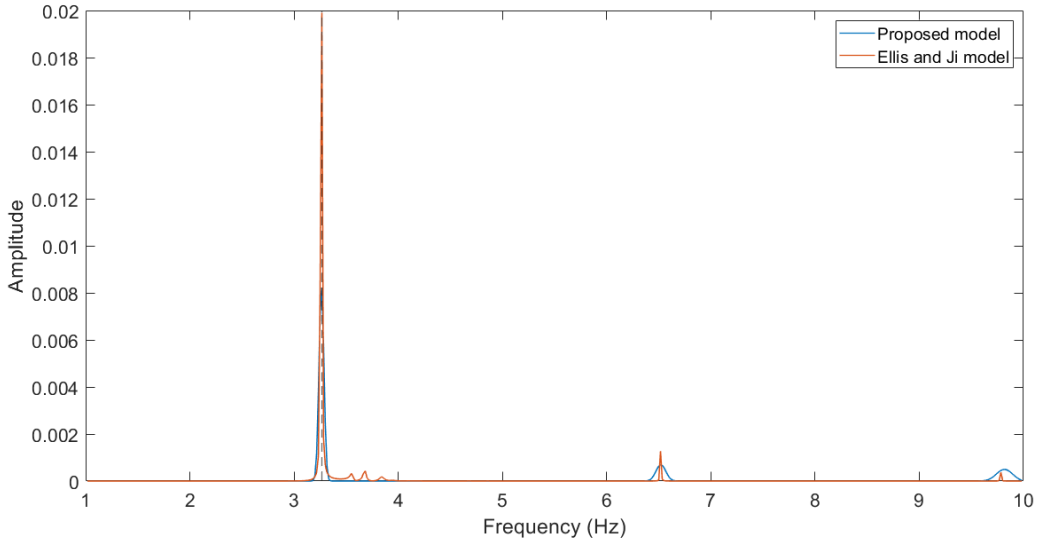

Figure 5.28: Mean PSD responses for a single person performing "skipping 1"

Conversely, the moderate excitation frequency of "skipping 2" (2.62Hz) enables the excitation of two dominant modes (having natural frequencies of 5.23 and 7.85Hz) near the second and third harmonics of the PSD load model, respectively (see Figure 5.29). In contrast, the first and second harmonics are dominant for ISO 10137 model without exciting higher natural modes. Larger coordination factors are also noticed for the proposed load model, which results in higher RMS responses than ISO 10137 model.

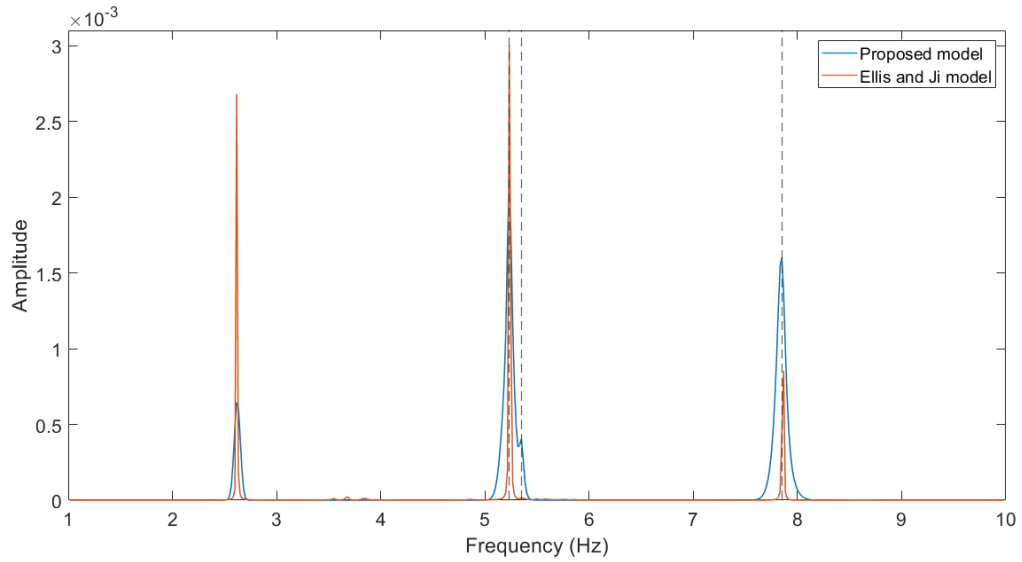

Figure 5.29: Mean PSD responses for a single person performing "skipping 2"

- **Conclusion**

The existence of the spread of energy (termed leakage [71]) in the PSD model allows the excitation of multiple natural modes simultaneously. On the other hand, the response of time domain load models is solely governed by the dominant harmonic of the load, so that the excitation of more than one dominant natural mode is not possible. Hence, the proposed model is suitable for the evaluation of the response of modern buildings comprising multi-span or multi-panel floors ([20], [22], [75]), which are characterized by multiple closely spaced natural modes.

5.4.3 Comparison of responses from existing frequency domain model

As outlined in Section 2.5.2.2, the principal frequency domain load model existing in the literature for crowd-rhythmic activities is that proposed by Xiong and Chen [89]. This random field model is compared with the proposed PSD load model in this section, based on experiments conducted on an existing floor under crowd jumping activities.

5.4.3.1 Presentation of the experiments

The analysed structure is a 12×12m² floor located in China (see Figure 5.30). Xiong et al. [91] carried out two test campaigns on this floor: Experimental Modal Analysis and vibration tests under jumping crowds.

Figure 5.30: Floor tested by Xiong et al. [91]

Firstly, the modal properties of the floor were determined using hammer impact excitations, which resulted in the fundamental mode having parameters presented in Table 5.10 and a modal shape shown in Figure 5.31. It was assumed that the response of the structure is dominated by the fundamental mode with a sinusoidal modal shape. Indeed, resonance is likely to occur for this mode (having natural frequency of 5.35Hz) at the second harmonic of the rhythmic load characterized by an excitation frequency ranging between 1.5 and 3.5Hz ([45], [81]).

Parameter	Natural frequency (Hz)	Modal mass (t)	Damping ratio (%)
Value	5.35	30	1.57

Table 5.10: Modal properties of the tested floor [91]

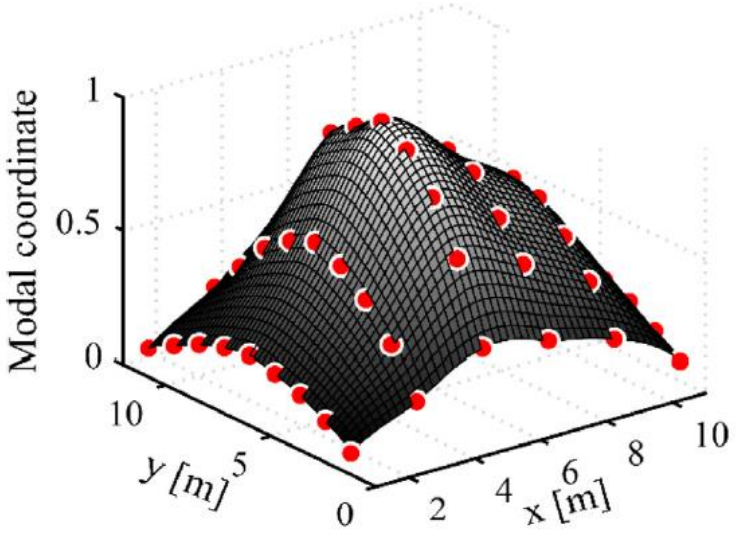

Figure 5.31: Fundamental modal shape (modified from [91])

Secondly, vibration experiments were conducted for "normal jumping" activity at a low frequency with the guidance of a metronome (see Figure 5.32). Investigated crowd sizes were 25, 36, 49 and 64, with the participation of 64 individuals of Tongji University. Participants were uniformly distributed over the floor and performed activities for about 30s twice, while accelerations were measured at the centre of the floor.

Figure 5.32: 64 individuals jumping [91]

5.4.3.2 Determination of floor response

For each crowd size, the mean RMS acceleration of the two activity windows was calculated from time-domain records by Xiong et al. [91]. In sequence, the random field model proposed by Xiong and Chen [89] was used to predict the floor response. The method consists of performing 1000 Monte Carlo simulations to generate load parameters related to the coherence function and the response was calculated for each sample. The five and ninety-five percentiles of the obtained RMS accelerations were then adopted as a lower and an upper value, respectively [91].

On the other hand, the response of the floor was evaluated using the proposed PSD load model. Among investigated activities (see Section 3.4.2.1), "jumping jack" is qualified as a low frequency jumping (see Section 4.3.2.2), which is close to the normal jumping performed in experiments. The load parameters of this activity (mean values of Table 4.5) were then adopted for this comparison, assuming a time duration of 30s and a maximum frequency of 10Hz. Given that the scope of coordination factor for "jumping jack" was successfully extended from 16 to 32 individuals (see Section 5.3.3), it was considered applicable for all tested crowd sizes (25, 36, 49 and 64 individuals).

Moreover, the mean mass of the individuals was taken as 60kg, similarly to what was found for Tongji University participants in another research [89]. In addition, the distance between individuals was considered equal to 1.5m in both directions. In fact, it is the maximum distance resulting in a low density of participants (which is the scope of the proposed model) enabling an equivalent modelling related to the random field proposed by Xiong and Chen [89]. The response of the analysed floor was then computed for the investigated group sizes (up to 64 individuals) based on the procedure detailed in Section 4.2.5.1. Figure 5.33 illustrates a PSD response for the case of 64 individuals, where the second harmonic of the load (with a frequency of 4.72Hz) is clearly dominant.

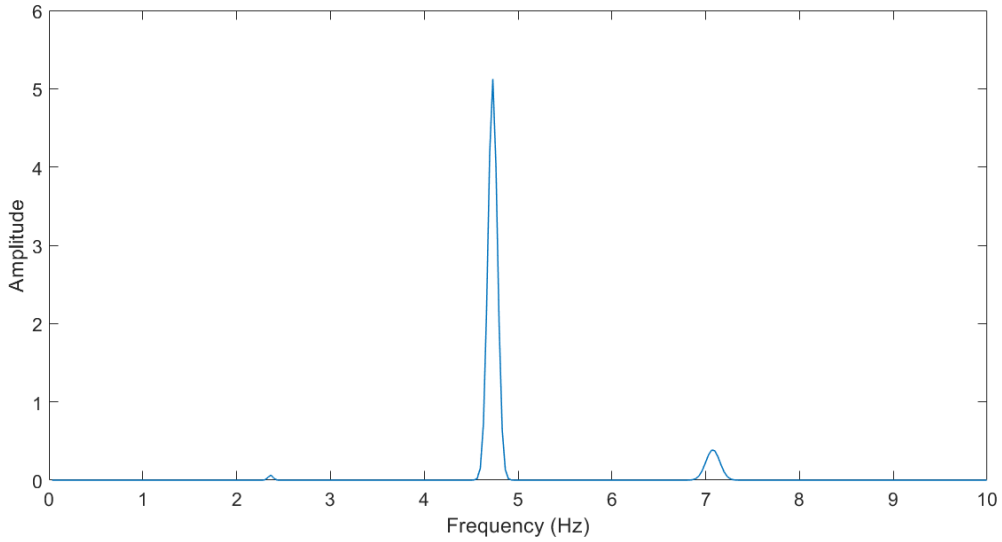

Figure 5.33: PSD acceleration for 64 individuals jumping

5.4.3.3 Comparison of RMS accelerations

Calculated vibrational responses of the floor are the mean experimental RMS accelerations, the 5 and 95 percentile of RMS accelerations obtained by Xiong and Chen model [89], and the RMS accelerations resulting from the proposed PSD model. These responses are plotted against crowd size in Figure 5.34.

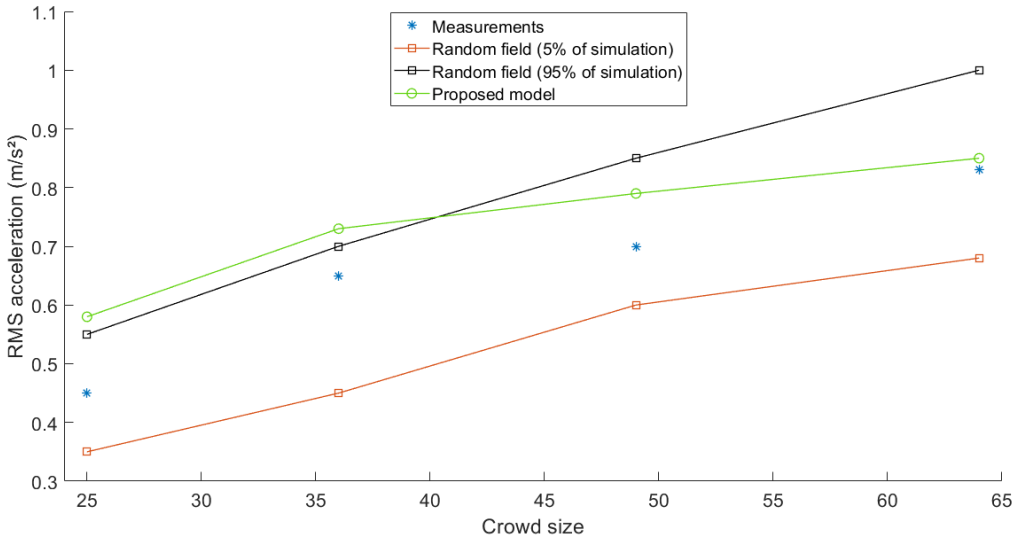

Figure 5.34: Comparison of numerical and experimental RMS accelerations for jumping activities

The proposed PSD model produces plausible differences in terms of RMS responses compared to the model of Xiong and Chen. Indeed, more conservative results were found for 25 and 36 persons (with maximum relative difference of 5.5% to the 95 percentile), whilst responses for 49 and 64 persons lie between the 5 and 95 percentiles of the random field model. Discrepancies could be attributed to the differences between "jumping jack" and "normal jumping" activities especially in terms of leg contact to the ground (leading to different amplitudes). The proposed simplification of Xiong and Chen model has then a limited impact on floor accelerations.

The RMS responses of the proposed model begin far from their experimental counterparts (relative difference of 29%) compared to Xiong and Chen model. However, when the crowd size is rising, a growth with a decreasing rate is observed for experimental responses. This tendency is reproduced by the proposed model, whereas a linear increase is noticed for both 5 and 95 percentiles of Xiong and Chen model. This difference could be due to the fact that the latter model considers that all individuals have a high synchronization degree with the guidance of metronome. In reality, this degree could not be reached for higher crowd sizes, where a phase delay between participants always exists depending on their reaction to the audible stimulus. The proposed model effectively considers this effect as it was based on experiments made under conditions close to real life situations, thus confirming the extension of the coordination factor to 64 individuals for the analysed activity.

The above results provide a first indication that reasonable differences exist between the proposed model and Xiong and Chen random field model. The higher RMS responses for small crowd sizes obtained by the proposed model is compensated by responses close to measurements due to the consideration of the observed lack of coordination between individuals.

5.5 Equivalent crowd-rhythmic load model

In this section, an equivalent load model formulation is established, based on the crowd-rhythmic load model proposed in Chapter 4 and verified in Section 5.3. This formulation allows a more straightforward prediction of floor responses subjected to such activities.

5.5.1 Variation of floor response by crowd size

As highlighted in Section 4.3.4.1, the main difference between loads and responses against crowd size is that RMS displacements are decreasing more severely than RMS forces. The observed difference is due to the transition from forces to displacements using the modal properties of the floor.

Based on the response calculation procedure described in Section 2.6.2, involved parameters for response prediction (other than those of the PSD load model) are time parameters, excitation and response amplitudes of modal shapes as well as modal parameters (natural frequency, modal mass, damping ratio). The factor that varies with the number of individuals is the excitation amplitude of modal shapes. Using the fundamental mode of the floor specimen (see Section 3.3.2), excitation modal amplitudes are calculated for up to 16 individuals and corresponding mean values are presented in Table 5.11.

Crowd size	1	2	4	8	16
Mean amplitude of modal shape	0.79	0.72	0.74	0.55	0.48

Table 5.11: Amplitudes of modal shapes for excitation positions by crowd size

The mean amplitude of modal shapes gradually decreases for an increasing number of individuals. In fact, the fundamental mode has a regular shape with maximum amplitude at centre and lower amplitudes far away. With an increasing number of participants, the uniform distribution over the floor imposes to place individuals far from the centre which results in lower amplitudes of modal shape for the fundamental mode. This could be responsible for the relative decrease of the crowd responses compared to the crowd forces.

In terms of excitation, the previous remark shows that the response of the floor is mainly governed by the mean amplitude of modal shapes for all individuals, independently of their specific positions on the floor. This opens the way for an equivalent formulation of the crowd load model (similar to the model adopted for pedestrians walking on footbridges [5]) presented in the next section.

5.5.2 Equivalent load model formulation

Consider a floor structure having M natural modes where a group of N individuals performs rhythmic activities in a coordinated manner. Each individual k is supposed to have a known position on the floor ($x_{0,k}$; $y_{0,k}$) and a known body mass m_k. The associated PSD load model $S_{p,N,k}(f)$ is provided by:

$$S_{p,N,k}(f) = \left[C(N) m_k g \alpha\right]^2 \sum_{i=1}^{3} \left[a_i^2 \exp\left(-\frac{\left(f - i f_p\right)^2}{(i\delta)^2} \right) \right] \tag{5.1}$$

where m_k is the body mass of the k^{th} individual, g the gravity acceleration (9.81m/s²), and for each activity: $C(N)$ is the coordination factor, f_p the excitation frequency, α the amplitude coefficient, δ the bandwidth coefficient and a_i the relative coefficient of the i^{th} harmonic (see Table 4.4).

The cross-PSD between two individuals k and l $S_{p,N,k,l}(f)$ is calculated by:

$$S_{p,N,k,l}(f) = \sqrt{S_{p,N,k}(f) S_{p,N,l}(f)} \tag{5.2}$$

The PSD matrix of generalized forces $\left[S_{p^*}(f)\right]$ is then obtained by:

$$\left[S_{p^*}(f)\right] = \left[\Phi_p\right]^T \left[S_{p,N}(f)\right] \left[\Phi_p\right] \tag{5.3}$$

where $\left[S_{p,N}(f)\right]$ is the PSD matrix of crowd loads ($N \times N$) (see Section 4.2.4) and $\left[\Phi_p\right]$ the modal shape matrix of excitation positions ($N \times M$), such that:

$$\left[\Phi_p\right]_{n,k} = \Phi_{p,n,k} \tag{5.4}$$

Here, $\Phi_{p,n,k}$ is the modal amplitude of the n^{th} mode related to the position of the k^{th} individual ($x_{0,k}$; $y_{0,k}$).

Using the previous remark about the response variation against crowd size, the N load models corresponding to each individual on the floor could be reduced to only one equivalent load model $S_{p,N}(f)$ expressed by:

$$S_{p,N}(f) = \left[N C(N) \bar{m} g \alpha\right]^2 \sum_{i=1}^{3} \left[a_i^2 \exp\left(-\frac{\left(f - i f_p\right)^2}{(i\delta)^2} \right) \right] \tag{5.5}$$

where $\bar{m}$ is the mean body mass of individuals. This load is supposed to be applied on the floor with a modal amplitude $\bar{\Phi}_{p,n}$ for each mode n calculated by:

$$\bar{\Phi}_{p,n} = \frac{1}{N} \sum_{k=1}^{N} \Phi_{p,n,k} \tag{5.6}$$

Using the modal shape vector for all natural modes $\{\Phi_p\}$, the equivalent PSD matrix of generalized forces is deduced by:

$$\left[S_{p^*}(f)\right] = \left\{\Phi_p\right\}^T S_{p,N}(f) \left\{\Phi_p\right\} \tag{5.7}$$

This matrix is then adopted in the procedure described in Section 2.6.2 to calculate RMS responses of floors subjected to rhythmic activities.

5.5.3 Verification on tested floors

In order to verify the previous formulation, RMS accelerations were calculated for the laboratory floor under the conditions corresponding to those presented in Section 5.4.2. Both the exact PSD load model (see Section 4.2.4) and the equivalent crowd load model presented earlier were used. Table 5.12 provides obtained results in terms of mean RMS responses.

Activity	Load model	RMS acceleration (m/s²)				
		1	2	4	8	16
Jumping 1	Exact	0.154	0.202	0.334	0.439	0.709
	Equivalent	0.154	0.202	0.335	0.438	0.712
Jumping 2	Exact	0.223	0.264	0.396	0.483	0.742
	Equivalent	0.223	0.264	0.397	0.482	0.746
Skipping 1	Exact	0.0794	0.100	0.142	0.147	0.177
	Equivalent	0.0794	0.100	0.143	0.147	0.178
Skipping 2	Exact	0.173	0.234	0.356	0.396	0.509
	Equivalent	0.173	0.234	0.358	0.395	0.511

Table 5.12: Comparison of RMS accelerations between the exact and equivalent load models for the laboratory floor

In a similar manner, RMS accelerations were computed for the parking floor (having 20 natural modes below 10Hz) with the parameters detailed in Section 5.4.2. Results for the exact and equivalent load models are given in Table 5.13.

Activity	Load model	RMS acceleration (m/s²)					
		1	2	4	8	16	32
Jumping 1	Exact	0.0555	0.119	0.187	0.262	0.482	0.689
	Equivalent	0.0559	0.119	0.187	0.265	0.484	0.693
Jumping 2	Exact	0.0917	0.120	0.178	0.210	0.246	0.458
	Equivalent	0.0913	0.121	0.177	0.210	0.248	0.462
Skipping 1	Exact	0.0248	0.0366	0.0498	0.0647	0.0786	0.148
	Equivalent	0.0248	0.0367	0.0499	0.0648	0.0789	0.148
Skipping 2	Exact	0.0204	0.0375	0.0536	0.0594	0.0719	0.142
	Equivalent	0.0203	0.0375	0.0536	0.0596	0.0725	0.143

Table 5.13: Comparison of RMS accelerations between the exact and equivalent load models for the parking floor

For both cases, RMS responses obtained by the equivalent load model are notably close to those calculated with the exact PSD load model. Almost identical accelerations were noticed for smaller groups, and slight differences occur for crowd sizes starting from 16 individuals due to more variability in terms of modal shapes. This provides a first verification of the proposed formulation for single-mode and multi-modal floor structures.

5.6 Conclusions

An experimental investigation conducted on a full-scale floor structure is presented in this chapter. The objective is to verify and extend the crowd-rhythmic load model identified in Chapter 4. After carrying out Experimental Modal Analysis, a number of up to 32 individuals perform rhythmic activities on the floor, adopting the same protocol as for the laboratory floor. The calculation of RMS accelerations using the established PSD load models and the dominant modal basis leads to comparable results related to their experimental counterparts (the mean relative difference is 9.8% and 17.5% for jumping and skipping, respectively). Furthermore, it is verified that the scope of coordination factors for jumping activities can be extended for up to 32 individuals using the hyperbolic functions. However, coordination factors related to skipping activities, expressed by power functions for up to 16 individuals, are found to be characterized by a constant plateau between 16 and 32 persons.

The proposed load models are then compared with existing models in the literature in terms of single person loads and coordination factors. The calculation of equivalent Dynamic Load Factors (DLFs) reveals comparable DLF amplitudes for the first harmonic and greater DLFs for higher ones, indicating that the proposed model adequately considers the spread of energy due to "intra-subject variability". Moreover, three groups of existing coordination factors have been reported for jumping activities (linear decrease followed by a plateau, power decrease, and gradual decrease by crowd size). Proposed factors are close to the third group with less-conservative values. On the other hand, a further power trend is used in the proposed models for skipping activities, leading to higher coordination factors for larger crowds in comparison to the existing model due to the presence of the plateau starting from 16 persons.

In terms of acceleration response, it is concluded that the proposed load models are less-sensitive to the excitation frequency for single-mode floors compared to existing time domain load models. For multi-modal floors, the existence of the spread of energy (termed leakage [71]) in the PSD models allows the excitation of multiple closely spaced modes simultaneously. This thus leads to an improved response estimation using the proposed load models for such widely used floor structures. Furthermore, comparison with the random field model proposed by Xiong and Chen [89] indicates that the coordination as observed in experiments has a considerable effect on the floor response. Although the proposed model predicts more conservative responses for smaller crowds, it considers the realistic synchronization degree sufficiently well, which provides close results to measurements for an increasing number of individuals.

Finally, an equivalent load model formulation is established based on the above verified load model. The usage of such formulation enables a more straightforward calculation of floor responses subjected to crowd-rhythmic activities, which will be discussed in the next chapter.

6 Prediction of floor responses to crowd-rhythmic loads

6.1 Introduction

In the field of structural dynamics, a simple yet reliable method is still a pre-requisite for the serviceability assessment of floor structures subjected to human movements, especially for crowd-rhythmic activities with a coordinated motion ([50], [90]). Unfortunately, existing guidelines dealing with this issue do not give a complete insight about the subject. As stated in Chapter 2, guidelines for comfort assessment of floors (SCI P354 [81] and AISC DG 11 [63]) are mainly dedicated to a single person exciting the floor. Alternatively, supplementary guidance documents provide more exhaustive information to take into account crowd loads during the response evaluation process. For instance, BS 6399-1 [9] proposes coordination factors for the case of crowds jumping. However, it was discovered that applying this guideline leads to much higher floor responses than have so far been found in practice [65]. The UK recommendations [49] present a crowd load model to be used in the response analysis of floors. However, the model is based primarily upon bouncing crowds [26], and restricted to groups of 50 or more individuals only [50]. ISO 10137 [45] proposes a jumping crowd load model including coordination factors for different levels of synchronization. Several methods for the response evaluation of floors using that model are listed, but without giving further details about their practical application.

In that context, detailed spectrum methods for the calculation of floor responses due to jumping crowds have been suggested. Chen et al. [14] established an acceleration spectrum based on individual jumping force measurements inspired by earthquake applications. However, resulting responses are conservative and the group effect is roughly considered (characterized by simulations from individual jumps). This was overcame by Xiong et al. [91] who proposed a response calculation procedure for jumping groups based on a random field model, although the practical implementation of such method is quite laborious (requiring Monte Carlo simulations).

In this chapter, methods for the prediction of the floor response against crowd-rhythmic activities are suggested, accounting for the crowd load models established in the previous chapters. Firstly, a general method for the response evaluation of multi-modal floors is established and a sensitivity study is carried-out in order to analyse and validate the proposed method. Secondly, a simplified method for the response calculation of single-mode floors is suggested, verified and applied to an existing floor structure.

6.2 General method for floor response calculation

This section presents a general method to calculate the response of floors subjected to rhythmic activities based on the equivalent crowd load model formulation proposed in Section 5.5 together with the random vibration theory. This method is applicable to all types of floors and rhythmic activities, assuming that corresponding load model parameters are known.

6.2.1 Calculation procedure

The configuration of the floor detailed in Section 2.6 is adopted in this section, with the same notations as those used in Section 5.5.2. The maximum investigated excitation frequency for human activities is 10Hz [31].

The equivalent load model representing a given crowd-rhythmic activity $S_{p,N}(f)$ (expressed by Eq. (5.5)) is rewritten by:

$$S_{p,N}(f) = \left[NC(N)\bar{m}g\alpha\right]^2 \bar{S}_p(f) \tag{6.1}$$

where:

$$\bar{S}_p(f) = \sum_{i=1}^{3}\left[a_i^2 \exp\left(-\frac{\left(f - if_p\right)^2}{(i\delta)^2}\right)\right] \tag{6.2}$$

The PSD term of generalized forces $\left[S_{p^*_{m,n}}(f)\right]$ is formulated from Eq. (5.7) by:

$$S_{p^*_{m,n}}(f) = \bar{\Phi}_{p,m}\bar{\Phi}_{p,n}S_{p,N}(f) \tag{6.3}$$

Here, $\bar{\Phi}_{p,m}$ and $\bar{\Phi}_{p,n}$ are the mean modal amplitudes at all excitation positions for the m^{th} and n^{th} modes, respectively (obtained by Eq. (5.6)).

The PSD term of modal coordinates $S_{q,m,n}(f)$ is then rewritten from Eq. (2.63) by:

$$S_{q,m,n}(f) = \bar{\Phi}_{p,m}\bar{\Phi}_{p,n}H_m(\omega)\bar{H}_n(\omega)S_{p,N}(f) \tag{6.4}$$

where $H_n(\omega)$ is the transfer function related to the n^{th} mode expressed by:

$$H_n(\omega) = \frac{1}{M_n(\omega_n^2 - \omega^2 + 2j\xi_n\omega_n\omega)} \tag{6.5}$$

In the above equation, ω_n, M_n and ξ_n are the circular frequency, the modal mass and the damping ratio of the n^{th} mode, respectively, and j the imaginary unit.

This leads to the PSD term of displacement responses $S_{d,m,n}(f)$ obtained from Eq. (2.65) by:

$$S_{d,m,n}(f) = \left[NC(N)\bar{m}g\alpha\right]^2 \Phi_{r,m}\Phi_{r,n}\bar{\Phi}_{p,m}\bar{\Phi}_{p,n}H_m(\omega)\bar{H}_n(\omega)\bar{S}_p(f) \tag{6.6}$$

where $\Phi_{r,m}$ and $\Phi_{r,n}$ are the modal amplitudes at the response point for the m^{th} and n^{th} modes, respectively. Corresponding PSD term of acceleration responses $S_{a,m,n}(f)$ is given by:

$$S_{a,m,n}(f) = (2\pi f)^4 S_{d,m,n}(f) \tag{6.7}$$

The total PSD of accelerations is then deduced by:

$$S_a(f) = \sum_{m=1}^{M}\sum_{n=1}^{M} S_{a,m,n}(f) \tag{6.8}$$

Finally, the RMS acceleration a_{rms} is computed by:

$$a_{rms} = \sqrt{\int_0^{+\infty} S_a(f)df} \tag{6.9}$$

6.2.2 Sensitivity study

The accuracy of the general method presented in Section 6.2.1 must be checked against the exact calculation method detailed in Section 2.6.2 (based on the crowd PSD load model described in Section 4.2.4). To accomplish that, a floor configuration described below is adopted as an initial case study and the associated input parameters are varied in order to determine their influence on the floor acceleration.

The initial floor has an area of 12×10m², with one natural mode having natural frequency of 7Hz, total mass of 50t (modal mass of 41% of the mass, assuming rigid boundary conditions [40]), damping ratio of 2%, and a sinusoidal modal shape $\Phi(x,y)$ corresponding to the classical fundamental mode of isotropic plates [83] expressed by:

$$\Phi(x,y) = \sin\left(\frac{\pi x}{L_x}\right)\sin\left(\frac{\pi y}{L_y}\right) \tag{6.10}$$

where L_x and L_y are the length and width of the floor, respectively.

The duration of the rhythmic activity is assumed equal to 30s, with a time step of 0.0078s and a uniform body mass of individuals equal to 75kg.

6.2.2.1 Influence of response parameters

The response of the floor presented earlier is calculated at first considering the rhythmic action performed by a single person. The centre of the floor is considered as both the excitation and the response position. Although the investigated rhythmic activities have different load parameters, they are characterized by the same formulation of the PSD load model. Hence, the influence of response parameters is analysed only for "jumping 1" activity, which would be the same for other activities.

First of all, the influence of three parameters can be directly deduced from the formulation of the PSD response of the floor (given by Eq. (6.6)) as follows:

- A linear dependence exists between the floor acceleration and the amplitude coefficient α (see Eq. (6.1));
- The modal mass M_n is inversely proportional to the floor acceleration (see Eq. (6.5));
- A hyperbolic decrease of the floor response is highlighted against the damping ratio ξ (see Eq. (6.5)).

Given that the possible variation range of the modal mass M_n is much larger than the damping ratio ξ, the decrease of the RMS response would be stronger for the first parameter compared to the second. Consequently, if a mitigation of response is needed, the modal mass is to be increased first, followed by the damping ratio in case of insufficient performance or economic reasons.

The influence of remaining load parameters is analysed by generating 50 equidistant values in the interval $[\bar{p} - \sigma_p,\ \bar{p} + \sigma_p]$, where $\bar{p}$ is the mean value of parameter p (f_p or δ) and σ_p the corresponding standard deviation, both taken from Table 4.5. The generation parameters for "jumping 1" activity are summarized in Table 6.1.

Parameter	Symbol	Units	Mean	Standard deviation	Samples
Excitation frequency	f_p	Hz	2.36	0.21	50
Bandwidth coefficient	δ	Hz	0.035	0.01	50

Table 6.1: Generation parameters of the PSD load model

Figure 6.1 displays the RMS acceleration of the floor against each analysed load model parameter.

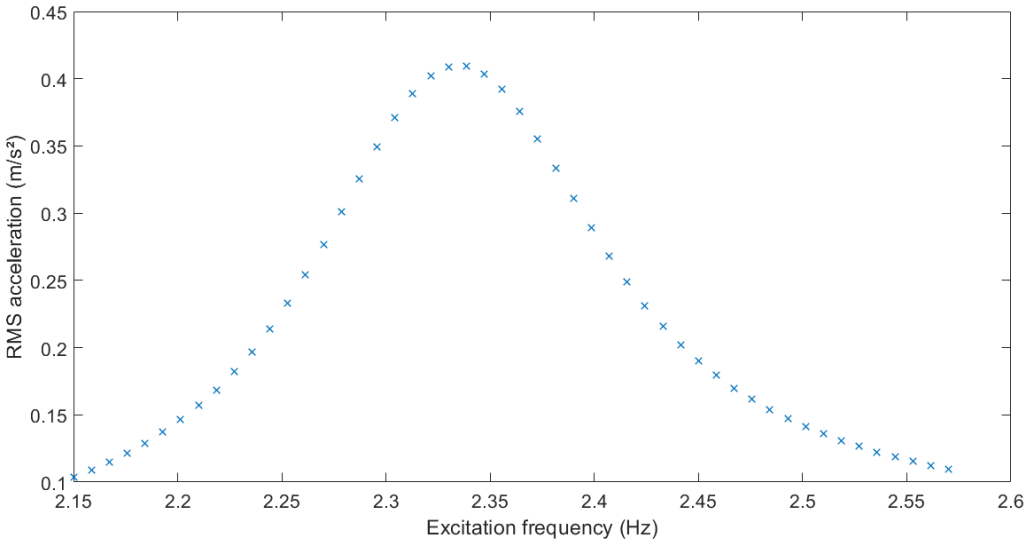

(a) Parameter f_p

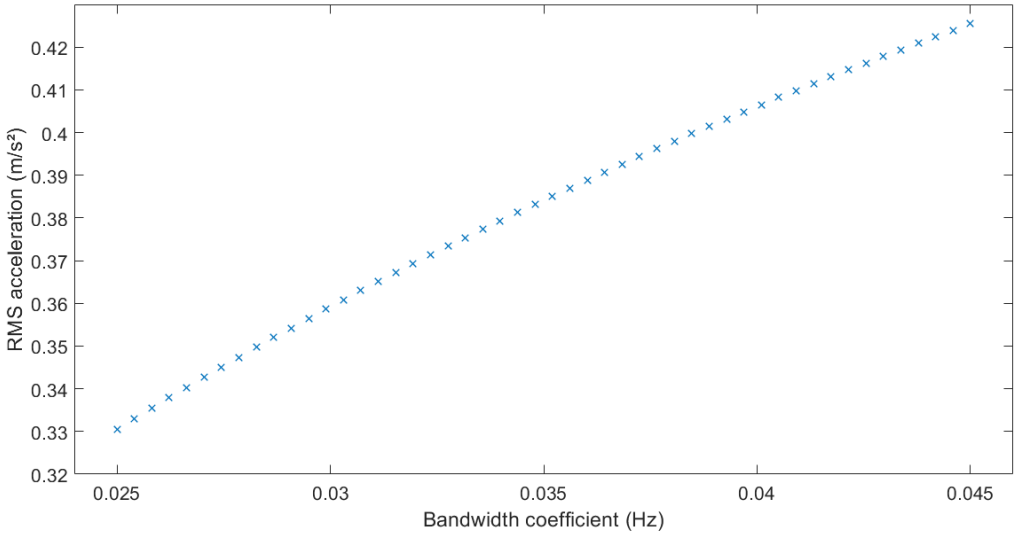

(b) Parameter δ

Figure 6.1: Variation of RMS acceleration against PSD load model parameters

The response of the floor is highly sensitive to the excitation frequency f_p. Indeed, the RMS acceleration gradually increases with the excitation frequency f_p until it reaches its maximum value at 2.32Hz followed by a gradual decrease. At this frequency, resonance occurs at the third harmonic of the load (6.96Hz) close to the natural frequency of the floor (7Hz). For practical response evaluations, the choice of an excitation frequency of 2.32Hz would be a worst-case scenario for the assessment of human comfort on the analysed floor.

On the other hand, an increasing tendency against parameter δ is found, characterized by a decreasing rate at higher values. This means that, in terms of response, the variation of the excitation frequency during motion (controlled by δ) is less influential than the variation of the impact energy of the rhythmic activity (quantified by α).

In addition, the influence of the natural frequency of the floor f_n is investigated using equidistant values between 2 and 10Hz (with a step of 0.1Hz). The RMS response of the floor is then calculated using the mean values of load parameters for "jumping 1" activity (see Table 4.5). The resulting RMS acceleration is plotted as a function of natural frequency in Figure 6.2.

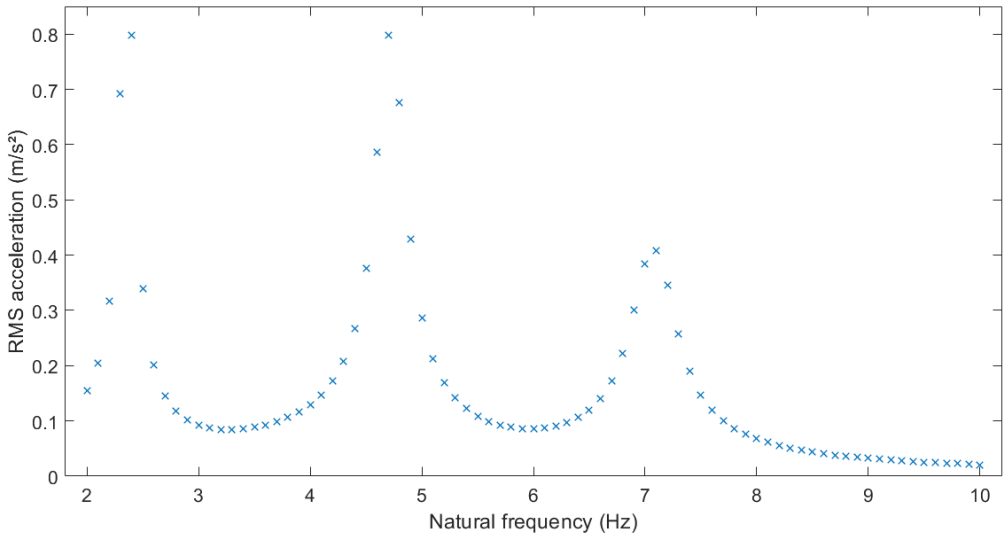

Figure 6.2: Variation of RMS acceleration against floor natural frequency

As the mean excitation frequency is 2.36Hz, the variation of the natural frequency f_n enables resonance to occur three times: at the first harmonic (f_p=2.36Hz, f_n=2.4Hz), the second harmonic ($2f_p$ =4.72Hz, f_n =4.7Hz) and the third harmonic of the load ($3f_p$ =7.08Hz, f_n =7.1Hz). The same bell shape as noticed for f_p (see Figure 6.1(a)) is reproduced for the natural frequency f_n at each resonant peak, indicating that the RMS response is also sensitive to this modal parameter.

Therefore, the interaction between f_n and f_p has been further analysed. For each f_n between 2 and 10Hz (with a step of 0.5Hz), the RMS response was calculated for the same values of f_p used above (with generation parameters given in Table 6.1). The obtained RMS accelerations are illustrated in terms of mean values and standard deviations in Figure 6.3. Maximum responses are found near resonance (at the first harmonic for f_n =2.5Hz and the second harmonic for f_n =4.5Hz and 5Hz). Furthermore, when the response is substantial, its variation with regards to the excitation frequency is also greater. This is due to the high sensitivity of the PSD response related to f_p near resonance. This confirms that the response of the floor is mainly dependent on these two parameters, which makes their accurate determination compulsory for a convenient response evaluation of floors subjected to human activities.

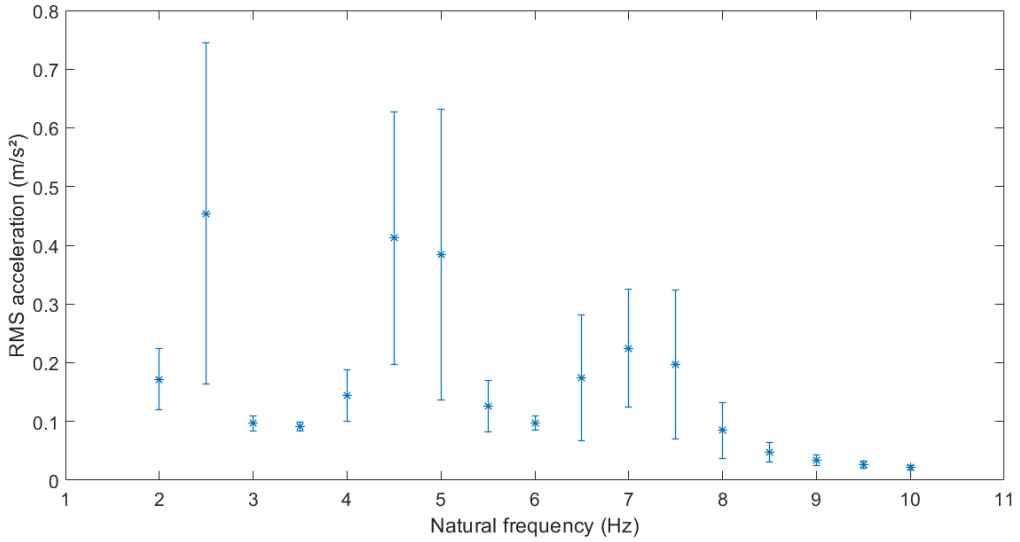

Figure 6.3: RMS accelerations (Mean in asterisk marks, standard deviation in error bars) for each natural frequency (assuming multiple excitation frequencies)

6.2.2.2 Comparison of floor responses

The modal properties of the floor are generated using equidistant values characterized by the parameters provided in Table 6.2. Subsequently, the floor acceleration is computed at centre for 1, 2, 4, 8 and 16 individuals uniformly distributed over the floor for the four studied rhythmic activities (with coordination factors provided in Table 5.6). The corresponding load parameters are generated using 50 equidistant values in the interval $[\bar{p} - \sigma_p,\ \bar{p} + \sigma_p]$, where $\bar{p}$ is the mean value of parameter p (f_p, α and δ) and σ_p the corresponding standard deviation, both taken from Table 4.5 for each investigated activity. Both response calculation methods (exact method, general method) are used for that purpose. Results of RMS acceleration are presented in Appendix C.1 in terms of mean values and standard deviations.

Parameter	Symbol	Units	Min	Max	Step
Natural frequency	f_n	Hz	2	10	0.1
Total mass	M	t	10	200	10
Damping ratio	ξ	%	0.5	10	0.5
Length	L_x	m	7	20	1
Width	L_y	m	6	15	1

Table 6.2: Variation range of floor modal properties

After investigating all parameters in their variation range, it is noticed that RMS response amplitudes depend on the load parameters characterizing each studied activity. It can also be deduced that the coefficient of variation of RMS responses (ratio of the standard deviation to the mean value) is almost the same for all investigated crowd sizes. The standard deviation is greater for an increasing number of individuals because it is more difficult to coordinate the motion of a larger crowd compared to a smaller one. The fluctuation of the response is also more important when varying the floor modal properties compared to the PSD load model parameters. The reason behind this is that the modal properties figure twice in FRFs (see Eq. (6.5)) whereas the load parameters are only used once in the PSD load model (see Eq. (6.2)). On the other hand, the lowest standard deviations are noticed after the variation of dimensions L_x and L_y, as they are supposed to affect only the fundamental modal shape.

The major remark highlighted from response results is that the general method provides RMS accelerations notably close to the exact method for all investigated crowd sizes and parameters related to the load model and the floor structure, which shows its accuracy for single-mode floors.

The vibrational floor response is also investigated for the case of multiple natural modes. As similar results are found for the four activities in the above analysis, "jumping 1" activity is solely used in the present study. The floor is assumed to have a number of 1, 4, 8 and 16 bending modes, where each natural mode n is characterized by a modal shape $\Phi_n(x,y)$ similar to that of isotropic plates expressed by [83]:

$$\Phi_n(x,y) = \sin\left(\frac{n\pi x}{L_x}\right)\sin\left(\frac{\pi y}{L_y}\right) \tag{6.11}$$

Remaining modal properties were defined by equidistant values for natural frequencies between 3 and 10Hz, total masses between 20 and 200t and damping ratios between 1 and 10% (using the step values provided in Table 6.2). The response was evaluated at the point with coordinates (x_r=2L_x/3, y_r=2L_y/3) which was also the position of excitation for the case of one individual. The reason for choosing this point instead of the centre of the floor is that the latter presents zero modal amplitudes for many natural modes, which eliminates their contribution in the final response. Table 6.3 summarizes RMS responses obtained with the exact and general methods. Results are close between the two methods, confirming that the general method remains efficient for the RMS response calculation of multi-modal floors too.

Number of modes	Method	RMS acceleration for "jumping 1" (m/s²)				
		1	2	4	8	16
1	Exact	0.0676	0.124	0.184	0.299	0.497
	General	0.0676	0.123	0.184	0.300	0.497
4	Exact	0.116	0.237	0.353	0.575	0.954
	General	0.116	0.237	0.354	0.576	0.954
8	Exact	0.191	0.252	0.348	0.576	0.956
	General	0.191	0.252	0.349	0.577	0.957
16	Exact	0.285	0.452	0.352	0.581	0.964
	General	0.285	0.451	0.352	0.582	0.964

Table 6.3: RMS acceleration by crowd size for multiple natural modes

6.3 Simplified method for floor response calculation

A simplified method for the calculation of vibrational response of floors under rhythmic activities is presented in this section. This method is derived from the general method detailed in Section 6.2, and applicable to several floors encountered in practice.

6.3.1 Scope of the method

This method is available for floors satisfying two conditions:

- They are dominated by only one natural mode in the frequency range between 0 and 10Hz (corresponding to human excitation ([31]);
- They are characterized by a regular modal shape (close to the classical sinusoidal one).

Modal analysis (using experimental techniques or numerical modelling) should be carried out in order to verify that a given floor fulfils the latter requirements. For the case of composite steel and concrete construction, these conditions are verified for regular floors encountered in practice [81]. Indeed, the first condition mainly corresponds to floors characterized by a limited number of spans and panels. These floors also primarily comprise structural components with a small amount of non-structural partitions. The second condition is usually satisfied for floors having a shape that could be obtained from rectilinear grids with limited curves on plan [81].

6.3.2 Response calculation procedure

The floor settings presented in Section 2.6 are adopted in this section. The floor is supposed to fulfil the conditions of Section 6.3.1 (see Figure 6.4).

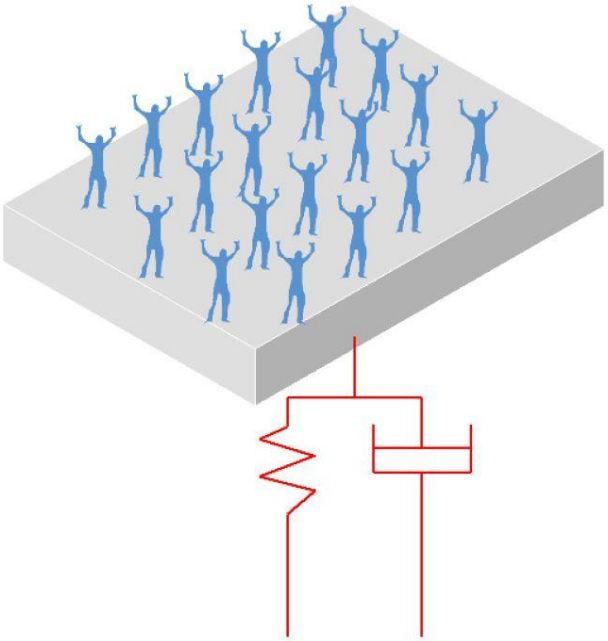

Figure 6.4: Single-mode floor subjected to crowd-rhythmic activities [90]

The calculation procedure described in Section 6.2.1 is applied using the equivalent PSD load model $S_{p,N}(f)$ obtained by Eq. (6.1) reminded below:

$$S_{p,N}(f) = \left[NC(N)\bar{m}g\alpha\right]^2 \bar{S}_p(f)$$

where $\bar{S}_p(f)$ is given by Eq. (6.2). The PSD of generalized forces $S_{p^*}(f)$ is simplified to only one term due to the presence of the unique fundamental mode of vibration as follows:

$$S_{p^*}(f) = \bar{\Phi}_p^2 S_{p,N}(f) \tag{6.12}$$

Here, $\bar{\Phi}_p$ is the mean of the fundamental modal amplitudes at the N excitation positions (obtained by Eq. (5.6)).

The PSD of the modal coordinate $S_q(f)$ is also reduced to:

$$S_q(f) = \bar{\Phi}_p^2 \left|H_1(f)\right|^2 S_{p,N}(f) \tag{6.13}$$

where $H_1(f)$ is the transfer function obtained by Eq. (6.5) for n=1 and ω=2πf, which gives:

$$\left|H_1(f)\right|^2 = \frac{1}{M_1^2\left[16\pi^4\left(f_1^2 - f^2\right)^2 + \left(8\pi^2\xi_1 f_1 f\right)^2\right]} \tag{6.14}$$

This leads to the PSD of the acceleration response $S_a(f)$ calculated by:

$$S_a(f) = \left[NC(N)\bar{m}g\alpha\right]^2 \Phi_r^2 \bar{\Phi}_p^2 (2\pi f)^4 \left|H_1(f)\right|^2 \bar{S}_p(f) \tag{6.15}$$

Here, Φ_r is the fundamental modal amplitude at the response location.

Eq. (6.15) is rewritten by:

$$S_a(f) = \sum_{i=1}^{3} S_{a,i}(f) \tag{6.16}$$

where $S_{a,i}(f)$ is the PSD response due to the i^{th} harmonic of the load given by:

$$S_{a,i}(f) = \left[NC(N)\bar{m}g\alpha\right]^2 \Phi_r^2 \bar{\Phi}_p^2 (2\pi f)^4 \left|H_1(f)\right|^2 a_i^2 \exp\left(-\frac{\left(f - if_p\right)^2}{(i\delta)^2}\right) \tag{6.17}$$

The RMS response $a_{rms,i}$ due to the i^{th} harmonic is then expressed by:

$$a_{rms,i}^2 = \int_0^{+\infty} S_{a,i}(f)df = \gamma_N a_i^2 \int_0^{+\infty}\left[f^4 \left|H_1(f)\right|^2 \exp\left(-\frac{\left(f - if_p\right)^2}{(i\delta)^2}\right)\right]df \tag{6.18}$$

where

$$\gamma_N = (2\pi)^4 \left[NC(N)\bar{m}g\alpha\right]^2 \Phi_r^2 \bar{\Phi}_p^2 \tag{6.19}$$

The integral given by Eq. (6.18) is approximated using two main simplifications. Firstly, the exponential function of the PSD load model (see Eq. (6.17)) is replaced by a bilinear function. Since the amplitude of the exponential function at $f=i(f_p \pm 2\delta)$ equals $0.018 \ll 1$, these values are considered as lower and upper frequencies (with zero amplitude) of the bilinear function $B_i(f)$ expressed as follows:

$$B_i(f) = \begin{cases} 1 + \left(\dfrac{f - if_p}{2i\delta}\right), & i(f_p - 2\delta) \le f \le if_p \\ 1 - \left(\dfrac{f - if_p}{2i\delta}\right), & if_p \le f \le i(f_p + 2\delta) \end{cases} \tag{6.20}$$

An illustration of the exponential and bilinear functions for the first load harmonic with f_p=2Hz and δ=0.05Hz is shown in Figure 6.5. It can be observed that the energy distribution is almost the same between the two functions. The obtained normalized load energy (variance) is 0.09 and 0.10 for the exponential and the bilinear function, respectively, A slightly conservative floor response is then expected when adopting the bilinear function. The same remarks mentioned earlier are made for higher load harmonics.

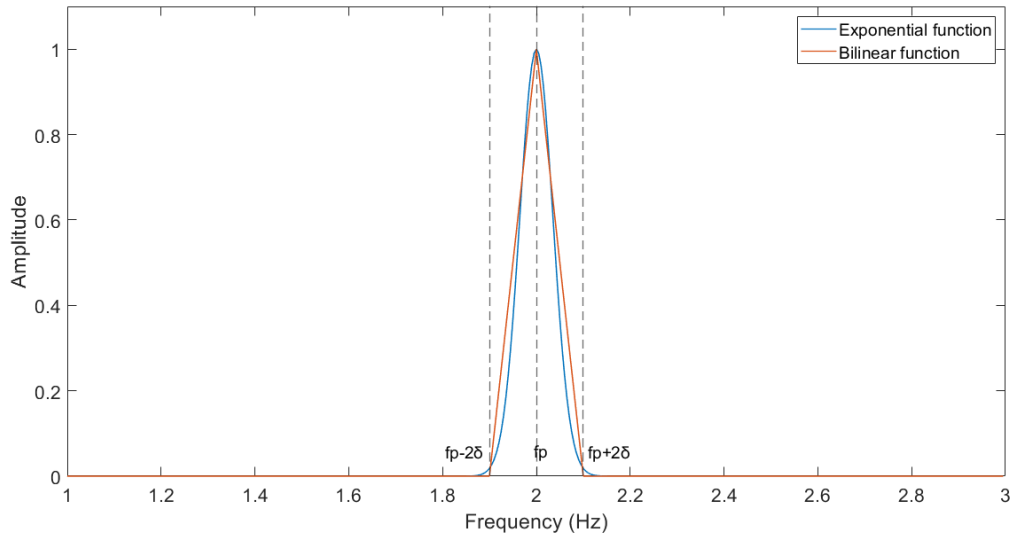

Figure 6.5: Comparison between exponential and bilinear functions for the PSD load model (first harmonic, excitation frequency of 2Hz)

Secondly, a closed-form expression of the bilinear function $B_i(f)$ is established. Indeed, the identified values of the bandwidth coefficient δ are all below 0.15Hz for all investigated activities (see Table 4.5), such that $\delta \ll f_p$. Hence, it is assumed that the energy content of the i^{th} harmonic could be concentrated at the corresponding peak [91]. Given that the enclosed area of the bilinear function curve equals $2i\delta$ (as illustrated in Figure 6.5), the following approximation applies:

$$\exp\left(-\frac{\left(f-if_p\right)^2}{(i\delta)^2}\right) \approx B_i(f) \approx \left(2i\delta\right)\Delta(f-if_p) \tag{6.21}$$

where Δ is the Dirac-delta function. This function has an integral property for a given function $Z(f)$ and a constant b expressed by:

$$\int_0^{+\infty} Z(f)\Delta(f-b)df = Z(b) \tag{6.22}$$

Using the approximation of the exponential function provided by Eq. (6.21), the application of Eq. (6.22) provides the following integral approximation:

$$\int_0^{+\infty}\left[f^4\left|H_1(f)\right|^2\exp\left(-\frac{\left(f-if_p\right)^2}{(i\delta)^2}\right)\right]df \approx \left(2i\delta\right)(if_p)^4\left|H_1(if_p)\right|^2 \tag{6.23}$$

This leads to an approximate expression of Eq. (6.18) given by:

$$a_{rms,i}^2 \approx \gamma_N\, a_i^2\left(2i\delta\right)(if_p)^4\left|H_1(if_p)\right|^2 \tag{6.24}$$

The RMS response of the floor a_{rms} is then deduced by:

$$a_{rms} = \sqrt{\int_0^{+\infty} S_a(f)df} = \sqrt{\sum_{i=1}^{3} a_{rms,i}^2} \tag{6.25}$$

6.3.3 Chart illustration for investigated activities

The response calculation procedure presented in Section 6.3.2 is illustrated for the four investigated activities. The objective is to elaborate simplified charts allowing to predict RMS accelerations for the most encountered cases in practice.

For each load harmonic *i*, a normalized RMS acceleration $\bar{a}_{rms,i}$ is obtained from Eq. (6.24) by eliminating all proportional factors (not characterizing the harmonic) as follows:

$$\bar{a}_{rms,i}^2 = \left[\frac{M_1^2}{\gamma_N (2\delta f_p^4)}\right] a_{rms,i}^2 \tag{6.26}$$

which gives, after substitution:

$$\bar{a}_{rms,i}^2 = \frac{a_i^2 \, i^5}{\left[16\pi^4 \left(f_1^2 - \left(if_p\right)^2\right)^2 + \left(8\pi^2 \xi_1 f_1 if_p\right)^2\right]} \tag{6.27}$$

The total normalized RMS acceleration $\bar{a}_{rms}$ is then deduced by:

$$\bar{a}_{rms} = \sqrt{\sum_{i=1}^{3} \bar{a}_{rms,i}^2} \tag{6.28}$$

The response is calculated for the most frequent rhythmic load case. Hence, the load parameters (including the excitation frequency f_p) are the identified mean values taken from Table 4.5. In addition, coefficients a_i (i={1, 2, 3}) are provided in Table 4.4, whereas coordination factors are given in Table 5.6 for the considered activity.

Similarly to earthquake engineering [14], the response charts represent the variation of floor accelerations with respect to the natural frequency for fixed values of damping ratios. The damping ratio of most floors ranges between 1 and 4%, as proposed by design guidelines for floor vibration analysis ([40], [63], [81]). Therefore, response charts are established for four values of damping ratio: 1%, 2%, 3% and 4%.

For each damping ratio and rhythmic activity, the simplified charts are established by varying the natural frequency f_1 and calculating the corresponding normalized RMS accelerations given by Eq. (6.28). The interval of variation of f_1 should represent floors satisfying the first condition of Section 6.3.1, and is thus taken between 2 and 10Hz (with a step of 0.01Hz). Figure 6.6 illustrates obtained response charts for the four investigated rhythmic activities.

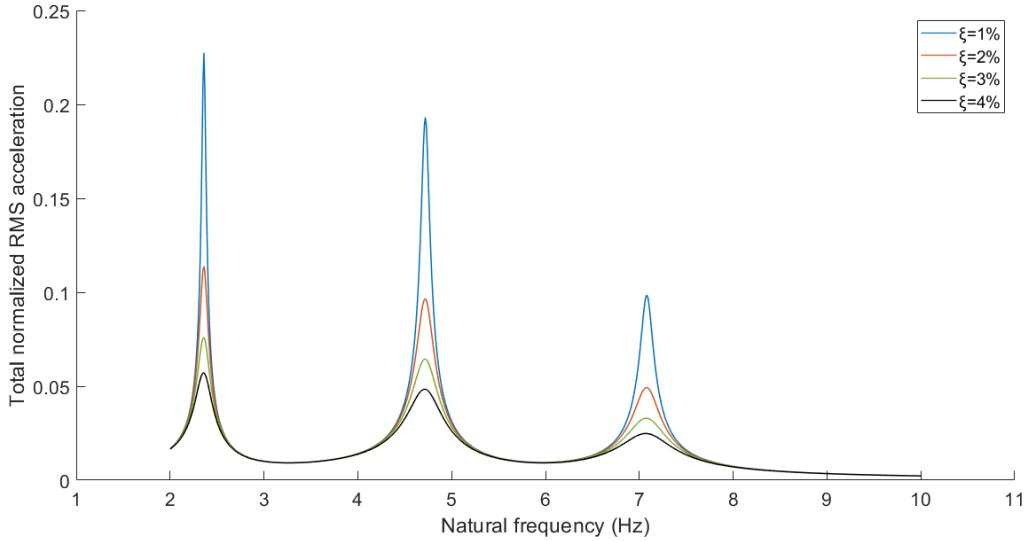

(a) Jumping 1

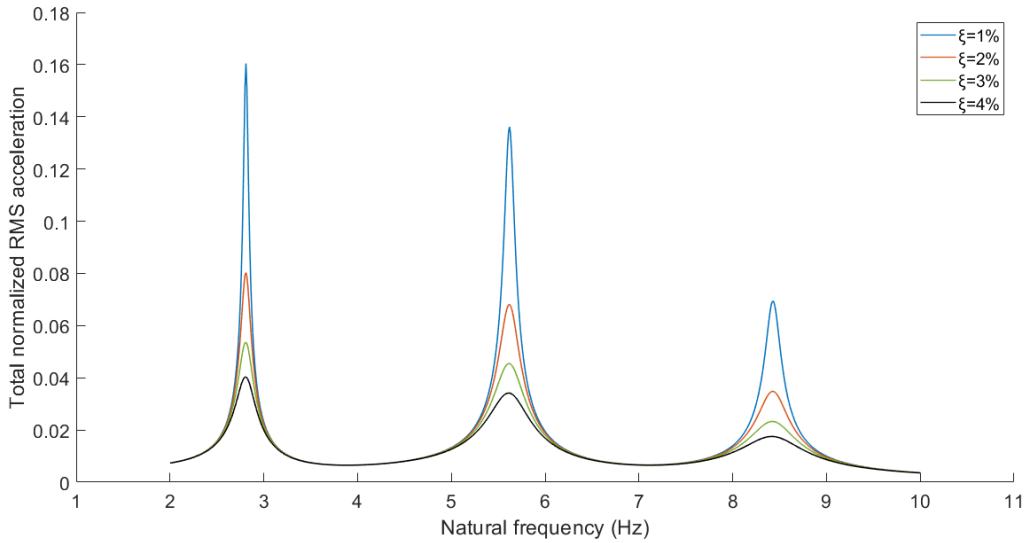

(b) Jumping 2

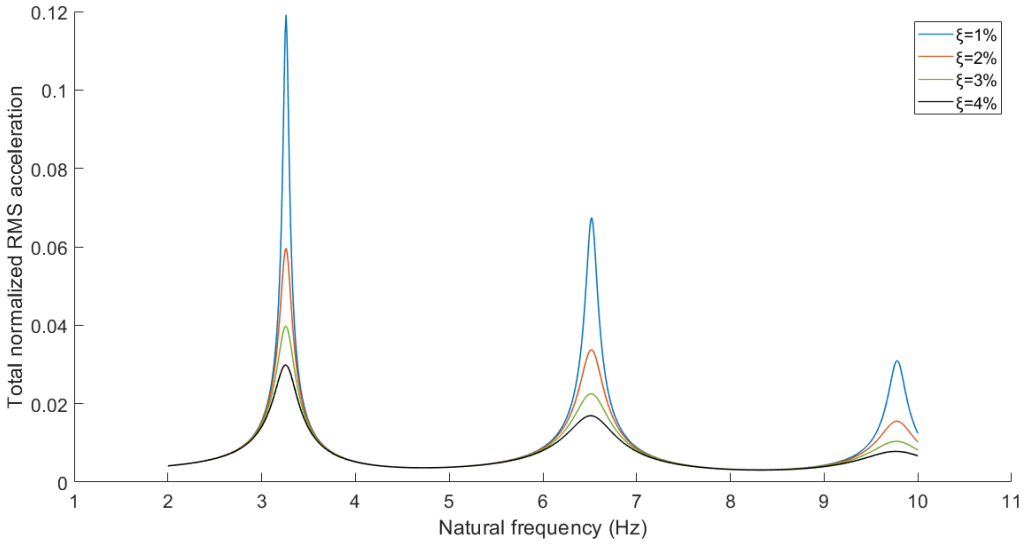

(c) Skipping 1

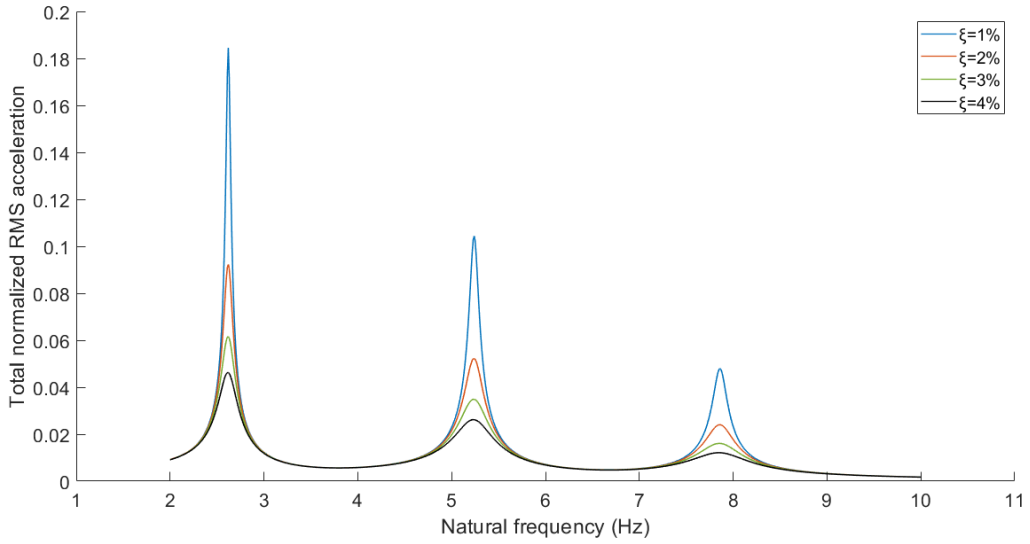

(d) Skipping 2

Figure 6.6: Total normalized RMS acceleration against floor natural frequency

For all investigated activities, maximum normalized RMS accelerations $\bar{a}_{rms}$ occur at each of the three harmonics of the load due to resonance, whereas a gradual decrease of the response is noticed between two harmonics. This is similar to the effects noticed in the sensitivity study carried out in Section 6.2.2.1 for the general method. Moreover, the increase in floor response for lower damping ratios takes places with a sharper resonant peak allowing faster reduction of the response away from the three harmonics of the load.

Knowing the damping ratio and the natural frequency of the floor along with additional parameters characterizing Eq. (6.26), a simplified estimation of RMS acceleration a_{rms} could then be made for each rhythmic activity considering the most probable floor vibration case by:

$$a_{rms} = \frac{\sqrt{2\delta\gamma_N}\, f_p^2}{M_1}\bar{a}_{rms} \tag{6.29}$$

6.3.4 Sensitivity study

The accuracy of the simplified method in terms of floor responses is assessed in comparison with the general method presented in Section 6.2. The same floor configuration used in the sensitivity study of Section 6.2.2 is adopted here. This floor meets the requirements of Section 6.3.1 for the application of the simplified method considering the fundamental mode.

The duration of each activity is considered equal to 30s, with a time step of 0.0078s and a uniform body mass of individuals equal to 75kg. Corresponding coordination factors are provided in Table 5.6.

The modal properties of the floor, together with the load parameters of the four analysed rhythmic activities, are generated using the same instructions as for Section 6.2.2.2. For each set of parameters and investigated activity, RMS responses are calculated at centre for 1, 2, 4, 8 and 16 individuals uniformly distributed over the floor, using both the general method (see Section 6.2.1) and the simplified method (see Section 6.3.2). RMS acceleration results, in terms of mean values and standard deviations for the four studied activities, are presented in Appendix C.2. As an illustration, Figure 6.7 displays mean RMS accelerations against crowd size obtained for both methods after varying the excitation frequency f_p of "jumping 1" activity.

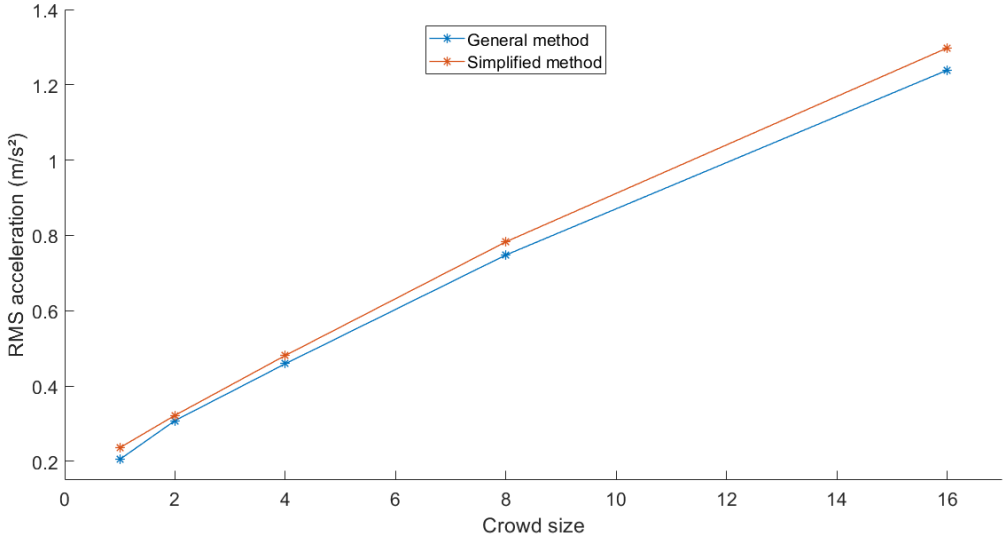

Figure 6.7: Mean RMS accelerations against crowd size for the general and simplified method (after varying the excitation frequency of "jumping 1")

The RMS acceleration difference between the two methods increases when the excitation frequency is likely to cause resonance to the analysed floor. This could be attributed to the concentration of energy in the closed-form expression (see Eq. (6.21)), which contributes to a slight overestimation of responses in resonant cases whereas the inverse effect is observed when resonance does not occur [88]. For the investigated activities, the mean excitation frequency of "jumping 1" (f_p=2.36Hz) leads to a third harmonic close to the floor fundamental frequency (f_n=7Hz), whereas the latter natural frequency is close to the second harmonic of "skipping 1" (f_p=3.26Hz). Maximum differences then occur for "jumping 1" and "skipping 1" for jumping and skipping activities, respectively. Moreover, the same relative difference between RMS accelerations is maintained by crowd size for each activity and set of parameters. This means that the accuracy of the simplified method would not change even when used for larger crowds.

From an overall point of view, the simplified method provides slightly conservative responses than the general method (with more fluctuated values). This is due to the difference between the exponential and bilinear functions in terms of load energy as outlined in Section 6.3.2. However, a good agreement of RMS responses is observed between the two methods (with a relative difference between 2.5% and 12.6%), thus confirming the application of the simplified method for the calculation of floor responses due to investigated activities. This method could then be used by engineers to have a quick estimation of the response of floors subjected to crowd-rhythmic activities.

6.3.5 Recommended parameters

6.3.5.1 Load parameters

The range of PSD load parameters for each investigated rhythmic activity is given in Table 4.5. However, their choice depends on the comfort level agreed by the stakeholders. Recommendations for this regard detailed in Section 4.3.2.2 for a general response evaluation are also applied to the simplified method. The same potential load case scenarios are considered for design: usual/mean load case (related to the most frequent situation) or occasional/maximum load case (causing the highest floor responses).

6.3.5.2 Modal shape and distribution of individuals

Presuming that the modal shape of the floor is not provided, it is recommended to use the classical sinusoidal shape $\Phi(x,y)$ given by Eq. (6.10) reminded below:

$$\Phi(x,y) = \sin\left(\frac{\pi x}{L_x}\right)\sin\left(\frac{\pi y}{L_y}\right)$$

where L_x and L_y are the length and width of the floor, respectively.

When performing rhythmic activities, individuals can be distributed in several ways [43]. This includes uniform, interval, triangular or diagonal line distributions, as can be seen in Figure 6.8.

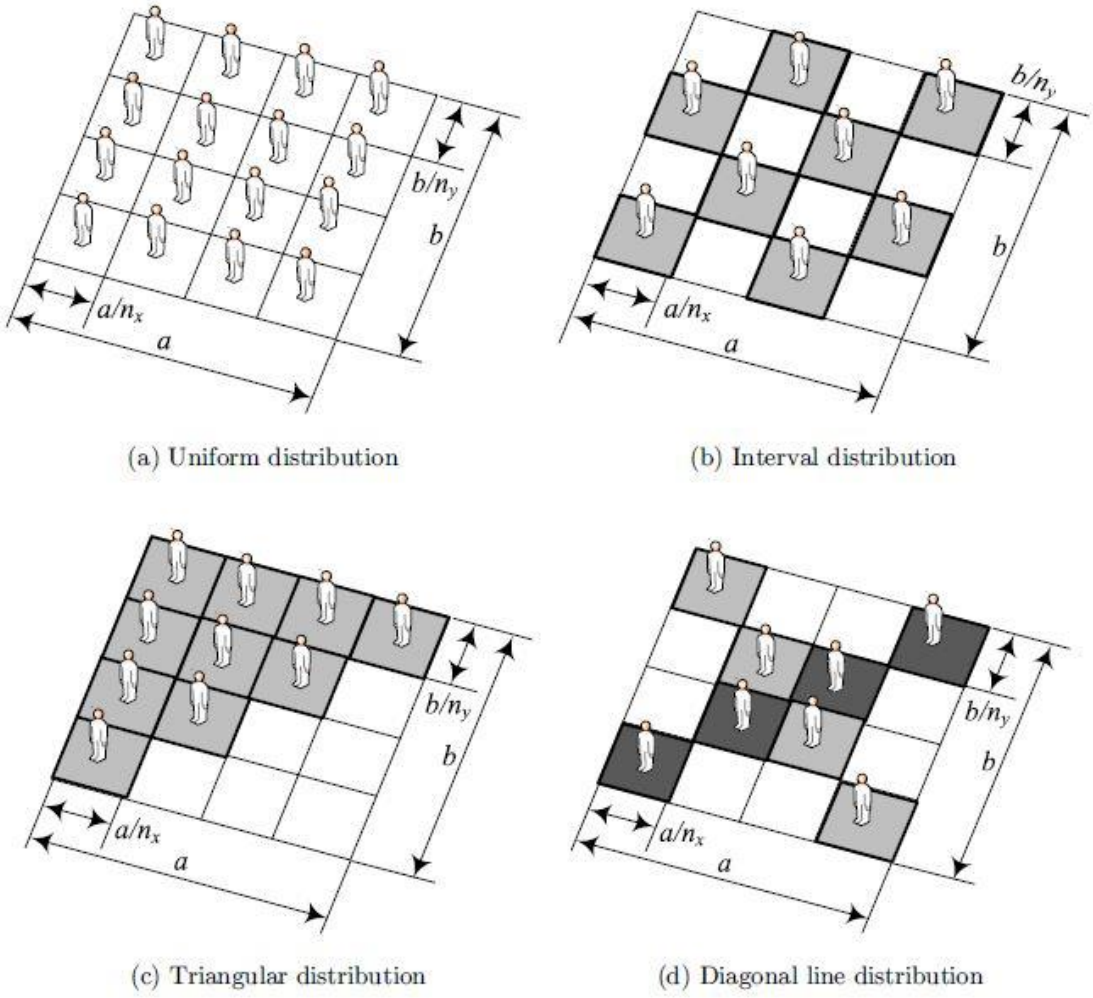

Figure 6.8: Potential distributions of individuals on a floor structure [43]

However, the uniform distribution is more likely to be encountered in real situations of rhythmic activities. Moreover, when adopting this distribution, the sinusoidal shape enables to have a stepwise decrease of modal amplitudes related to excitation positions for an increasing crowd size (as outlined in Section 5.5.1). In case no specific positions of rhythmic activities are defined by the stakeholders, a distribution having the latter property is thus suggested for response prediction. As remarkable differences of responses are noticed with stepwise changes of crowd size [31], proposed positions are made for 1, 2, 4, 8, 16, 32 and 64 individuals, as illustrated in Figure 6.9. An area of 3×2m² is occupied by each person for crowd sizes between 1 and 4, against an area of 2×1.5m² for crowd sizes between 8 and 64. The same distribution could be applied to other numbers of individuals using the previous areas per person.

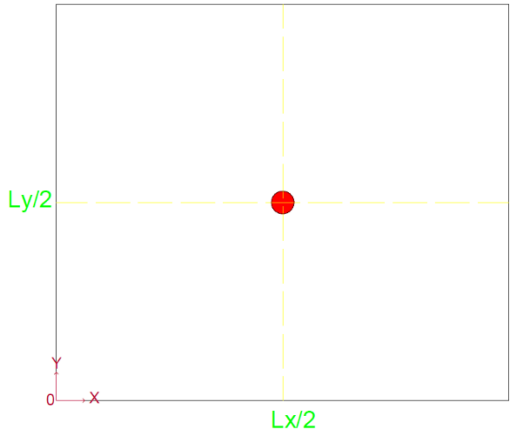

(a) 1 person

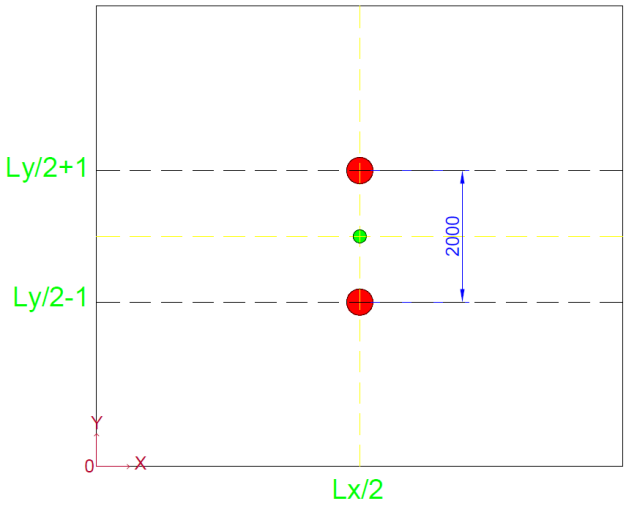

(b) 2 individuals

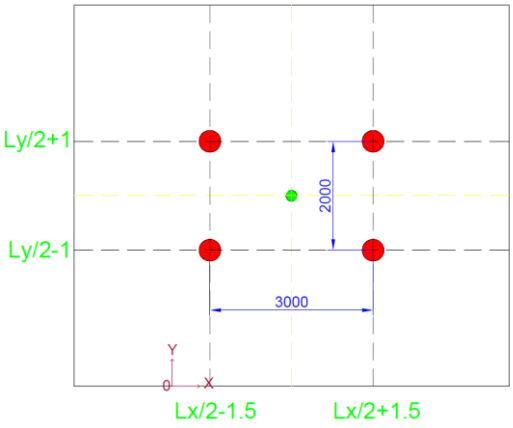

(c) 4 individuals

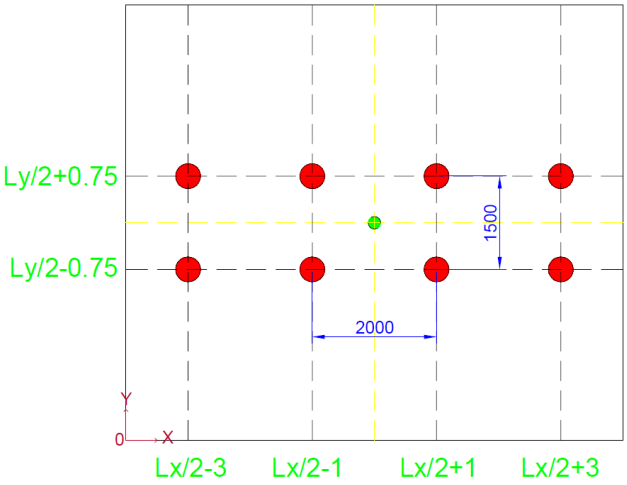

(d) 8 individuals

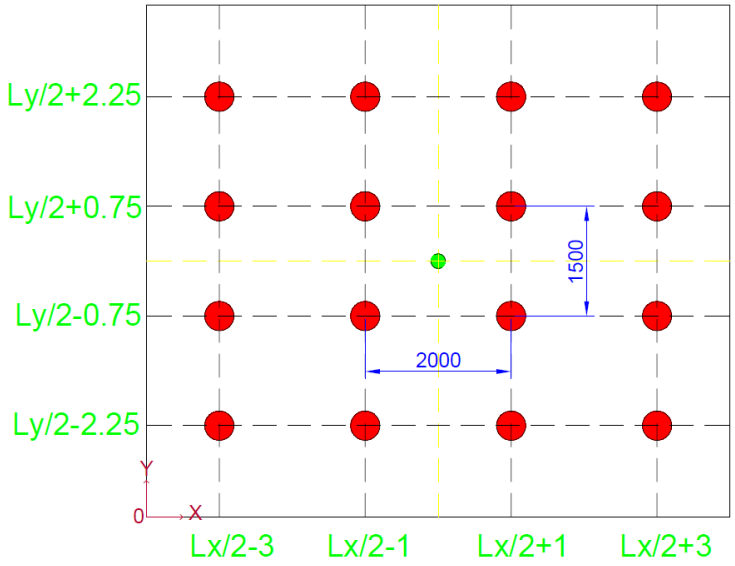

(e) 16 individuals

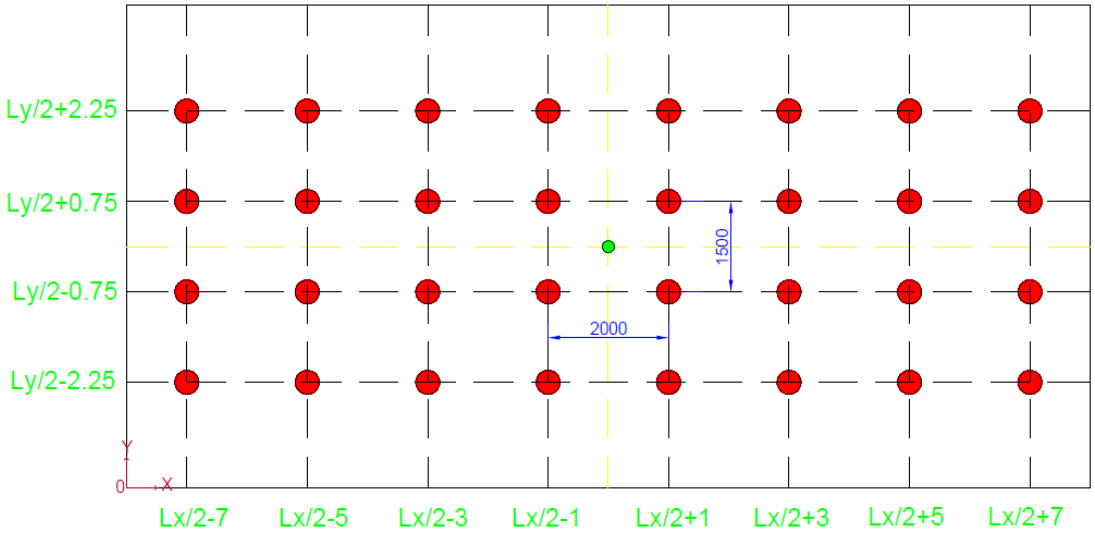

(f) 32 individuals

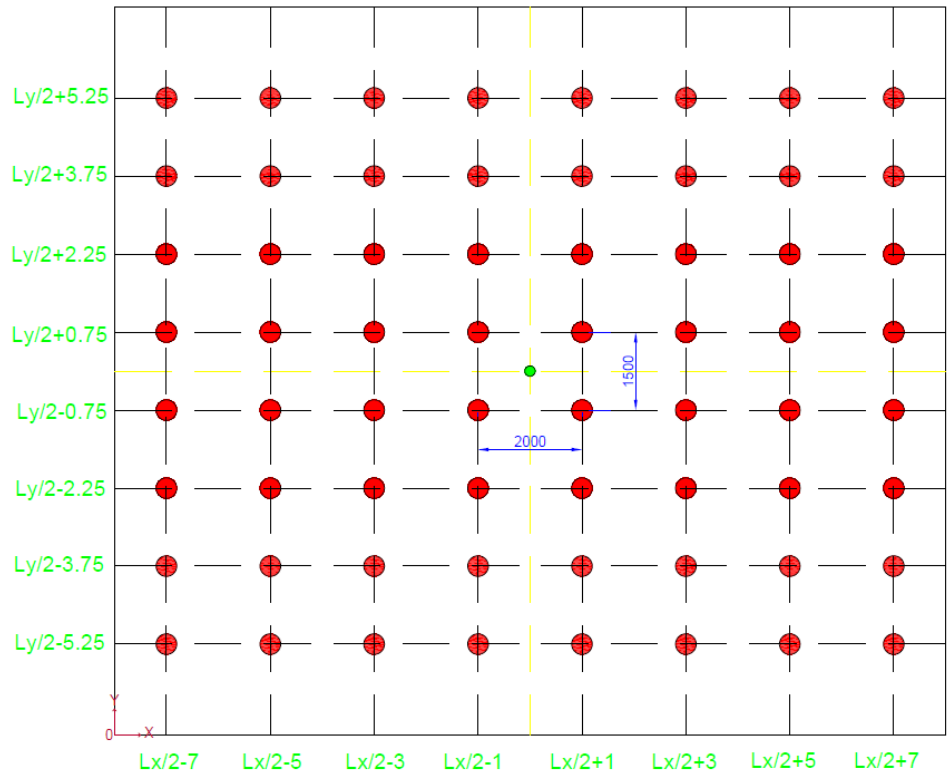

(g) 64 individuals

Figure 6.9: Proposed distribution of individuals for floor response prediction (coordinates of excitation positions in green)

6.3.5.3 Verification on the floor specimen

The response using recommended modal shape and distribution of individuals was compared against their experimentally determined counterparts for the laboratory floor presented in Chapter 3 (satisfying the conditions of Section 6.3.1). The same conditions as those listed in Section 5.4.2 were adopted for that purpose, and the simplified method presented in Section 6.3.2 was used to calculate the response of the floor. The switch from the experimental to the suggested modal shape (given by Eq. (6.10)) was analysed first, and resulting RMS responses for the four investigated activities are summarized in Table 6.4.

Activity	Modal shape	RMS acceleration (m/s²)				
		1	2	4	8	16
Jumping 1	Experimental	0.160	0.210	0.348	0.455	0.739
	Recommended	0.183	0.252	0.406	0.482	0.727
Jumping 2	Experimental	0.219	0.259	0.390	0.473	0.732
	Recommended	0.251	0.311	0.455	0.500	0.720
Skipping 1	Experimental	0.0840	0.106	0.151	0.156	0.188
	Recommended	0.0962	0.127	0.176	0.165	0.185
Skipping 2	Experimental	0.180	0.244	0.373	0.411	0.533
	Recommended	0.206	0.293	0.435	0.435	0.524

Table 6.4: Effect of modal shape on RMS acceleration by crowd size

It can be seen that RMS accelerations between the experimental and recommended modal shapes are close. The maximum relative difference is 20%. This difference is proportional to

the modal amplitudes, which is higher for the simplified modal shape for all numbers of participants except 16.

However, when using the simplified modal shape, the RMS response for the case of 8 persons is lower or equal to that of 4 persons for skipping activities. This unacceptable tendency is due to the fact that individuals are not distributed in an exactly symmetrical way in experiments, which leads to modal amplitudes much lower for the case of 8 persons compared to those for 4 persons. Instead, the suggested distribution presented in Figure 6.9 was used for both modal shapes. Corresponding RMS responses for all investigated activities are provided in Table 6.5.

Activity	Modal shape	RMS acceleration (m/s²)				
		1	2	4	8	16
Jumping 1	Experimental	0.201	0.242	0.320	0.496	0.801
	Recommended	0.204	0.264	0.354	0.515	0.742
Jumping 2	Experimental	0.274	0.299	0.358	0.516	0.793
	Recommended	0.278	0.326	0.397	0.535	0.735
Skipping 1	Experimental	0.105	0.122	0.139	0.170	0.204
	Recommended	0.107	0.133	0.154	0.176	0.189
Skipping 2	Experimental	0.226	0.281	0.342	0.448	0.577
	Recommended	0.229	0.307	0.379	0.465	0.535

Table 6.5: RMS acceleration by crowd size assuming proposed distribution of individuals

The switch from the experimental to the proposed distribution of individuals contributes to higher RMS responses for all crowd sizes except for the case of 4 persons. However, the maximum obtained relative difference is 11%, indicating close values between the two cases of modal shapes. It is also noticed that when using both recommended modal shapes and distribution of individuals, the trend of RMS responses against crowd size is corrected especially between 4 and 8 persons for skipping activities compared to that presented in Table 6.4. This confirms the usage of such recommendations in the calculation of the response of the analysed floor.

6.3.6 Steps for application of the simplified method

Based on the information provided thus far, the procedure for predicting the structural response of floors using the simplified method can be divided into the following six steps:

(1) Determine dimensions and modal properties of the floor related to the fundamental mode (natural frequency, modal mass, damping ratio) after verification of the conditions presented in Section 6.3.1.
(2) Define the number of individuals N and their body mass (use 75kg otherwise).
(3) Define the rhythmic activity and the equivalent PSD load model $S_{p,N}(f)$ (provided by Eq. (6.1)). The instructions detailed in Section 6.3.5.1 are applied for the choice of load parameters (considering usual/mean or occasional/maximum load cases).
(4) Calculate the mean amplitude of modal shape related to excitation positions. Adopt the suggested distribution for the N individuals from Figure 6.9 in case of no pre-determined positions. Use the proposed modal shape (given by Eq. (6.10)) if unknown.
(5) Specify a position for the evaluation of the response, then compute the response variance of each harmonic with Eq. (6.24) using the procedure presented in Section 6.3.2.
(6) Deduce the floor RMS acceleration by Eq. (6.25).

6.4 Illustrative example for response prediction

The simplified method detailed in Section 6.3 is applied to an existing floor structure in order to illustrate the procedure of calculating the acceleration response due to rhythmic activities including jumping and skipping.

6.4.1 Presentation of the structure

The existing building is composed of one storey open-plan office (along with the ground floor), as shown in Figure 6.10. The investigated structure is a steel-concrete composite floor located at the first storey, with a total area of 28.5×13.5m².

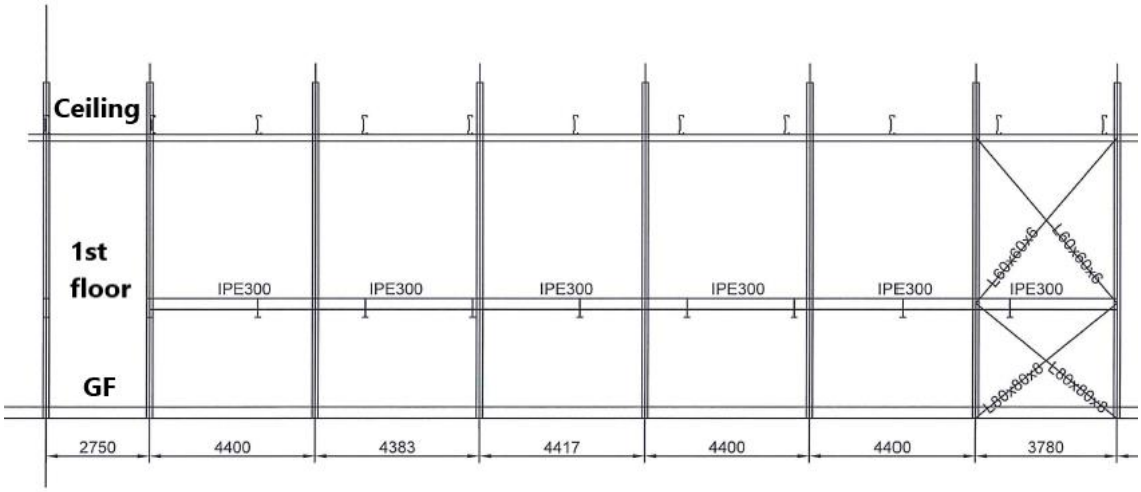

Figure 6.10: Inside layout of the existing building (dimensions in mm)

The analysed area comprises a 120mm thick composite concrete deck, with 0.75mm thick profiled steel sheet of Cofraplus 60 type. The composite floor is supported underneath by welded I-beams, and the connection is achieved by shear studs with 19mm diameter and 100mm height. The secondary beams have a 490×5 web and 140×10 flanges, except for one beam which has a 490×5 web and 140×15 flanges. The primary beams are formed of hot-rolled IPE330 at the upper part and IPE300 at the lower part. The columns are made of hot-rolled IPE330. All beams are considered to be simply supported. Figure 6.11 illustrates a plan view of the analysed floor. The class of concrete used in the deck is C25/30 and the steel grade adopted in the other structural members is S275 for hot-rolled profiles and S355 for welded I-beams.

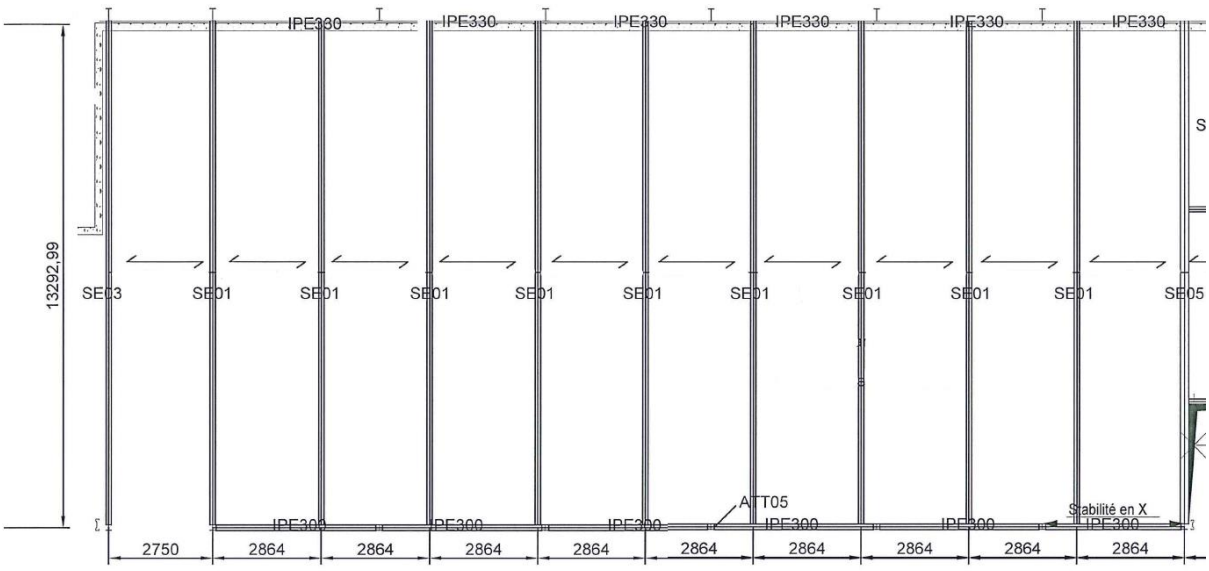

Figure 6.11: Plan view of the analysed floor (dimensions in mm)

6.4.2 Modal analysis

The floor structure is modelled by the Finite Element Method using ANSYS. A FEM configuration similar to that adopted for the floor specimen (see Section 3.2.2) is used in this case, and the corresponding model is shown in Figure 6.12.

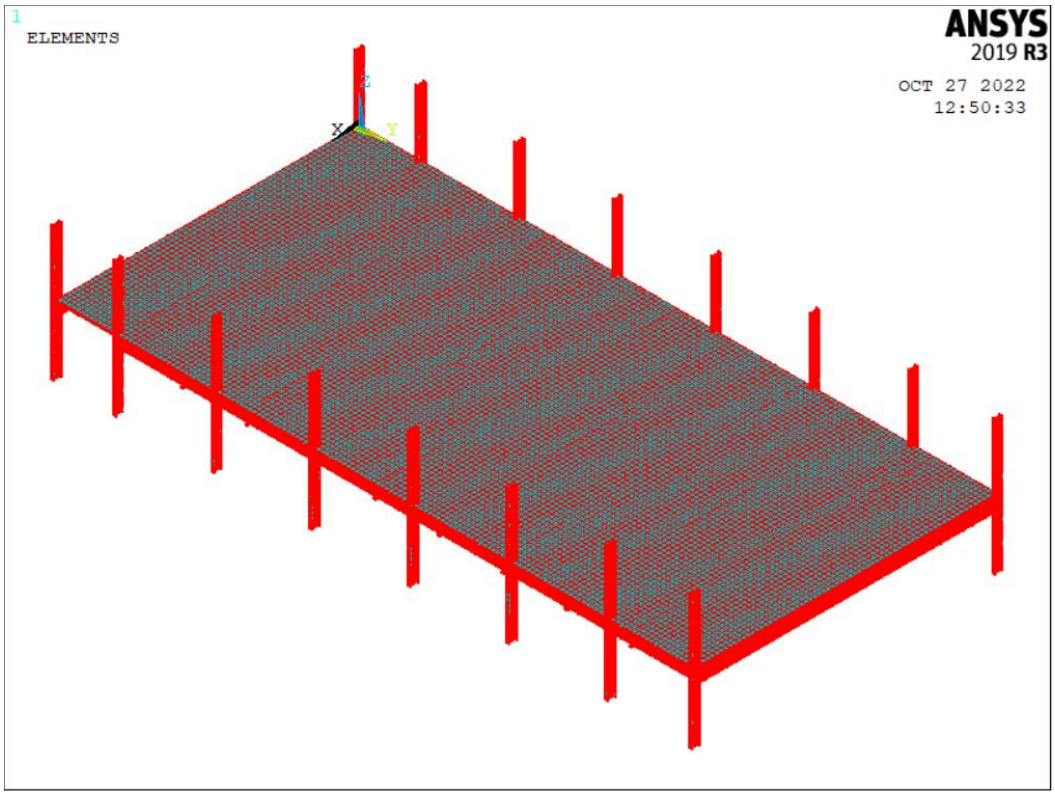

Figure 6.12: FEM model of the analysed floor

Modal analysis is performed using Block-Lanczos eigenvalue extraction method. Results for the fundamental mode are given in Table 6.6. The damping ratio of 3% is taken for the investigated floor according to related design guidelines ([40], [63], [81]).

Parameter	Natural frequency (Hz)	Modal mass (t)	Damping ratio (%)
Value	3.40	24.62	3

Table 6.6: Modal properties of the analysed floor

Corresponding modal shape is illustrated in Figure 6.13, which is close to a regular sinusoidal shape. Assuming that the response of the floor is majorly governed by its fundamental mode of vibration, the simplified response evaluation method could then be applied when the floor is subjected to crowd-rhythmic activities.

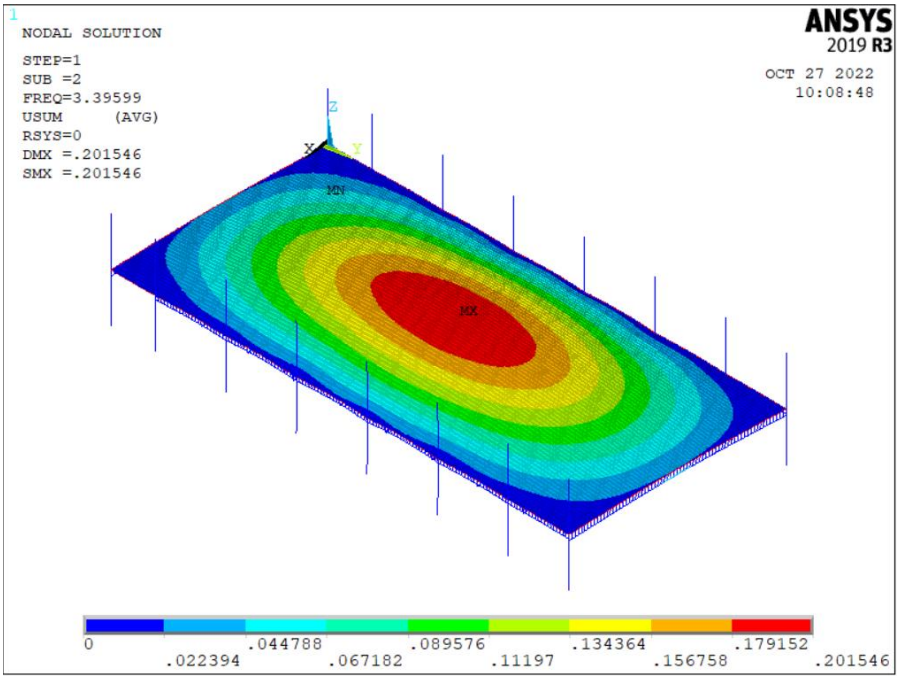

Figure 6.13: Fundamental modal shape of the analysed floor

6.4.3 Evaluation of floor acceleration

As the floor presents a large surface, the acceleration response is evaluated for a number of 1, 2, 4, 8, 16, 32 and 64 individuals. The duration of the rhythmic activity is considered equal to 30s with a maximum frequency of 10Hz. The simplified method detailed in Section 6.3 is applied to the four investigated rhythmic activities and the above crowd sizes.

For the sake of clarity, only the case of 16 individuals performing jumping jack ("jumping 1") is selected to illustrate the response prediction steps proposed in Section 6.3.6. Calculation results related to each step are summarized as follows:

(1) Dimensions: L_x=28.5m, L_y=13.5m;
Modal properties: f_1=3.40Hz, M_1=24.62t, ξ_1=3%.
(2) Rhythmic excitation by 16 individuals, each having a body mass of 75kg. The distribution suggested in Section 6.3.5 is adopted and corresponding positions are shown in Figure 6.14.

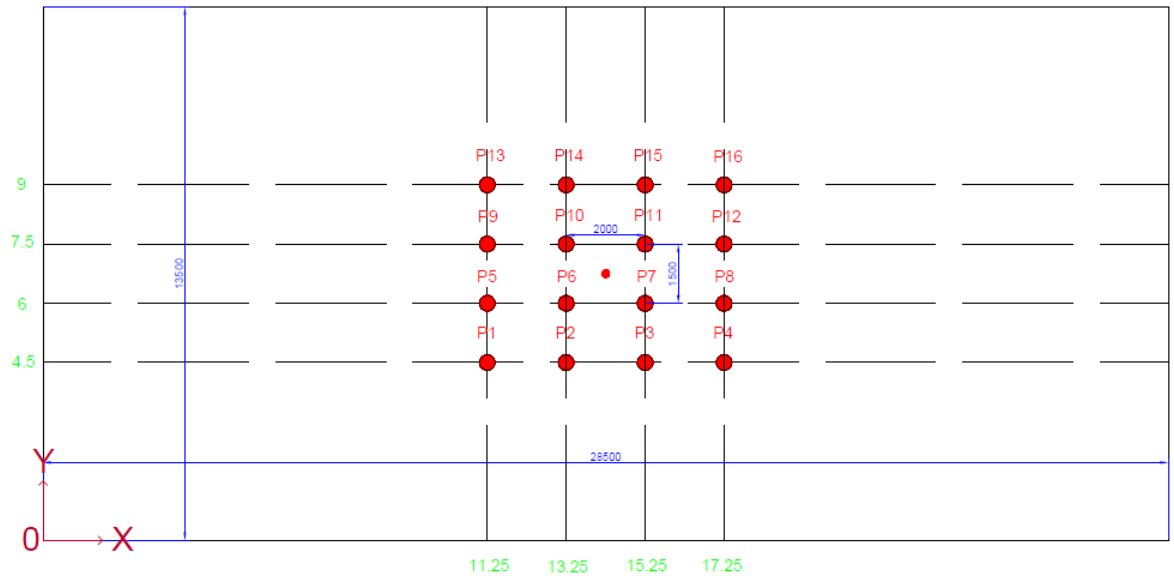

Figure 6.14: Positions of 16 individuals for response prediction (dimensions in mm)

(3) Rhythmic activity: "jumping 1", usual/mean load case (see Section 4.3.2.2); Parameters of the equivalent PSD load model (see Table 4.5): f_p=2.36Hz, α=4.64, δ=0.035Hz, a_i=[1, 0.6, 0.25], $C(N)$=0.44+0.56/N.

(4) The modal shape recommended in Section 6.3.5 is used, which resulted in amplitudes given in Table 6.7. The mean amplitude is $\bar{\Phi}_p$= 0.9.

y \ x	11.25	13.25	15.25	17.25
9	P13 (0.82)	P14 (0.86)	P15 (0.86)	P16 (0.82)
7.5	P9 (0.93)	P10 (0.98)	P11 (0.98)	P12 (0.93)
6	P5 (0.93)	P6 (0.98)	P7 (0.98)	P8 (0.93)
4.5	P1 (0.82)	P2 (0.86)	P3 (0.86)	P4 (0.82)

Table 6.7: Excitation modal amplitudes for 16 individuals (coordinates in m)

(5) The response is evaluated at the floor centre (Φ_r=1). The RMS acceleration $a_{rms,i}$ for each harmonic i is computed by Eq. (6.24):

$$a_{rms,i}^2 \approx \gamma_N \, a_i^2 \, (2i\delta)(if_p)^4 \left|H_1(if_p)\right|^2$$

where:

$$\begin{cases} \gamma_N = (2\pi)^4 \left[16\, C(16)\, \bar{m} g \alpha\right]^2 \Phi_r^2 \, \bar{\Phi}_p^2 \\ \left|H_1(if_p)\right|^2 = \dfrac{1}{M_1^2 \left[16\pi^4 \left(f_1^2 - (if_p)^2\right)^2 + \left(8\pi^2 \xi_1 f_1 if_p\right)^2\right]} \end{cases}$$

which gives, after numerical substitution:

$$a_{rms,i}^2 \approx \frac{3028\, a_i^2\, i^5}{\left[\left(457 - 220i^2\right)^2 + 361i^2\right]}$$

(6) Using the above equation for the three harmonics of the load, the floor RMS acceleration a_{rms} is deduced by Eq. (6.25):

$$a_{rms} = \sqrt{\sum_{i=1}^{3} a_{rms,i}^2} \approx \sqrt{0.0536 + 0.1934 + 0.0198} = 0.517 m/s^2$$

6.4.4 Assessment of human comfort

The method detailed earlier for 16 individuals performing "jumping 1" is applied to the other rhythmic activities and crowd sizes (see Section 6.4.3), and resulting RMS responses are summarized in Table 6.8. The criterion of the SCI P354 guideline [81], based on the evaluation of RMS accelerations, is adopted for the assessment of human comfort. The RMS response limit proposed by this guideline is 0.6m/s² for floors subjected to vertical vibrations induced by crowd movements, related to a response factor of 120 (see Table 2.10).

Activity	RMS acceleration (m/s²)						
	1	2	4	8	16	32	64
Jumping 1	0.0757	0.106	0.169	0.295	0.517	0.901	1.354
Jumping 2	0.125	0.157	0.228	0.370	0.616	1.045	1.547
Skipping 1	0.272	0.365	0.501	0.690	0.898	1.625	2.491
Skipping 2	0.0537	0.0774	0.114	0.168	0.234	0.419	0.642

Table 6.8: RMS acceleration by crowd size for the four investigated activities (regarding human comfort to vibrations, green accelerations are acceptable, red accelerations are unacceptable)

Maximum RMS responses occur at "skipping 1", since the excitation frequency of this activity (3.26Hz) is the closest one to the fundamental natural frequency (3.4Hz) among investigated activities, thus leading to a resonant regime at the first harmonic of the load. This makes unacceptable accelerations to appear at a relatively small crowd size (beginning from 8 individuals). Conversely, "skipping 2" presents the minimum RMS responses which are all acceptable towards human comfort except for 64 individuals. In fact, this activity is performed under an excitation frequency lower than "jumping 2" and has coordination factors lower than "jumping 1". Response amplitudes for both jumping activities range between those obtained for skipping ones, with an exceedance of the acceleration limit starting from 16 and 32 individuals for "jumping 2" and "jumping 1", respectively. In general, the floor presents tolerable levels of acceleration due to crowd-rhythmic activities for up to 16 persons, and remedial measures must be undertaken to reduce the response of the floor when subjected to larger crowd sizes.

6.5 Conclusions

This chapter introduces practical methods for the evaluation of floor responses when subjected to crowd-rhythmic activities. Firstly, a general method to predict the response of multi-modal floors is proposed. This method is based on the equivalent rhythmic load model established in Section 5.5 along with the random vibration theory. A sensitivity study is then carried out by varying the PSD load parameters and the floor modal properties, indicating that the response is mainly dependent on the frequency of the performed activity and the natural frequency of the floor. Slight differences are also noticed between the exact and general methods in terms of accelerations. Secondly, a simplified method for the evaluation of the response of single-mode

floors due to rhythmic activities is established, based on an approximation of the exponential function representing the PSD load model. A sensitivity study carried out on this method reveals slightly conservative accelerations compared to those obtained by the general method (maximum relative difference of 12.6%). Recommended modal shapes and distributions of individuals over the floor are also provided for the implementation of this method if undefined. The steps for application of the simplified method are finally illustrated on an existing floor structure for up to 64 individuals performing the four investigated rhythmic activities.

7 Conclusions and recommendations for future work

This thesis covered various aspects concerning the vibration analysis of floor structures subjected to crowd-rhythmic activities. The major aim was to establish a robust and user-friendly load model followed by a practical method for the evaluation of the floor response. The main conclusions of the present study are summarized in this chapter, and recommendations for future work are then suggested.

7.1 Main conclusions

Seeking for a reliable load model for rhythmic activities, a modelling approach in the frequency domain was adopted by means of simplified Power Spectral Density (PSD) functions. In comparison with time domain load models, this spectral model had the advantage to excite multiple natural modes simultaneously, which is appropriate for floors having multiple bays or panels. "Intra-subject variability" was also considered in the proposed model, as it had a bell shape allowing a spread of energy (leakage) in the vicinity of the peak of each harmonic. This makes responses to be evaluated more accurately in resonant and non-resonant cases compared to time domain models characterized by sharp peaks at each harmonic of the load. The identification of PSD load parameters from measured forces due to a single person was made by the least-squares method, more straightforward for such nonlinear optimization problems. The adoption of this technique allowed for the entire signal record to be used resulting in the consideration of the intra-subject variability effects during the rhythmic action. Coordination factors were derived from the best-fit curves describing the variation of crowd RMS forces against crowd size. The combination of the two elements cited above resulted in the total spectral load model, which is simpler to handle compared to a classical random field model.

In order to determine the parameters of the load model described earlier, a first test campaign was conducted on a floor specimen designed to have only one mode excited by human-induced loads (with a natural frequency below 10Hz). This included Experimental Modal Analysis and human-induced vibration tests. Four rhythmic activities were investigated (jumping jack, quick jumping, skipping on feet toes, skipping on feet soles), with groups of up to 16 uniformly distributed individuals. Participants were asked to move comfortably while subjected to audible and visual stimulus to be as close as possible to real life situations. Both forces and displacement responses were recorded during activities. Although resulting PSD load models were influenced by the type of coordination stimulus, the consideration of multiple activity windows enabled to have an interval of variation for each load parameter (mean ± standard deviation). This allowed the usage of identified load models for similar situations. In the present case, obtained parameters were quite different among the four rhythmic activities. The load energy was rather concentrated at the peaks of each harmonic, except for quick jumping where a spread of energy is noticed. The amplitude had the highest variability as the impact on the floor differs at each sequence of activity. Recommendations regarding the definition of load parameters for design purposes were then provided depending on the considered comfort level (to be determined by the stakeholders). Furthermore, coordination factors were found to exhibit a hyperbolic decrease with respect to crowd size for jumping activities (see Figure 4.16(a)) against lower values for skipping activities characterized by an exponential decrease (see Figure 4.16(b)). The contact mode of the foot on the floor had an impact on the crowd synchronization as coordination factors were higher for skipping on soles compared to skipping on toes. The crowd PSD load models were then used to determine RMS displacements on the floor specimen. The mean relative difference between numerical and experimental responses was found between

7.2% and 21.8% for the four investigated activities. This was due to variabilities noticed both during experiments and throughout the load identification process.

An experimental investigation of a full-scale floor structure was realized afterwards, so that the previously developed spectral load models could be verified and their scope extended. After carrying out Experimental Modal Analysis, a number of up to 32 individuals performed rhythmic activities on the floor, adopting the same protocol as for the laboratory floor, and corresponding accelerations were measured. The calculation of RMS accelerations using the established PSD load models and the dominant modal basis resulted in comparable responses related to their experimental counterparts (the mean relative difference was 9.8% and 17.5% for jumping and skipping, respectively). Discrepancies could be attributed to the variation of motion from an activity window to another, or to the slight difference in the coordination stimulus between the two experiments. Furthermore, it was verified that the scope of coordination factors for jumping activities could be extended for up to 32 individuals using the hyperbolic functions. However, coordination factors related to skipping activities, expressed by power functions for up to 16 individuals, were found to be characterized by a constant plateau between 16 and 32 persons in order to have responses in the same order of measurements.

Equivalent Dynamic Load Factors (DLFs) were then computed to compare the proposed PSD load models with existing time domain load models. This revealed comparable DLF amplitudes for the first harmonic, but greater DLFs were obtained for higher harmonics since the energy content within harmonics had a larger width by harmonic order. The proposed model thus adequately considers the load effects due to “intra-subject variability”. Moreover, three groups of existing coordination factors were found for jumping activities (linear decrease followed by a plateau, power decrease, and gradual decrease by crowd size). Suggested factors were close to the third group with less-conservative values. Conversely, a further power trend was used in the proposed models for skipping activities leading to higher coordination factors for larger crowds compared to the existing model due to the presence of the plateau beginning from 16 persons. On the other hand, comparison with the predictions of the proposed PSD load models with three of the most relevant time domain models in the literature confirmed the advantages of the spectral modelling approach in terms of response accuracy (less-sensitivity to excitation frequency and resonant cases, excitation of multiple closely spaced natural modes). Comparison with an existing random field model also indicated that the experimental coordination has a noticeable effect on the floor responses, which was effectively considered in the proposed model especially for larger crowds (despite more conservative responses for smaller groups).

In the floor specimen, RMS displacements exhibited a stronger decrease against crowd size compared to RMS forces. This was attributed to the reduction of the mean amplitudes of fundamental modal shape at excitation positions for an increasing number of participants. An equivalent load model for crowd-rhythmic activities was then proposed with regard to this observation, followed by a general method to predict the response of multi-modal floors based on the random vibration theory. A sensitivity study was made by varying the PSD load parameters and the floor modal properties, indicating that the response is mainly dependent on the frequency of the performed activity and the natural frequency of the floor. Slight differences were also noticed between the exact method (using the initial PSD load model formulation) and the general method in terms of accelerations. In addition, a simplified method for the evaluation of the response of single-mode floors due to rhythmic activities was established, based on an approximation of the exponential function representing the PSD load model. A sensitivity study

carried out on this method provided slightly conservative accelerations compared to those obtained by the general method (relative difference between 2.5% and 12.6%). Recommended modal shapes and distributions of individuals over the floor were also provided for the application of this method if undefined.

Both general and simplified response prediction methods could be implemented in a software to be simply used by engineers. After defining vibration acceptance criterion by the stakeholders, the proposed methods could then be used to quickly assess building floors for human comfort when exposed to crowd-rhythmic activities. The findings of this research might also represent a first step in the inclusion of this type of methods in the forthcoming editions of Eurocodes for practical application.

7.2 Recommendations for future work

The proposed spectral load models could be used for the four investigated rhythmic activities which are one of the most encountered activities in practice. However, they are only applicable in their experimental range of excitation frequency (presented in Table 4.5), with a low density of occupants (inferior to 0.3 person/m²) and crowd sizes between 1 and 32.

Based on studies performed during this research, recommendations for future work can be summarized as follows:

- In order to enlarge the scope of the proposed load models, supplementary tests should be carried out with other coordination stimulus encountered in real life and larger crowd sizes than the maximum number of 32 individuals adopted in this work. The density of the group could be analysed in moderate or high cases (more than 1 person/3m² investigated here). Full-scale structures having various geometrical and material properties might also be tested to later verify the proposed models.
- In the same context, in case when conservative results in terms of crowd-induced loads are needed, people who are familiar and experienced to synchronize their motion in a group should be involved.
- A further verification of the suggested load models could be made by monitoring existing floors during real-life events (fitness sessions at gymnasiums, football matches at grandstands, etc.). After determining the modal properties of the floors, accelerations might be measured for a long period of time. Corresponding loads could also be obtained by means of inverse identification techniques.
- Additional rhythmic activities might be investigated such as bouncing, aerobics, foot-stamping, hand-clapping, etc. On the other hand, human activities performed in a random way (walking and running for example) could also be analysed since they are more likely to occur in many floors (hospitals, public transport venues, commercial centres, etc.). In that case, spectral load models usually include a combined time and spatial characterization of the crowd motion.
- The relation between the crowd and the structure was assumed independent. However, the presence of the crowd might alter the dynamic properties of the floor (mainly in terms of natural frequency and damping) and the movement of the group might be influenced if the structure is moving perceptibly. These are some effects of the human-structure interaction phenomenon that could be further investigated.

References

[1] Abd El-Hamid, A.S., Eissa, A.H., and Radwan, A. Levenberg-Marquardt's Algorithm used for PID Controller Parameters Optimization. Global Journal of Research In Engineering 15, 1 (2015), 090499.

[2] Agilent Tehnologies. The fundamentals of modal testing. Application Note 243-3, 2000.

[3] Alves, N.K.C., Roitman, N., and Magluta, C. Dynamic response under human movements. Materials and Structures 32, 1 (1999), 31-37.

[4] An, Q., Ren, Q., Liu, H., Yan, X., and Chen, Z. Dynamic performance characteristics of an innovative Cable Supported Beam Structure–Concrete Slab Composite Floor System under human-induced loads. Engineering Structures 117 (2016), 40-57.

[5] Association Française de Génie Civil. Sétra: Evaluation du comportement vibratoire des passerelles piétonnes sous l'action des piétons, 2006 [in French].

[6] Association française de normalisation. NF EN 1993-1-1/NA: Eurocode 3 - Design of steel structures - National Annex to NF EN 1993-1-1:2005 - Part 1-1: general rules and rules for buildings, 2013.

[7] Bachmann, H., and Ammann, W. Vibrations in structures: induced by man and machines. IABSE - AIPC - IVBH, Third edition, Zürich, 1987.

[8] Bihina, G. Analyse du comportement au feu des planchers mixtes acier-béton constitutés de poutres cellulaires. PhD thesis, France, Université Blaise Pascal-Clermont-Ferrand II, 2011 [in French].

[9] British Standards Institution. BS 6399-1:1996 - Loading for Buildings - Part 1: Code of Practice for Dead and Imposed Loads, London, 1996.

[10] British Standards Institution. BS 6472:1992 - Guide to evaluation of human exposure to vibration in buildings (1Hz to 80Hz), London, 1992.

[11] British Standards Institution. BS 6841:1987 - Guide to measurement and evaluation of human exposure to whole-body mechanical vibration and repeated shock, London, 1987.

[12] Brownjohn, J.M., Pavic, A., and Omenzetter, P.A. Spectral density approach for modelling continuous vertical forces on pedestrian structures due to walking. Canadian Journal of Civil Engineering 31, 1 (2004), 65-77.

[13] Catterou, T., Castaign, J-B., Munier, L., Group Induced Vibration on Light Floor - Essais en laboratoire. Test report, FCBA, 2022 [in French].

[14] Chen, J., Li, G., and Racic, V. Acceleration response spectrum for predicting floor vibration due to occupants jumping. Engineering Structures 112 (2016), 71-80.

[15] Chen, J., Wang, H., and Wang, L. Experimental investigation on single person's jumping load model. Earthquake Engineering and Engineering Vibration 14, 4 (2015), 703-714.

[16] Chen, S., Zhang, R., and Zhang, J. Human-induced vibration of steel–concrete composite floors. Proceedings of the Institution of Civil Engineers-Structures and Buildings, 171, 1 (2018), 50-63.

[17] Clough, R., and Penzien, J. Dynamics of structures. Computers and Structures, 1995.

[18] Comer, A.J., Williams, M.S., and Blakeborough, A. Experimental determination of crowd load and coherency when jumping on a rigid raked grandstand. In proceedings of the 25th International Modal Analysis Conference IMAC (Orlando, Florida, February 2007).

[19] Comité Euro-International du Béton. CEB Bulletin d'information 209. Vibration Problems in Structures - Practical Guidelines. Paris, 1991.

[20] Costa-Neves, L.F., da Silva, J.S., De Lima, L.R.O., and Jordão S. Multi-storey, multi-bay buildings with composite steel-deck floors under human-induced loads: The human comfort issue. Computers and Structures 136 (2014), 34-46.

[21] de Brito, V.L., and Pimentel, R.L. Cases of collapse of demountable grandstands. Journal of performance of constructed facilities 23, 3 (2009), 151-159.

[22] De Silva, S., and Thambiratnam, D. Vibration characteristics of concrete-steel composite floor structures. ACI Structural Journal 108, 6 (2011), 706-714.

[23] De Silva, S.S., and Thambiratnam, D.P. Dynamic characteristics of steel-deck composite floors under human-induced loads. Computers & Structures 87, 17-18 (2009), 1067-1076.

[24] Denoël V. Rapport de mesures sur un plancher de parking à Nantes. Test report, University of Liège, 2020 [in French].

[25] Deutsches Institut für Normung e.V. DIN 4150-2: Vibrations in buildings - Part 2: Effects on persons in buildings, June 1999 [German standard].

[26] Duarte, E., and Ji, T. Action of individual bouncing on structures. Journal of structural engineering 135, 7 (2009), 818-827.

[27] Ebrahimpour, A. and Sack, R.L. Design live loads for coherent crowd harmonic movements. Journal of Structural Engineering118, 4 (1992), 1121-1136.

[28] El Asri, Y., Lukić, M., Hjiaj, M., Couchaux, M., and Denoël, V. Crowd size effect on floor vibration response due to random and rhythmic excitations. In Proceedings of the 27th International Congress on Sound and Vibration ICSV (Online, July 2021).

[29] El Asri, Y., Denoël, V., Couchaux, M., Hjiaj, M., and Lukić, M. Vibration comfort of floors: State-of-the-art. Revue Construction Métallique 4 (2021), 41-78.

[30] El Asri, Y., Naudet, B., and Couchaux, M. Dimensionnement d'un plancher de laboratoire : note de calcul détaillée. CTICM Report: DRV/19-RCM-125/001-A, 2021 [in French].

[31] Ellis, B.R., and Ji, T. Loads generated by jumping crowds: experimental assessment. BRE IP4/02, CRC Ltd., London (2002), 1-12.

[32] Ellis, B.R., and Ji, T. Loads generated by jumping crowds: numerical modelling. Structural Engineer 82, 17 (2004), 35-40.

[33] Ellis, B.R., and Ji, T. The response of structures to dynamic crowd loads. Building Research Establishment, 2004.

[34] Ellis, B.R., and Littler, J.D. Response of cantilever grandstands to crowd loads. Part 2: load estimation. Proceedings of the Institution of Civil Engineers-Structures and Buildings 157, 5 (2004), 297-307.

[35] Ellis, B.R., Ji, T., and Littler, J.D. The response of grandstands to dynamic crowd loads. Proceedings of the Institution of Civil Engineers-Structures and Buildings 140, 4 (2000), 355-365.

[36] European Committee for Standardization. EN 1992-1-1: Eurocode 2: Design of concrete structures - Part 1-1: general rules and rules for buildings, 2005.

[37] European Committee for Standardization. EN 1993-1-1: Eurocode 3: Design of steel structures - Part 1-1: General rules and rules for buildings, 2005.

[38] European Committee for Standardization. EN 1994-1-1: Eurocode 4: Design of composite steel and concrete structures - Part 1-1: General rules and rules for buildings, 2005.

[39] Faísca, R.G. Characterization of dynamic loads due to human activities. PhD thesis, COPPE/UFR, Rio de Janeiro, Brazil, Civil Engineering Department, 2003 [in Portuguese].

[40] Feldmann, M., Heinemeyer, C., Lukic, M., Caetano, E., Cunha, Á., Goldack, A., Keil, A., Schlaich, M., Hicks, S., Smith, A., Hechler, O., Obiala, R., Galanti, F., and Waarts, P. Human-Induced Vibrations of Steel Structures (HiVoSS). RFCS, 2008.

[41] Fernández Martínez, J., Hermanns, L.K.H., Alarcón Álvarez, E., and Cara Cañas, F.J. Modelling Crowd Load for Floor Vibration Analysis. In Proceedings of the 6th Congress on Numerical Methods in Engineering CMN (Coimbra, Portugal, June 2011).

[42] Ferrarotti, A., and Tubino, F. Generalized equivalent spectral model for serviceability analysis of footbridges. Journal of Bridge Engineering 2, 6 (2016), 04016091.

[43] Gao, Y.A., Yang, Q.S., Dong, Y., Chen, C., and Ye, T.P. Dynamic behaviour of slab induced by pedestrian traffic. International Journal of Structural Stability and Dynamics 19, 12 (2019), 1950154.

[44] Gaspar, C.M., and da Silva, J.G.S. Influence of the human rhythmic activities modelling on the composite floors dynamic response. Journal of Civil Engineering and Architecture Research 2, 1 (2015), 429-437.

[45] International Organisation for Standardization. ISO 10137: Bases for design of structures - Serviceability of buildings and walkways against vibration, 2007.

[46] International Organisation for Standardization. ISO 2631-1: Mechanical vibration and shock - Evaluation of human exposure to whole-body vibration - Part 1: General requirements, 1997.

[47] International Organisation for Standardization. ISO 2631-2:1989: Evaluation of human exposure to whole-body vibration - Part 2: Human exposure to continuous and shock-induced vibrations in buildings (1 to 80 Hz), 1989.

[48] International Organisation for Standardization. ISO 2631-2:2003: Mechanical vibration and shock - Evaluation of human exposure to whole-body vibration - Part 2: Vibration in buildings (1Hz to 80Hz), 2003.

[49] IStructE/DCLG/DCMS Joint Working Group, Dynamic Performance Requirements for Permanent Grandstands: Recommendations for Management Design and Assessment, Institution of Structural Engineers, London, 2008.

[50] Jones, C.A., Reynolds, P., and Pavic, A. Vibration serviceability of stadia structures subjected to dynamic crowd loads: A literature review. Journal of Sound and Vibration 330, 8 (2011), 1531-1566.

[51] Kumar, P., and Kumar, A. Human induced vibration in structures. International Journal of Mechanical Engineering and Robotics Research 1, 1 (2014), 44-54.

[52] Kutner, M.H., Nachtsheim, C.J., Neter, J. and Li W. Applied Linear Statistical Models. McGraw-Hill/Irwin, Fifth edition, New York, 2005.

[53] Lee, K., Lee, S.H., Kim, G.C., and Woo S.S. Global vertical resonance phenomenon between steel building and human rhythmic excitations. Journal of Constructional Steel Research 92 (2014), 164-174.

[54] Li, G., Ji, T., and Chen, J. Determination of the dynamic load factors for crowd jumping using motion capture technique. Engineering Structures 174 (2018), 1-9.

[55] Li, Z., Zhang, Q., and Fan, F. A stochastic approach for generating individual jumping loads considering different jumping force patterns. Journal of Building Engineering 62 (2022), 105378.

[56] Lukić, M., and Molina, L. Vibration de planchers. CTICM Report: DRV/13-RCM-125/001-A, 2017 [in French].

[57] Máca, J., and Rokoš, O. Modelling of Synchronized Jumping Crowds on Grandstands, Procedia Engineering 190 (2017), 645–652.

[58] Martínez, J.F., Hermanns, L., de Lerma, A.F., and Álvarez, E.A. Jumping load models applied on a gymnasium floor. Engineering Structures 125 (2016), 26-38.

[59] Mathworks. MATLAB for data processing and visualization, training course notebook, 2020.

[60] Mathworks. Optimization techniques in MATLAB, training course notebook, 2021.

[61] Mohammed, A.S., Pavic, A., and Racic, V. Improved model for human induced vibrations of high-frequency floors. Engineering Structures 168 (2018), 950-966.

[62] Muhammad, Z.O. and Reynolds, P., Vibration Serviceability of Building Floors: Performance Evaluation of Contemporary Design Guidelines, Journal of Performance of Constructed Facilities 33, 2 (2019), 04019012.

[63] Murray, T.M., Allen, D.E. and Ungar, E.E. Floor Vibrations Due to Human Activity. Steel Design Guide Series N°11, American Institute of Steel Construction and Canadian Institute of Steel Construction, 2003.

[64] Nhleko, S., Zingoni, A., and Moyo, P. A variable mass model for describing load impulses due to periodic jumping. Engineering Structures 30, 6 (2008), 1760-1769.

[65] Parkhouse, J.G., and Ewins, D.J. Crowd-induced rhythmic loading. Proceedings of the Institution of Civil Engineers-Structures and Buildings 159, 5 (2006), 247-259.

[66] Paz, M., and Kim, Y.H. Structural Dynamics: Theory and Computation. Springer Nature Switzerland AG, Sixth edition, 2019.

[67] Pernica, G. Dynamic load factors for pedestrian movements and rhythmic exercises. Canadian Acoustics 18, 2 (1990), 3-18.

[68] Piccardo, G., and Tubino, F. Equivalent spectral model and maximum dynamic response for the serviceability analysis of footbridges. Engineering Structures 40 (2012), 445-456.

[69] Piersol, A., and Paez, T. Harris' shock and vibration handbook. McGraw-Hill Handbooks, Sixth edition, New York, 2001.

[70] Preumont, A. Random vibration and spectral analysis. Kluwer Academic Publishers, Dordrecht, 1994.

[71] Racic, V., and Pavic, A. Mathematical model to generate near-periodic human jumping force signals. Mechanical Systems and Signal Processing 24, 1 (2010), 138-152.

[72] Racic, V., Brownjohn, J.M.W., and Pavić, A. Dynamic loading factors of individual jogging forces. In Proceedings of the 4th ECCOMAS Thematic Conference on Computational Methods in Structural Dynamics and Earthquake Engineering COMPDYN (Kos Island, Greece, June 2013).

[73] Racic, V., Pavic, A., and Brownjohn, J.M.W. Modern facilities for experimental measurement of dynamic loads induced by humans: A literature review. Shock and Vibration 20, 1 (2013, 53-67.

[74] Richardson, M.H., and Formenti, D.L. Parameter estimation from frequency response measurements using rational fraction polynomials. In Proceedings of the 1st International Modal Analysis Conference IMAC (Orlando, Florida, November 1982).

[75] Richter dos Santos, E.A., Almeida de Sousa, F., and Santos da Silva, J.G. Human Comfort Assessment of Steel-Concrete Composite Floors Subjected to People Dynamic Loads. In proceedings of the international colloquium on Stability and Ductility of Steel Structures SDSS (Aveiro, Portugal, September 2022).

[76] Royvaran, M., Avci, O, and Davis, B. Analysis of floor vibration assessment methods using a large database of floors framed with W-shaped members subjected to walking excitation. Journal of Constructional Steel Research 164 (2020), 105764.

[77] Salyards, K.A., and Firman, R.J. Experimental Investigation of Dynamic Load Estimation Using Small-Scale Testing. Dynamics of Civil Structures, Volume 4. Springer, New York, NY, 2011, 25-32.

[78] Sedlacek, G., Heinemeyer, C., Butz, C., Volling, B., Waarts, P., Van Duin, F., Hicks, S., Devine, P., and Demarco, T. Generalisation of criteria for floor vibrations for industrial, office, residential and public building and gymnastic halls. Technical Rep. No. Eur 21972 EN, Technical steel research, 2006.

[79] Shih, C.Y., Tsuei, Y.G., Allemang, R.J., and Brown, D.L. Complex mode indication function and its applications to spatial domain parameter estimation. Mechanical systems and signal processing 2, 4 (1988), 367-377.

[80] Sim, J., Blakeborough, A., Williams, M.S., and Parkhouse, G. Statistical model of crowd jumping loads. Journal of structural engineering 134, 12 (2008), 1852-1861.

[81] Smith, A.L., Hicks, S.J., and Devine, P.J. Design of Floors for Vibration: A New Approach (Revised Edition, February 2009). SCI publication P354, the Steel Construction Institute, 2009.

[82] Tatara, T., and Ptasznik, B. Vibrations of sports stadium grandstand structure due to crowd-jumping loads. In Proceedings of the 5th ECCOMAS Thematic Conference on Computational Methods in Structural Dynamics and Earthquake Engineering COMPDYN (Crete Island, Greece, May 2015).

[83] Timoshenko, S., and Woinowsky-Krieger, S. Theory of plates and shells. McGraw-Hill, Vol. 2, New York, 1959.

[84] Vanmarcke, E. Random fields: analysis and synthesis. The MIT Press, Third printing, Massachusetts, 1988.

[85] Venuti, F., and Tubino, F. Numerical validation of the generalized equivalent spectral model through crowd dynamics simulations. In proceedings of the XI International Conference on Structural Dynamics EURODYN (Athens, Greece, November 2020).

[86] Vijayan, A., Abraham, N.M., and SD, A.K. Analysis of structures subjected to crowd loads, Procedia Structural Integrity 14 (2019), 696-704.

[87] Wyatt, T.A. Design guide on the vibration of floors. SCI P076, the Steel Construction Institute, 1989.

[88] Xiong, J., and Chen, J. Power spectral density function for individual jumping load. International Journal of Structural Stability and Dynamics 18, 02 (2018), 1850023.

[89] Xiong, J., and Chen, J. Random field model for crowd jumping loads. Structural safety 76 (2019), 197-209.

[90] Xiong, J., Duan, S., Qian, H., and Pan, Z. Equivalent Dynamic Load Factor of Different Non-Exceedance Probability for Crowd Jumping Loads. Buildings 12, 4 (2022), 450.

[91] Xiong, J., Duan, S., Qian, H., and Pan, Z. Multi-mode response spectrum for multi-harmonic crowd jumping loads. Applied Mathematical Modelling 111 (2022), 696-712.

[92] Yao, S., Wright, J.R., Pavic, A., and Reynolds, P. Experimental study of human-induced dynamic forces due to jumping on a perceptibly moving structure. Journal of Sound and Vibration 296, 1-2 (2006), 150-165.

[93] Živanović, S. Probability-based estimation of vibration for pedestrian structures due to walking. PhD thesis, United Kingdom, Department of Civil and Structural Engineering, University of Sheffield, February 2006.

[94] Živanović, S., Pavic, A., and Reynolds, P. Vibration serviceability of footbridges under human-induced excitation: a literature review. Journal of sound and vibration 279, 1-2 (2005), 1-74.

[95] Živanović, S., Pavić, A., and Reynolds, P. Probability-based prediction of multi-mode vibration response to walking excitation. Engineering Structures 29, 6 (2007), 942-954.

Appendix A: Constructional details related to the laboratory floor

A.1. Connection details

Details are presented for the four connection types used in the laboratory floor.

The column bases were pinned and placed on a mortar to obtain a uniform surface. Load cells were placed between two 300×300×30 and 300×300×20 plates to measure compressive forces, whereas lateral forces were supported by four rods with diameter of 20mm. Distribution of the loads to the ground was made by 650×650×40 plates. Four cleat angles were placed two at each direction to restrain horizontal displacements. This connection is presented in Figure A.1 for column B2. Other columns were connected using the same technique detailed earlier, but had variable heights (see Table 3.1).

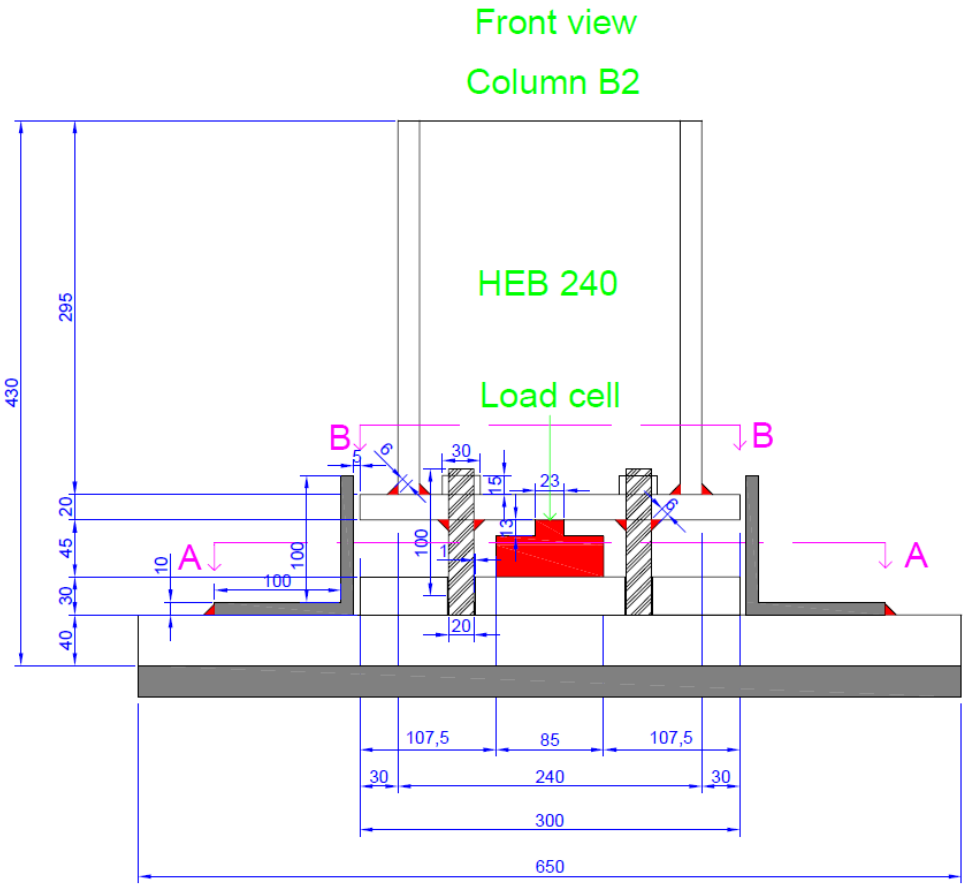

(a) Front view

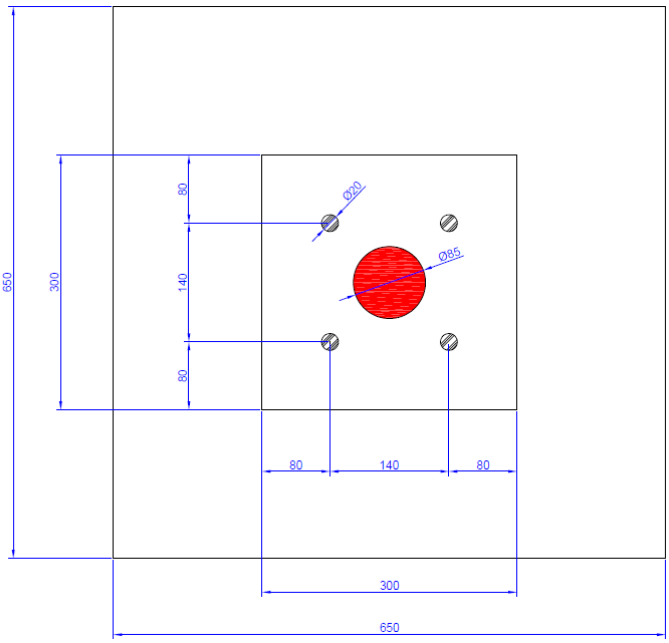

(b) Section A-A

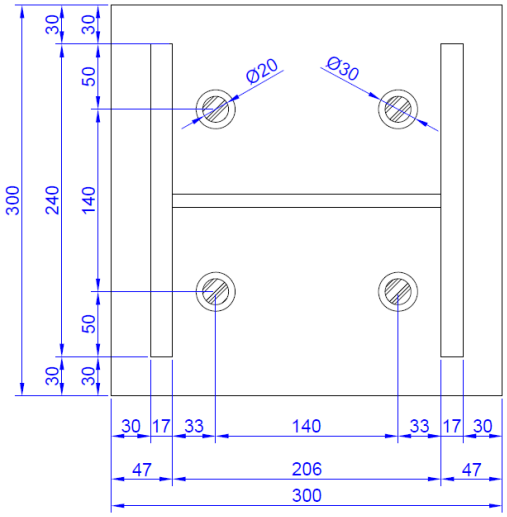

(c) Section B-B

Figure A.1: Column base connection

Connections between primary beams and columns were achieved by four M24 class 8.8 bolts (see Figure A.2). They were fixed between the lower flange of each primary beam and a 270×270×20 steel plate located at the upper part of each column. This connection was assumed rigid.

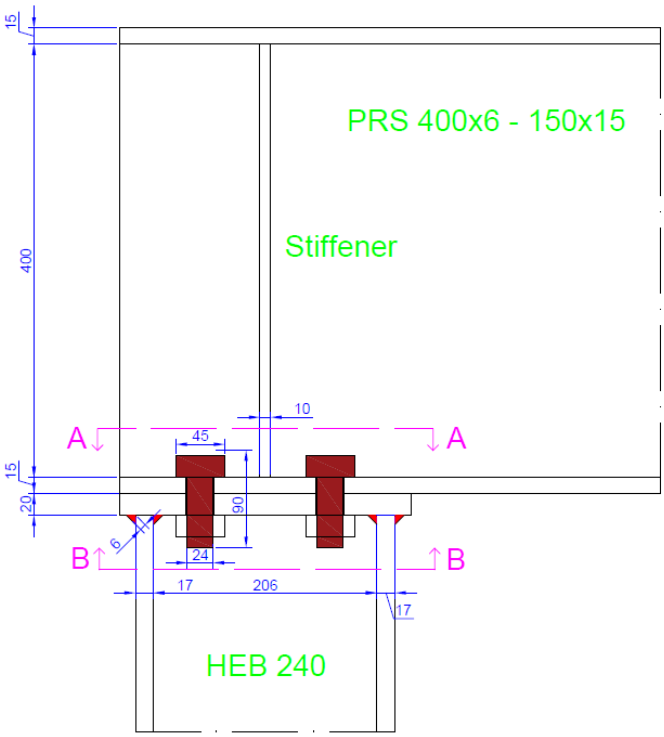

(a) Front view

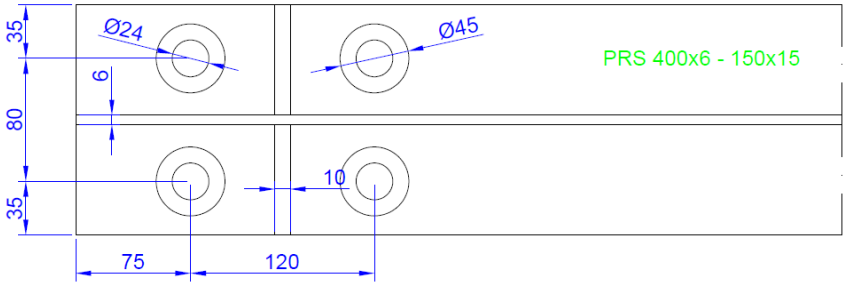

(b) Section A-B

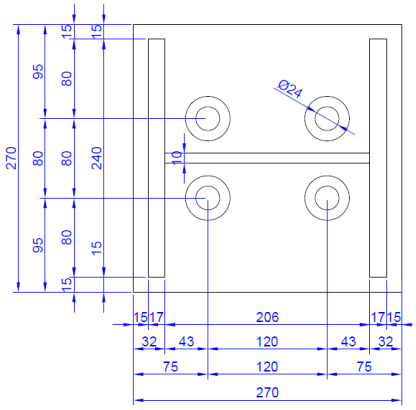

(c) Section B-B

Figure A.2: Connection between primary beams and columns

Connections between edge secondary beams and primary beams were made by two 150×400×20 steel plates and four M16 class 8.8 bolts (see Figure A.3). Two stiffeners were placed between the web of each primary beam to guarantee an efficient and rigid connection.

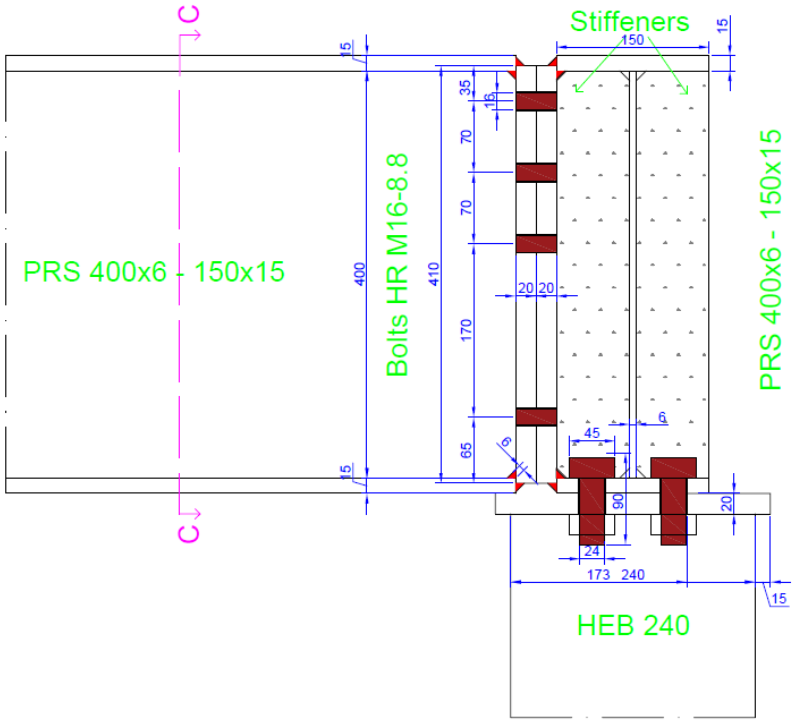

(a) Front view

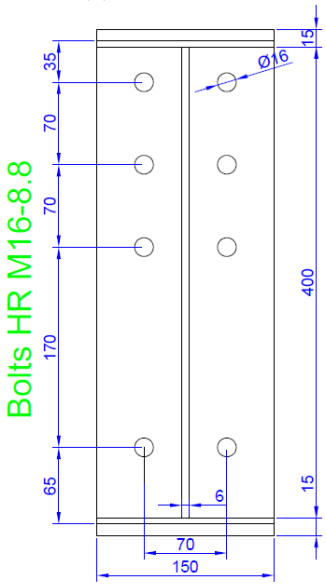

(b) Section C-C

Figure A.3: Connection between edge secondary and primary beams

Connections between intermediate secondary beams and primary beams were realized by 70×70×7 double web cleat angles (see Figure A.4). Six M16 class 8.8 bolts connected the web cleat to the secondary beam, and the cleats to the primary beam, respectively.

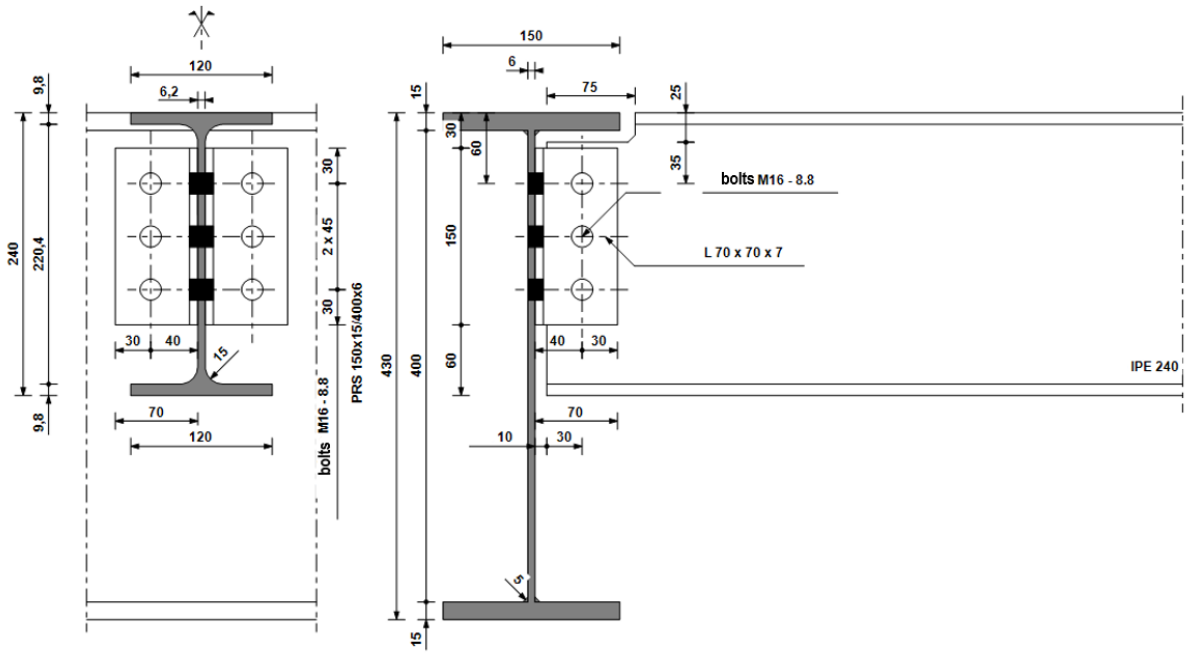

Figure A.4: Connection between intermediate secondary beams and primary beams

A.2. Floor construction stages

Floor construction begins with assembling all structural elements using connections detailed in Section A.1. Figure A.5 illustrates two of the realized connections.

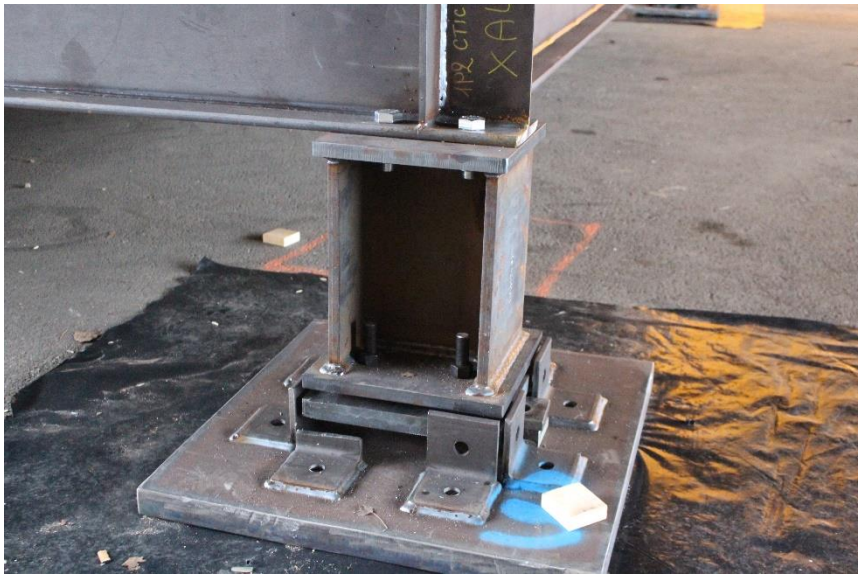

(a) Column

(b) Edges beams

Figure A.5: Realized connections

The second stage is to weld shear connectors to primary beams (with a spacing of 200mm) and secondary beams (with a spacing of 207mm) as can be seen in Figure A.6.

Figure A.6: Shear connectors welded to beams

The third stage is to put the steel decking profile on the floor elements (see Figure A.7). Shear connectors of the secondary beams were located between the ribs of the steel sheet. Curbs with 2mm thickness and 150mm height were also mounted on the four edges in order to delimit the concrete surface.

Figure A.7: Floor with steel decking profile

The final stage is to prepare the reinforced concrete slab with ST25C steel mesh and C25/30 class concrete to have a 15cm thick composite slab (see Figure A.8).

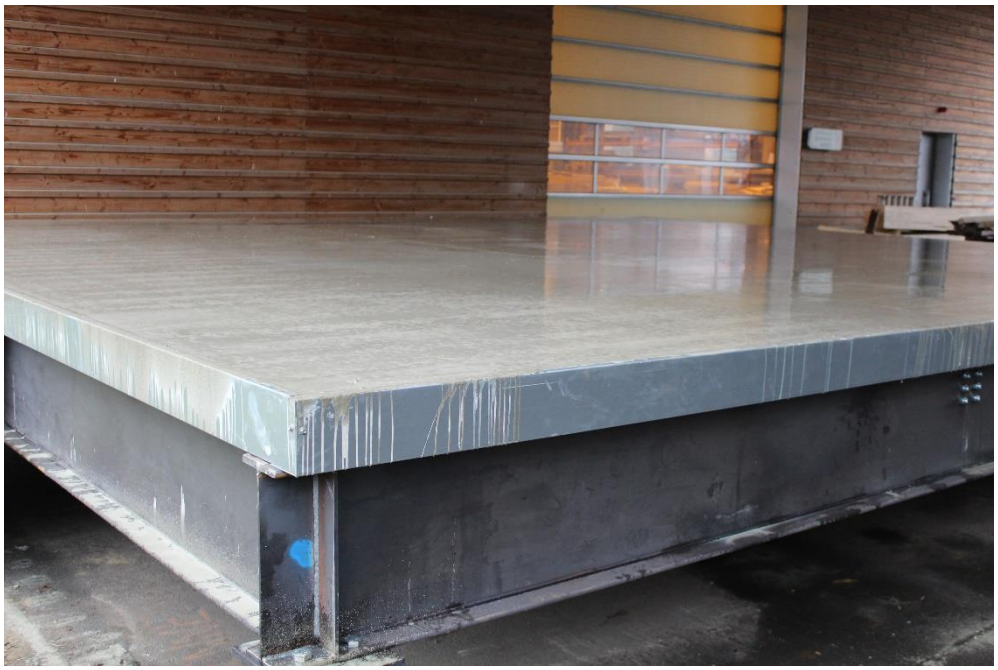

Figure A.8: Floor with composite slab

A.3. Concrete properties

Specifications of concrete used in the floor specimen are summarized in Table A.1.

Specification	Value
Standard	BPS NF EN 206/CN
Class	C25/30
Exposition	XC1 (F)
Chloride	Cl^- (0.4%)
D_{max}	16mm
Consistency	S4
Cement	CEM II/ A-LL 42.5 N CE CP2 NF

Table A.1: Concrete specifications

Six cylinders were taken during concrete casting, three of them were tested to get compressive strength and three others to determine Young's Modulus. Both tests were realized 28 days after the casting. The results are presented in Table A.2.

Test number	Compressive strength (MPa)		Young's modulus (GPa)	
	Test value	Mean	Test value	Mean
1	29.6		27.8	
2	29.7	29.8	26.9	28.1
3	30.2		29.6	

Table A.2: Concrete compressive strength and Young's modulus

Appendix B: Numerical accelerations using several crowd-rhythmic load models

Appendix B: Numerical accelerations using several rhythmic load models

The present appendix is a complement to the comparison made between the proposed PSD load models and the existing time domain models described in Section 5.4.2. Calculated acceleration responses (mean ± standard deviation) using the previous load models are presented. All investigated rhythmic activities were considered, for either the laboratory/single-mode floor or the parking/multi-modal floor in Section B.1 and B.2, respectively.

B.1. Calculated accelerations for a single-mode floor

Load model	RMS acceleration for "jumping 1" (m/s²)				
	1	2	4	8	16
Proposed model	0.154±0.037	0.202±0.049	0.334±0.081	0.439±0.11	0.709±0.17
Ellis and Ji [31]	0.0954±0.023	0.140±0.034	0.233±0.056	0.281±0.068	0.395±0.096
Faisca [39]	0.151±0.037	0.258±0.062	0.466±0.11	0.597±0.14	0.932±0.23
ISO 10137 [45]	0.106±0.026	0.193±0.047	0.395±0.096	0.567±0.14	0.875±0.21

Load model	RMS acceleration for "jumping 2" (m/s²)				
	1	2	4	8	16
Proposed model	0.223±0.054	0.264±0.064	0.396±0.096	0.483±0.12	0.742±0.18
Ellis and Ji [31]	0.101±0.024	0.150±0.036	0.251±0.061	0.308±0.075	0.438±0.11
Faisca [39]	0.173±0.042	0.296±0.072	0.536±0.13	0.686±0.17	1.071±0.26
ISO 10137 [45]	0.079±0.019	0.144±0.035	0.295±0.072	0.424±0.10	0.659±0.16

Load model	RMS acceleration for "skipping 1" (m/s²)				
	1	2	4	8	16
Proposed model	0.0794±0.019	0.100±0.024	0.142±0.035	0.147±0.036	0.177±0.043
ISO 10137 [45]	0.0436±0.011	0.0562±0.013	0.0815±0.020	0.0861±0.021	0.106±0.026

Load model	RMS acceleration for "skipping 2" (m/s²)				
	1	2	4	8	16
Proposed model	0.173±0.042	0.234±0.057	0.356±0.086	0.396±0.096	0.509±0.12
ISO 10137 [45]	0.0507±0.012	0.0653±0.016	0.0947±0.023	0.100±0.024	0.123±0.030

B.2. Calculated accelerations for a multi-modal floor

Load model	RMS acceleration for "jumping 1" (cm/s²)					
	1	2	4	8	16	32
Proposed model	5.55±2.4	11.9±4.7	18.7±7.4	26.2±11.4	48.2±21.1	68.9±35.9
Ellis and Ji [31]	3.71±1.7	8.75±3.6	14.6±6.1	20.8±9.4	34.0±15.3	46.1±23.7
Faisca [39]	3.38±1.2	9.33±3.4	16.1±5.9	21.6±7.6	37.4±14.2	50.4±22.6
ISO 10137 [45]	4.27±2.0	11.9±5.0	23.4±9.8	37.7±17.5	66.0±30.2	82.5±44.8

Load model	RMS acceleration for "jumping 2" (cm/s²)					
	1	2	4	8	16	32
Proposed model	9.17±2.9	12.0±4.1	17.8±5.9	21.1±8.2	24.6±15.1	45.8±14.6
Ellis and Ji [31]	4.36±2.1	8.06±4.2	13.7±7.2	16.9±9.6	22.3±15.6	33.5±12.9
Faisca [39]	5.79±1.9	12.3±4.4	21.7±7.6	24.7±10.2	33.4±20.0	56.1±21.1
ISO 10137 [45]	3.99±2.2	8.91±5.2	17.8±10.3	24.5±15.5	32.6±26.9	43.3±20.4

Load model	RMS acceleration for "skipping 1" (cm/s²)					
	1	2	4	8	16	32
Proposed model	2.48±0.7	3.65±1.2	4.98±1.7	6.47±2.1	7.86±3.1	14.8±4.8
ISO 10137 [45]	2.44±0.8	3.81±1.3	5.39±1.9	7.38±2.4	9.18±3.3	12.1±3.7

Load model	RMS acceleration for "skipping 2" (cm/s²)					
	1	2	4	8	16	32
Proposed model	2.04±0.7	3.75±1.8	5.36±2.5	5.94±2.5	7.19±2.7	14.2±4.3
ISO 10137 [45]	1.21±0.4	2.30±1.0	3.14±1.3	3.43±1.2	4.02±1.4	4.40±1.2

Appendix C: Sensitivity study results

This appendix summarizes the findings of the sensitivity studies performed in Chapter 6 for the four investigated rhythmic activities. The floor responses are given in terms of RMS accelerations (mean ± standard deviation). Numerical results are presented for the general and the simplified method in Section C.1 and C.2, respectively.

C.1. Results for the general method

The response of the floor was calculated using the instructions presented in Section 6.2.2 using two different methods:

- The exact method using the exact PSD load model (see Section 4.2.4) and the calculation procedure presented in Section 2.6.2;
- The general method using the equivalent load model (see Section 5.5) and the calculation procedure detailed in Section 6.2.1.

The next tables present resulting RMS accelerations by crowd size. For each set of parameters, the upper line is obtained by the exact method and the lower line by the general method.

Investigated parameter	RMS acceleration for "jumping 1" (m/s²)				
	1	2	4	8	16
f_p	0.225±0.101	0.308±0.138	0.458±0.205	0.746±0.334	1.238±0.555
	0.225±0.101	0.308±0.138	0.459±0.206	0.748±0.335	1.239±0.555
α	0.384±0.034	0.526±0.047	0.783±0.070	1.275±0.113	2.116±0.188
	0.384±0.034	0.526±0.047	0.784±0.070	1.278±0.114	2.117±0.188
δ	0.382±0.028	0.523±0.039	0.779±0.057	1.268±0.093	2.104±0.154
	0.382±0.028	0.523±0.038	0.780±0.057	1.270±0.093	2.105±0.154
f_p, α, δ	0.223±0.098	0.305±0.134	0.455±0.199	0.740±0.325	1.228±0.539
	0.223±0.098	0.305±0.134	0.455±0.200	0.742±0.325	1.229±0.539
f_n	0.167±0.171	0.228±0.235	0.340±0.349	0.553±0.568	0.918±0.943
	0.167±0.171	0.228±0.234	0.340±0.350	0.554±0.569	0.918±0.944
M_g	0.346±0.418	0.473±0.573	0.704±0.853	1.147±1.389	1.903±2.305
	0.346±0.418	0.473±0.572	0.706±0.854	1.149±1.391	1.904±2.306
ξ	0.255±0.213	0.350±0.291	0.521±0.434	0.848±0.706	1.407±1.172
	0.255±0.213	0.349±0.291	0.521±0.435	0.849±0.708	1.407±1.173
f_n, M_g, ξ	0.144±0.242	0.198±0.331	0.294±0.492	0.479±0.802	0.795±1.331
	0.144±0.242	0.197±0.330	0.295±0.493	0.480±0.803	0.795±1.331
L_x, L_y	0.384	0.522±0.019	0.772±0.054	1.257±0.170	2.050±0.349
	0.384	0.522±0.019	0.772±0.055	1.257±0.170	2.051±0.349

Appendix C: Sensitivity study results

Investigated parameter	RMS acceleration for "jumping 2" (m/s²)				
	1	2	4	8	16
f_p	0.118±0.001	0.145±0.002	0.196±0.002	0.296±0.003	0.468±0.005
	0.117±0.001	0.145±0.002	0.196±0.002	0.297±0.003	0.469±0.005
α	0.117±0.015	0.145±0.019	0.195±0.026	0.295±0.039	0.466±0.061
	0.117±0.015	0.144±0.019	0.196±0.026	0.296±0.039	0.467±0.061
δ	0.116±0.020	0.144±0.024	0.194±0.033	0.293±0.049	0.464±0.078
	0.116±0.019	0.144±0.024	0.194±0.033	0.294±0.049	0.464±0.078
f_p, α, δ	0.120±0.036	0.148±0.045	0.200±0.061	0.302±0.092	0.477±0.145
	0.120±0.036	0.148±0.045	0.200±0.061	0.303±0.092	0.477±0.145
f_n	0.270±0.219	0.334±0.271	0.452±0.366	0.682±0.553	1.078±0.874
	0.270±0.219	0.334±0.271	0.452±0.367	0.683±0.554	1.078±0.875
M_g	0.105±0.127	0.130±0.158	0.176±0.213	0.265±0.321	0.420±0.508
	0.105±0.127	0.130±0.157	0.176±0.213	0.266±0.322	0.420±0.508
ξ	0.113±0.004	0.139±0.005	0.188±0.007	0.284±0.010	0.449±0.016
	0.113±0.004	0.139±0.005	0.188±0.007	0.285±0.010	0.449±0.016
f_n, M_g, ξ	0.240±0.453	0.296±0.560	0.400±0.756	0.604±1.141	0.955±1.804
	0.240±0.453	0.296±0.559	0.401±0.757	0.605±1.144	0.955±1.805
L_x / L_y	0.117	0.144±0.005	0.193±0.014	0.291±0.039	0.452±0.077
	0.117	0.143±0.005	0.192±0.014	0.291±0.039	0.452±0.077

Investigated parameter	RMS acceleration for "skipping 1" (m/s²)				
	1	2	4	8	16
f_p	0.124±0.019	0.163±0.025	0.208±0.032	0.267±0.041	0.329±0.051
	0.123±0.019	0.162±0.025	0.209±0.032	0.267±0.041	0.330±0.051
α	0.121±0.007	0.159±0.010	0.204±0.013	0.261±0.016	0.323±0.020
	0.121±0.008	0.159±0.010	0.204±0.013	0.262±0.016	0.323±0.020
δ	0.121±0.011	0.159±0.015	0.203±0.019	0.261±0.025	0.322±0.031
	0.121±0.012	0.159±0.015	0.204±0.019	0.261±0.025	0.322±0.031
f_p, α, δ	0.127±0.039	0.167±0.052	0.214±0.066	0.274±0.085	0.339±0.104
	0.127±0.039	0.167±0.051	0.214±0.066	0.275±0.085	0.339±0.104
f_n	0.125±0.121	0.165±0.160	0.211±0.204	0.271±0.262	0.334±0.323
	0.125±0.121	0.165±0.159	0.212±0.204	0.271±0.262	0.334±0.323
M_g	0.109±0.132	0.143±0.174	0.183±0.222	0.235±0.285	0.290±0.351
	0.109±0.132	0.143±0.173	0.184±0.222	0.236±0.285	0.290±0.352
ξ	0.101±0.017	0.133±0.023	0.170±0.029	0.218±0.037	0.269±0.046
	0.101±0.017	0.132±0.022	0.170±0.029	0.218±0.037	0.269±0.046
f_n, M_g, ξ	0.113±0.213	0.149±0.281	0.191±0.360	0.245±0.461	0.302±0.569
	0.113±0.213	0.149±0.281	0.191±0.360	0.245±0.462	0.302±0.569
L_x, L_y	0.121	0.158±0.006	0.201±0.014	0.258±0.035	0.313±0.053
	0.121	0.158±0.006	0.201±0.014	0.258±0.035	0.313±0.053

Investigated parameter	RMS acceleration for "skipping 2" (m/s²)				
	1	2	4	8	16
f_p	0.052±0.006	0.073±0.008	0.100±0.011	0.137±0.016	0.181±0.021
	0.051±0.006	0.073±0.008	0.100±0.012	0.137±0.016	0.182±0.021
α	0.050±0.004	0.070±0.006	0.096±0.008	0.132±0.011	0.175±0.014
	0.050±0.004	0.070±0.006	0.096±0.008	0.133±0.011	0.175±0.014
δ	0.049±0.008	0.069±0.011	0.095±0.015	0.131±0.020	0.173±0.027
	0.049±0.008	0.069±0.011	0.096±0.015	0.131±0.020	0.173±0.027
f_p, α, δ	0.050±0.007	0.071±0.009	0.097±0.013	0.134±0.018	0.177±0.024
	0.050±0.007	0.071±0.010	0.098±0.013	0.134±0.018	0.177±0.024
f_n	0.111±0.120	0.157±0.169	0.216±0.232	0.297±0.318	0.392±0.421
	0.111±0.120	0.157±0.169	0.216±0.232	0.297±0.319	0.392±0.421
M_g	0.045±0.054	0.063±0.076	0.087±0.105	0.119±0.144	0.157±0.190
	0.045±0.054	0.063±0.076	0.087±0.105	0.119±0.144	0.157±0.191
ξ	0.046±0.003	0.065±0.005	0.089±0.006	0.123±0.008	0.163±0.011
	0.046±0.003	0.065±0.004	0.090±0.006	0.123±0.008	0.163±0.011
f_n, M_g, ξ	0.099±0.157	0.140±0.222	0.191±0.305	0.263±0.419	0.348±0.554
	0.099±0.157	0.139±0.222	0.191±0.305	0.264±0.420	0.348±0.554
L_x, L_y	0.050	0.070±0.003	0.095±0.007	0.130±0.018	0.169±0.029
	0.050	0.069±0.002	0.095±0.007	0.130±0.018	0.169±0.029

C.2. Results for the simplified method

The response of the floor was computed according to the indications presented in Section 6.3.4. For that purpose, the general method explained above was adopted together with the simplified method (whose response is obtained using the instructions of Section 6.3.2).

The following tables provide calculated RMS accelerations by crowd size. For each set of parameters, the upper line is obtained by the general method and the lower line by the simplified method.

Appendix C: Sensitivity study results

Investigated parameter	RMS acceleration for "jumping 1" (m/s²)				
	1	2	4	8	16
f_p	0.225±0.101	0.308±0.138	0.459±0.206	0.748±0.335	1.239±0.555
	0.236±0.115	0.322±0.157	0.481±0.234	0.783±0.381	1.298±0.631
α	0.384±0.034	0.526±0.047	0.784±0.070	1.278±0.114	2.117±0.188
	0.421±0.037	0.575±0.051	0.859±0.076	1.399±0.124	2.318±0.206
δ	0.382±0.028	0.523±0.038	0.780±0.057	1.270±0.093	2.105±0.154
	0.419±0.036	0.573±0.049	0.856±0.073	1.394±0.119	2.309±0.196
f_p, α, δ	0.223±0.098	0.305±0.134	0.455±0.200	0.742±0.325	1.229±0.539
	0.234±0.110	0.319±0.151	0.477±0.225	0.777±0.367	1.287±0.607
f_n	0.167±0.171	0.228±0.234	0.340±0.350	0.554±0.569	0.918±0.944
	0.175±0.181	0.239±0.248	0.356±0.370	0.580±0.602	0.961±0.998
M_g	0.346±0.418	0.473±0.572	0.706±0.854	1.149±1.391	1.904±2.306
	0.378±0.458	0.518±0.627	0.772±0.935	1.258±1.523	2.085±2.524
ξ	0.255±0.213	0.349±0.291	0.521±0.435	0.849±0.708	1.407±1.173
	0.261±0.186	0.357±0.254	0.533±0.379	0.868±0.618	1.437±1.024
f_n, M_g, ξ	0.215±0.495	0.294±0.677	0.439±1.010	0.715±1.645	1.185±2.725
	0.207±0.439	0.283±0.601	0.422±0.897	0.687±1.461	1.138±2.421
L_x, L_y	0.384	0.522±0.019	0.772±0.055	1.257±0.170	2.050±0.349
	0.420	0.571±0.021	0.845±0.060	1.376±0.186	2.245±0.382

Investigated parameter	RMS acceleration for "jumping 2" (m/s²)				
	1	2	4	8	16
f_p	0.117±0.001	0.145±0.002	0.196±0.002	0.297±0.003	0.469±0.005
	0.122±0.002	0.150±0.002	0.204±0.003	0.308±0.004	0.486±0.006
α	0.117±0.015	0.144±0.019	0.196±0.026	0.296±0.039	0.467±0.061
	0.121±0.016	0.150±0.020	0.203±0.027	0.306±0.040	0.484±0.063
δ	0.116±0.019	0.144±0.024	0.194±0.033	0.294±0.049	0.464±0.078
	0.120±0.018	0.148±0.023	0.201±0.031	0.303±0.046	0.478±0.073
f_p, α, δ	0.120±0.036	0.148±0.045	0.200±0.061	0.302±0.092	0.477±0.145
	0.123±0.036	0.152±0.044	0.206±0.059	0.311±0.090	0.491±0.142
f_n	0.270±0.219	0.334±0.271	0.452±0.367	0.683±0.554	1.078±0.875
	0.274±0.253	0.339±0.312	0.459±0.423	0.693±0.639	1.094±1.008
M_g	0.105±0.127	0.130±0.157	0.176±0.213	0.266±0.322	0.420±0.508
	0.109±0.132	0.135±0.163	0.182±0.221	0.276±0.334	0.435±0.527
ξ	0.113±0.004	0.139±0.005	0.188±0.007	0.285±0.010	0.449±0.016
	0.117±0.004	0.145±0.005	0.196±0.007	0.296±0.010	0.467±0.016
f_n, M_g, ξ	0.240±0.453	0.296±0.559	0.401±0.757	0.605±1.144	0.955±1.805
	0.270±0.554	0.333±0.684	0.451±0.926	0.681±1.399	1.075±2.208
L_x, L_y	0.117	0.143±0.005	0.192±0.014	0.291±0.039	0.452±0.077
	0.121	0.149±0.005	0.200±0.014	0.302±0.041	0.468±0.080

Appendix C: Sensitivity study results

Investigated parameter	RMS acceleration for "skipping 1" (m/s²)				
	1	2	4	8	16
f_p	0.123±0.019	0.162±0.025	0.209±0.032	0.267±0.041	0.330±0.051
	0.129±0.020	0.170±0.026	0.218±0.033	0.280±0.042	0.345±0.052
α	0.121±0.008	0.159±0.010	0.204±0.013	0.262±0.016	0.323±0.020
	0.127±0.008	0.167±0.010	0.214±0.013	0.275±0.017	0.338±0.021
δ	0.121±0.012	0.159±0.015	0.204±0.019	0.261±0.025	0.322±0.031
	0.126±0.011	0.166±0.015	0.213±0.019	0.273±0.025	0.337±0.030
f_p, α, δ	0.127±0.039	0.167±0.051	0.214±0.066	0.275±0.085	0.339±0.104
	0.132±0.040	0.174±0.052	0.224±0.067	0.287±0.086	0.353±0.106
f_n	0.125±0.121	0.165±0.159	0.212±0.204	0.271±0.262	0.334±0.323
	0.132±0.128	0.174±0.169	0.223±0.217	0.287±0.279	0.353±0.342
M_g	0.109±0.132	0.143±0.173	0.184±0.222	0.236±0.285	0.290±0.352
	0.114±0.138	0.150±0.182	0.192±0.233	0.247±0.299	0.304±0.368
ξ	0.101±0.017	0.132±0.022	0.170±0.029	0.218±0.037	0.269±0.046
	0.106±0.018	0.140±0.023	0.179±0.030	0.230±0.038	0.283±0.047
f_n, M_g, ξ	0.113±0.213	0.149±0.281	0.191±0.360	0.245±0.462	0.302±0.569
	0.123±0.237	0.162±0.312	0.207±0.401	0.266±0.514	0.328±0.633
L_x, L_y	0.121	0.158±0.006	0.201±0.014	0.258±0.035	0.313±0.053
	0.127	0.166±0.006	0.211±0.015	0.270±0.037	0.328±0.056

Investigated parameter	RMS acceleration for "skipping 2" (m/s²)				
	1	2	4	8	16
f_p	0.051±0.006	0.073±0.008	0.100±0.012	0.137±0.016	0.182±0.021
	0.054±0.006	0.076±0.008	0.105±0.011	0.144±0.016	0.191±0.021
α	0.050±0.004	0.070±0.006	0.096±0.008	0.133±0.011	0.175±0.014
	0.052±0.004	0.074±0.006	0.101±0.008	0.139±0.011	0.184±0.015
δ	0.049±0.008	0.069±0.011	0.096±0.015	0.131±0.020	0.173±0.027
	0.052±0.008	0.073±0.011	0.100±0.015	0.138±0.021	0.182±0.027
f_p, α, δ	0.050±0.007	0.071±0.010	0.098±0.013	0.134±0.018	0.177±0.024
	0.053±0.007	0.075±0.010	0.103±0.014	0.141±0.019	0.186±0.025
f_n	0.111±0.120	0.157±0.169	0.216±0.232	0.297±0.319	0.392±0.421
	0.117±0.129	0.165±0.182	0.227±0.251	0.312±0.345	0.412±0.456
M_g	0.045±0.054	0.063±0.076	0.087±0.105	0.119±0.144	0.157±0.191
	0.047±0.057	0.066±0.080	0.091±0.110	0.125±0.152	0.166±0.201
ξ	0.046±0.003	0.065±0.004	0.090±0.006	0.123±0.008	0.163±0.011
	0.049±0.003	0.069±0.005	0.095±0.006	0.130±0.009	0.172±0.011
f_n, M_g, ξ	0.099±0.157	0.139±0.222	0.191±0.305	0.264±0.420	0.348±0.554
	0.103±0.164	0.146±0.231	0.201±0.317	0.276±0.436	0.364±0.576
L_x, L_y	0.050	0.069±0.002	0.095±0.007	0.130±0.018	0.169±0.029
	0.052	0.073±0.003	0.010±0.007	0.137±0.019	0.178±0.030

INSA INSTITUT NATIONAL DES SCIENCES APPLIQUÉES RENNES

INSA de RENNES
Service de la Recherche

AVIS DU JURY SUR LA REPRODUCTION DE LA THESE SOUTENUE

Titre de la thèse:
Vibration of floor structures subjected to crowd-rhythmic activities

Nom Prénom de l'auteur : EL ASRI YOUSSEF

Membres du jury :
- Monsieur COUCHAUX Maël
- Monsieur DENOËL Vincent
- Monsieur SCHWARTZ Cédric
- Monsieur COSTA NEVES Luis
- Monsieur HJIAJ Mohammed
- Monsieur BATOU Anas
- Monsieur BATTINI Jean-Marc
- Madame TUBINO Federica

Président du jury : ANAS BATOU

Date de la soutenance : 24 Février 2023

Reproduction de la these soutenue

☒ Thèse pouvant être reproduite en l'état
☐ Thèse pouvant être reproduite après corrections suggérées

Fait à Rennes, le 24 Février 2023

Signature du président de jury

A. BATOU

Le Directeur,

Vincent BRUNIE

Titre : Vibration des planchers soumis à des activités rythmiques de foule

Mots clés : Planchers de bâtiment, vibrations induites par l'homme, effet de groupe rythmique, évaluation vibratoire en service.

Résumé : De nos jours, les planchers de bâtiment souffrent de vibrations excessives produites par l'activité humaine. Ceci est plus remarquable lorsqu'un groupe de personnes tente d'exercer des activités rythmiques de manière coordonnée. Les effets sur les occupants recevant ces vibrations peuvent aller de la perception, l'inconfort ou même la panique.
Cette thèse vise à établir une approche fréquentielle de modélisation des activités rythmiques de foule et proposer des méthodes pour évaluer la réponse vibratoire des planchers soumis à ces cas de charge. Le Chapitre 2 présente d'abord une revue de littérature sur le sujet. Le Chapitre 3 décrit la première campagne expérimentale effectuée sur un plancher de laboratoire où des groupes d'individus exerçaient des activités rythmiques dans des conditions proches de la pratique.
Un modèle de charge caractérisant les activités rythmiques de groupe dans le domaine fréquentiel est développé au Chapitre 4. Celui-ci comprend un modèle spectral pour une seule personne combiné avec des coefficients de coordination pour un groupe d'individus. La procédure pour identifier les paramètres de charge associés est détaillée puis appliquée aux résultats d'essais de laboratoire pour quatre activités rythmiques. De tels modèles ont été validés dans le Chapitre 5 sur la base d'essais vibratoires réalisés sur un plancher existant, avec une extension de leur domaine d'application. Après comparaison avec des modèles de la littérature, les modèles ainsi obtenus sont utilisés dans le Chapitre 6 pour établir des méthodes pratiques pour la prédiction de la réponse des planchers soumis à des activités rythmiques de groupe.

Title : Vibration of floor structures subjected to crowd-rhythmic activities

Keywords : Building floors, human-induced vibration, rhythmic group effect, vibration serviceability assessment.

Abstract : Nowadays, building floors are prone to excessive vibrations induced by human actions, especially when a group of people perform rhythmic activities in a coordinated manner. Resulting effects on the floor occupants vary from perception, discomfort or even panic.
This thesis addresses the development of a spectral modelling approach related to crowd-rhythmic activities and proposes methods for predicting the response of floors subjected to such load cases. Chapter 2 presents a literature review about the vibration of floors subjected to rhythmic activities. Chapter 3 describes the first experimental campaign carried out on a floor specimen where individuals performed various rhythmic activities while subjected to audible and visual stimulus.
A frequency-domain load model characterizing crowd-rhythmic activities is established in Chapter 4, comprising a spectral load model for a single person, combined with coordination factors for multiple individuals. The procedure to identify the crowd model parameters is detailed afterwards and applied to laboratory measurements for four investigated rhythmic activities. The developed models are then validated and their scope extended in Chapter 5, based on experiments realized on a full-scale floor. These crowd load models are then compared with existing models in the literature and used in Chapter 6 to propose design-oriented methods for the evaluation of floor responses due to crowd-rhythmic activities.